

STUDIES ON ADSORPTION OF ETHYL ACETATE VAPOR IN MOLECULAR SIEVES

THESIS

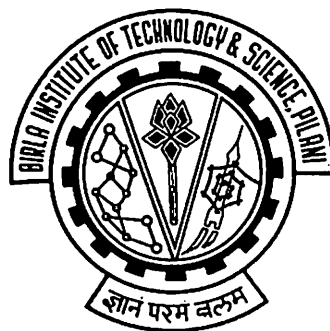
Submitted in partial fulfillment
of the requirements for the degree of
DOCTOR OF PHILOSOPHY

By

MANJARE SAMPATRAO DAGU

Under the Supervision of

Dr. A.K. GHOSHAL
Assistant Professor
IIT, Guwahati



**BIRLA INSTITUTE OF TECHNOLOGY AND SCIENCE
PILANI (RAJASTHAN) INDIA**

2004

ACKNOWLEDGEMENTS

I wish to express my deep sense of gratitude and sincere thanks to my thesis supervisor *Dr. A. K. Ghoshal*, Assistant Professor, IIT, Guwahati for his valuable guidance, keen interest and constructive encouragement throughout the period of this research work, without which, this work would not have seen the light of the day. It has been a great privilege for me to work under his guidance.

I thank *Prof. B.V. Babu*, Group Leader, Chemical Engineering Group and *Prof. R.P. Vaid*, Professor Chemical Engineering Group, the members of Doctoral Advisory Committee, for their kind suggestions, moral support and assistance.

My special thanks go to *Prof. S. Venkateswaran*, Vice-Chancellor, B.I.T.S. for giving me an opportunity to do research at the Institute. I also thank *Prof. L. K. Maheshwari*, Director, B.I.T.S., *Prof. K. E. Raman*, Deputy Director (Administration), B.I.T.S., *Prof. V. S. Rao*, Deputy Director (Off-Campus Programme), B.I.T.S. and *Prof. A. K. Sarkar*, Dean Instruction Division and Faculty Division I for providing the necessary infrastructure and other facilities. I also express my gratitude for the kindness and affection shown in enquiries about the work and the encouragement given by *Prof. Ravi Prakash*, Dean, Research and Consultancy Division. I thank *Mr. Sanjay D. Pohekar* of Research and Consultancy Division for helping me in finalizing the report. I am also thankful to *Dr. B.A. Metri* and *Dr. P.A. Thakurdesai*, Research and Consultancy Division, for their encouragement.

I express my sincere thanks to *Prof. R. K Gupta*, former member of Doctoral Advisory Committee and *Prof. R.K Patnaik*, former Dean, Instruction Division and Faculty Division I. for their guidance and invaluable assistance.

I am thankful to *Mr. Basudeb Munshi*, *Mr. H.K. Mohanta*, *Mr. Rakesh Angira*, *Mr. Ashish Chaurasia*, *Mr. Suresh Gupta*, and *Mr. Amol Deshpande* for their timely help and support during this research work.

I acknowledge contributions of *Prof. B.R. Natarajan*, *Prof. T.N.S. Mathur* and *Dr. V. S. Moholkar*, *Mrs. Manjuri Kumar* and other members Chemical Engineering Group with a sense of gratitude.

I extend special thanks to *Dr. Ajit Pratap Singh*, Instruction Division; *Dr. M.K. Deshmukh*, Coordinator, Center for Renewable Energy And Environment Development (CREED); *Dr. B.M. Deshpande*, IPC unit; *Dr. N. Rajesh*, Chemistry Group; *Dr. K.S.Raju*, Group Leader, Civil Engineering Group; *Dr. Neeraj Kumar Sachdev*, Humanities Group and *Mr. I.*

Ramakrishna, Civil Engineering Group for their help and encouragement throughout my research work.

I sincerely thank *Mr. Janardhanan, Ms. Gunjeet Bhaiya, Mr. Kalyan Patil, Mr. U.K. Reddy, Mr. S. Karthick* and *Shraddesh Malviya*, M.E. Chemical students, for their assistance in conducting experiments and preparing report.

I would like to thank *Mr. S.S.Nandal, Mr. Banwarilal Darji, Mr. Rajkumar Budania, Madanlal Jangir* and *Mr. Rajkumar Saini*, workshop, for helping in fabrication of experimental setup.

I express my sincere thanks to *Mr. Jangvir, Mr. Shankarmal, Mr. Jeevan, Mr. Babulal* and *Mr. Amarlal*, Chemical Engineering Laboratory for their assistance in setting up of experimental setup. I sincerely thank *Mr. Babulal Saini, Mr. Jamunadhar Saini, and Mr. Mathuram* for their cooperation during the preparation of this research report. I also express my special thanks to *Mr. K. N. Sharma* for his help in preparing drawings.

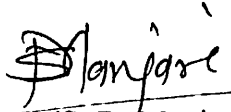
I would like to thank members of Reprography, Xerox and Printing Sections for their prompt services. I would like to thank one and all who have helped me in myriad ways throughout the course of this work.

I extend very special expression of gratitude to *Mrs. A.K. Ghoshal, Mrs. K.N. Sharma, and Mrs. K.L. Nangia* for their encouragement and moral support during my research work.

I am deeply indebted to my parents, brother, and all other family members for their constant encouragement, patience, and moral support. This work would not have been completed without their support.

I would like to record my special affection and thanks to my wife *Neeta*, whose constant persuasion and moral support has been a source of inspiration to me. I also thank my daughters *Bhagayashree, Madhura*, and my nephew *Krishna* for cheerfully sacrificing the time that rightfully belonged to them.

Last but not the least, I humbly acknowledge that I owe my being and my abilities in completing the research work to the God, the Almighty.


(S. D. Manjare)

CONTENTS

Abstract	i
Summary	iii
List of Tables	viii
List of Figures	x
List of Symbols	xv
Chapters	

1. Introduction & Literature Survey	
1.1. Introduction	1
1.1.1.Regulations	2
1.1.2.Recovery /Removal of VOCs	3
1.1.2.1 Absorption	
1.1.2.2 Condensation	
1.1.2.3 Adsorption	
1.1.2.4 Membrane Based Separation	
1.1.3.Selection of Adsorbent	9
1.1.4.Zeolites	11
1.1.4.1 Types of Molecular Sieves	
1.1.4.2 Structural Aspects of Molecular Sieves	
1.1.5.Role of Ethyl Acetate	15
1.1.6.Importance of Problem	19
1.1.7.Objective of the Work	20
1.2. Literature review	21
1.2.1.Available Control/ Abatement Techniques	21
1.2.2.Equilibrium and Rate Studies	23
1.2.3.Dynamic Studies	30
1.2.4.Conclusion on Literature Survey	33
2. Model Development	
2.1. Models for Adsorption Isotherm	39
2.1.1.Freundlich Adsorption Isotherm	40
2.1.2.Langmuir Adsorption Isotherm	40
2.1.3.Langmuir-Freundlich Adsorption Isotherm	41

CONTENTS

Abstract	i
Summary	iii
List of Tables	viii
List of Figures	x
List of Symbols	xv
Chapters	

1. Introduction & Literature Survey

1.1. Introduction	1
1.1.1.Regulations	2
1.1.2.Recovery /Removal of VOCs	3
1.1.2.1 Absorption	
1.1.2.2 Condensation	
1.1.2.3 Adsorption	
1.1.2.4 Membrane Based Separation	
1.1.3.Selection of Adsorbent	9
1.1.4.Zeolites	11
1.1.4.1 Types of Molecular Sieves	
1.1.4.2 Structural Aspects of Molecular Sieves	
1.1.5.Role of Ethyl Acetate	15
1.1.6.Importance of Problem	19
1.1.7.Objective of the Work	20
1.2. Literature review	21
1.2.1.Available Control/ Abatement Techniques	21
1.2.2.Equilibrium and Rate Studies	23
1.2.3.Dynamic Studies	30
1.2.4.Conclusion on Literature Survey	33

2. Model Development

2.1. Models for Adsorption Isotherm	39
2.1.1.Freundlich Adsorption Isotherm	40
2.1.2.Langmuir Adsorption Isotherm	40
2.1.3.Langmuir-Freundlich Adsorption Isotherm	41

2.1.4. Determination of Isotherm Model Parameters	41
2.2. Mass Transfer Mechanism	41
2.2.1. Determination of Mass Transfer Coefficient	42
2.2.1.1. Mass Transfer Coefficient Determination Using Uptake Rates	
2.2.1.2. Mass Transfer Coefficient Determination Using the LDF Rate Expression	
2.3. Model For Dynamic Study	43
2.3.1. Physical Structure of the Problem	47
2.3.2. Model Development for Dynamic Study	48
2.3.2.1. Assumptions	
2.3.2.2. Model Development	
2.3.3. Discretized Equations	54
2.4. Heat transfer Coefficient Between Fluid and Solid	57
2.5. Axial Dispersion Co-efficient	57
2.6. Numerical Solution	58
3. Experimental	
3.1. Isotherm Experiments	60
3.1.1. Experimental Setup and Procedure	60
3.2. Dynamic Studies – Experimental	61
3.2.1. Experimental Setup	61
3.2.2. Experimental Procedure	63
3.3. Materials	64
3.4. Analytical Technique	64
4. Results and Discussion	
4.1. Equilibrium and Kinetic Studies	70
4.1.1. Determination of Isotherms	70
4.1.2. Suitability of Different Isotherm Models	71
4.1.3. Determination of Model Parameters	73
4.1.4. Determination of Mass Transfer Coefficient	73
4.1.4.1 Mass Transfer Coefficient Determination Using the Uptake Curve Method	
4.1.4.2 Mass Transfer Coefficient Determination Using the LDF Rate Equation	

4.1.5. Determination of Heat of Adsorption	78
4.1.6. Conclusions on the Equilibrium & Kinetic Studies	78
4.2. Dynamic Studies	97
4.2.1. Introduction	97
4.2.2. Experimental Results	98
4.2.2.1 Adsorption on 5A and 13X Molecular Sieves	
4.2.2.2 Effect of Inlet Concentration	
4.2.2.3 Effect of inlet Velocity	
4.2.2.4 Effect of Bed Height	
4.2.3. Validation of the Model	102
4.2.4. Simulation Studies	105
4.2.4.1 Effect of Adsorbate Inlet Concentration, Inlet superficial Velocity and Bed Length	
4.2.4.2 Effect of Bed Diameter	
4.2.4.3 Effect of Overall Mass Transfer Coefficient, k	
4.2.4.4 Effect of Saturation Adsorption Capacity, q_s	
4.2.4.5 Effect of Heat of Adsorption, $-\Delta H$	
4.2.4.6 Effect of Bed to Wall Heat Transfer Coefficient, h_w	
4.2.4.7 Effect of Solid to Gas Heat transfer Coefficient, h	
4.2.4.8 Effect of Axial Dispersion Coefficient, D_a	
4.2.5. Conclusions from Dynamic Studies	112
Conclusions	142
Future Scope of Work	145
References	146
Appendix – I	154
Appendix – II	158
Appendix – III	186

ABSTRACT

Adsorption behavior of ethyl acetate (EA) from air on molecular sieves (E-merck 5A and 13X) is studied through experimental investigation on equilibrium, kinetics and through both experimental and theoretical investigations on dynamic adsorption. Equilibrium adsorption isotherms of ethyl acetate are obtained from the experimentally generated data on E-merck 5A and 13X molecular sieves in the temperature range of 308-328 K. Three isotherm models namely Freundlich, Langmuir, and Langmuir-Freundlich are used to correlate experimental data. The isotherms for ethyl acetate on E-merck 5A and 13X molecular sieves are typically of Brunauer Type – I. Of the three models, Langmuir isotherm model best represented the experimental data. Model parameters such as saturation capacity of adsorbent q_s , Langmuir constant b , and Freundlich constant n ; temperature dependency of model parameters; and heat of adsorption values are determined. Equilibrium adsorption capacity of ethyl acetate in E-merck 13X molecular sieve is higher and the sieve behaves closer to ideal behaviour than E-merck 5A molecular sieve. Overall mass transfer coefficient, k to understand the kinetics of adsorption is determined using Uptake rate and Linear Driving Force (LDF) rate methods. It is observed that k was independent of the flow rate and inlet concentration of ethyl acetate; values of k by LDF method were lower than the ones by uptake method; and adsorption was controlled by pore diffusion. Mass transfer coefficient obtained by Uptake method and heat of adsorption values for both the sieves are of the order of 10^{-4} s^{-1} and 10^5 J/kg respectively.

Dynamic adsorption behavior is studied experimentally through generation of concentration and temperature breakthrough curves with variations of input variables such as inlet concentration (c_0), inlet velocity (v_0) and bed length (L) in non-isothermal, non-adiabatic fixed bed adsorber containing pellets of 5A and 13X molecular sieves with feed mixture of

Ethyl Acetate (EA) and air. The experimental observations on effects of inlet concentration of EA, feed flow rate and bed height are analysed. A mathematical model is developed from mass and energy balance principles and is validated with the experimental data using the parameters determined from adsorption equilibrium and kinetic studies. Detailed simulation studies are carried out to study the effects of different parameters such as inlet concentration (c_o), inlet velocity (v_o), bed length (L), overall mass transfer coefficient (k), saturation capacity (q_s), heat of adsorption ($-\Delta H$), bed to wall heat transfer coefficient (h_w), solid to gas heat transfer coefficient (h) and axial dispersion coefficient (D_a) on the behavior of the adsorption system and the results are analysed. Early concentration breakthrough with higher inlet adsorbate (EA) concentration, constant pattern breakthrough curves with the changes of inlet adsorbate (EA) concentration, inlet velocity, and saturation adsorption capacity have been observed. Change of bed diameter, bed to wall heat transfer coefficient, and solid gas heat transfer coefficient don't significantly influence the concentration breakthrough curves.

KEY WORDS

Adsorption isotherm; Adsorption kinetics; Adsorption dynamics; ethyl acetate; E-merck 5A; E-merck 13X; Heat of adsorption; LDF method; Mass transfer coefficient; Mathematical model; Molecular sieves; Uptake curve method

SUMMARY

Emissions of Volatile Organic Compounds (VOCs) to the atmosphere are limited by government regulations because VOCs have been implicated as major contributor to photochemical smog and ozone formation, which adversely affects plant and human life. In the present study, adsorption behavior of ethyl acetate (EA), the VOC of concern, in molecular sieves has been studied. To understand the adsorption behavior of ethyl acetate in molecular sieves (E-merck 5A & 13X), detailed experimentation on equilibrium and dynamic studies and theoretical dynamic studies have been performed.

The Thesis has been presented mainly in four chapters and their contents are briefly presented below:

CHAPTER - I

Chapter I presents the introduction on the environmental regulations for VOCs emissions at national and international levels; impact of VOCs on the environment and the available control techniques; detailed discussion on the adsorbent with merits and demerits; several details on molecular sieves; and characteristic features of ethyl acetate and its impact on the environment. Then it discusses on the importance of the problem and objectives of the present study. The chapter category wise presents the extensive literature survey on the topics namely available control/abatement techniques; equilibrium and rate studies; and dynamic studies.

CHAPTER - II

This chapter discusses different adsorption isotherm models and the methodologies to determine the model parameters such as saturation adsorption capacity, Langmuir and

Freundlich constants and heat of adsorption from the experimental equilibrium adsorption isotherm data. Mechanism of mass transfer and methods of determining overall mass transfer coefficient by Uptake curve method and Linear Driving Force (LDF) method from the experimental data collected during isotherm studies have been discussed. The chapter then deals with the detailed development of the mathematical model with necessary initial and boundary conditions applicable to the system from the mass and energy balance equations applied for a differential section of the packed bed adsorber. Finally, the chapter presents the discretisation of the developed models and the numerical solution procedure.

CHAPTER - III

Experimental scheme and procedure for equilibrium, kinetic and dynamic studies have been presented in this chapter.

The adsorption isotherm setup was a glass U-tube containing a known weight of molecular sieve kept in constant temperature water bath. The molecular sieves used are type 5A and 13X (E-Merck, (1/16)"cylindrical pellets). The concentration of EA in air was varied maintaining different flow rates as well as different levels of EA in the saturator(s). Weight change of the U-tube containing molecular sieve was measured time-to-time using electronic balance. The experiments were performed for several concentration levels of ethyl acetate at four different temperatures 35°C, 40°C, 45°C and 55°C using 5A molecular sieve and at three different temperatures 35°C, 45°C and 55°C using 13X molecular sieve. The concentration of ethyl acetate vapor in the inlet stream was measured with the help of Gas Chromatography (GC) using AT 1000 column and Flame Ionization Detector (FID).

The apparatus for the dynamic studies consists of a dehydration column, saturators, knockout pot(s), flow meter, packed-bed adsorption column (S.S. pipe of ID 10 cm, thickness 0.2 cm and length 40 cm), and a constant temperature water bath. Thermocouple probes at equal

spacing (6 cm) were provided on the wall of the column at different radial locations to measure the temperature of the packed bed column along its length. After each run the sieves were taken out and heated overnight at 300 deg C for regeneration and cooled to room temperature. The variables studied are superficial velocity, inlet concentration of ethyl acetate, and bed length.

CHAPTER – IV

This chapter discusses the results of equilibrium and dynamic studies on ethyl acetate (EA) adsorption on E-merck 5A and 13X molecular sieves.

The results of equilibrium studies are discussed in the form of isotherms for 5A molecular sieve at four different temperatures 35°C, 40°C, 45°C and 55°C and for 13X molecular sieve at three different temperatures of experiment 35°C, 45°C and 55°C. The equilibrium capacities of 5A and 13X molecular sieves at different temperatures 35°C, 45°C and 55°C have been compared. Three isotherm models namely Langmuir, Freundlich and Langmuir-Freundlich are used to fit in the experimental equilibrium data. The model parameters such as Freundlich constant K , Langmuir constant b , saturation capacity q_s , and Freundlich and Langmuir-Freundlich exponent n have been obtained. The quantitative suitability of the models has been tested after calculating the standard deviations of the models' predictions from the experimental data.

Then the chapter discusses the results obtained from dynamic adsorption studies that include experimental study, model validation and dynamic simulation studies. At first, from the experimental data, effects of changes in input variables such as inlet superficial velocity, inlet concentration of EA and bed height have been analysed and performance of both the sieves towards adsorption of EA has been compared. Then, verification of the validity of the model

has been attempted through the comparison of the concentration and temperature histories measured at the end of the bed with those obtained from the proposed model. The model has been simulated after taking values of the input parameters such as Langmuir constant, equilibrium adsorption capacity, heat of adsorption and overall mass transfer coefficients as have been calculated from equilibrium studies. A quantitative assessment of the quality of the model has been made, by calculating standard deviation at each experimental point. Finally, The mathematical model was simulated with different values of the parameters such as adsorbate inlet concentration, inlet superficial velocity, bed length, bed diameter, overall mass transfer coefficient, saturation capacity, heat of adsorption, bed to wall heat transfer coefficient, solid to gas heat transfer coefficient, and axial dispersion coefficient and the results have been analysed.

The major inferences, which can be drawn from the present studies, are:

- The isotherms for ethyl acetate on E-merck 5A and 13X molecular sieves are typically of Brunauer Type – I.
- Of the three isotherm models tested Langmuir isotherm model best explains the equilibrium adsorption behavior of EA on E-merck 5A and 13X molecular sieves.
- Equilibrium adsorption capacity of ethyl acetate in E-merck 13X molecular sieve is higher and the sieve behaves closer to ideal behaviour than E-merck 5A molecular sieve.
- Mass transfer is controlled by pore diffusion. Also, no significant effect of concentration of EA on mass transfer coefficient has been observed.
- Mass transfer coefficient obtained by Uptake method is of the order of 10^{-4} s^{-1} . LDF method also can be an alternative to Uptake method if provided with properly designed data collection and analysis unit.

- Heat of adsorption values in both the sieves have been of the order of 10^5 J/kg
- Early concentration breakthrough with higher inlet adsorbate (EA) concentration, constant pattern breakthrough curves with the changes of inlet adsorbate (EA) concentration, inlet velocity, and saturation adsorption capacity have been observed.
- Effect of bed diameter, bed to wall heat transfer coefficient, and solid gas heat transfer coefficient is insignificant on the concentration breakthrough curves.

List of Tables

- Table 1.1** Commercial applications of molecular sieve as adsorbent
- Table 1.2** Zeolite types in commercial applications
- Table 1.3** Specifications of ethyl acetate
- Table 4.1.1** Equilibrium capacities and mass transfer coefficients for ethyl acetate in E-merck 5A molecular sieve at 35 deg C
- Table 4.1.2** Equilibrium capacities and mass transfer coefficients for ethyl acetate in E-merck 5A molecular sieve at 40 deg C
- Table 4.1.3** Equilibrium capacities and mass transfer coefficients for ethyl acetate in E-merck 5A molecular sieve at 45 deg C
- Table 4.1.4** Equilibrium capacities and mass transfer coefficients for ethyl acetate in E-merck 5A molecular sieve at 55 deg C
- Table 4.1.5** Equilibrium capacities and mass transfer coefficients for ethyl acetate in E-merck 13X molecular sieve at 35 deg C
- Table 4.1.6** Equilibrium capacities and mass transfer coefficients for ethyl acetate in E-merck 13X molecular sieve at 45 deg C
- Table 4.1.7** Equilibrium capacities and mass transfer coefficients for ethyl acetate in E-merck 13X molecular sieve at 55 deg C
- Table 4.1.8** Statistical analysis of fitting of experimental isotherm data to different isotherm models for ethyl acetate adsorption in E-merck 5A molecular sieve
- Table 4.1.9** Statistical analysis of fitting of experimental isotherm data to different isotherm models for ethyl acetate adsorption in E-merck 13X molecular sieve
- Table 4.1.10** Isotherm parameters for ethyl acetate adsorption in E-merck 5A molecular sieve
- Table 4.1.11** Isotherm parameters for ethyl acetate adsorption in E-merck 13X molecular sieve
- Table 4.1.12** Heat of adsorption values of ethyl acetate adsorption in E-merck 5A and 13X molecular sieves evaluated based on Langmuir and Langmuir – Freundlich models
- Table 4.2.2.1** Variables studied in packed bed adsorption experiments

Table 4.2.2.2 Operating conditions for adsorption of ethyl acetate on E-merck 5A molecular sieves

Table 4.2.2.3 Operating conditions for adsorption of ethyl acetate on E-merck 13X molecular sieves

Table 4.2.3.1 Values of model input parameters for simulation of experimental runs

Table 4.2.3.2 Statistical analysis results: model vs. experiment (in 5A molecular sieves)

Table 4.2.3.3 Statistical analysis results: model vs. experiment (in 13X molecular sieves)

Table 4.2.4.1 Variables with range of values used for theoretical study of ethyl acetate adsorption

Table 4.2.4.2 Base values of model input parameters for ethyl acetate adsorption

LIST OF FIGURES

- Figure 1.1** (a) Secondary building units and (b) Commonly occurring polyhedral units in zeolites framework structures
- Figure 1.2** Line representation of zeolite structure: (a) sodalite cage or truncated octahedron (b) type A zeolite unit cell (c) unit cell of types X and Y or fau (d) cation sites in type A (there are eight I, three II, and twelve III sites per unit cell); (e) cation sites in types X and Y (16 I, 32 I', 32 II, 32 II', 48 III, and 32 III' sites per unit cell).
- Figure 2.1** Section of packed bed column
- Figure 2.2** Coordinate system
- Figure 3.1.1** Experimental set up for equilibrium studies
- Figure 3.1.2** Photograph of experimental setup for equilibrium studies
- Figure 3.2.1** Experimental set up for Dynamic studies
- Figure 3.2.2** Photograph of experimental setup for dynamic studies
- Figure 3.4.1** Photograph of gas chromatography
- Figure 4.1.1** Ethyl acetate adsorption isotherms at different temperatures in E-merck 5A molecular sieve
- Figure 4.1.2** Ethyl acetate adsorption isotherms at different temperatures in E-merck 13X molecular sieve
- Figure 4.1.3** Comparison of equilibrium capacities of ethyl acetate in E-merck 5A and 13X molecular sieves at 35 deg C
- Figure 4.1.4** Comparison of equilibrium capacities of ethyl acetate in E-merck 5A and 13X molecular sieves at 45 deg C
- Figure 4.1.5** Comparison for equilibrium capacities of ethyl acetate in E-merck 5A and 13X molecular sieve at 55 deg C
- Figure 4.1.6** Fitting of Freundlich model with experimental data at 45 deg C in E-merck 5A and 13X molecular sieves
- Figure 4.1.7** Fitting of Langmuir model with experimental data at 45 deg C in 5A and 13X molecular sieves
- Figure 4.1.8** Fitting of Langmuir- Freundlich model with experimental data at 45 deg C in E-merck 5A and 13X molecular sieves

- Figure 4.1.9** Comparison of different isotherm models' predictions with experimental equilibrium data of ethyl acetate in E-merck 5A molecular sieves at 35 deg C
- Figure 4.1.10** Comparison of different isotherm models' predictions with experimental equilibrium data of ethyl acetate in E-merck 5A molecular sieves at 40 deg C
- Figure 4.1.11** Comparison of different isotherm models' predictions with experimental equilibrium data of ethyl acetate in E-merck 5A molecular sieves at 45 deg C
- Figure 4.1.12** Comparison of different isotherm models' predictions with experimental equilibrium data of ethyl acetate in E-merck 5A molecular sieves at 55 deg C
- Figure 4.1.13** Comparison of different isotherm models' predictions with experimental equilibrium data of ethyl acetate in E-merck 13X molecular sieves at 35 deg C
- Figure 4.1.14** Comparison of different isotherm models' predictions with experimental equilibrium data of ethyl acetate in E-merck 13X molecular sieves at 45 deg C
- Figure 4.1.15** Comparison of different isotherm models' predictions with experimental equilibrium data of ethyl acetate in E-merck 13X molecular sieves at 55 deg C
- Figure 4.1.16** Determination of overall mass transfer coefficient using uptake rate for ethyl acetate in E-merck 5A molecular sieve
- Figure 4.1.17** Determination of overall mass transfer coefficient using uptake rate for ethyl acetate in E-merck 13x molecular sieve
- Figure 4.1.18** Determination of overall mass transfer coefficient using LDF model in E-merck 5A molecular sieve
- Figure 4.1.19** Determination of overall mass transfer coefficient using LDF model in E-merck 13X molecular sieve
- Figure 4.1.20** Determination of heat of adsorption of ethyl acetate adsorption in E-merck 5A molecular sieves based on Langmuir model
- Figure 4.1.21** Determination of heat of adsorption of ethyl acetate adsorption in E-merck 13X molecular sieves based on Langmuir model
- Figure 4.2.2.1** Comparison between concentration breakthrough curves in E-merck 5A and 13X molecular sieves for ethyl acetate adsorption
- Figure 4.2.2.2** Comparison between concentration breakthrough curves in E-merck 5A and 13X molecular sieves for ethyl acetate adsorption

- Figure 4.2.2.3** Effect of inlet concentration on experimental concentration breakthrough curves in E-merck 5A molecular sieve of ethyl acetate in air
- Figure 4.2.2.4** Effect of inlet concentration on experimental concentration breakthrough curves in E-merck 13X molecular sieve of ethyl acetate in air
- Figure 4.2.2.5** Effect of inlet concentration on experimental temperature breakthrough curves in E-merck 13X molecular sieve of ethyl acetate in air
- Figure 4.2.2.6** Effect of inlet velocity on experimental concentration breakthrough curves in E-merck 5A molecular sieve of ethyl acetate in air
- Figure 4.2.2.7** Effect of inlet velocity on experimental concentration breakthrough curves in E-merck 13X molecular sieve of ethyl acetate in air
- Figure 4.2.2.8** Effect of inlet velocity on experimental temperature breakthrough curves in E-merck 13X molecular sieve of ethyl acetate in air
- Figure 4.2.2.9** Effect of bed heights on experimental concentration breakthrough curves in E-merck 5A molecular sieve of ethyl acetate in air
- Figure 4.2.2.10** Effect of bed heights on experimental concentration breakthrough curves in E-merck 13X molecular sieve of ethyl acetate in air
- Figure 4.2.2.11** Effect of bed heights on experimental temperature breakthrough curves in E-merck 13X molecular sieve of ethyl acetate in air
- Figure 4.2.3.1** Comparison of experimental concentration breakthrough curve of ethyl acetate in E-merck 5A molecular sieve with simulated results for run DS3
- Figure 4.2.3.2** Comparison of experimental temperature breakthrough curve of ethyl acetate in E-merck 5A molecular sieve with simulated results for run DS3
- Figure 4.2.3.3** Comparison of experimental concentration breakthrough curve of ethyl acetate in 5A molecular sieve with simulated results for run DS4
- Figure 4.2.3.4** Comparison of experimental temperature breakthrough curve of ethyl acetate in 5A molecular sieve with simulated results for run DS4
- Figure 4.2.3.5** Comparison of experimental concentration breakthrough curve of ethyl acetate in 5A molecular sieve with simulated results for run DS9
- Figure 4.2.3.6** Comparison of experimental temperature breakthrough curve of ethyl acetate in 5A molecular sieve with simulated results for run DS9
- Figure 4.2.3.7** Comparison of experimental concentration breakthrough curve of ethyl acetate in 13X molecular sieve with simulated results for run DS15

- Figure 4.2.3.8** Comparison of experimental temperature breakthrough curve of ethyl acetate in 13X molecular sieve with simulated results for run DS15
- Figure 4.2.3.9** Comparison of experimental concentration breakthrough curve of ethyl acetate in 13X molecular sieve with simulated results for run DS16
- Figure 4.2.3.10** Comparison of experimental temperature breakthrough curve of ethyl acetate in 13X molecular sieve with simulated results for run DS16
- Figure 4.2.3.11** Comparison of experimental concentration breakthrough curve of ethyl acetate in 13X molecular sieve with simulated results for run DS17
- Figure 4.2.3.12** Comparison of experimental temperature breakthrough curve of ethyl acetate in 13X molecular sieve with simulated results for run DS17
- Figure 4.2.3.13** Comparison of experimental concentration breakthrough curve of ethyl acetate in E-merck 13X molecular sieve with simulated results for increased k and calculated k for run DS 15
- Figure 4.2.3.14** Comparison of experimental temperature breakthrough curve of ethyl acetate in E-merck 13X molecular sieve with simulated results for increased k and calculated k for run DS 15
- Figure 4.2.4.1** Effect of inlet concentration on concentration breakthrough curve of ethyl acetate
- Figure 4.2.4.2** Effect of inlet concentration on temperature breakthrough curve of ethyl acetate
- Figure 4.2.4.3** Effect of inlet velocity on concentration breakthrough curve of ethyl acetate
- Figure 4.2.4.4** Effect of inlet velocity on temperature breakthrough curve of ethyl acetate
- Figure 4.2.4.5** Effect of bed height on concentration breakthrough curve of ethyl acetate
- Figure 4.2.4.6** Effect of bed height on temperature breakthrough curve of ethyl acetate
- Figure 4.2.4.7** Effect of bed diameter on concentration breakthrough curve of ethyl acetate
- Figure 4.2.4.8** Effect of bed diameter on temperature breakthrough curve of ethyl acetate
- Figure 4.2.4.9** Effect of mass transfer coefficient on concentration breakthrough curve of ethyl acetate
- Figure 4.2.4.10** Effect of mass transfer coefficient on temperature breakthrough curve of ethyl acetate
- Figure 4.2.4.11** Effect of saturation capacity on concentration breakthrough curve of ethyl acetate

- Figure 4.2.4.12** Effect of saturation capacity on temperature breakthrough curve of ethyl acetate
- Figure 4.2.4.13** Effect of heat of adsorption on concentration breakthrough curve of ethyl acetate
- Figure 4.2.4.14** Effect of heat of adsorption on temperature breakthrough curve of ethyl acetate
- Figure 4.2.4.15** Effect of bed to wall heat transfer coefficient h_w on concentration breakthrough curve of ethyl acetate
- Figure 4.2.4.16** Effect of bed to wall heat transfer coefficient h_w on temperature breakthrough curve of ethyl acetate adsorption
- Figure 4.2.4.17** Effect of solid to fluid heat transfer coefficient on concentration breakthrough curve of ethyl acetate adsorption
- Figure 4.2.4.18** Effect of solid to fluid heat transfer coefficient on temperature breakthrough curve of ethyl acetate adsorption
- Figure 4.2.4.19** Effect of dispersion coefficient on concentration breakthrough curve of ethyl acetate adsorption
- Figure 4.2.4.20** Effect of dispersion coefficient on temperature breakthrough curve of ethyl acetate adsorption
- Figure AI-1** GC peak for standard sample and area of the peak
- Figure AI-2** GC peak for column inlet sample and area of the peak.

List of Symbols

A_o	Bed cross-sectional area, (m^2)
A	Interstitial area, (m^2)
a_p	External surface area per unit volume of adsorbent, (m^2/m^3)
b	Langmuir constant (m^3/kg)
b_o	Pre-exponential factor in equation 2.3 (m^3/kg)
c	Concentration of adsorbate in fluid phase (kg/m^3)
c_o	Concentration of adsorbate in the fluid phase at the inlet, (kg/m^3)
C_p	Specific heat ($J/kg \cdot K$)
D	Column Diameter, (m)
D_a	Axial Dispersion Coefficient, (m^2/sec)
D_c	Intracrystalline diffusivity, (m^2 / sec)
D_m	Molecular diffusivity, (m^2/sec)
d_{pr}	Particle diameter (m)
h	Overall heat transfer coefficient between adsorbent particle and fluid ($J/sec \cdot m^2 \cdot K$)
h_w	Overall heat transfer coefficient at column wall ($J/sec \cdot m^2 \cdot K$)
$(-\Delta H)$	Heat of adsorption (J/kg)
J	Mass flux adsorbate in fluid phase, ($kg/m^2 \cdot sec$)
J_h	Heat flux through fluid, ($J/m^2 \cdot sec$)
K	Freundlich constant
k	Mass transfer coefficient, (sec^{-1})
k_c	Thermal conductivity of the gas, ($J/s \cdot m \cdot K$)
L	Adsorbent bed length (m)

Nu	Nusselt number, $\frac{hd_{pr}}{k_c}$
n	Exponent in equation 2.1 and 2.4 and number of data points in equation 2.6
Pr	Prandtl number, $\frac{Cp_g \mu_g}{k_c}$
q^*	Amount adsorbed at Equilibrium, (kg/kg)
q	Amount adsorbed at any time, (kg/kg)
q_s	Saturation capacity of adsorbent, (kg/kg)
R	Column radius, (m)
R_p	Particle radius, (m)
r	Radial co-ordinate for microparticle or crystal, m
Re_p	Particle Reynolds number, $\frac{d_p v_o \rho_g}{\mu_g \varepsilon}$
R_u	Universal gas constant, (J/ kg mole. K)
r_c	Crystal radius, (m)
t	Time, (sec)
Δt	Time increment, (sec)
T	Temperature, (K)
v_o	Superficial velocity, (m/sec)
v	Interstitial velocity, (m/sec)
x	Column thickness, (m)
z	Axial distance, (m)
Δz	Incremental change in length, (m)

Greek symbols

ε	Bed Porosity
ρ	Density, (kg/m ³)
τ_p	Tortuosity factor
μ	Viscosity, (kg/m.sec)
π	3.14

Subscripts

o	Initial condition
b	Bed
g	Gas
p	Particle
s	Solid
t	Value at time t
$t + \Delta t$	Value at $t + \Delta t$
w	Wall
z	Value at space grid z
$z + 1$	Value at $z + 1$
$z - 1$	Value at $z - 1$
$z + \Delta z$	Value at space grid $z + \Delta z$

CHAPTER I

INTRODUCTION AND LITERATURE SURVEY

Among the gaseous air pollutants, volatile organic compounds (VOCs) have attracted major attention because of their common occurrence in the atmosphere and their harmful effects. This chapter discusses different VOCs with their sources of emission, impact on environment, regulations with emission limits, and their recovery/removal techniques. Detailed discussion has been made particularly on ethyl acetate (EA), the VOC of concern in the present study; adsorption process with different adsorbents and the technique used for EA separation in this study. Importance of the problem and objectives of the work have been explained. Finally, the chapter concludes with an exhaustive literature review relevant to the topic.

1.1 Introduction

Volatile Organic Compounds are among the most common air pollutants emitted from chemical, petrochemical and allied industries. Emissions of VOCs originate from breathing and loading losses from storage tanks, venting of the process vessels, leaks from piping and equipment, wastewater streams and heat exchanger systems (Ghoshal and Manjare, 2002). Emissions from burning coal, oil, gasoline and evaporation at gasoline service stations also contribute to baseline level of different volatile organic compounds found in air. Vehicle emissions, chemical manufacturing, evaporation of automotive fuels, petroleum based products and chemical solvents are some other sources emitting hazardous VOCs in air. Some common examples of VOCs emitted from chemical process industries are

acetaldehyde, acetone, benzene, carbon tetrachloride, ethyl acetate, ethylene glycol, hexane, naphthalene, styrene, toluene, xylene etc. (Gupta and Verma, 2002; Ruhl, 1993).

VOCs have been implicated as a major contributor to photochemical smog, which can cause haze, damage to plant and animal life, eye irritation, and respiratory problem for humans (Hwang et al 1997). VOCs in combination with nitrogen oxides are responsible for ground level ozone and smog. VOCs participate in photochemical reactions to form ozone, which is a primary component of smog (Khan et al 1999). While ozone in the upper atmosphere is beneficial, ozone at ground level is quite undesirable/hazardous. The atmospheric ozone layer protects us from sun's dangerous ultraviolet rays. Ground level ozone however is a highly reactive gas that has adverse effects on the normal functioning of lungs in healthy humans. Breathing air with ozone concentrations above air quality standards aggravates symptoms of people with pulmonary diseases and increases the rate of asthma attacks. Prolonged exposure to ozone causes permanent damage to lung tissue and interferes in the functioning of the immune system. Because of VOCs adverse effects on human health and its role in ozone formation, emissions of VOCs to the atmosphere are required to be kept within limits set by government regulations as a means of protecting the environment from air pollution.

1.1.1 Regulations

International Level: Regulation on controlling organic vapour pollutants in air has been issued worldwide. In the ambient air quality standards, stipulated by the US Environmental Protection Agency, the maximum 3-h concentration of hydrocarbon content is $1.6 \times 10^{-4} \text{ kg/m}^3$ (0.24 ppm), not to be exceeded in one year (Khan et al 1999). Reduction of VOCs emissions in an area that exceeds the current national ambient air quality standard for ozone of 0.12 ppm is mandated under Title I of the US Clean Air Act Amendment of 1990. In addition,

Title III of the amendments requires reduction of the emissions of 189 hazardous pollutants, most of which are also included under the definition of VOCs (Ruddy and Carroll, 1993). The recently passed European Community stage emissions limit is 35 g total organic compounds (TOC) per cubic meter gasoline loaded (35 g TOC/m³). Similarly, the United States Environmental Protection Agency Standard 40 Code of Federal Regulations (CFR) part 63 has established an emission limit of 10 g TOC/m³. The German TA-Luft standard, the most stringent known gasoline emission regulation, has set an emissions limit of 150 mg TOC (excluding methane) per cubic meter of loaded product (0.15 g TOC/m³) (Khan and Ghoshal, 2000; Ruddy and Carroll, 1993; Pezolt et al 1997).

National level: The Air Prevention and Control of Pollution Act, 1981 intended to achieve effective control over air pollution caused for various reasons. The act contemplates establishment of central and state boards to lay down the standards of emission of air pollutants from industrial plants for improvement of air quality. Later, The Environmental Protection Act, 1986 was brought into force, which also deals with the aspects of hazardous chemicals (Bhole and Parwate, 1998). Also the Clean Air Act, 1990 (amendment) and the Factory Act, 1986 (amendment) limit the emission of commonly hazardous chemicals. Though these chemicals include many of the VOCs, no separate regulation mentioning the VOCs has been implemented so far (Khan and Ghoshal, 2000).

1.1.2 Recovery/ Removal of VOCs

The increasing awareness of the necessity for environmental safety and pollution control has diverted the attention of researchers across the world to look for better and efficient methods of VOCs recovery or removal from the effluent gas streams. Due to the adverse effects of VOCs emissions in the environment, the gaseous streams from vents and emission stacks are subjected to suitable abatement techniques, essentially to bring down the VOCs

concentration below the permissible levels before their release into the atmosphere. As the emission tolerance gets lower (ppm and ppb concentration levels) with increasing stringent environmental regulation, the control strategies for VOCs require a fresh and systematic approach.

There are various methods employed for the removal or recovery of VOCs from gaseous wastes. Listed below are some of the commonly identified techniques with some light thrown on the process advantages and disadvantages.

1.1.2.1 Absorption

Absorption, or scrubbing, is often used to separate gaseous streams containing high concentrations of organics, especially water-soluble compounds such as methanol, ethanol, isopropanol, butanol, acetone, and formaldehyde (Moretti, 2002). Absorption system can be designed to handle capacity of 55 to 2830 m³/min gas with VOCs concentration ranges from 500 to 5,000 ppm. Absorber can achieve VOC removal efficiencies of 95 to 98 % (William and Lead, 1997).

The use of absorption as the primary control technique for organic vapours is subject to several limiting factors. One factor is the availability of a suitable solvent. The VOC must be soluble in the absorbing liquid. Some common solvents that may be useful for VOC include water, mineral oils or other non-volatile petroleum oils. Another factor is the availability of vapour/liquid equilibrium data for the specific organic/solvent system in question. Such data are necessary for the design of absorber systems; however, they are not readily available for uncommon organic compounds.

Another consideration in the use of absorption is the treatment or disposal of the material removed from the absorber. In most cases, the scrubbing liquid containing the VOC is regenerated by stripping, where the VOC is desorbed from the absorbent liquid, typically at elevated temperature and/or vacuum. The VOC is then recovered as a liquid in a condenser. The stripping process may create water disposal problems that may require a wastewater treatment system to handle the contaminants.

1.1.2.2 Condensation

Condensation of a component or a mixture of components at their respective saturation temperatures is a common approach for industrial separation of gases. Condensation is achieved by chilling, pressurization or both, of the waste gas stream. Condensation is most efficient for VOCs with boiling points above 38 °C at relatively high concentrations above 5,000 ppm. Low-boiling VOCs can require extensive cooling or pressurization, which sharply increases operating costs. Condensation is best suited to mono solvent systems that produce liquid product, which require further treatment to separate various chemical species. Recovered VOCs can be reused within the process, used as wash solvents during equipment cleanup, burned as an alternative boiler fuel.

1.1.2.3 Adsorption

Physical adsorption has been found to be more significant in case of separation process. Physical adsorption occurs when adsorbate molecules are held on the surface and in the pores of adsorbent by the weak van der Waals force of attraction and is generally characterized by low heat of adsorption, and by the fact that the adsorption equilibrium is reversible and rapidly established (Ruthven, 1984). Activated carbon or zeolites are often used in physical adsorption.

Activated carbon based adsorption

VOCs are removed from the inlet air by physical adsorption onto the surface of the carbon. The system is sized according to the maximum flow and concentrations expected, and anything less usually improves efficiency. Carbon adsorption systems are flexible and are inexpensive to operate. Installation costs are often lower than those of other systems (Ruhl, 1993; Stenzel, 1993). The adsorption capacity of activated carbon for a given VOC is often represented by an adsorption isotherm that gives the amount of VOC adsorbed (adsorbate) to the equilibrium pressure (concentration) at constant temperature.

Activated carbon is a good adsorbent because of its large surface area, which is result of its vast infrastructure of pores. The pore structure may be pictured as having many small pores branching off from large ones, which are open through the entire particle. In a commercially available activated carbon solvent recovery plant, solvent laden air passes through a tank containing a bed of activated carbon. The solvent is adsorbed on the carbon surface and clean air is exhausted to atmosphere. When all of the available surfaces of the carbon pores are occupied it will not capture any additional solvent. Now to recover solvent for reuse, it must be released from the carbon surface. This is most commonly done by heating the carbon with steam. The hotter the carbon, the less solvent it can hold, so as steam heats the carbon, solvent is released and flushed away by the steam. The mixture of steam and solvent is condensed by cooling and then separated in the simplest case by gravity decanting. The carbon then can be reused as well. The batch process of adsorption and desorption is described above can be made continuous by the use of multiple carbon beds so that one is off-line for desorption while the others is on adsorption. Regeneration can be done on-site with hot air or hot nitrogen also, depending upon process conditions and local utilities.

Moisture is one of the crucial parameters to dictate the efficiency and effectiveness of adsorption processes. Halogenated compounds are strongly affected with increased relative humidity, whereas aromatic compounds are weakly affected. However, water vapour competes with the VOCs in the emission stream for adsorption sites on the carbon surface, emission stream humidity level exceeding 60 % RH are not desirable (Khan and Ghoshal, 2000). Activated carbon is the right adsorbent for high capacity, non-selective adsorption of gases at ambient temperature, suitable for most VOCs with molecular weights between 40 and 150 and boiling points from 38 °C to 65 °C.

Zeolite based adsorption

As elaborated in earlier section, it has been recognized that activated carbon is the most suitable adsorbent for this application (Rhul, 1993). However, Blocki (1993) pointed out that the applications of activated carbon present some disadvantages as these are flammable, difficult to regenerate for high boiling solvents, promotes polymerization or oxidation of some solvents to toxic or insoluble compounds, and require humidity control. Therefore, it is necessary for new type of adsorbent to replace the activated carbon. As a result, hydrophobic zeolite is now considered as an alternative adsorbent since it has good properties such as thermal stability and hydrophobicity (Blocki 1993; Takeuchi et al 1995). Hydrophobic zeolite can be manufactured with precise pore size, allowing selective adsorption of some compounds while excluding others.

Zeolites are inorganic materials that have a crystalline structure and fixed pore size. The homogenous pore size prevent molecules larger than a certain size from entering the lattice, so zeolites are some times called molecular sieves, which allow them to adsorb selectively. The non-flammable, thermally stable, and hydrophobic characteristics of zeolite can also play an important role in adsorption. The thermal stability and hydrophobicity of zeolite

increases with the Si/Al ratio in the zeolite framework. Synthetic hydrophobic zeolite, a pure crystalline silica molecular sieve, is non-flammable and is capable of withstanding temperatures as high as 850 °C (Deng and Lin, 1995). Furthermore, hydrophobic zeolite has a low affinity for water. Hydrophobic zeolites are also non-flammable, so it can be used for some compounds that might fire with activated carbon (e.g. cyclo-hexane). The cost of hydrophobic zeolite is still very high, so its use is economically limited to applications for which activated carbon is not well suited.

Important parameters which determine the performance of adsorption process are: i) Retentive ability, ii) Pressure, iii) Concentration, iv) Particulate concentration, v) Type of adsorbent, vi) Desorption methods, vii) Fire suppression, and viii) Steam recovery.

1.1.2.4 Membrane Based Separations

Several researchers are pursuing research for recovery of VOCs from air by membranes. But an established membrane separation technology for VOCs recovery is yet to be commercialised economically due to the following limitations (Lyandres et al, 1989).

- Application to narrow range of molecular size
- Very high operational feed pressure (100-200 psig)
- Strict maintenance of pH
- Scale build-up
- Bacterial fouling

Further research is continued in these areas to get through the above shortcomings. Thus, to summarise, amongst the techniques discussed above, adsorption technology has picked up considerable growth in the commercial application because of the following reasons (Serbezov and Sortirchos, 1997).

- Development of more selective synthetic adsorbent
- Development of advanced concepts like Pressure Swing Adsorption (PSA), Temperature Swing Adsorption (TSA), Fluidised Bed Adsorption (FBA), Moving Bed Adsorption (MBA), etc.

DOW Chemical Company has installed the SORBATHENE unit (based on Pressure Swing Adsorption, PSA) in 1987, as an economic alternative for the recovery of VOCs (Pezolt et al, 1997). Though this technology has been patented and used in United States and Europe, still it has many limitations. For example, this technology was initially applicable only to control the emissions of chlorinated solvents and monomers. Their research activities are continually expanding the list of recoverable compounds and exploring adsorption based separation processes (Pezolt et al 1997).

In view of above, the present research deals with adsorption technology to separate EA present in air using packed bed adsorber. The following section describes in detail different adsorbents and the corresponding selection of the adsorbents used for the present study.

1.1.3 Selection of Adsorbent

The role of the adsorbent is to provide the surface area required for selective sorption of the preferentially adsorbed species (Ruthven et al 1994). A high selectivity is the primary requirement, but a high capacity is also desirable since the capacity determines the size and therefore the cost of the adsorbent beds. A large specific surface area is preferable for providing large adsorption capacity, but the creation of a large internal surface area in a limited volume inevitably gives rise to large numbers of small sized pores between adsorption surfaces. The size of the micropores determines the accessibility of adsorbate

molecules to the internal adsorption surface, so the pore size distribution of micropores is another important property for characterizing adsorptivity of adsorbents.

Commercial adsorbents, which exhibit ultraporosity and which are generally used for separation of gas and vapour mixture include the activated carbons, activated clay, silica gel, activated alumina and the crystalline alumino-silicate zeolites. Except zeolites, all others do not possess ordered crystalline structure and the pores are non-uniform. The distribution of diameters may vary widely (20 to several thousand angstrom). Hence, all molecular species, with the possible exception of high molecular weight polymer materials, may enter the pores.

Certain materials (zeolites and carbon molecular sieves) that have very fine and uniformly sized micropores show significant differences in sorption rates as a result of steric hindrance to diffusion within the micropores. Such adsorbents offer the possibility of achieving an efficient kinetic separation based on differences in sorption rate rather than on difference in sorption equilibrium. Especially materials such as zeolite and carbon molecular sieves can be specifically engineered with precise pore size distributions and hence tuned for a particular separation. Surface polarity corresponds to affinity with polar substances such as water or alcohols. If the surface is polar, generally as a result of the presence of ions or polar molecules strongly bound to the solid surface, it will preferentially attract polar molecules- in particular water. This is because the field-dipole and/or field gradient-quadrupole interactions provide additional contributions to the energy of adsorption. This additional energy will arise only when conditions are fulfilled (i.e., a polar or quadrupolar molecule and a polar adsorbent). If either of these is lacking, there can be no significant electrostatic contribution to the energy of sorption. Thus polar adsorbents are termed as hydrophilic while adsorbents having a non-polar surface are termed as hydrophobic.

In recent times, the advent of synthetic molecular sieves as physical adsorbents, in spite of being expensive, enhanced the prospect of adsorption technology. New economic industrial separation operations based on adsorption were made possible by the use of commercially available molecular sieves, which have the following advantages:

- They provide good capacity with gases of low relative humidity.
- They are applicable to gases at elevated temperatures.
- They can be used to adsorb water selectively.
- They can be used to remove other selective impurities together with water.
- They can be used for adiabatic drying.
- They are not damaged by liquid water.

Commercial applications of molecular sieves are listed in Table-1.1.

1.1.4 Zeolites (Molecular Sieves)

1.1.4.1 Type of Molecular Sieves

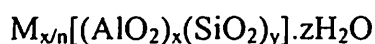
Many different types of molecular sieves are available commercially. They represent both synthetic and natural zeolites. The products are solids as powders, pellets, beads, tablets and mesh. The most widely used molecular sieves are synthetic zeolites in pelleted form. Some commercially available zeolite types are listed in Table – 1.2.

1.1.4.2 Structural Aspects of Molecular Sieves

The crystalline zeolites of commercial interest are based on a three dimensional network of AlO_4 and SiO_4 tetrahedra which are linked by the sharing of oxygen atoms. In considering the zeolite frameworks, it is convenient to consider the structures as built up from assemblages of secondary building units, which are themselves polyhedral made up of several SiO_4 and

AlO₄ tetrahedra. The secondary building units and some of the commonly occurring polyhedra are schematically shown in the Figure 1.1. In the diagram, each of the vertexes represents the location of a Si or Al atom while the lines represent, approximately, the diameters of the oxygen atoms, which are very much larger than the tetrahedral Si or Al atoms. Each aluminum atom introduces one negative charge on the framework, which must be balanced by an exchangeable cation. The exchangeable cations are located at preferred sites within the framework and play a very important role in determining the properties of the adsorbent. Changing the exchangeable cation by ion exchange provides a useful and widely exploited means of modifying the adsorptive properties.

Chemically, the structural formula for the unit cell can be represented as



where M = exchange cation of valence n, z = number of water molecules in unit cells. The sum (x+y) is constant for a particular unit cell. Unit cells are shown in Figure 1.2 (b) and (c). The water molecules can be removed with ease upon heating and evacuation, leaving an almost unaltered aluminosilicate skeleton with a void fraction between 0.2 and 0.5. The skeleton has a regular structure of cages, which are usually interconnected by six windows in each cage. The cages can imbibe or occlude large amounts of guest molecules in place of water. The size of window apertures, which can be controlled by fixing the type and number of cations, ranges from 3 Å to 10 Å. The sorption may occur with great selectivity because of size of the aperture (and to a lesser extent because of the surface property in the cages) and hence the name molecular sieve.

The Si/Al ratio in a zeolite is never less than 1.0 but there is no upper limit and pure silica analogs of some of the zeolite structures have been prepared. The adsorptive properties show a systematic transition from the aluminum-rich sieves, which have very high affinities for

eight corners of the cavity. Type II is at the eight member aperture, directly obstructing the entrance. Type III is near the four member ring inside the cavity. Type A zeolites are synthesized in the sodium form, with 12 sodium cations occupying all eight sites in I and three sites in II, plus one site in III. This is the commercial type 4A zeolite, with an effective aperture size of 3.8 \AA . The sodium form can be replaced by various other cations or by a hydrogen ion. The commercial type 3A zeolite is formed by exchanging Na^+ with K^+ , resulting in a smaller effective aperture size due to the large K^+ . The aperture size of the sodium form can also be increase by exchanging Na^+ with Ca^{+2} or Mg^{+2} , since two Na^+ are replaced by one bivalent cation. The form of the exchanged Ca^{+2} or Mg^{+2} is type 5A with rather unobstructed and larger apertures.

The skeletal structure of types X and Y zeolites are the same as that of the naturally occurring faujasite. The sodalite units are linked through six member prisms, as shown in the unit cell in Figure 1.2 (c). Each unit cell contains 192 $(\text{Si}, \text{Al})\text{O}_4$ tetrahedra. The number of aluminium ions per unit cell varies from 96 to 77 for type X zeolite, and from 76 to 48 for type Y zeolite. This framework has the largest central cavity volume of any known zeolite, amounting to about 50% void fraction in the dehydrated form. A unit cell, when fully hydrated, contains approximately 235 water molecules, mostly in the central cavity. The aperture is formed by the twelve -member oxygen rings with a free diameter of approximately 7.4 \AA . Three major locations are: centre of the six-member prism (I) and opposite to I in the sodalite cage (I'); similar to I and I' but further from the central cavity (II and II'); and at the twelve member aperture (III and III'). The commercial 10X zeolite contains Ca^{+2} as the major cation, and Na^+ is the major cation for 13X zeolite.

So, to conclude, molecular sieve zeolites are increasingly being used in commercial separation and VOCs recovery, due to their ability to preferentially adsorb particular

molecule and excluding others (Jasra and Bhat, 1987). Again, molecular sieve, being the most scientific and versatile adsorbent, could be a good option as adsorbent instead of activated carbon where recovery of an industrial component is concerned (Ruthven and Sircar, 1995).

Hence, though there are several adsorbents available for adsorption of a single component from air stream (EA from air in the present case), in the present research work molecular sieves (e-merck 5A and 13X) have been used. It seems that activated carbon could be enough for EA adsorption as there is no selectivity involved. The reported literature (discussed elsewhere in this chapter) provides information that the adsorptive capacity of the fibrous carbon cloth and crushed activated carbon for ethyl acetate from inert gas was 0.223 g EA/gm of fibrous cloth and 0.175 g EA/gm of crushed activated carbon respectively. Also the adsorptive capacity of the activated carbon for ethyl acetate from aqueous solution was 0.15 g EA / gm of activated carbon. Till date as such no information is available on the adsorption of EA using zeolites from air to make it free from EA. Again, since 5A molecular sieve has comparable pore size with the size of EA, 13X molecular sieve has also been used to compare the performances of the two molecular sieves for separation of ethyl acetate from air. The subsequent section of this chapter discusses in detail on properties and sources of emission of EA and its impact on environment.

1.1.5 Role of Ethyl Acetate as an Air Pollutant

Ethyl Acetate is a clear, volatile, inflammable liquid with a characteristic fruity odor detectable at 7 to 50 ppm. This is produced by the esterification of acetic acid with ethyl alcohol in the presence of catalysts. It has been recognized as one of the hazardous volatile organic compounds present in the air (Khan and Ghoshal, 2000). Specifications of ethyl acetate have been presented in Table 1.3.

Sources of Emission

The following operations involve the emission of ethyl acetate into the environment:

- Manufacture and transportation of ethyl acetate being used as a solvent in dry cleaning and for celluloid, shellacs, and lacquers
- Manufacture of smokeless powder, artificial silk and patent leathers, and preparation of photographic films and plates
- Manufacture of linoleum and plastic woods, flexible packaging, adhesives, paints, dyes, pharmaceuticals, drug intermediates, ethyl acetoacetate, acetic acid, n-nitrosodiethanolamine, artificial fruit flavorings and essences, and perfumes and fragrances, and during use of duplicator fluid
- Used as a co-extractant of camphor, fats, oils, and antibiotics

Product Description

Ethyl acetate is a flammable liquid and vapor. It has been assigned a flammability rating of 3 (serious fire hazard) by the National Fire Protection Association (NFPA) (www.osha.gov).

- Toxicity

The acute toxicity of ethyl acetate is low. Ethyl acetate vapor causes eye, skin and respiratory tract irritation at concentrations above 400 ppm. Exposure to high concentrations may lead to headache, nausea, blurred vision, central nervous system depression, dizziness, drowsiness and fatigue. Ingestion of ethyl acetate may cause gastrointestinal irritation and with larger amounts central nervous system depression. Eye contact with the liquid can produce temporary irritation and lacrimation. Skin contact produces irritation. No chronic systemic effects have been reported in humans and ethyl acetate has not been shown to be a carcinogen, reproductive or developmental toxin.

- **Flammability and Explosibility**

Ethyl acetate is a flammable liquid (NFPA rating = 3) and its highly flammable vapor can travel a considerable distance to an ignition source and flash back. It forms explosive mixtures with air at a concentration of 2-11% by volume. Hazardous gases produced in ethyl acetate fires include CO₂ and CO. Carbon dioxide or dry chemical extinguishers should be used for ethyl acetate fires. Flammable limits in air (% by volume): Lower, 2.0; Upper, 11.5.

- **Reactivity and Incompatibility**

Conditions contributing to its instability include heat sparks and open flame. Contact with strong oxidizers, strong alkalis and strong acids may cause fires and explosions. Ethyl acetate reacts vigorously with chlorosulphonic acid, lithium aluminum hydride, 2-chloromethyl furan, oleum, and potassium t-butoxide. Ethyl acetate also attacks some forms of plastics, rubbers and coatings.

- **Storage and handling**

Ethyl acetate should be handled in the laboratory using the basic prudent practices, supplemented by the additional precautions for dealing with highly flammable substances. In particular ethyl acetate should be used in areas free of ignition sources and quantities greater than 1 liter should be stored in tightly sealed metal containers in areas separate from oxidizers.

- **Exposure limits (www.osha.gov).**

The current Occupational Safety and Health Administration (OSHA) Permissible Exposure Limit (PEL) for ethyl acetate is 400 ppm (1400 milligrams per cubic meter (mg/m³)) as an 8-hour Time-Weighted Average (TWA) concentration.

The National Institute for Occupational Safety and Health (NIOSH) has established a Recommended Exposure Limit (REL) for ethyl acetate of 400ppm (1400 mg/m³) as a TWA for up to a 10-hour workday and a 40-hour workweek.

The American Conference of Government Industrial Hygienists (ACGIH) has assigned ethyl acetate a Threshold Limit Value (TLV) of 400 ppm (1400 mg/m³) as a TWA for a normal 8-hour workday and a 40-hour workweek.

- **Rationale for Limits**

The NIOSH limit is based on the risk of eye and respiratory irritation. The ACGIH limit is based on the risk of adverse health effects and irritation.

Hazardous Effects

- **Effects on Animals**

Ethyl acetate is a respiratory tract irritant and at high concentrations, it causes narcosis and depression of heart function (Hathaway et al 1991). The oral lethal dose 50 percent kill (LD 50) for acute exposure to ethyl acetate is 4935 mg/kg for rabbits and 5620 mg/kg for rats and 8-hour rat inhalation lethal concentration 50 percent kill (LC 50) are 1600ppm (Sax and Lewis, 1989). Cats exposed to 9000 ppm for 8 hours suffered from respiratory irritation and laboured breathing. Cats exposed for 45 minutes to 20,000 ppm showed deep narcosis, while exposure to 43,000 ppm for 14 to 16 minutes was lethal, symptoms of autopsy, pulmonary edema, haemorrhage and hyperemia of lungs were noted. Repeated 4-hour exposures to 2000 ppm were well tolerated by experimental animals such that no changes in the cellular components of the blood were noted. However, repeated exposure of rabbits to 4450 ppm caused liver damage and secondary anemia, with elevated white blood cell counts (NLM, 1992). Conjunctival irritation without corneal damage occurred in rabbits exposed chronically to ambient ethyl acetate concentrations that were intolerable to humans. Liquid

ethyl acetate instilled into the eyes of rabbits cause orbital irregularities of the cornea that completely resolved within 2 days (Grant, 1986).

- **Effects on humans**

Ethyl acetate is an irritant of the eyes and the upper respiratory tract at concentrations above 400 ppm (NLM, 1992). Unacclimated human volunteers experienced nose and throat irritation at 400 ppm, but no adverse symptoms were found in workers exposed to 375 to 1500 ppm ethyl acetate for several months. Ethyl acetate occasionally causes sensitization, with inflammation of the mucous membranes and eczema of the skin (Hathaway et al 1991). Workers exposed chronically to ethyl acetate concentrations ranging from 0.015 to 0.05 mg/m³ and 0.02 to 0.08 mg/m³ amyl acetate in air showed only redness of the conjunctiva (Grant, 1986). Signs and symptoms of exposure include the following:

(a) Acute exposure: Ethyl acetate causes irritation, redness and tearing of the eyes and irritation of the nose and throat. It is a defatting agent and may cause skin dryness after acute exposure. Sensitisation of the lining of the nose may occur with symptoms of inflammation (swelling, runny nose, redness of lining).

(b) Chronic exposure: Chronic exposure of the skin to ethyl acetate may cause dermatitis; no other systemic effects have been reported from the chronic exposure to ethyl acetate (Grant, 1986).

1.1.6 Importance of the Problem

Ethyl acetate is an important solvent used in petrochemical and polymer industries. It is commonly emitted from industrial plants and is often a constituent of industrial wastes (Tan and Liou, 1988). Ethyl acetate vapour present in air is one of the toxic Volatile Organic Compounds (VOCs) (Khan and Ghoshal, 2000). Stringent regulations have already been

enforced in different countries for VOCs emissions (Khan et al 1999). Many researchers across the world engaged themselves to find out economically feasible solution for the removal or recovery of VOCs for an environment-friendly technique. The details have been discussed later in this chapter. Though the toxicity of EA may not be so alarming, still it is also an environmental necessity to enquire after the techniques and processes for the removal or recovery of EA from air. Till date very little information is available on removal or recovery of EA from air. Adsorption is becoming more and more important as the basis of separation processes for gas mixtures due to the development of useful continuous and batch techniques and the use of new synthetic adsorbents with molecular sieve properties (Costa, et al 1991). The present research work aims at investigating the potential of adsorption technique and the molecular sieves for separation of EA from polluted air.

1.1.7 Objective of the work

Realising the importance of the problem the present research work has been undertaken with the following objectives:

- Adsorption equilibrium and kinetic studies for ethyl acetate in different molecular sieves, namely E-merck 5A and E-merck 13X.
- Evaluation of equilibrium and kinetic parameters as input to the model for dynamic studies.
- Comparison of adsorption capacities, kinetic and breakthrough data of different molecular sieves.
- Comparison of model prediction with the experimental adsorption behaviour.
- Adsorption dynamic studies in detail to understand the mechanism of ethyl acetate adsorption in different molecular sieves.

1.2 Literature Review

Adsorption has been recognized as the most practical regenerative methods for separating and recovering VOCs from the industrial flue gas streams. In recent years, new adsorbent materials (Lo et al 1996) and sorption methods have been actively studied for the efficient separation of VOCs from polluted air streams (Singh et al 2002). The detailed literature survey has been conducted for adsorption of VOCs/hydrocarbons on activated carbon and zeolite materials.

The literature survey presented here has been divided into three categories as below.

1. Available control /abatement techniques for controlling VOCs
2. Determination of equilibrium adsorption relation and kinetic parameters
3. Adsorption modeling and simulation supported by experimental data in some cases

1.2.1 Available Control/Abatement Techniques

Several research papers have been published in the literature mentioning the different control/ abatement techniques for controlling VOCs. Depending on the nature of pollutant, concentration of pollutant in exit streams, and other operating conditions, available control/abatement technique can be selected. Different control/abatement techniques studied by different authors are mentioned below.

Cantrell (1982) analysed several techniques to recover vapours from loading operations and processing units in the process and related industries. They concluded that as the value of feedstock continues to increase the value of vapours lost from processing facilities would also increase and favour the use of updated technology to minimize overall production costs and ensure environmental requirements are met. The author has discussed activated carbon adsorption for hydrocarbon separation.

Ruhl (1993) recognized adsorption as a proven and reliable pollution control technology that has the benefit of recovering valuable materials for reuse. His study highlighted the use of adsorbent, activated carbon, primarily for the recovery of important solvents like toluene, heptane, acetone, ethyl acetate, etc. He recommended the use of other adsorbents like hydrophobic zeolites with precise pore size, allowing selective adsorption of some specific VOCs.

Pezolt et al (1997), researchers from the DOW Chemical Company, successfully applied the SORBTHENE Solvent Recovery Unit technology, a pressure swing adsorption process, to meet the increasingly stringent gasoline and light hydrocarbon vapour emission standards. A field trial demonstrated 99+% recovery efficiencies at a major US gasoline storage and distribution terminal.

Ghoshal and Manjare (2002) studied several advanced concepts of adsorption in view of providing economic solutions for separation of VOCs from gaseous mixture. Their work was an attempt to establish a qualitative guideline for the selection of the appropriate technique (from amongst PSA, TPSA, TCPSA, SMBA) for recovery of VOCs, keeping in view the type and concentration of VOCs, VOCs vs. adsorbent suitability and the extent of separation required.

Moretti (2002) studied the abatement technologies available for controlling emissions of volatile organic compounds and hazardous air pollutants and the criteria for choosing among them.

1.2.2 Equilibrium and Rate Studies

Varieties of research work on adsorption equilibrium and kinetic studies for selected VOCs have been published in recent years. Different theories have been used for determination of the type of adsorption equilibrium relation and kinetic rate parameters. The relevant studies concerning the equilibrium relation and rate parameters are mentioned below.

Riekert (1971) studied the kinetic patterns of sorption, desorption and sorbate exchange for several C₂- C₅ hydrocarbons in synthetic zeolites of the mordenite T and Y structures. They concluded that the rate observations can best be represented by a model of sorption on interstitial sites in the solid, rather than by a model based on the analogy with macroporous sorbents. The number of vacant sites changes in time during the process of sorption, whereas it can remain constant if one sorbate is exchanged against another one.

Ruthven and Doetisch (1976) investigated the kinetics of sorption of four representative hydrocarbons namely, n-heptane, hexane, benzene and methylbenzene on 13X zeolite crystals. Extensive diffusivity data are presented showing the dependence on sorbate concentration and temperature. The form of concentration dependence of the diffusivity for these systems was very similar to that of the small mono-atomic and diatomic molecules in 5A zeolite. Thus the key factor, which determines the diffusion behavior, was the relative size of diffusing molecule and sieve window. For these hydrocarbons in the 13X sieve, as for the mono-atomic and diatomic gases in 5A, the critical diameters of the diffusing molecules are all appreciably smaller than the free diameter of the windows.

Jasra and Bhat (1987) reported measurements on sorption kinetics of n-paraffins viz. n-heptane, n-nonane, n-decane, n-dodecane, and n-tridecane on molecular sieve 5A from m-xylene, p-xylene, ethyl benzene, and methyl cyclohexane. Apparent diffusivity coefficients

have been determined from the kinetic data. The effect of carbon chain length, preadsorbed water and different nonadsorbing solvents on the kinetics of the sorption has been examined.

Kubota et al., (1989) studied the adsorption of propylene gas on molecular sieves 4A pellets. The heat of adsorption and the effective diffusion coefficient of propylene gas were estimated and measured, respectively. It was observed from kinetic studies that the transfer of the adsorbable species within the molecular sieve pellet was controlled and limited by micropore diffusion.

Yeh et al (1989) reported experimental results for equilibrium adsorption and diffusivities of CH_4 , C_2H_6 and CO_2 in type A zeolite containing mixed sodium and potassium ions. The percolation model interprets the equilibrium adsorption data, and stochastic results are derived for the diffusivity in zeolites with mixed cations.

Costa et al (1991) studied equilibrium adsorption isotherms of ethylene, propane, propylene, and carbon dioxide on 13X zeolite. Experimental data of adsorption isotherms were fitted to Langmuir, Prausnitz, and BET equations, showing the best results with Prausnitz isotherms. Binary adsorption isotherms for all binary systems were also obtained.

Cal et al (1994) developed adsorption isotherms for the adsorption of acetone and benzene onto activated carbon fibres (ACF). The isotherms were then fitted to Freundlich equation and Dubinin-Radushkevich equation. The measured adsorption isotherms of acetone and benzene were well fitted to modelled results using Freundlich and Dubinin-Radushkevich equations.

Olivier et al (1994) measured adsorption isotherms of butane, 2-methylpropane and 1-butene on activated carbon. The adsorption equilibria were correlated by the Flory-Huggins form of

the vacancy solution model. It was found that compounds with the same number of carbon atoms, the capacity increases with the presence of a double bond and decreases with a branched structure.

Malek and Farooq (1996) studied different isotherm models for correlating equilibrium results of methane, ethane and propane in activated carbon. They investigated the limiting behaviours as well as the pressure and temperature derivatives of the equilibrium isotherm models.

Ruthven and Kaul (1996) have reported the experimental equilibrium isotherms, Henry's law constants, and heats of sorption for adsorption of n-hexane, benzene, toluene, p-xylene, mesitylene, naphthalene, trimethylbenzene (TMP), and hexamethylbenzene (HMB) in La-exchanged zeolite Y.

Triebe et al (1996) studied the adsorption of methane, ethane, and ethylene on molecular sieve zeolites to determine the potential for the separation of ethylene from light hydrocarbons. The molecular sieves chosen for the study were H-modemite and 13X, CaX, 4A and 5A zeolites. Henry's law constant were determined over a variety of temperature changes. Equilibrium separation factors for the ethylene/methane system were provided for all zeolites over various temperature changes.

Silva and Rodrigues (1997a) studied the adsorption and diffusion of n-pentane in pellets of 5A zeolite. The adsorption equilibrium was interpreted with a model of localized adsorption in a homogenous surface, assuming that a molecule when adsorbed occupies a certain number of active sites with no interaction with sorbed molecules. Kinetic data clearly showed that the macropore diffusion was the controlling mass-transfer mechanism.

Yun and Choi (1997) studied adsorption isotherms of benzene and methylbenzene vapours on activated carbon. The study showed that the maximum adsorption capacity of benzene on activated carbon is higher than that of methylbenzene.

Yun et al (1998a) studied the adsorption equilibria of dichloromethane, 1,1,1-trichloroethane and trichloroethylene on activated carbon. The Toth and Dubinin-Radushkevich equations were used to correlate experimental isotherms. Thermodynamic properties such as the isosteric heat of adsorption and Henry's constant were calculated. It was found that values of isosteric heat of adsorption were varied with surface loading. Henry's constant showed that the order of adsorption affinity is 1,1,1-trichloroethane, trichloroethylene and dichloromethane.

Yun et al. (1998b) reported the experimental isotherms and prediction results for adsorption of benzene, toluene, dichloromethane and 1,1-dichloro-1-fluoroethane on hydrophobic Y-type zeolite. Isotherm showed the type-V shape according to the classification by Brunauer et al. (1940) The Clausius-Clapeyron equation used to calculate the isosteric heat of adsorption provided simple and reliable prediction of adsorption equilibrium relationships at various temperatures.

Dolidovich et al (1999) reported some findings on theoretical and experimental research studies of mechanical, structural, physical and chemical properties, micro- and macro kinetic adsorptive, catalytic and regenerative characteristics of heterogeneous alumina catalyst-adsorbents used for decontamination of individual volatile organic compounds (VOC), such as acetone, benzene, butylacetate, butylalcohol, xylene, ethyl acetate and their multi-component mixtures. They discussed the novel technologies of VOC decontamination in fixed, moving and fluidized catalyst-adsorbent beds. They found the adsorptive capacity of

the fibrous carbon cloth and crushed activated carbon for ethyl acetate from inert gas was 0.223 g EA/gm of fibrous cloth and 0.175 g EA/gm of crushed activated carbon respectively.

Silva and Rodrigues (1999) investigated the propylene and propane single adsorption isotherms and mass transfer kinetics over 13X and 4A zeolite pellets. Their work showed that 13X zeolite shows a higher loading capacity and lower mass transfer resistance while 4A zeolite shows the highest selectivity for propylene. Kinetic studies indicated that the macropore diffusion controls the mass transfer inside 13X zeolite pellets while micropore diffusion controls the propylene adsorption on 4A zeolite pellets.

Padin et al (2000) studied the gas phase separation of propane-propylene system with new sorbents, two new sorbents namely, NaLi -type A zeolite (NaLiA) and aluminophosphate AlPO_{14} -14 zeolite have been proposed for separation of propane-propylene system by adsorption. NaLiA is based on the principle of partially replacing some of the large Na^+ cations in commercial 4A (NaA) zeolite with smaller Li^+ cations in order to improve C_3H_6 uptake rates while at same time limiting C_3H_8 adsorption. AlPO_{14} -14_zeolite is capable of sterically excluding C_3H_8 due to its unique pore structure. In both cases, 99% propylene product purities could be obtained at reasonably high recoveries and throughputs.

Choudary et al (2002) studied the equilibrium adsorption isotherms of ethylene, ethane, propylene and propane on an Ag^+ -impregnated clay-based alkene-selective adsorbent, Olesorb-1. This adsorbent exhibited very high adsorption capacities, heats of adsorption and adsorption selectivity for ethylene and propylene over the corresponding alkanes. The adsorption selectivity was described to the interaction between the silver ions and the π electrons of the alkene molecules. The selectivity decreased with increasing alkene composition in the gas phase. A sharp decrease in the ethylene and propylene heats of

adsorption was observed with increasing coverage. The diffusion of the alkenes was rapid compared to that of the corresponding alkanes. The isotherm data correlated well with the Langmuir- Freundlich isotherm model for all the systems.

Ding et al (2002) have studied the kinetics of single component adsorption on activated carbon using a heterogenous vacancy solution theory (VST) of adsorption. Experimental equilibrium data of five hydrocarbons viz. ethane, propane, butane, benzene, and toluene and polar compounds, CO₂ and SO₂ were fitted to heterogeneous VST model to obtain isotherm parameters. The adsorption isotherm was developed to account for the adsorbate non-ideality due to size difference between the adsorbate molecule and the vacant site, while incorporating adsorbent heterogeneity through a pore-width-related potential energy. The transport processes in the bidisperse carbon considers couple mass transfer in both macropore and micropore phase simultaneously.

Grande et al (2002) presented the equilibrium and kinetic data for propane and propylene adsorption on pellets and crystals of 5A zeolite. The kinetic data presented indicate that the transport of sorbate in the pellet is controlled by macropore diffusion.

Huang et al (2002) investigated the gas-phase adsorption of acetone and n-hexane by activated carbons with different pore structures. A bituminous coal was chosen as the precursor of activated carbon and high porosity carbons were produced via a chemical activation route using KOH as the chemical reagent. Increasing the activation temperature increased both the porosity and the pore size. The equilibrium adsorption capacity for organic compounds increased with carbon porosity, but not proportionately. By incorporating pore size distribution with the Dubinin-Radushkevich equation using an inverse proportionality between the micropore size and adsorption energy, the isotherms for adsorption onto

different carbons were predicted. Simulations indicated that the adsorption energy, which is an inverse function of the micropore size, determines the adsorption capacity.

Prasetyo et al (2002) studied surface diffusion of strongly adsorbing hydrocarbon vapours on activated carbon. Propane, n-butane, n-hexane, benzene, and ethanol were used as diffusing adsorbate on a commercial activated carbon. It was found that the surface diffusivity of these strongly adsorbing vapours increases rapidly with loading, and the surface diffusion flux contributes significantly to the total flux and cannot be ignored. The surface diffusivity increases with temperature according to the Arrhenius law, and for the paraffins tested it decreases with the molecular weight of the adsorbate.

Singh et al (2002) studied the adsorption behavior of hexane and benzene in a single-component and in a mixture system onto activated carbon fabric cloth. The experimental adsorption isotherm data were correlated with Langmuir and Freundlich adsorption isotherms. The adsorption of n-hexane was found to be more in comparison to benzene. Kinetic studies concluded that internal diffusion controls the adsorption of benzene and n-hexane on activated carbon cloth.

Zhou et al (2002) had experimentally proved the enhancement effect of preadsorbed water on methane storage on activated carbon. Adsorption isotherms of methane on dry and wet activated carbon with different water content were measured. A sudden change in the methane uptake mechanism that was indicated by the inflection point of isotherms was observed. The measured amount adsorbed always decreased with the increasing water content of carbon before the inflection point.

1.2.3 Dynamic Studies

Several research articles based on theoretical and experimental studies for adsorption of selected VOCs have been reported in the literature. Follows below are the discussion on such relevant literatures related to adsorption of selected VOCs.

Sowerby and Crittenden (1988) performed column studies to determine the ability of silicalite to selectively remove the alcohols (ethanol, n-propanol, 2-propanol, 1-butanol, 2-butanol, 1-pentanol) from vapour streams containing high concentrations of water. The phenomenon of roll up was observed for both water and each alcohol studied. The magnitude of each roll-up and the analysis of the breakthrough curves suggest that the rate of mass transfer in the crystalline structure of silicalite not only decreases as the carbon chain length increases for straight chain alcohols but also is higher for straight chain alcohols than for the corresponding branched chain isomers.

Tan and Liou (1988) studied desorption of ethyl acetate from activated carbon by supercritical carbon dioxide. It was found that the adsorptive capacities after several regeneration cycles were still close to that of virgin carbon and remained stable. The effect of temperature, pressure, and flow rate on regeneration efficiency was also investigated. Regeneration was more favourable at higher pressures, but optimal temperature was found to depend on pressure. A one parameter mathematical model assuming linear desorption kinetics was proposed which agreed well with the experimental data. They also reported the adsorptive capacity of the activated carbon for ethyl acetate from aqueous solution to be 0.15 g EA / gm of activated carbon.

Ritter and Yang (1991) studied experimentally and theoretically the separation of dimethyl methylphosphonate (DMMP) vapour from air in activated carbon using Pressure Swing Adsorption (PSA). Different operating variables, like feed concentration, cycle time, volumetric purge to feed ratio and high to low pressure ratio were studied to know effect of these variables on the process performance.

Huang et al (1993) studied experimentally and theoretically the adsorption of acetone vapour from a nitrogen stream using a fixed bed of activated carbon. A linear driving force mass transfer model was used to fit the experimental data and was found to provide a good fit to the experimental data. The system was found to be an intraparticle mass transfer controlled process.

Liu and Ritter (1996) theoretically studied the removal of benzene vapour from nitrogen using an activated charcoal using pressure swing adsorption (PSA). The parameters i) effect of purge to feed ratio ii) effect of pressure level iii) effect of pressure ratio iv) effect of feed flow rate v) effect of feed concentration vi) effect of heat transfer coefficient vii) effect of cycle time viii) effect of adsorption step time and ix) effect of bed length to diameter ratio were investigated to ascertain their effects on the process performance. The trends from the parametric study showed that the process performance was affected significantly by all of these parameters.

Martinez and Basmadjian (1996) presented a general adsorption isotherm for gases and gas mixtures which separates due to adsorbate size, loss of symmetry or chemical dissociation, clustering and molecular interactions in the adsorbate phase. They studied adsorption of CO₂, ethane, ethylene and isobutane and their mixtures on zeolite 13X.

Hwang et al (1997) studied both experimentally and theoretically the adsorption and regeneration of methylene chloride vapour in a fixed bed of activated carbon, using nitrogen as carrier gas. A non-equilibrium, non-isothermal and non-adiabatic mathematical model was developed to calculate the concentration and temperature curves for both adsorption and regeneration runs. A linear driving force mass transfer model was found to be an acceptable fit to experimental data. Experimental and modelling results were used to study the effects of operation variables, such as, initial bed temperature, feed concentration of adsorption step and purge temperature. Also, regeneration efficiency was discussed on the basis of specific energy requirement and purge gas consumption.

Ray (1997) spotlighted the economic removal of malodorous and toxic organics by means of adsorption with activated carbon. They studied the adsorption of VOCs viz butane, decane, toluene, methyl chloride, methylene chloride, formaldehyde, methyl alcohol, and isopropyl alcohol.

Silva and Rodrigues (1997b) performed a detailed study of adsorption and diffusion of n-hexane in commercial pellets of 5A zeolite. The adsorption equilibrium was interpreted with a model of localized adsorption in a homogenous surface, assuming that a molecule when adsorbed occupies a certain number of active sites with no interaction between sorbed molecules. The effect of temperature, partial pressure of sorbate and total flow rate was studied in a fixed bed.

Silva and Rodrigues (1997c) studied the adsorption of feed mixtures of n-pentane, isopentane and nitrogen in fixed-bed adsorbers containing pellets of 5A zeolite. The effects of the partial pressure of the sorbate, temperature, and total flow rate of the mixture on the behaviour of the system were experimentally analysed and compared with model predictions.

Suyadal et al (2000) investigated the adsorption of trichloroethylene (TCE) vapour in a laboratory-scale packed-bed adsorber using granular activated carbon (GAC). They studied the effects of TCE inlet concentration, operating temperature and mass of the adsorbent on the TCE breakthrough curves and tested the deactivation model for these curves by using the analogy between the adsorption of TCE and the deactivation of catalyst particles. It was found that the deactivation model describes the experimental breakthrough curves more accurately compared to the adsorption isotherms given in the literature.

Cheng et al (2002) discussed the electrothermal desorption, an electricity promoted desorption technology. It is extremely straightforward and efficient when the adsorbent is electrically conductive. Electrochemical desorption shows distinct advantages over the traditional methods. They studied desorption of benzene from activated carbon using the electrothermal desorption.

Gupta and Verma (2002) studied the removal of di-methyl chloride (DMC) and toluene in air by cryogenic condensation and adsorption. They found out that condensation is a suitable and efficient method of VOC removal if emissions levels are high (>1%) while adsorption would be the preferred technique if the VOC emission levels are low i.e., parts per million (ppm), or sub ppm. Their work draws the conclusion that if the concentration of VOCs in the effluent stream varies over a wide range, condensation followed by adsorption is an effective technique to control the emissions.

1.2.4 Conclusion on Literature Survey

The detailed literature survey reveals that several researchers have been concerned since a few decades for the removal/recovery of VOCs / hydrocarbons. They studied different VOCs / hydrocarbons include hexane, benzene, n-heptane, i-pentane, propane, propylene, heptane,

methylbenzene, methyl chloride, trichloroethylene, ethylene, ethane, di-methyl chloride, toluene, acetone and methane. They have been using adsorption as the technique with different kinds of adsorbents. Adsorbents used were activated carbon, molecular sieves 5A and 13X, and sometimes specifically developed adsorbents. Most of the reported studies have focussed on the equilibrium and kinetic studies and their adsorption behaviour as a single component as well as multi-component systems. Results of these studies were to conclude on whether the mass transfer was micropore or macropore diffusion controlled; adsorptive capacities of the adsorbents; suitability of the type of isotherm to represent the equilibrium; and on the effects of parameters controlling the dynamics of the system. A few desorption studies have also been reported to conclude upon the ease of recovery. A few available reported literatures on adsorption of ethyl acetate provide information that the adsorptive capacity of the fibrous carbon cloth and crushed activated carbon for ethyl acetate from inert gas was 0.223 g EA/gm of fibrous cloth and 0.175 g EA/gm of crushed activated carbon respectively. Also the adsorptive capacity of the activated carbon for ethyl acetate from aqueous solution was 0.15 g EA / gm of activated carbon. Till date as such no information is available on the equilibrium adsorption of EA onto molecular sieves, type of isotherm suitably representing equilibrium adsorption behaviour, isotherm and kinetic parameters during the process of adsorption and identification of pertinent parameters and their effects on the dynamic adsorption behaviour of EA from air in fixed bed of molecular sieves. Keeping these in view and realising the importance of the problem, the present research problem has been undertaken to generate data for ethyl acetate adsorption in molecular sieves to meet up the aforementioned objectives.

Table 1.1: Commercial applications of molecular sieve as adsorbent

A	For Purification	B	For Bulk Separation
I	Drying of: Natural Gas (including LNG) Cracked Gas (Ethylene Plants) Refrigerant	I	Normal/iso-paraffin separation
II	CO ₂ removal from: Natural Gas Cryogenic air separation plants	II	Xylene separation
III	Sulphur compound removal Sweetening of natural gas or liquefied petroleum gas	III	Olefin separation
IV	Pollution Abatement Removal of Hg, NO _x , SO _x	IV	Oxygen from air

Table 1.2: Zeolite types in commercial applications

Zeolite Minerals	Synthetic Zeolites
Mordenite	Na, K, Ca forms
Chabazite	X- Na, Ca, Ba forms
Erionite	Y- Na, Ca, NH ₄ , rare earths
Clinoptilolite	L- K, NH ₄ forms Omega- Na, H forms Zeolon-H, Na forms Mordenite ZSM-5- various forms F-K form W-K form

Table 1.3: Specifications of ethyl acetate

Name	Ethyl Acetate
Classification	Ester
Formula	$\text{CH}_3\text{COOC}_2\text{H}_5$
Molecular Weight	88
Physical Properties	Colourless liquid Boiling Point 77°C , Melting Point -84°C
Solubility	Freely soluble in alcohol and acetone, moderately soluble in water (9 g/100 ml)
Vapor Density	3.0 (air = 1.0)
Vapor Pressure	76 mm Hg at 20°C
Flash Point	-4°C
Auto Ignition Temperature	427°C
Relative Density	0.895 to 0.898 at $27^\circ\text{C}/27^\circ\text{C}$
Toxicity Data	
LC ₅₀ oral (rat)	5620 mg/kg
LC ₅₀ inhale (rat)	1600 ppm
PEL (OSHA)	400 ppm (1400 mg/m ³)
TLV-TWA (ACGIH)	400 ppm (1440 mg/m ³)

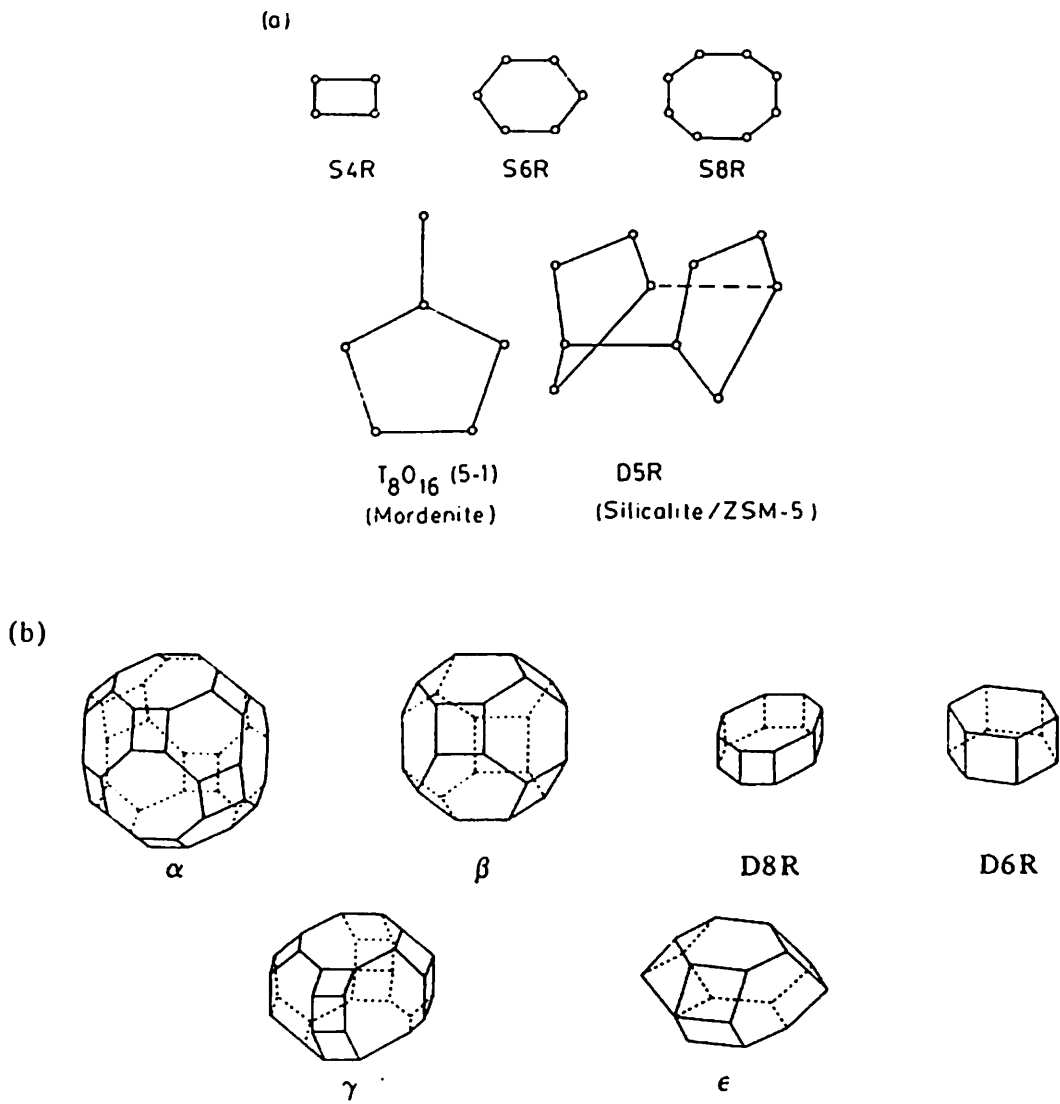


Figure 1.1: (a) Secondary building units and (b) Commonly occurring polyhedral units in zeolites framework structures

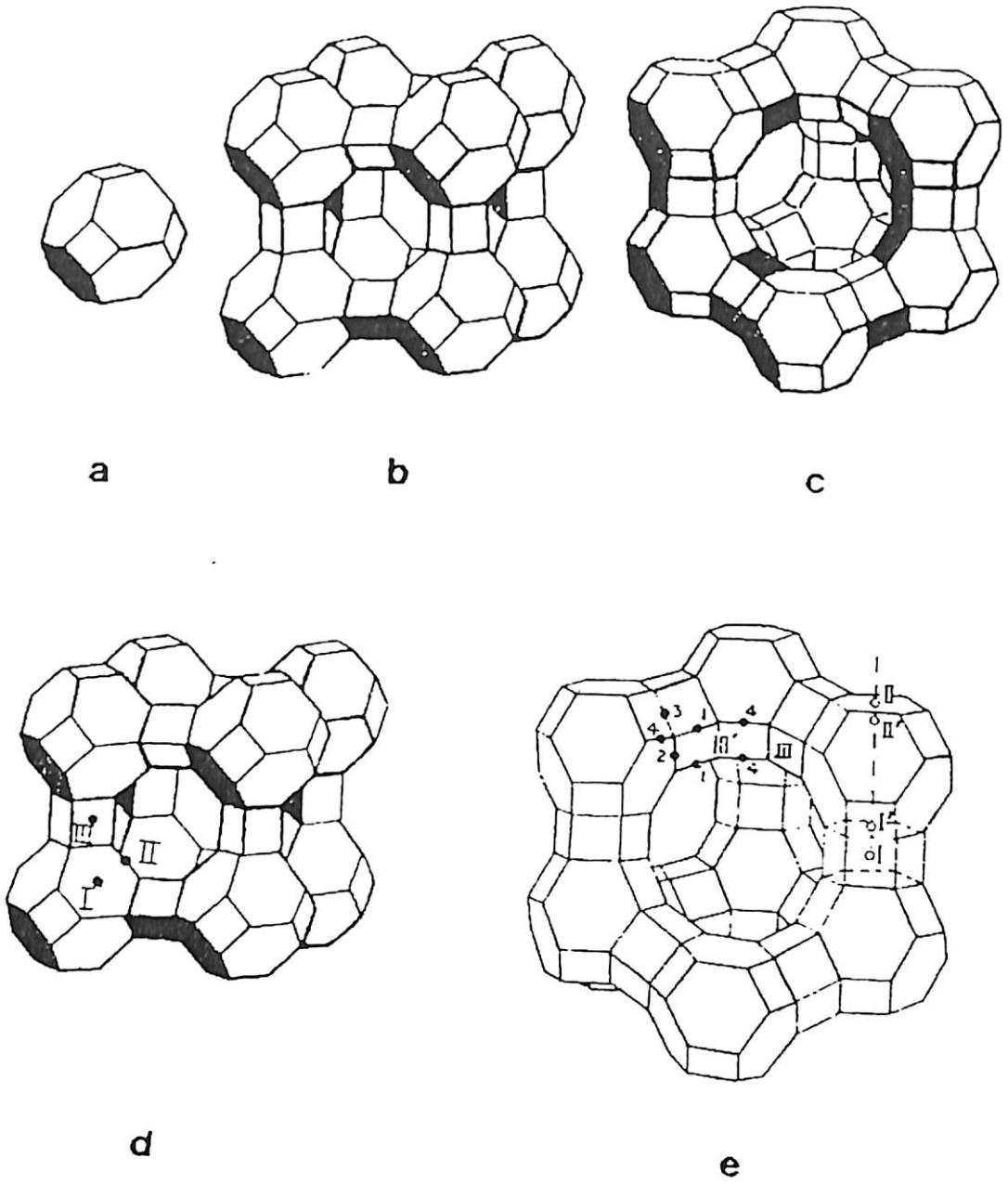


Figure 1.2: Line representation of zeolite structure: (a) sodalite cage, or truncated octahedron (b) type A zeolite unit cell (c) unit cell of types X and Y, or faujasite (d) cation sites in type A (there are eight I, three II, and twelve III sites per unit cell) (e) cation sites in types X and Y (16 I, 32 I', 32 II, 32 II', 48 III, and 32 III' sites per unit cell).

CHAPTER II

MODEL DEVELOPMENT

The successful application of adsorption as an industrial separation technology requires intensive study of phenomena such as equilibria and the kinetics of adsorption, coupled with mathematical model that correctly describes the dynamics of adsorption columns (Silva & Rodrigues, 1997a). To understand the adsorption behaviour of ethyl acetate (EA) using molecular sieves (E-merck 5A & 13X) for the present study, detailed experimentation on equilibrium study and dynamic study have been performed. The generated experimental data on adsorption isotherm have been used to correlate the type of isotherm most suitable for EA adsorption. The generated breakthrough data have been used to validate the dynamic model, which has been used subsequently for theoretical study on the dynamics of EA adsorption. This chapter discusses three different equilibrium isotherm models, which have been tested to find the best suitable one for EA adsorption. It also presents the mass transfer mechanism and thereafter the models for determination of mass transfer coefficients. Finally, the mathematical model developed from fundamental mass & energy balance equations for the dynamic study has been discussed in detail along with the scheme of numerical solution.

2.1 Models for Adsorption Isotherm

An adsorption isotherm equation is an expression of the relation between the amount of solute adsorbed and the concentration of the solute in the fluid phase at a given temperature. A number of equilibrium isotherm models can be utilized for correlating equilibrium results. Some of these models have gained more importance than others due to their simplicity and ubiquitous applicability. Accuracy of an isotherm model is generally a function of the number of independent parameters in the model, while its popularity in relation to process

application is generally a function of its mathematical simplicity (Malek & Farooq, 1996). Amongst the several isotherm models reported so far, the commonly used isotherm models such as Freundlich isotherm, Langmuir isotherm and Langmuir-Freundlich isotherm have been discussed below. These models have been used to correlate the generated isotherm data in the present study and the details have been presented in section 4.1.

2.1.1 Freundlich Adsorption Isotherm

The Freundlich isotherm is expressed as

$$q^* = Kc^n \quad (2.1)$$

Where, q^* is amount adsorbed at equilibrium (kg/kg), K and n are Freundlich constants and c is concentration of adsorbate in the fluid phase inside column (kg/m³).

2.1.2 Langmuir Adsorption Isotherm

The Langmuir equation may be written as

$$\frac{q^*}{q_s} = \frac{bc}{1 + bc} \quad (2.2)$$

Where, q_s is saturation capacity of adsorbent (kg/kg), b is Langmuir adsorption equilibrium constant (m³/kg) and c is concentration of adsorbate in the fluid phase in side column (kg/m³).

Van't Hoff equation (Ruthven 1984), relates the Langmuir adsorption equilibrium constant b to the free energy of adsorption.

$$b = b_o e^{\frac{-\Delta H}{R_u T_g}} \quad (2.3)$$

where, ΔH is heat of adsorption (J/kg), R_u is universal gas constant (J/kg/K) and T_g is gas phase temperature (K).

2.1.3 Langmuir-Freundlich Adsorption Isotherm

To obtain greater flexibility in empirical correlations, the Langmuir and Freundlich isotherms are combined to express Langmuir – Freundlich adsorption isotherm and is represented by

$$\frac{q^*}{q_s} = \frac{bc^n}{1 + bc^n} \quad (2.4)$$

The equilibrium constant b is related to the free energy of adsorption by equation 2.3 and n is Langmuir-Freundlich constant.

2.1.4 Determination of Isotherm Model Parameters

Isotherm model parameters are determined by fitting the experimental equilibrium data using the different isotherm models discussed above and reported in section 4.1. Temperature dependency of Langmuir constant b has been calculated using Van't Hoff equation (Eq. 2.3).

2.2 Mass Transfer Mechanism

In a composite adsorbent, there exist three distinct resistances viz. external film resistance, macropore resistance and micropore resistance. Under practical conditions of operation, the external film resistance is seldom, if ever, rate limiting so that the sorption/desorption rate is generally controlled by either macropore or micropore diffusion or by the combined effects of these resistances.

In general mass transfer mechanism of an adsorption process with molecular sieve zeolites as adsorbent includes five steps viz. fluid-film transfer, macropore diffusion, surface adhesion, surface diffusion and micropore diffusion. Since the surface adhesion rate approximates the order of the collision frequency of the gas molecules on the solid surface, which is much greater than that for the rate process, equilibrium has been assumed to achieve instantaneously at the interfaces. Pore diffusion and surface diffusion generally take place

simultaneously. In molecular sieves, pore diffusion is the significant mode of transport (Ruthven & Loughlin, 1972). Combination of the film transfer and pore diffusion can be represented as an overall rate controlling step and the corresponding resistance is the overall mass transfer resistance and inverse is the overall mass transfer coefficient which may vary with adsorbate adsorbent system and operating conditions. Usually the overall mass transfer coefficient is determined from the uptake curve as being discussed later. Apart from this usual procedure, an attempt has also been made here in the present study to determine the overall mass transfer coefficient using Linear Driving Force (LDF) rate equation, which has been described subsequently.

2.2.1 Determination of Mass Transfer Coefficient

The overall mass transfer coefficient has been determined from uptake rate and LDF rate expressions. The procedures have been explained in detail in section 4.1.

2.2.1.1 Mass Transfer Coefficient Determination Using Uptake Rates

For most particle shapes, representation as an equivalent sphere is an acceptable approximation and transport may therefore be described by a diffusion equation, written in spherical coordinate with the assumption of constant diffusivity as

$$\frac{\partial q}{\partial t} = D_c \left(\frac{\partial^2 q}{\partial r^2} + \frac{2}{r} \frac{\partial q}{\partial r} \right) \quad (\text{Ruthven, 1984}) \quad (2.5)$$

The solution of this equation with suitable initial and boundary conditions (Ruthven, 1984)

for the uptake curve is given by the familiar expression

$$\frac{q}{q^*} = 1 - \frac{6}{\pi^2} \sum_{n=1}^{\infty} \frac{1}{n^2} \exp\left(-\frac{n^2 \pi^2 D_c t}{r_c^2}\right) \quad (2.6)$$

where, q/q^* is the fractional approach to equilibrium.

Equation (2.6) can be used to find the diffusional time constant, D_c/r_c^2 . This expression converges rapidly in the long time region since the higher terms of the summation become vanishingly small. For fractional uptakes greater than 70% only the first term may be retained to obtain.

$$1 - \frac{q}{q^*} \approx \frac{6}{\pi^2} \exp\left(-\frac{\pi^2 D_c t}{r_c^2}\right) \quad (\text{Ruthven, 1984; Yang, 1987}) \quad (2.7)$$

In the long time region a plot of $\ln\left(1 - \frac{q}{q^*}\right)$ versus t should be linear with slope $-\pi^2 \frac{D_c}{r_c^2}$ and intercept $\ln(6/\pi^2)$. Such a plot provides in principle, a simple method of both checking the conformity of an experimental uptake curve with the diffusion equation and determining the diffusional time constant. Overall mass transfer coefficient (k) in LDF expression is approximately related to the diffusional time constant by the relation, $k = 15(D_c/r_c^2)$. The validity of this approximation has been confirmed for many different initial and boundary condition (Yang, 1987).

2.2.1.2 Mass Transfer Coefficient Determination Using the LDF Rate Expression

In most adsorption systems, the kinetics is controlled mainly by intra-particle diffusion. The diffusion-controlled kinetics may be satisfactorily represented by the following Linear Driving Force expression (LDF).

$$\frac{\partial q}{\partial t} = k(q^* - q) \quad (\text{Yang 1987}) \quad (2.8)$$

2.3 Model for Dynamic Study

In the industrial application of adsorbents, which is usually contacted by fluid flowing through a packed bed, the overall dynamics of the packed bed system control the design and determine the efficiency of the process. From the perspective of a designer, prediction of the

breakthrough curve from basic kinetic and equilibrium data is necessary since this provides a method of predicting dynamic capacity of a the column without recourse to extensive experimentation. The complexity of the dynamic behaviour of an adsorption column is directly related to the number of components and nature of operation since these factors determine the number of mass transfer zones or transitions. Adsorption systems can be classified with increasing complexity as follows (Ruthven, 1984).

1. Single Transition System (Single Mass Transfer Zone)
 - a. One adsorbable component plus inert carrier: isothermal or near isothermal operation
 - b. Two adsorbable components (no carrier): isothermal or near isothermal operation

2. Two Transition Systems (Two Mass Transfer Zones)
 - a. Two adsorbable components plus inert carrier: isothermal operation
 - b. Three adsorbable components (no carrier): isothermal operation
 - c. One adsorbable component plus inert carrier: adiabatic operation
 - d. Two adsorbable components (no carrier): adiabatic operation

3. Multiple Transition Systems (Multiple Mass Transfer Zones)
 - a. Four or more components: isothermal operation
 - b. Three or more components: adiabatic operation
 - c. Three components, isothermal operation with selectivity reversal
 - d. Two components, adiabatic operation with selectivity reversal

The dynamic behaviour of an adsorption system may be classified according to the nature of the mass transfer front and the complexity of the mathematical model required describing the system. Solely the form of the equilibrium relationship determines the nature of the mass

transfer front, while the complexity of the mathematical model depends on the concentration level, the choice of rate equation, and the choice of flow model.

Following classification provides a useful framework for more detailed analysis.

1) Nature of equilibrium relationship

(a) *Linear Isotherm*: It is characterized by dispersive behaviour. Analytical solutions for step or pulse response can generally be found.

(b) *Favourable response*: Concentration front approaches constant pattern form. Analytical solutions for asymptotic constant pattern profile are easily obtained, but a general analytical solution for the breakthrough curve or pulse response is only possible in a few special cases.

(c) *Unfavourable isotherm*: It is also characterized by dispersive behaviour. It is most commonly observed during desorption of a favourably adsorbed species. Analytical solutions are generally not possible.

2) Isothermal or near isothermal

(a) *Isothermal*: Heat transfer resistance can be neglected. The spreading of the concentration front is due entirely to axial dispersion and mass transfer resistance. This is the usual situation in a chromatographic system in which the adsorbable component is present only at low concentration in an inert carrier.

(b) *Near Isothermal*: Heat transfer between fluid and solid is slow enough to cause additional broadening of the concentration front although heat transfer between the column and the surroundings is still fast enough to prevent the formation of a distinct thermal front and associated secondary mass transfer zone.

3) *Concentration level of adsorbable components*

- (a) *Trace systems*: The adsorbable component is present only at low concentration in an inert carrier. Changes in fluid velocity across the mass transfer zone are therefore negligible.
- (b) *Nontrace systems*: The adsorbable species are present at sufficiently high concentration levels to cause a significant variation in fluid velocity across the mass transfer zone. Such effects are usually significant only for gaseous systems.

4) *Flow model*

- (a) *Plug flow*: Axial dispersion is neglected so that the term $-D_a \partial^2 c / \partial z^2$ can be dropped, thus producing a first order hyperbolic equation.
- (b) *Dispersed plug flow*: Axial dispersion is significant so that the term $-D_a \partial^2 c / \partial z^2$ must be retained.

5) *Complexity of kinetic model*

- (a) *Negligible mass transfer resistance*: Instantaneous equilibrium is assumed at all points in the column.
- (b) *Single mass transfer resistance*:
 - (i) *Linear rate expression*:

$$\frac{\partial q}{\partial t} = k(q^* - q) \quad (2.9)$$

The rate coefficient is an overall effective mass transfer coefficient (lumped parameter).

- (ii) *Diffusion model*: The dominant mass transfer is intraparticle diffusion, which is described by the diffusion equation with associated boundary conditions.

(c) *Two mass transfer resistances*

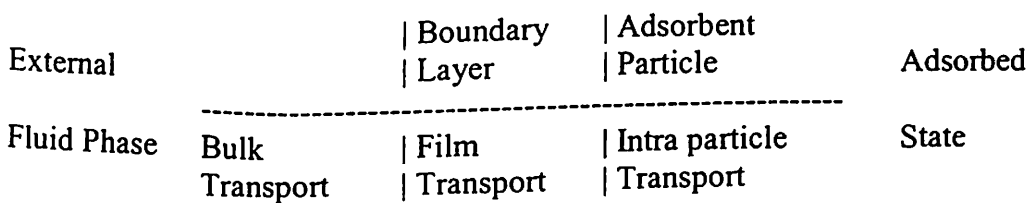
- (i) External fluid film resistance plus intraparticle diffusion
- (ii) Two internal diffusion resistances (macropore and micropore).

(d) *Three mass transfer resistances*

It includes external film resistance plus two intraparticle diffusional resistances (macropore and micropore). Such a model is sufficiently general to provide a realistic description of almost all-practical systems.

2.3.1 Physical Structure of the Problem

A mathematical model of fixed bed adsorber is very useful to obtain a proper design and to define optimal operating conditions for the adsorber. Adsorption on a solid particle can generally be regarded as a mass transport in which the rate expression shall include the transfer processes both inside and outside the adsorbent particle. There are essentially three consecutive transport steps associated with adsorption as illustrated below.



The first step, bulk transport of solute in the external fluid phase, is usually rapid because of mixing and convective flow. The second step, film transport involves diffusion of solute through a thin film or fluid dynamic boundary layer. Except for a small amount of adsorption that occurs to the exterior of the adsorbent, the solute then diffuses within the pore volume of the adsorbent and/or along pore-wall surfaces to an active adsorption site (intraparticle transport).

The actual adsorption of solute on interior surface sites is generally considered to be very rapid, equivalent to an equilibrium reaction and thus a negligible factor in this context of overall adsorption rate. Film and intraparticle transport are thus the major factors controlling the rates of adsorption by porous adsorbents of which the intraparticle transport is the predominant one and hence the control is mainly governed by the intraparticle transport.

2.3.2 Model Development for Dynamic Study

The system considered here for the mathematical model is a non-isothermal adsorption column packed with porous molecular sieve pellets through which an inert gas, air free from dust particles, carbon dioxide and moisture (non-adsorbable component), as carrier flows steadily along with the adsorbable component (ethyl acetate for the present case).

2.3.2.1 Assumptions

The following assumptions have been made while developing of the mathematical model.

1. Constant and uniform void fraction throughout the bed
2. Constant inlet feed flow rate
3. Complete radial mixing
4. Constant axial dispersion of heat and mass
5. Air free from moisture, carbon dioxide and particulates acts as an inert carrier gas
6. The feed consists of a small concentration of the adsorbable component, and the frictional pressure drop through the bed is negligible so that the linear velocity through the bed has been considered constant
7. Constant heat and mass transfer resistances throughout the bed because of little velocity variation across the bed
8. Negligible initial temperature difference across the bed

9. The equilibrium relationship for the adsorbing component is represented by the Langmuir isotherm with Langmuir constant, b showing the normal exponential temperature dependence
10. Temperature within the solid particle is homogeneously distributed
11. Temperature dependence of gas and solid properties are neglected
12. Change of fluid phase density with time is neglected
13. The mass transfer rate is represented by a linear driving force rate expression in which the mass transfer coefficient is the overall mass transfer coefficient (lumped parameter)
14. Bulk flow of heat and conduction in the axial direction are considered in the heat balance equation. An overall heat transfer coefficient has been used to account for heat loss from the system and the temperature of the column wall is assumed to be the same as the feed temperature. This implies a uniform temperature across the column radius with all heat transfer resistance concentrated at the wall.

2.3.2.2 Model Development

Development of the mathematical model based on fundamental balance equations considering a differential length Δz (Figure 2.1) and time Δt has been discussed below.

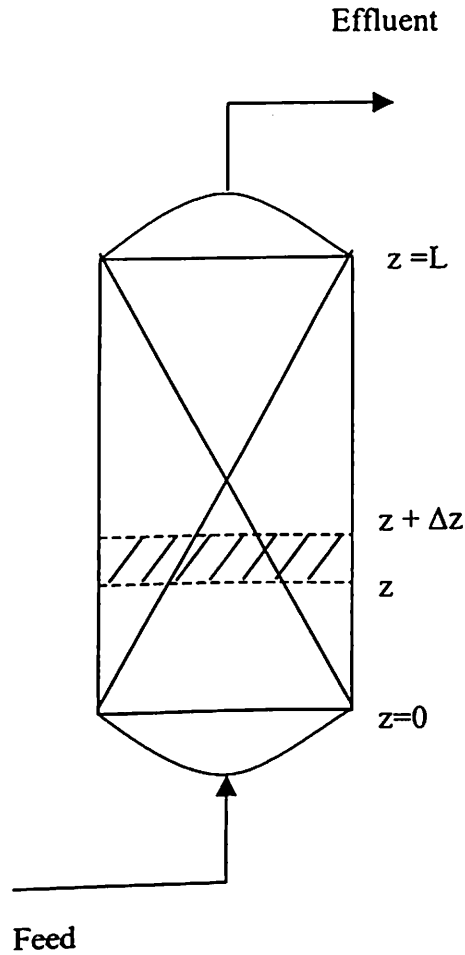


Figure 2.1: Section of packed bed column

Overall mass balance:

Since velocity and density of the fluid has been assumed as constant during the adsorption process, the overall mass balance became redundant.

Component mass balance:

Fluid phase component mass balance:

$$\begin{aligned} \text{Component mass in} + \text{Component mass generation} - \text{Component mass depletion} = \\ \text{Component mass out} + \text{Component mass accumulation} + \text{Component mass transferred to} \\ \text{solid phase} \end{aligned} \quad (2.10)$$

Mass in by convection = $cAv\Delta t|_z$

Mass in by diffusion = $JA\Delta t|_z$

Mass generation = zero

Mass depletion = zero

Mass out by convection = $cAv\Delta t|_{z+\Delta z}$

Mass out by diffusion = $JA\Delta t|_{z+\Delta z}$

Mass accumulation = $cA\Delta z|_{t+\Delta t} - cA\Delta z|_t$

Mass transferred to solid = $q\rho_b A_o \Delta z|_{t+\Delta t} - q\rho_b A_o \Delta z|_t$

$$J = -D_a \frac{\partial c}{\partial z}$$

Substituting all these terms in equation 2.10, rearranging and taking $\text{Lim}_{\Delta t \rightarrow 0}$ and $\text{Lim}_{\Delta z \rightarrow 0}$,

the final expression becomes

$$\frac{\partial c}{\partial t} = D_a \frac{\partial^2 c}{\partial z^2} - \frac{v_o}{\varepsilon} \frac{\partial c}{\partial z} - \frac{\rho_b}{\varepsilon} \frac{\partial q}{\partial t} \quad (2.11)$$

Solid phase component mass balance:

Component mass in + Component mass generation – Component mass depletion =

Component mass out + Component mass accumulation (2.12)

Mass in = mass transferred from fluid phase = $k(q^* - q)\rho_s A_o \Delta z(1 - \varepsilon)\Delta t$

Mass generation = zero

Mass depletion = zero

Mass out by convection = zero

Mass out by diffusion = zero

Mass accumulation = $q\rho_s (1 - \varepsilon) A_o \Delta z|_{t+\Delta t} - q\rho_s (1 - \varepsilon) A_o \Delta z|_t$

Substituting all these terms in equation 2.12, rearranging and taking $\text{Lim}_{\Delta t \rightarrow 0}$ and $\text{Lim}_{\Delta z \rightarrow 0}$,

the equation takes the form

$$\frac{\partial q}{\partial t} = k (q^* - q) \quad (2.13)$$

Energy balance:

Fluid phase energy balance:

Amount of energy in + Amount of energy generated – Amount of energy depleted = Amount of energy out + Amount of energy accumulated + Amount of energy lost to wall

$$(2.14)$$

$$\text{Energy in by convection} = \rho_g A v C_{p_g} T_g \Delta t \Big|_z$$

$$\text{Energy in by diffusion} = J_h A \Delta t \Big|_z$$

$$\text{Amount of energy in by transfer from solid phase} = h a_p (T_s - T_g) A_o (1 - \varepsilon) \Delta z \Delta t$$

$$\text{Amount of energy generation} = \text{zero}$$

$$\text{Amount of energy depletion} = \text{zero}$$

$$\text{Amount of energy accumulated} = \rho_g A_o \Delta z \varepsilon C_{p_g} T_g \Big|_{t+\Delta t} - \rho_g A_o \Delta z \varepsilon C_{p_g} T_g \Big|_t$$

$$\text{Amount of energy out by convection} = \rho_g A v C_{p_g} T_g \Delta t \Big|_{z+\Delta z}$$

$$\text{Amount of energy out by diffusion} = J_h A \Delta t \Big|_{z+\Delta z}$$

$$\text{Amount of energy lost to wall} = h_w \pi D (T_g - T_w) \Delta z \Delta t$$

$$J_h = -k_c \frac{\partial T_g}{\partial z}$$

Substituting all these terms in equation 2.14, rearranging and taking $\text{Lim}_{\Delta t \rightarrow 0}$ and $\text{Lim}_{\Delta z \rightarrow 0}$,

the equation becomes

$$\frac{\partial T_g}{\partial t} = \frac{ha_p}{\rho_s C_{p_s}} \frac{(1-\varepsilon)}{\varepsilon} (T_s - T_g) + \frac{k_c}{\rho_s C_{p_s}} \frac{\partial^2 T_g}{\partial z^2} - \frac{v_o}{\varepsilon} \frac{\partial T_g}{\partial z} - \frac{2h_w(T_g - T_w)}{R\varepsilon\rho_s C_{p_s}} \quad (2.15)$$

Solid phase energy balance:

Amount of energy in + Amount of energy generated = Amount of energy transferred
+ Amount of energy accumulated (2.16)

Amount of energy in with the adsorbate is negligible in comparison to the amount of heat generation due to adsorption.

$$\text{Amount of energy generated} = \frac{\partial q}{\partial t} (-\Delta H) \rho_s A_o \Delta z \Delta t (1 - \varepsilon)$$

$$\text{Amount of energy transferred} = ha_p (1 - \varepsilon) A_o \Delta z (T_s - T_g) \Delta t$$

$$\text{Amount of energy accumulated} = \rho_s C_{p_s} A_o \Delta z (1 - \varepsilon) T_s |_{t+\Delta t} - \rho_s C_{p_s} A_o \Delta z (1 - \varepsilon) T_s |_t$$

Substituting all these terms in equation 2.16, rearranging and taking $\text{Lim}_{\Delta t \rightarrow 0}$ and $\text{Lim}_{\Delta z \rightarrow 0}$, the equation takes the form

$$\frac{\partial T_s}{\partial t} = \frac{(-\Delta H)}{C_{p_s}} \frac{\partial q}{\partial t} - \frac{ha_p}{\rho_s C_{p_s}} (T_s - T_g) \quad (2.17)$$

Initial and Boundary Conditions:

Fluid phase component mass balance:

Initial condition:

$$\text{At } t = 0 \text{ for all } z, c = 0 \text{ i.e. } c|_{t=0} = 0 \quad (2.18)$$

Lower boundary condition:

$$\text{At } z = 0 \text{ for } t > 0, v_o c_o = v_c \varepsilon - D_a \varepsilon \frac{\partial c}{\partial z} |_{z=0} \quad (2.19)$$

Upper boundary condition:

$$\text{At } z = L \text{ for } t > 0, \frac{\partial c}{\partial z} = 0 \quad (2.20)$$

Initial condition for solid phase mass balance:

$$\text{At } t = 0 \text{ for all } z, q = 0 \text{ i.e. } q|_{t=0} = 0 \quad (2.21)$$

Fluid phase energy balance:

Initial condition:

$$\text{At } t = 0 \text{ for all } z, T_g = T_{go} \text{ i.e. } T_g|_{t=0} = T_{go} \quad (2.22)$$

Lower boundary condition:

$$\text{At } z = 0 \text{ for } t > 0, v_o T_{go} = v T_g \varepsilon - \frac{k_c}{\rho_g C_{Pg}} \frac{\partial T_g}{\partial z} \Big|_{z=0} \quad (2.23)$$

Upper boundary condition:

$$\text{At } z = L \text{ for } t > 0, \frac{\partial T_g}{\partial z} \Big|_{z=L} = 0 \quad (2.24)$$

Solid phase energy balance:

Initial condition:

$$\text{At } t = 0 \text{ for all } z, T_s = T_{so} \text{ i.e. } T_s|_{t=0} = T_{so} \quad (2.25)$$

2.3.3 Discretized Equations:

Fluid phase component mass balance:

$$c_z^{t+1} = [a - bv_o] c_{z+1}^t + [c] c_z^t + [a + bv_o] c_{z-1}^t - d(q_z^{t+1} - q_z^t)$$

$$\text{where, } a = \frac{D_a \Delta t}{\Delta z^2}, \quad b = \frac{\Delta t}{2\varepsilon \Delta z}, \quad \mathbf{M} = 1 - \frac{2\Delta t D_a}{\Delta z^2} \text{ and } d = \frac{\rho_b}{\varepsilon}$$

Fluid phase energy balance:

$$T_{g,z}^{t+1} = [f - gv_o] T_{g,z+1}^t + [h] T_{g,z}^t + [f + gv_o] T_{g,z-1}^t + k T_{s,z}^t + p$$

where,

$$f = \frac{k_c \Delta t}{\rho_g C_{pg} \Delta z^2}, \quad g = \frac{\Delta t}{2\varepsilon \Delta z}, \quad h = \left[1 - \frac{\Delta t h a_p (1 - \varepsilon)}{\rho_g C_{pg} \varepsilon} - \frac{2h_w}{R\varepsilon \rho_g C_{pg}} - \frac{2k_c \Delta t}{\rho_g C_{pg} \Delta z^2} \right],$$

$$k = \frac{\Delta t h a_p (1 - \varepsilon)}{\rho_g C_{pg} \varepsilon} \text{ and}$$

$$p = \frac{2h_w(T_w)}{R\varepsilon \rho_g C_{pg}}$$

Solid phase component mass balance:

$$q_z^{i+1} = q_z^i + k a_p \Delta t (q_z^{*i} - q_z^i)$$

Solid phase energy balance:

$$T_{s,z}^{i+1} = T_{s,z}^i + l (q_z^{*i} - q_z^i) - m (T_{s,z}^i - T_{g,z}^i)$$

$$\text{where, } l = \frac{\Delta t (-\Delta H) k a_p}{C_{ps}}, \quad m = \frac{h a_p \Delta t}{\rho_s C_{ps}}$$

Boundary conditions:

Fluid phase component mass balance:

Lower boundary:

$$c_z^i = c_o + \frac{D_a \varepsilon}{v_o} \frac{c_{z+1}^i - c_{z-1}^i}{2\Delta z}$$

Upper boundary:

$$c_{z+1} = c_{z-1}$$

Fluid phase energy balance:

Lower boundary:

$$T_{g,z}^i = T_{g0} + \frac{k_c \varepsilon}{\rho_g C_{pg} v_o} \frac{T_{g,z+1}^i - T_{g,z-1}^i}{2\Delta z}$$

Upper boundary:

$$T_{g,z+1} = T_{g,z-1}$$

The above model equations have been used for simulation in case of adsorption on E-merck 5A molecular sieve. In case of E-merck 13X molecular sieve, it has been observed that the above model equations with out the axial dispersion of heat and mass have satisfactorily described the experimental dynamic results. Hence, the following model equations have been used for discretization and thereafter simulation studies.

Component mass balance:

Fluid phase component mass balance:

$$\frac{\partial c}{\partial t} = -\frac{v_o}{\varepsilon} \frac{\partial c}{\partial z} - \frac{\rho_b}{\varepsilon} \frac{\partial q}{\partial t} \quad (2.26)$$

Solid phase component mass balance:

$$\frac{\partial q}{\partial t} = k (q^* - q) \quad (2.27)$$

Energy Balance:

Fluid phase energy balance

$$\frac{\partial T_g}{\partial t} = \frac{ha_p}{\rho_g C_{Pg}} \frac{(1-\varepsilon)}{\varepsilon} (T_s - T_g) - \frac{v_o}{\varepsilon} \frac{\partial T_g}{\partial z} - \frac{2h_w(T_g - T_w)}{R\varepsilon\rho_g C_{Pg}} \quad (2.28)$$

Solid phase energy balance:

$$\frac{\partial T_s}{\partial t} = \frac{(-\Delta H)}{C_{Ps}} \frac{\partial q}{\partial t} - \frac{ha_p}{\rho_s C_{Ps}} (T_s - T_g) \quad (2.29)$$

Initial and Boundary Conditions:

Fluid phase component mass balance:

Initial condition:

$$\text{At } t = 0 \text{ for all } z, c = 0 \text{ i.e. } c|_{t=0} = 0 \quad (2.30)$$

Lower boundary condition:

$$\text{At } z = 0 \text{ for } t > 0, c_o = c_{in} \quad (2.31)$$

Initial condition for solid phase component mass balance:

$$\text{At } t = 0 \text{ for all } z, q = 0 \text{ i.e. } q|_{t=0} = 0 \quad (2.32)$$

Fluid phase energy balance:

Initial condition:

$$\text{At } t = 0 \text{ for all } z, T_g = T_{go} \text{ i.e. } T_g|_{t=0} = T_{go} \quad (2.33)$$

Lower boundary condition:

$$\text{At } z = 0 \text{ for } t > 0, T_{go} = T_{gin} \quad (2.34)$$

Solid phase energy balance:

Initial condition:

$$\text{At } t = 0 \text{ for all } z, T_s = T_{so} \text{ i.e. } T_s|_{t=0} = T_{so} \quad (2.35)$$

2.4 Heat transfer Coefficient Between Fluid and Solid

From the analogy between heat and mass transfer between fluid and solid in fixed bed, the value of heat transfer coefficient can be computed from the equation below.

$$Nu = 2.0 + 1.1 \times Re_p^{0.6} Pr^{0.33} \text{ (Ruthven, 1984)} \quad (2.36)$$

2.5 Axial Dispersion Co-efficient

- * For gaseous flow in a packed bed, owing to larger magnitude of diffusion co-efficient in gas phase it is reasonable to expect axial dispersion co-efficient will be contributing factor for modelling mass transport at low Reynolds number. This can be expressed in terms of molecular diffusion co-efficient via a tortuosity factor, which accounts for the reduction in diffusivity because tortuosity flow paths, characteristic of the fixed bed.

Thus at very low flow rate (Butt, 1980)

$$D_a = \frac{D_m \varepsilon}{\tau_p} \quad (2.37)$$

at very large values of Reynolds number (Ruthven & Loughlin, 1971)

$$D_a = \frac{v_0 d_{pr}}{2\varepsilon} \quad (2.38)$$

Combining the low and high velocity contribution to D_a additively gives

$$D_a = \frac{D_m \varepsilon}{\tau_p} + \frac{v_0 d_{pr}}{2\varepsilon} \quad (2.39)$$

2.6 Numerical Solution:

Explicit method has been successfully utilized to approach towards the numerical solution of the model. In this explicit scheme, Forward difference for Time and Central difference for Space (FTCS) has been applied. The discretized equations hence march forward by means of point-by-point technique, wherein the changes in the concentration along column length and with passage of time are determined. Breakthrough curve formed for different concentrations helps to analyse the dynamic behaviour of the column. X-Y coordinate system is used to develop the model. Figure 2.2 represents the grid in which the X - direction corresponds to the space coordinate while the Y - direction to the time coordinate.

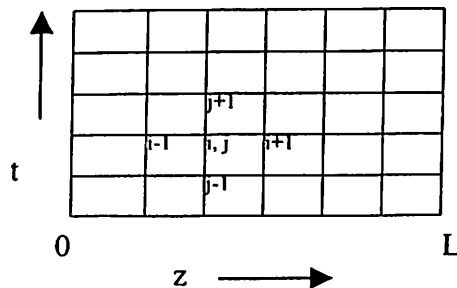


Figure 2.2: Coordinate system

CHAPTER III

EXPERIMENTAL

The emission control of volatile organic compounds (VOCs) by adsorption process has attracted special interest as a means of protecting the environment and human health from air pollution (Yun, et al.1998b). Ethyl acetate (EA), commonly used as a solvent in process industries, can be removed/recovered by adsorption process. As discussed earlier in chapter I, removal/recovery of ethyl acetate from air through adsorption using molecular sieves is yet to be reported in the literature. Even no equilibrium and kinetic studies for the same are reported so far.

To design adsorption facilities, data on adsorption equilibria are essential (Yang, 1987). For practical applications, adsorption equilibria must be known over a wide range of the operation temperature. Generated experimental data from equilibrium studies are used for determination of saturation capacity, isotherm model parameters, overall mass transfer coefficient and heat of adsorption

Dynamics studies are needed to understand the adsorber bed performances for the removal of ethyl acetate (EA) from the air stream; the effects of the geometric, physical, and operating parameters; mechanism of the process; relationship between temperature and concentration histories. Finally, the generated data from the experimental dynamic studies are used to validate the developed mathematical model, which in turn is used for detailed simulation studies.

This chapter deals with the experimental studies on equilibrium, kinetics and dynamics of ethyl acetate adsorption on pellets of E-merck 5A and 13X molecular sieves.

3.1 Isotherm Experiments

Adsorption isotherm of ethyl acetate, a toxic organic compound, has been studied for E-merck 5A at different temperatures 35°C, 40°C, 45°C and 55°C and for 13X molecular sieves at different temperatures 35°C, 45°C and 55°C. From the experimental data, overall mass transfer coefficient, isotherm model parameters and their temperature dependencies, saturation limit and heat of adsorption have been found out. The results obtained have been presented and discussed in detail in section 4.1.

3.1.1 Experimental setup and procedure

The adsorption isotherm setup, shown in Figure 3.1.1 was consisting of a borosilicate glass U-tube containing a known weight (approximately 1g) of preheated (at 300°C overnight and thereafter cooled) molecular sieve kept in constant temperature water bath. Compressed air from the compressor was passed through the air regulatory valve to supply air without fluctuations to the bottom of the pretreatment column, packed with glass wool, activated alumina, and silica gel. This column makes the air, sequentially, devoid of any dust particles, moisture content, and carbon dioxide content when it is passed through the column. Metered amount (through pre-calibrated rotameter) of pre-treated air was sent continuously into the U-tube after passing through saturators filled with ethyl acetate. To maintain a specific concentration the saturators were kept in constant temperature water bath. Temperature of the bath, level of ethyl acetate in saturation bottles and flow rate of air accounted for the variation of ethyl acetate concentration in the inlet stream. Knockout pot had been kept to avoid any entrainment of ethyl acetate droplets with air. Weight change of the U-tube containing molecular sieve was measured time-to-time using electronic metler balance

(accuracy 0.1mg). This was continued till the saturation limit. The concentration of ethyl acetate in air was measured before and after the experimental run by using gas chromatography. The average concentration was taken as inlet concentration. The changes in weight of U-tube were noted after regular time intervals. The experiment was continued till there was no change in weight of U-tube with molecular sieve i.e. till it reached into equilibrium. The experiments were performed for several concentration levels of ethyl acetate at four different temperatures 35°C, 40°C, 45°C and 55°C using 5A molecular sieve and at three different temperatures 35°C, 45°C and 55°C using 13X molecular sieve. The Photograph of experimental set up for equilibrium studies is shown in Figure 3.1.2.

3.2 Dynamic Studies - Experimental

For Dynamic studies, experiments were carried out in a semi-continuous mode to find out the adsorption behavior of ethyl acetate in molecular sieves E-merck 5A and E-merck13X. Adsorption was continued till the bed was fully saturated. After each run the sieves were taken out and heated overnight at 300 deg C for regeneration of saturated adsorbent. The variables studied were superficial velocity, inlet concentration of ethyl acetate, and bed length. The results obtained have been presented and discussed in detail in section 4.2.

3.2.1 Experimental Setup

The apparatus for the dynamic studies consists of a dehydration column, saturators, knockout pot(s), flow meter, packed-bed adsorption column, and a constant temperature water bath. Air regulatory valve ensured continuous supply of air from the compressor at constant pressure. A schematic diagram of the experimental set up is presented in Figure 3.2.1.

The fixed bed adsorber column was a S.S. pipe of ID 10 cm, thickness 0.2 cm and length 40 cm. The top and bottom of the column were connected with conical sections through flange

joints. A fine stainless steel screen was placed at the bottom of the column to support the solid adsorbent packing. The conical sections at the bottom and at the top of the column were provided with inlet and outlet connections respectively. Four thermocouple wells at equal spacing (6.0 cm) were provided on the wall of the column at different radial locations to measure the temperature of the packed bed column along its length. Two thermocouple probes were also provided at the bottom and at the top conical section to monitor the temperatures of inlet and outlet streams respectively. The conical section at the bottom of the column was packed with 0.3 cm Pyrex glass beads to achieve uniform distribution so as to avoid any possible entrance effects. Compressed and pretreated air was used as the carrier gas during adsorption step. Air, compressed in a two-stage compressor, was pretreated after passing through the dehydration column packed with glass wool, activated alumina and silica gel to remove dust particles, moisture, and carbon dioxide respectively from it. Flow rate of air containing ethyl acetate vapors was measured with pre-calibrated rotameter. Thermometer was used to measure the temperature of the water bath. Dial thermometers were used to measure the temperatures of different sections of the packed bed during adsorption. Metered amount of this air was bubbled through ethyl acetate kept in a series of saturators. To maintain a specific concentration the saturators were kept in constant temperature water bath. Temperature of the bath, level of ethyl acetate in saturation bottles and flow rate of air accounted for the variation of ethyl acetate concentration in the inlet stream. The knockout pot(s) were used to remove any possible entrainment of ethyl acetate droplets. Before performing adsorption experiment the adsorbent was heated to 300 °C overnight and then cooled to room temperature in glass desiccators. After each run the sieves were taken out and heated overnight at 300 deg C for regeneration and cooled to room temperature. The Photograph of experimental set up for dynamic studies is shown in Figure 3.2.2.

3.2.2 Experimental Procedure

Compressed air from the compressor was passed through the air regulatory valve to supply air without fluctuations to the bottom of the pretreatment column, packed with glass wool, activated alumina, and silica gel. This column makes the air, sequentially, devoid of any dust particles, moisture content, and carbon dioxide content when it is passed through the column. The pretreated air was then passed through saturators filled with ethyl acetate and then through knockout pot to avoid any possible entrainment. The saturators were kept in constant temperature water bath. The bath temperature was measured with thermometer. The metered amount (using precalibrated rotameter) of air and ethyl acetate mixture was then sent through adsorber column packed up to desired height, with regenerated molecular sieves. The inlet concentration of ethyl acetate vapor in air was measured several times, using gas chromatography at the start of the experiment and at the end of the experiment. The average concentration was taken as inlet concentration of ethyl acetate. The outlet concentration of ethyl acetate in air was measured at regular time interval, using gas chromatography. It was continued till outlet concentration was almost same as inlet concentration, indication of the bed saturation. Inlet and outlet temperatures were measured using thermometers kept in thermo wells, provided at bottom and top conical section of the adsorber column. The temperatures along the length of the column were measured at regular time interval using dial thermometers (precalibrated) kept in equally spaced (6.0 cm) thermo wells, provided on the wall of the column at different radial locations. After the bed was saturated, the flow of air and ethyl acetate mixture to column was stopped, and adsorbent were taken out for regeneration. The experiments were conducted for different inlet concentrations, flow rates and bed lengths. Concentration of EA has been varied by changing the ethyl acetate level in saturators, the temperature of water bath and by varying flow rates. The bed length was

varied by filling the column up to desired height. The details about the different experimental conditions are given in Tables 4.2.1.1 to 4.2.1.3 in section 4.2.

3.3 Materials

The adsorbents used were type 5A molecular sieve (E-Merck, (1/16)" cylindrical pellets) and 13X molecular sieve (E-Merck, (1/16)"cylindrical pellets). The adsorbate used was ethyl acetate vapor. Ethyl acetate (99% extra pure) was used to produce ethyl acetate vapor was manufactured by Sisco Chem Industries, Mumbai. Compressed air was used as a carrier gas.

3.4 Analytical Technique

The concentration of ethyl acetate vapor in the inlet stream was measured with the help of Gas Chromatography (GC) with AT 1000 column and Flame Ionization Detector (FID). The AT 1000 column used was made up of stainless steel material. The column was of 1.83 m length with outer and inner diameter as 3.175 mm and 2 mm respectively.

The temperature of oven was maintained at 80°C. The detector and column temperature was maintained at 120°C. Nitrogen gas was used as inert and hydrogen gas was used as fuel with air. Nitrogen and hydrogen flow rates were maintained at 30 ml/min. Air flow rate was maintained at 400 ml/min.

The gas calibration was done by taking known volume of (vapor + air) mixture in the micro syringe (Hamilton made, 500 µl capacity) collected from just above the surface of liquid ethyl acetate from ethyl acetate bottle and diluting it for different concentrations. Using Raoult's Law the concentration was found out for the collected sample. Antoine equation was used to find the vapor pressures of ethyl acetate at operating temperatures. For the known concentrations of ethyl acetate, standard areas were obtained and compared with areas

obtained for column outlet samples. The standard area peak, sample area peak and the detail procedure to determine the ethyl acetate vapor concentration in the air stream have been presented in Appendix I. The Photograph of gas chromatography is shown in Figure 3.4.1

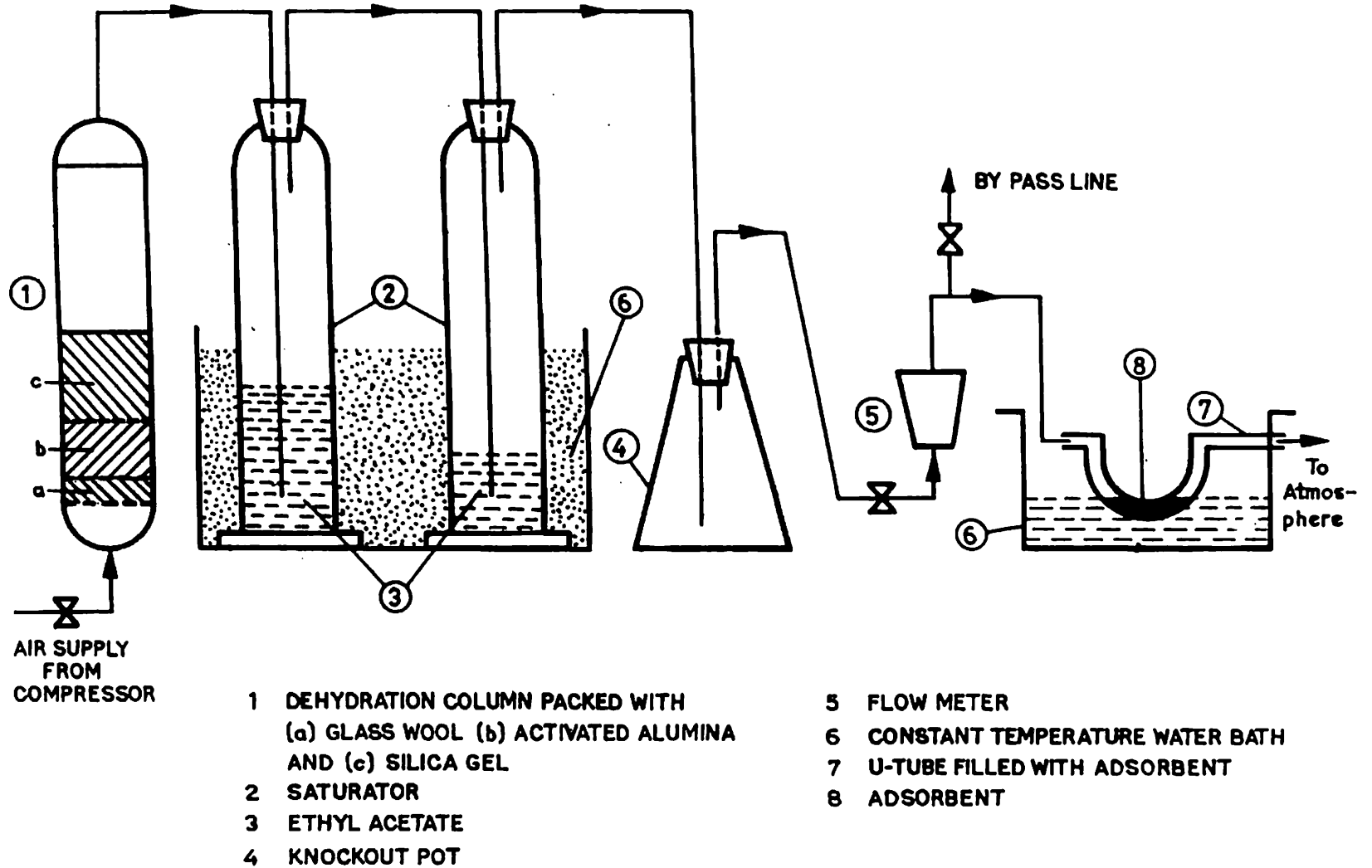


FIGURE 3.1.1 EXPERIMENTAL SET-UP FOR EQUILIBRIUM STUDIES



Figure 3.1.2 Photograph of experimental setup for equilibrium studies

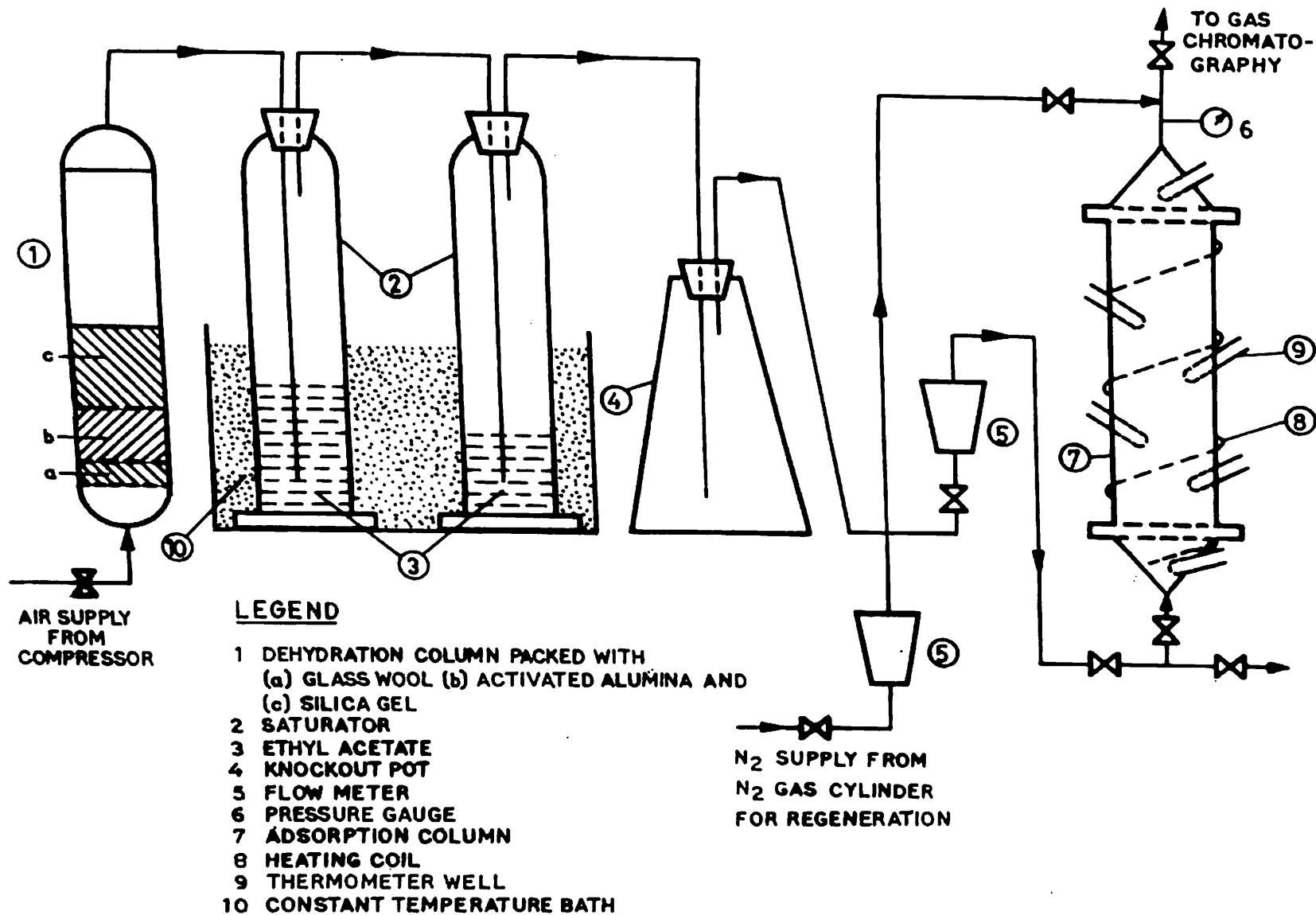


FIGURE 3.2.1 EXPERIMENTAL SET-UP FOR DYNAMIC STUDIES

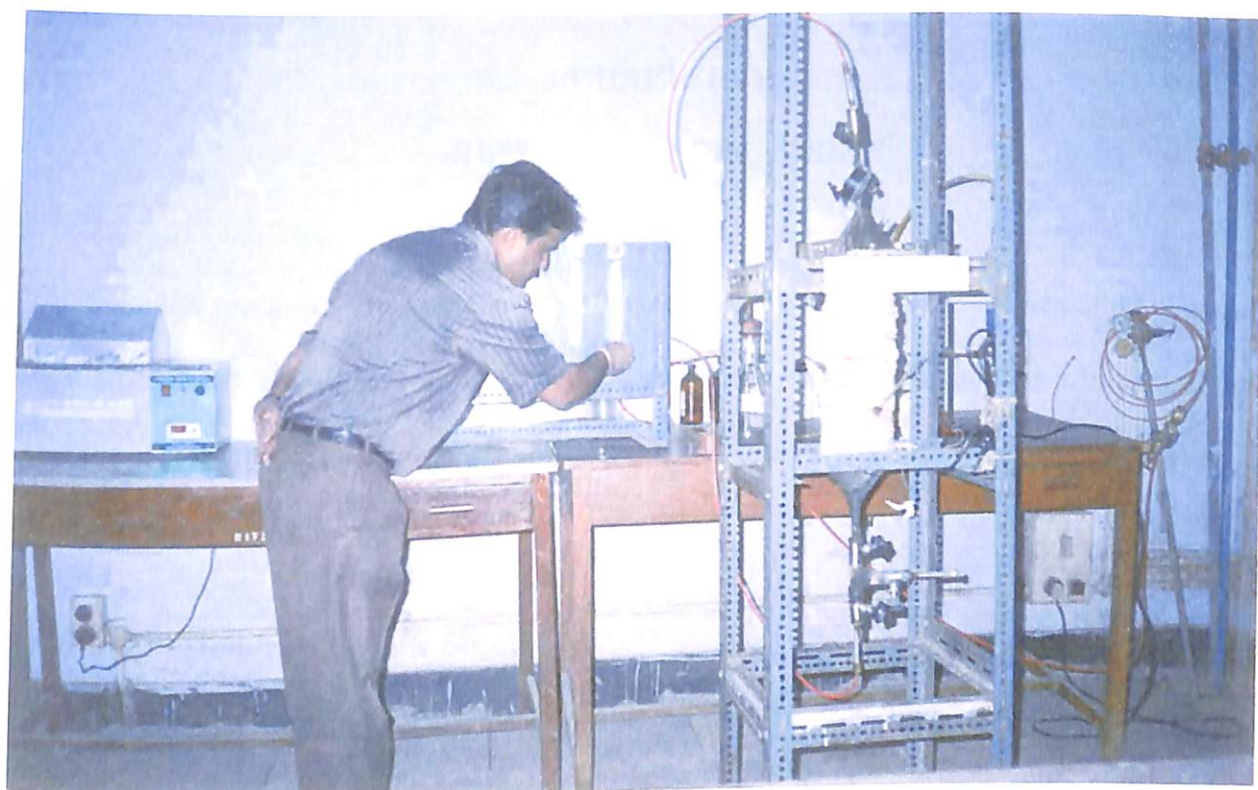


Figure 3.2.2 Photograph of experimental setup for dynamic studies

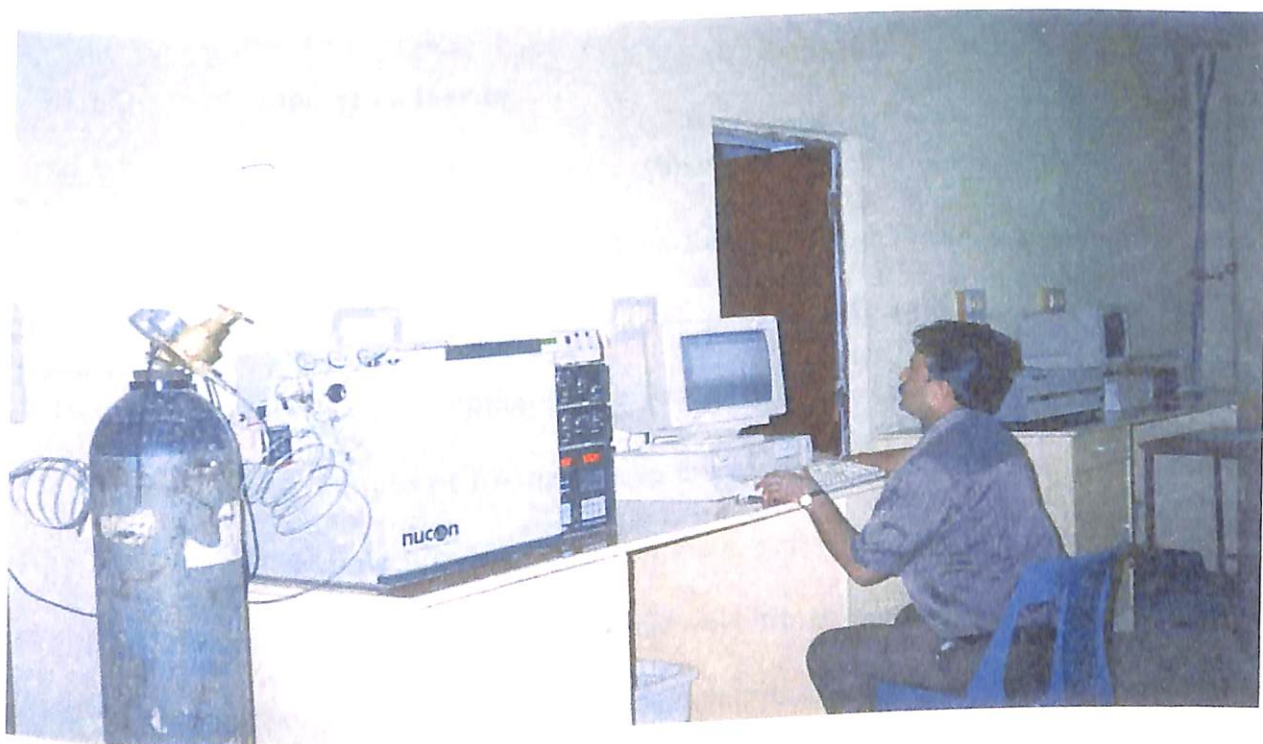


Figure 3.4.1 Photograph of gas chromatography

CHAPTER IV

RESULTS AND DISCUSSION

This chapter discusses the results on equilibrium, kinetic and dynamic studies of ethyl acetate (EA) adsorption on E-merck 5A and 13X molecular sieves. Results on equilibrium and kinetic studies are discussed in section 4.1 and results on dynamic studies are discussed in section 4.2.

4.1 Equilibrium and Kinetic Studies

Results on equilibrium and kinetic studies are discussed in following subsections in terms of: determination of isotherms, suitability of the different isotherm models with the experimental data, determination of model parameters, determination of Mass Transfer Coefficient, and determination of heat of adsorption.

4.1.1 Determination of Isotherms

The adsorption isotherm of ethyl acetate vapor has been determined at four different temperatures 35°C, 40°C, 45°C and 55°C in E-merck 5A molecular sieve and at three different temperatures 35°C, 45°C and 55°C in E-merck 13X molecular sieve. The experimental equilibrium adsorption capacities of the two molecular sieves for EA at different inlet concentrations of EA have been presented in Tables 4.1.1 to 4.1.7. Isotherm plots for a particular molecular sieve at a particular temperature have been obtained after plotting equilibrium adsorption capacities of the sieve for EA versus concentration of EA in air at the same temperature. Four experimentally determined isotherms in 5A molecular sieve at temperatures 35°C, 40°C, 45°C and 55°C have been presented in Figure 4.1.1. Similarly, three isotherms in 13X molecular sieve have been obtained at three different temperatures of experiment 35°C, 45°C and 55°C and presented in Figure 4.1.2. It is obvious from these

figures that the isotherms are typically of Brunauer Type – I. Again, temperature dependence of the adsorption capacities, as evident from the figures of both the molecular sieves, shows that at higher temperature the equilibrium capacity is less. Further the difference in capacities at two different temperatures goes on increasing with increase in concentration and reaches a constant value at higher concentration level of EA. This may be attributed to the fact of non-linear temperature dependence of equilibrium adsorption capacity.

Figures 4.1.3 to 4.1.5 represent the comparison for equilibrium capacities between 5A and 13X molecular sieves at temperatures 35°C, 45°C and 55°C respectively. It can be observed from the figures that capacity of ethyl acetate in 13X molecular sieve is higher than 5A molecular sieve at all concentrations and at all temperatures. This may be attributed to the fact that the comparable pore size of 5A molecular sieve with the molecular diameter of EA provides steric hindrance to the movement of the chain of EA into pores of 5A leading to lesser adsorption capacity. The same phenomenon is not true for 13X. The pore size in 13X is comparatively larger, allowing more layers of EA adsorption onto 13X as compared to 5A.

4.1.2 Suitability of the Different Isotherm Models with the Experimental Data

As discussed earlier in section 2.1, numbers of equilibrium isotherm models can be utilized for correlating experimental equilibrium results. In the present study, three isotherm models, namely, Langmuir, Freundlich and Langmuir-Freundlich have been used to fit in the experimental equilibrium data of ethyl acetate in 5A and 13X molecular sieves and to investigate the suitability of the isotherm models for the adsorbate-adsorbent system of study. From the fitting of the experimental equilibrium data with different isotherm models, model parameters such as Freundlich constant K , Langmuir constant b , saturation capacity q_s and Freundlich and Langmuir-Freundlich exponent n have been obtained.

In case of Freundlich model, the plot of $\ln(q)$ versus $\ln(c)$ provides the slope as n and intercept as K . Similarly, for Langmuir model, the plot of $1/(q \cdot c)$ versus $1/c$ provides the slope as $1/(bq_s)$ and intercept as $1/q_s$ and in case of Langmuir-Freundlich model, the plot of $\ln(1/(q_s/q) - 1)$ versus $\ln(c)$ provides the slope as n and intercept as $\ln(b)$. The sample plots on the fitting of experimental equilibrium data at 45°C to Freundlich, Langmuir and Langmuir-Freundlich models have been shown in Figures 4.1.6, 4.1.7 and 4.1.8 respectively.

After determination of the model parameters, different models' predictions have been compared with the experimental equilibrium data. Figures 4.1.9 to 4.1.12 show the comparison of different models' (Freundlich, Langmuir and Langmuir-Freundlich) predictions with the experimental data for ethyl acetate adsorption on E-merck 5A molecular sieve at four different temperatures 35°C, 40°C, 45°C and 55°C respectively. Similarly, Figures 4.1.13 to 4.1.15 represent the comparisons of different models' predictions with the experimental equilibrium data for ethyl acetate adsorption on 13X molecular sieve at three different temperatures 35°C, 45°C and 55°C respectively. From the figures above for both the sieves, it may be observed that Freundlich model shows large deviations from the experimental data whereas, Langmuir and Langmuir-Freundlich models show good agreement with the experimental results. Of the last two models, Langmuir model better represents the experimentally generated adsorption equilibrium data for both the sieves at all different temperatures.

The quantitative suitability of the models has also been tested after calculating the standard deviations of the models' predictions from the experimental data. The detailed statistical analysis in the form of standard deviation (STDEV), and coefficient of determination (R^2) for both the sieves 5A and 13X have been presented in Tables 4.1.8 and 4.1.9 respectively. The statistical analysis also shows that standard deviation is the least in case of Langmuir model,

lower in case of Langmuir-Freundlich model and much higher in case of Freundlich model for both the sieves at all different temperatures.

Therefore, it may be concluded from the above observations that either of Langmuir and Langmuir-Freundlich isotherm models satisfactorily explains the equilibrium adsorption behaviour of EA in E-merck 5A and 13X molecular sieves. Of the three models taken for the present study, the Langmuir model is the best suited one and Freundlich model is not acceptable for ethyl acetate adsorption from air in molecular sieves E-merck 5A and 13X within the range of the experimental conditions.

4.1.3 Determination of Model Parameters

The model parameters have been determined using the plots as mentioned in section 4.1.2. The estimated parameters for different models have been reported in Tables 4.1.10 and 4.1.11. The tables indicate that the saturation capacity decreases with increase in temperature for both 5A and 13X molecular sieves for all the three models. It has also been observed from the Tables 4.1.10 and 4.1.11 that the Freundlich constant, K and the Langmuir constant, b decrease with increase in temperature for both 5A and 13X molecular sieves. The decrease in values of K and b with increase in temperature implies the exothermicity of the adsorption process and the decrease of q_s with increase in temperature implies the decrease in saturation adsorption capacity at higher temperature establishing the fact that higher temperatures don't favour adsorption. The corresponding heat of adsorption values have been evaluated and discussed later in section 4.1.5.

4.1.4 Determination of Mass Transfer Coefficient

As has already been discussed in Chapter II, the experimental data of equilibrium isotherm studies have been utilised to determine the overall mass transfer coefficients, k of EA-E-

merck 5A and EA-E-merck 13X systems using Uptake curve method and Linear Driving Force (LDF) rate expression. The following two subsections discuss on the k values and compare the same determined by the above two methods.

4.1.4.1 Mass Transfer Coefficient Determination Using the Uptake Curve Method

As discussed in section 2.2.1.1, the overall mass transfer coefficient can be obtained from the

equation: $k = 15 \frac{D_c}{r_c^2}$, where the diffusional time constant $\frac{D_c}{r_c^2}$ can be found from the slope of

the plot of $\ln\left(1 - \frac{q}{q^*}\right)$ versus t.

Figures 4.1.16 and 4.1.17 are the sample plots for the determination of mass transfer coefficient using uptake rates for ethyl acetate in E-merck 5A and 13X molecular sieves respectively.

The values of the overall mass transfer coefficient found from uptake curve method (k_{uptake}) have been reported in Tables 4.1.1 to 4.1.4 for E-merck 5A and Tables 4.1.5 to 4.1.7 for E-merck 13X molecular sieves for different temperatures of study. It has been observed from the above tables that the values of k_{uptake} are of the order of 10^{-4} s^{-1} and lie mostly in the range of $(1.0 - 2.0) \times 10^{-4} \text{ s}^{-1}$ for both the molecular sieves. There have been a few cases when k_{uptake} is slightly less than $1.0 \times 10^{-4} \text{ s}^{-1}$ or slightly above $2.0 \times 10^{-4} \text{ s}^{-1}$. This may be due to associated experimental error while collecting the data required for evaluation of k_{uptake} . The k_{uptake} values determined for all the different operating conditions for both the sieves (Tables 4.1.1 – 4.1.7) don't show any distinct effect of flow rate on overall mass transfer coefficient. This indicates the insignificant external film resistance for mass transfer within the range of flow rates studied. It has also been clear from the tables that there is no distinct effect of

temperature on the overall mass transfer coefficient, k_{uptake} in the range of the temperature studied in the present investigation.

So from the values of overall mass transfer coefficient, k obtained by Uptake curve method it may be concluded that k_{uptake} is independent of temperature, concentration and flow rate in the range of experimental conditions in the present study. Further, independence of k_{uptake} on the flow rate apparently leads to the conclusion that pore diffusion is predominant for the present systems of study.

4.1.4.2 Mass Transfer Coefficient Determination Using the LDF Rate Expression

Though Uptake curve method (Ruthven, 1984) has been the established method to estimate the overall mass transfer coefficient for adsorption, an attempt has been made in this study to evaluate the same using Linear Driving Force (LDF) rate expression and then to compare the values with those obtained by Uptake curve method.

As discussed in section 2.2.1.2, the diffusion-controlled kinetics may be satisfactorily represented by the following LDF expression (Yang 1987).

$$\frac{\partial q}{\partial t} = k(q^* - q)$$

The LDF rate equation can be rearranged to $\frac{dq}{dt} = k(q^* - q)$ as $q = f(t)$ only

Then the plot of $\frac{dq}{dt}$ versus q provides a straight line with its slope as $(-k)$ and intercept as kq^* . In the present investigation, q has been taken as average of the q values between two time intervals. This has been calculated by noting the changes in weight of the U-tube containing molecular sieves with time, as already explained in section 3.1.1. Similarly, the rate of change of adsorption capacity $\frac{dq}{dt}$ has been taken as rate of change of average

adsorption capacity and calculated by dividing the difference in average adsorption capacities between two time intervals with the time interval.

Values of overall mass transfer coefficient (k_{LDF}) obtained by LDF rate expressions in E-merck 5A molecular sieves at four different temperatures 35°C, 40°C, 45°C and 55°C have been presented in Tables 4.1.1 to 4.1.4 respectively. Also a sample plot for the determination of k_{LDF} in E-merck 5A has been shown through Figure 4.1.18. It may be observed from the above tables that in some cases k_{LDF} values are in the order of 10^{-4} s^{-1} and are closer to the values of k_{uptake} . However majority of the k_{LDF} values for all the temperatures are in the order of 10^{-5} s^{-1} . The tables also show wide variations in some cases questioning the reliability of the method for calculation of overall mass transfer coefficient. But a close look into the tables further suggests that most of the values lie in the range of $(4.5 - 6.5) \times 10^{-5} \text{ s}^{-1}$, which are slightly lower than those obtained by Uptake method. Very frequent time intervals to collect the data would have improved the slope of the fitting curves thereby increasing the values of overall mass transfer coefficient. Widely scattered values in a few cases may be due to experimental errors. However, like the k_{uptake} values, the k_{LDF} values determined for all the different operating conditions in E-merck 5A molecular sieve (Tables 4.1.1 – 4.1.4) do not show any distinct effect of flow rate, temperature and concentration of EA on the mass transfer coefficient. This fact, thus, corroborates the conclusion of insignificant effect of external film diffusion and significant controlling role of pore diffusion. These observations also possibly allow us to conclude that, with a suitably designed data collection and analysis technique, LDF method may be an alternative method for determination of overall mass transfer coefficient in case of an adsorbate-adsorbent system.

In case of E-merck 13X molecular sieve, Tables 4.1.5 and 4.1.6 for temperatures 35°C and 45°C respectively indicate the k_{LDF} values mostly lying in the range of $(4.5 - 8.0) \times 10^{-5} \text{ s}^{-1}$, which is slightly lower than the values by uptake method, whereas for temperature 55°C the k_{LDF} values are of the order of 10^{-4} s^{-1} and lie in the range of $(1.0 - 2.0) \times 10^{-4} \text{ s}^{-1}$ (Table 4.1.7) i.e. higher than the k_{LDF} values in E-merck 13X molecular sieve at other temperatures of study. Like uptake curve method, the mass transfer coefficients obtained by LDF method do not indicate any distinct effect of flow rate and concentration of EA on them. Slightly higher k_{LDF} values at temperatures 35°C, 45°C and 55°C in 13X molecular sieve in comparison to 5A molecular sieve may be attributed to the fact that bigger pore size in 13X puts less resistance for the diffusive movement of EA. This is not the case in 5A as comparative pore size with the molecular diameter of EA restricts its movement in the pore resulting in lower k_{LDF} values. A sample plot for the determination of k_{LDF} in E-merck 13X has been shown through Figure 4.1.19.

Again, the k_{LDF} values obtained at different temperatures for 13X molecular sieve (Tables 4.1.5 to 4.1.7) reflect slight increase in mass transfer coefficient with increase in temperature, which is not the case for 5A molecular sieve. The difference in observation in the sieves may be explained as follows.

Comparable pore size in 5A with molecular size of EA may be playing a crucial role in diffusion as illustrated earlier so that in spite of increase in temperature the mass transfer coefficient might not have been influenced significantly. But relatively much higher pore size in 13X may help enhancing the diffusive movements of EA in the pores at higher temperatures. However, the above observations have not been found in Uptake curve method, which may be due to the principle of the method itself where the data for the calculations have been collected after 70% percent saturation. At that condition, due to

decreased freedom of movement of EA slight increase in temperature (as in the present investigation) may not significantly influence the diffusivity of EA in the pore.

Further observations on the k_{LDF} values suggest that except at 55°C in 13X, in all other conditions k_{LDF} is slightly lower than k_{uptake} . This difference may possibly be eliminated after taking experimental readings at very frequent time intervals, which could not be followed always in the present investigation due to some practical limitations.

4.1.5 Determination of Heat of Adsorption

Heat of adsorption values of EA in molecular sieves E-merck 5A and 13X have been calculated from the Langmuir constant (b) values (Tables 4.1.10 and 4.1.11) using equation-2.3 and making a plot of $\ln b$ versus $1/T$, which provides the slope as $-\Delta H/R_u$ and intercept as $\ln b_0$. Figure 4.1.20 and 4.1.21 shows the sample plot for determination of heat of adsorption of ethyl acetate in E-merck 5A and 13X molecular sieves in case of Langmuir model respectively. The values of the heat of adsorption of ethyl acetate vapor in 5A and 13X molecular sieves and the pre-exponential constants have been reported in Table 4.1.12 for both Langmuir and Langmuir –Freundlich models. Table 4.1.12 reflects that heat of adsorption values in both the sieves are of the order of 10^5 J/kg.

4.1.6 Conclusions on the Equilibrium and Kinetic Studies

The following conclusions may be made based on the results on equilibrium and kinetic studies of ethyl acetate adsorption in E-merck 5A and 13X molecular sieves.

- Isotherms are typically of Brunauer Type – I with non-linear temperature dependency of equilibrium adsorption capacities and either of Langmuir and Langmuir-Freundlich isotherm models satisfactorily explains the equilibrium adsorption behaviour of EA in

both molecular sieves. Langmuir model is the best suited one and Freundlich model is not acceptable for the present system of study.

- Equilibrium adsorption capacity of ethyl acetate in 13X molecular sieves is higher than 5A molecular sieves at all concentrations and temperatures of study.
- Insignificant effect of flow rate on overall mass transfer coefficient determined by both the Uptake and LDF methods is indicative of insignificant effect of external film diffusion and a significant controlling role of pore diffusion. Also no significant effect of concentration of EA on mass transfer coefficient has been observed.
- Mass transfer coefficient (k_{uptake}) obtained by Uptake method is of the order of 10^{-4} s^{-1} and lies in the range of $(1.0 - 2.0) \times 10^{-4} \text{ s}^{-1}$ for both the molecular sieves and has been independent of temperature in the range of the temperature studied in the present investigation.
- Mass transfer coefficient obtained by LDF method has shown different values for different sieves of study. In general, LDF method shows slightly lower values for overall mass transfer coefficient in comparison to Uptake method. Though the LDF method looks not to give consistent output, still this method can be an alternative to Uptake method if provided with properly designed data collection and analysis unit. In 5A molecular sieves, except a few cases, most of the k_{LDF} values lie in the range of $(4.5 - 6.5) \times 10^{-5} \text{ s}^{-1}$ and are independent of temperature. In 13X molecular sieves, slight increase in k_{LDF} values with increase in temperatures has been observed.
- Heat of adsorption values in both the sieves are of the order of 10^5 J/kg .

Table 4.1.1: Equilibrium capacities and mass transfer coefficients for ethyl acetate in E-merck 5A molecular sieve at 35 °C

Sr. No.	Run No.	Flow rate $Q \times 10^6$ (m^3/s)	c , (kg/m^3)	q , (kg/kg)	$k_{LDF} \times 10^5$ (s^{-1})	R^2	$k_{uptake} \times 10^4$ (s^{-1})	R^2
1	IS15	1.49	0.027	0.181	10.17	0.92	1.27	0.95
2	IS16	0.975	0.047	0.24	3.66	0.96	0.84	0.98
3	IS17	0.86	0.073	0.27	6.5	0.88	1.165	0.92
4	IS19	4.0	0.12	0.29	10.67	0.96	1.19	0.93
5	IS12	4.0	0.27	0.33	5.0	0.93	0.91	0.98
6	IS21	4.34	0.43	0.352	5.83	0.94	1.32	0.999
7	IS18	7.0	0.56	0.363	5.66	0.91	1.32	0.93
8	IS20	6.5	0.60	0.366	5.8	0.96	1.34	0.963

Table 4.1.2: Equilibrium capacities and mass transfer coefficients for ethyl acetate in E-merck 5A molecular sieve at 40 °C

Sr. No.	Run No.	Flow rate $Q \times 10^6$ (m^3/s)	c (kg/m^3)	q (kg/kg)	$k_{LDF} \times 10^5$ (s^{-1})	R^2	$k_{uptake} \times 10^4$ (s^{-1})	R^2
1	IS30	1.49	0.027	0.157	13.0	0.95	0.94	0.97
2	IS25	0.975	0.047	0.21	14.2	0.95	2.18	0.92
3	IS23	0.86	0.073	0.24	4.0	0.97	2.3	0.94
4	IS28	4.0	0.12	0.267	2.66	0.99	1.59	0.91
5	IS27	4.0	0.27	0.32	6.0	0.93	0.94	0.95
6	IS29	4.34	0.43	0.34	9.0	0.99	2.02	0.99
7	IS24	7.0	0.56	0.35	10.16	0.995	1.54	0.96
8	IS26	6.5	0.60	0.354	3.5	0.98	-	-

Table 4.1.3: Equilibrium capacities and mass transfer coefficients for ethyl acetate in E-merck 5A molecular sieve at 45 °C

Sr. No.	Run No.	Flow rate $Q \times 10^6$ (m^3/s)	c (kg/m^3)	q (kg/kg)	$k_{LDF} \times 10^5$ (s^{-1})	R^2	$k_{uptake} \times 10^4$ (s^{-1})	R^2
1	IS35	1.49	0.027	0.121	1.83	0.95	1.82	0.92
2	IS36	0.975	0.047	0.18	6.17	0.99	1.47	0.986
3	IS37	0.86	0.073	0.21	6.5	0.96	1.46	0.94
4	IS40	4.0	0.12	0.24	3.83	0.98	1.52	0.975
5	IS43	4.0	0.27	0.291	5.17	0.92	1.16	0.94
6	IS38	4.34	0.43	0.324	8.66	0.95	1.62	0.93
7	IS39	7.0	0.56	0.343	12.5	0.93	1.44	0.93
8	IS44	6.5	0.60	0.345	6.46	0.94	1.19	0.90

Table 4.1.4: Equilibrium capacities and mass transfer coefficients for ethyl acetate in E-merck 5A molecular sieve at 55 °C

Sr. No.	Run No.	Flow rate $Q \times 10^6$ (m^3/s)	c (kg/m^3)	q (kg/kg)	$k_{LDF} \times 10^5$ (s^{-1})	R^2	$k_{uptake} \times 10^4$ (s^{-1})	R^2
1	IS45	1.49	0.027	0.101	10.66	0.91	2.38	0.94
2	IS46	0.975	0.047	0.155	8.33	0.90	1.67	0.977
3	IS47	0.86	0.073	0.19	9.2	0.92	2.07	0.974
4	IS48	4.0	0.12	0.22	5.8	0.91	1.04	0.94
5	IS49	4.0	0.27	0.265	5.33	0.94	1.34	0.95
6	IS50	4.34	0.43	0.285	5.33	0.97	2.1	0.98
7	IS51	7.0	0.56	0.288	8.33	0.94	1.10	0.99
8	IS52	6.5	0.60	0.291	4.66	0.96	1.47	0.965

Table 4.1.5: Equilibrium capacities and mass transfer coefficients for ethyl acetate in E-merck 13X molecular sieve at 35 °C

Sr. No.	Run No.	Flow rate $Q \times 10^6$ (m^3/s)	c (kg/m^3)	q (kg/kg)	$k_{LDF} \times 10^5$ (s^{-1})	R^2	$k_{uptake} \times 10^4$ (s^{-1})	R^2
1	IS59	1.49	0.027	0.238	7.66	0.98	1.47	0.99
2	IS65	0.975	0.047	0.294	11.5	0.97	1.19	0.99
3	IS66	0.86	0.073	0.345	8.83	0.994	1.30	0.988
4	IS57	4.0	0.12	0.416	4.83	0.996	0.81	0.98
5	IS64	4.0	0.27	0.508	4.5	0.93	1.1	0.98
6	IS61	4.34	0.43	0.55	7.16	0.997	1.69	0.985
7	IS60	7.0	0.56	0.583	3.0	0.93	1.11	0.98
8	IS53	6.5	0.60	0.584	6.0	0.97	1.24	0.91

Table 4.1.6: Equilibrium capacities and mass transfer coefficients for ethyl acetate in E-merck 13X molecular sieve at 45 °C

Sr. No.	Run No.	Flow rate $Q \times 10^6$ (m^3/s)	c (kg/m^3)	q (kg/kg)	$k_{LDF} \times 10^5$ (s^{-1})	R^2	$k_{uptake} \times 10^4$ (s^{-1})	R^2
1	IS67	1.49	0.027	0.17	7.0	0.97	1.19	0.983
2	IS72	0.975	0.047	0.251	4.5	0.94	1.32	0.89
3	IS76	0.86	0.073	0.285	17.8	0.90	1.13	0.97
4	IS71	4.0	0.12	0.336	7.3	0.93	1.24	0.97
5	IS74	4.0	0.27	0.387	7.8	0.97	1.06	0.998
6	IS69	4.34	0.43	0.415	7.16	0.95	1.00	0.99
7	IS73	7.0	0.56	0.435	7.33	0.97	1.62	0.99
8	IS79	6.5	0.60	0.44	15.0	0.89	2.25	0.996

Table 4.1.7: Equilibrium capacities and mass transfer coefficients for ethyl acetate in E-merck 13X molecular sieve at 55 °C

Sr. No.	Run No.	Flow rate $Q \times 10^6$ (m^3/s)	c (kg/m^3)	q (kg/kg)	$k_{LDF} \times 10^5$ (s^{-1})	R^2	$k_{uptake} \times 10^4$ (s^{-1})	R^2
1	IS91	1.49	0.027	0.135	14.6	0.89	1.90	0.999
2	IS80	0.975	0.047	0.218	13.33	0.99	-	-
3	IS82	0.86	0.073	0.274	23.5	0.92	0.68	0.96
4	IS88	4.0	0.12	0.324	13.8	0.90	1.52	0.91
5	IS89	4.0	0.27	0.35	11.8	0.91	0.76	0.975
6	IS87	4.34	0.43	0.36	13.0	0.93	2.12	0.932
7	IS84	7.0	0.56	0.376	4.17	0.95	1.64	0.91
8	IS90	6.5	0.60	0.377	12.33	0.921	0.89	0.98

Table 4.1.8: Statistical analysis of fitting of experimental isotherm data to different isotherm models for ethyl acetate adsorption in E-merck 5A molecular sieve

Model	35°C		40°C		45°C		55°C	
	STDEV	R^2	STDEV	R^2	STDEV	R^2	STDEV	R^2
Freundlich	0.0087	0.984	0.0091	0.983	0.0083	0.984	0.0113	0.962
Langmuir	0.0037	0.997	0.0047	0.996	0.0034	0.994	0.003	0.997
Langmuir - Freundlich	0.0044	0.995	0.0081	0.985	0.0037	0.997	0.0036	0.995

Table 4.1.9: Statistical analysis of fitting of experimental isotherm data to different isotherm models for ethyl acetate adsorption in E-merck 13X molecular sieve

Model	35°C		45°C		55°C	
	STDEV	R ²	STDEV	R ²	STDEV	R ²
Freundlich	0.0202	0.964	0.014	0.9744	0.020	0.932
Langmuir	0.010	0.991	0.00243	0.9988	0.012	0.9822
Langmuir -Freundlich	0.018	0.973	0.003724	0.997	0.015	0.9795

Table 4.1.10: Isotherm parameters for ethyl acetate adsorption in E-merck 5A molecular sieve

Sr. No.	Temperature, °C	Freundlich		Langmuir		Langmuir- Freundlich		
		K	n	q _s , kg/kg	b, m ³ /kg	q _s , kg/kg	b, m ³ /kg	n
1	35	0.423	0.20	0.372	35.70	0.372	58.58	1.19
2	40	0.421	0.24	0.370	25.65	0.370	50.10	1.53
2	45	0.42	0.30	0.364	18.87	0.364	22.86	1.08
3	55	0.37	0.30	0.326	17.50	0.326	13.57	0.90

Table 4.1.11: Isotherm parameters for ethyl acetate adsorption in E-merck 13X molecular sieve

Sr. No.	Temperature, °C	Freundlich		Langmuir		Langmuir- Freundlich		
		K	n	q _s , kg/kg	b, m ³ /kg	q _s , kg/kg	b, m ³ /kg	n
1	35	0.704	0.283	0.587	23.65	0.587	131.64	1.64
2	45	0.531	0.267	0.467	21.87	0.467	20.9	0.99
3	55	0.473	0.272	0.440	17.79	0.440	9.62	0.76

Table 4.1.12: Heat of adsorption values of ethyl acetate adsorption in E-merck 5A and 13X molecular sieves evaluated based on Langmuir and Langmuir – Freundlich models

Sr No.	Model	5A		13X	
		-ΔH, J/kg x 10 ⁻⁵	b ₀ , m ³ /kg	-ΔH, J/kg x 10 ⁻⁵	b ₀ , m ³ /kg
1	Langmuir	3.37	3.0 * 10 ⁻⁴	1.30	2.69 * 10 ⁻¹
2	Langmuir-Freundlich	7.39	5.6 * 10 ⁻¹⁰	12.5	2.42 * 10 ⁻¹⁷

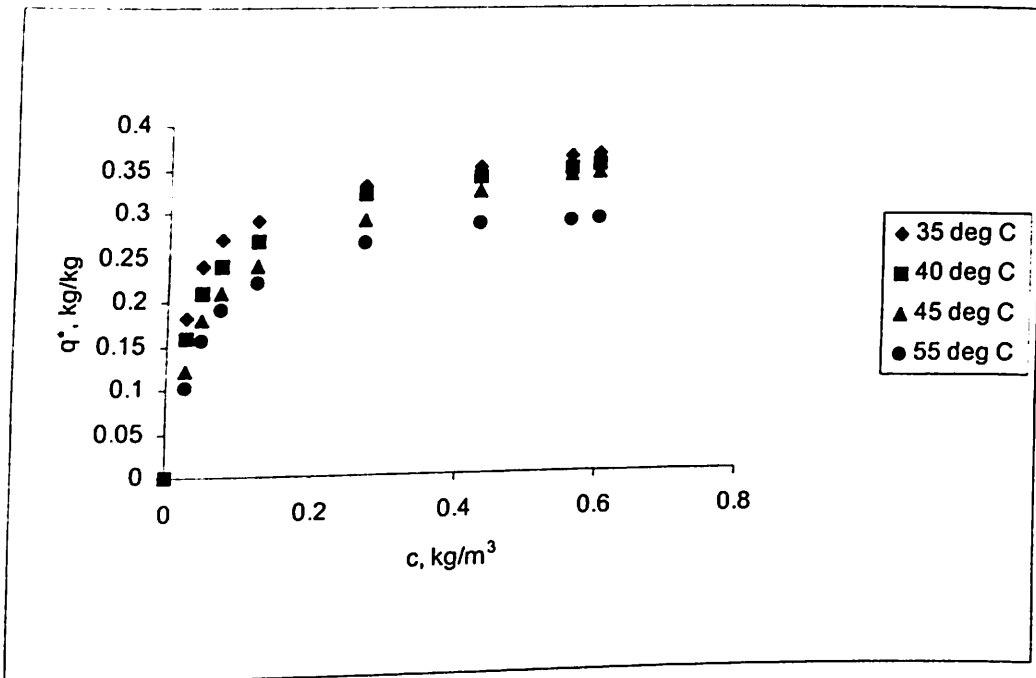


Figure 4.1.1: Ethyl acetate adsorption isotherms at different temperatures in E-merck 5A molecular sieve

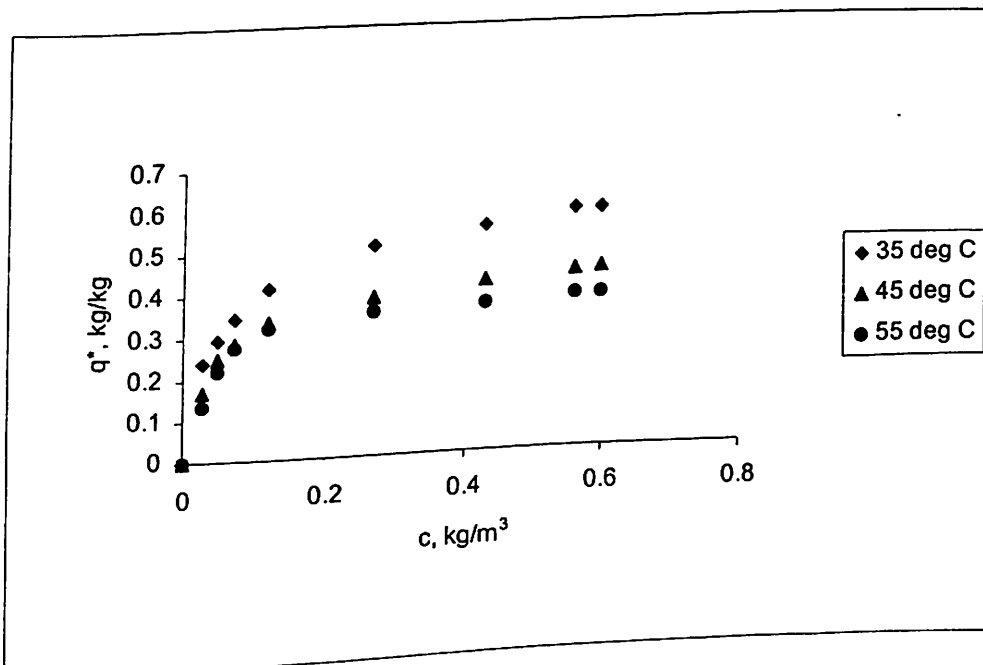


Figure 4.1.2: Ethyl acetate adsorption isotherms at different temperatures in E-merck 13X molecular sieve

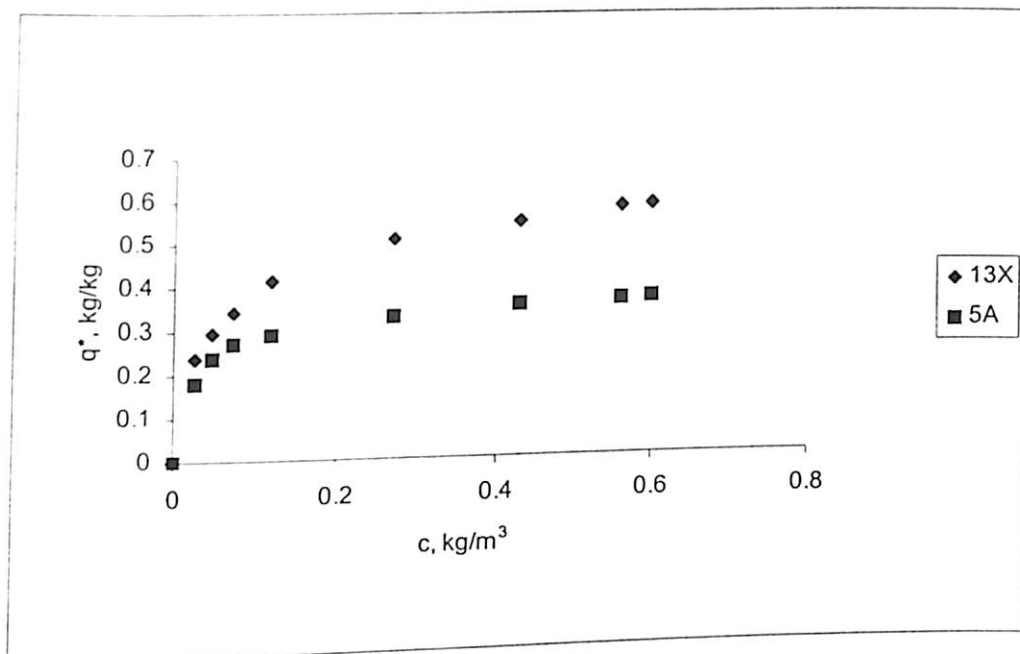


Figure 4.1.3: Comparison of equilibrium capacities of ethyl acetate in E-merck 5A and 13X molecular sieves at 35 deg C

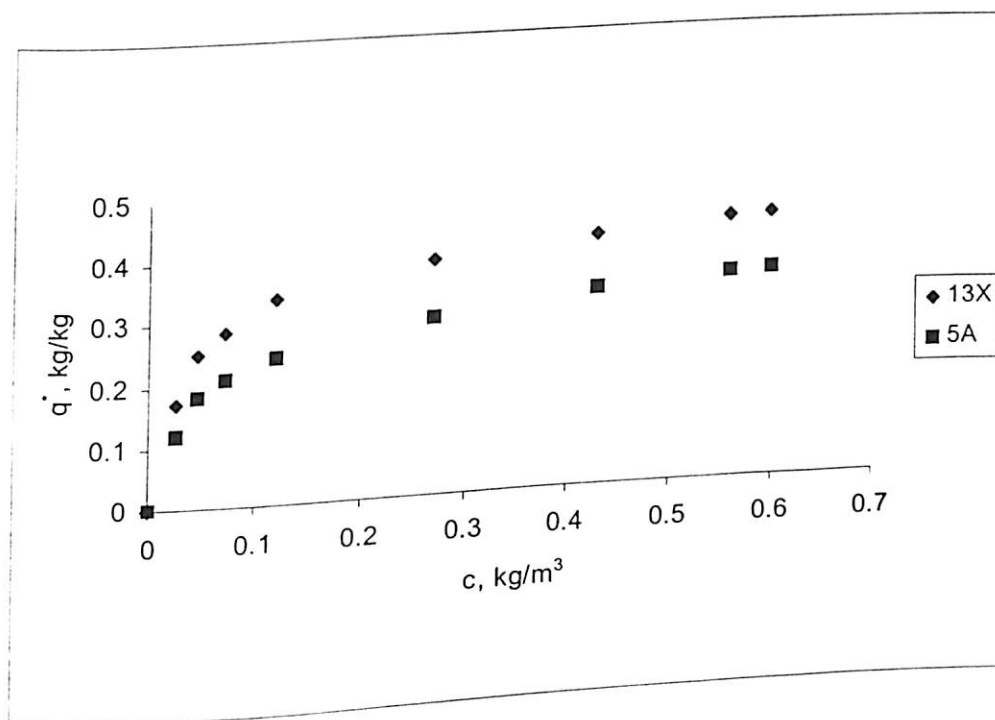


Figure 4.1.4: Comparison of equilibrium capacities of ethyl acetate in E-merck 5A and 13X molecular sieves at 45 deg C

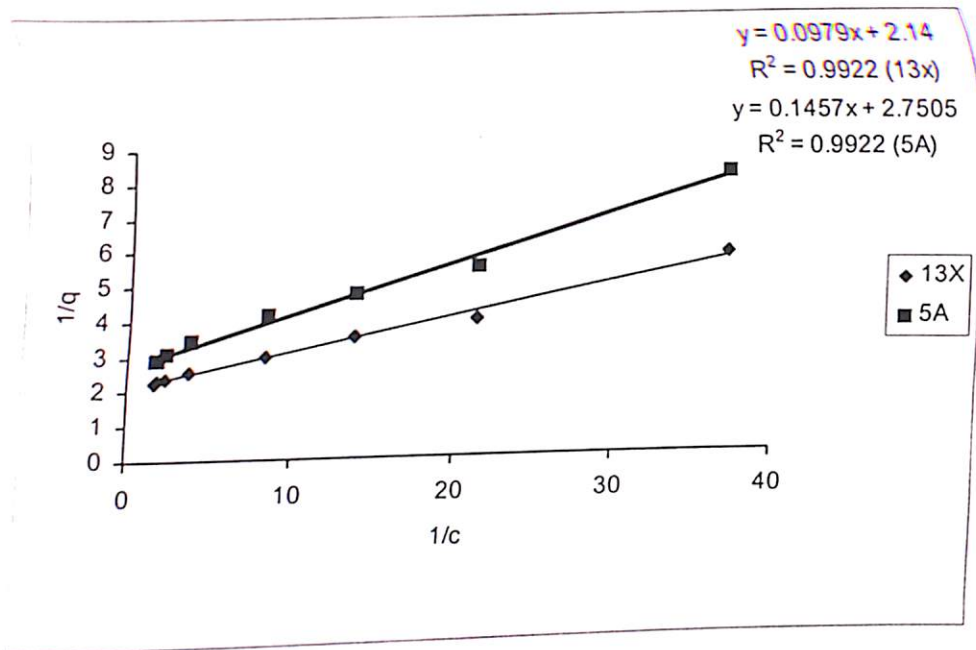


Figure 4.1.7: Fitting of Langmuir model with experimental data at 45 deg C in 5A and 13X molecular sieves

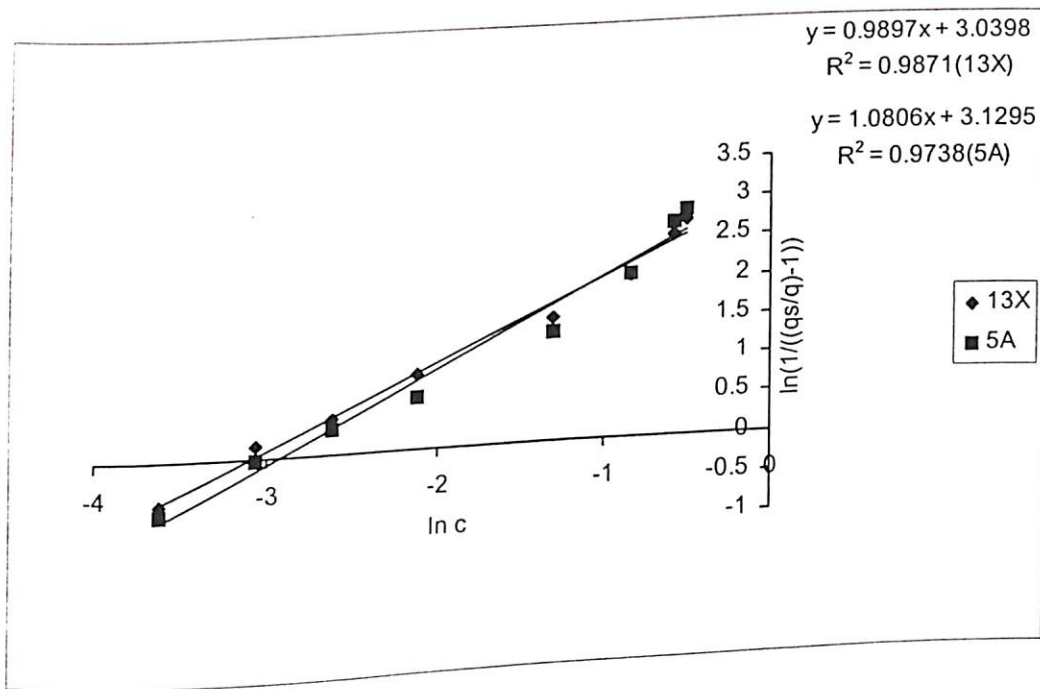


Figure 4.1.8: Fitting of Langmuir- Freundlich model with experimental data at 45 deg C in E-merck 5A and 13X molecular sieves

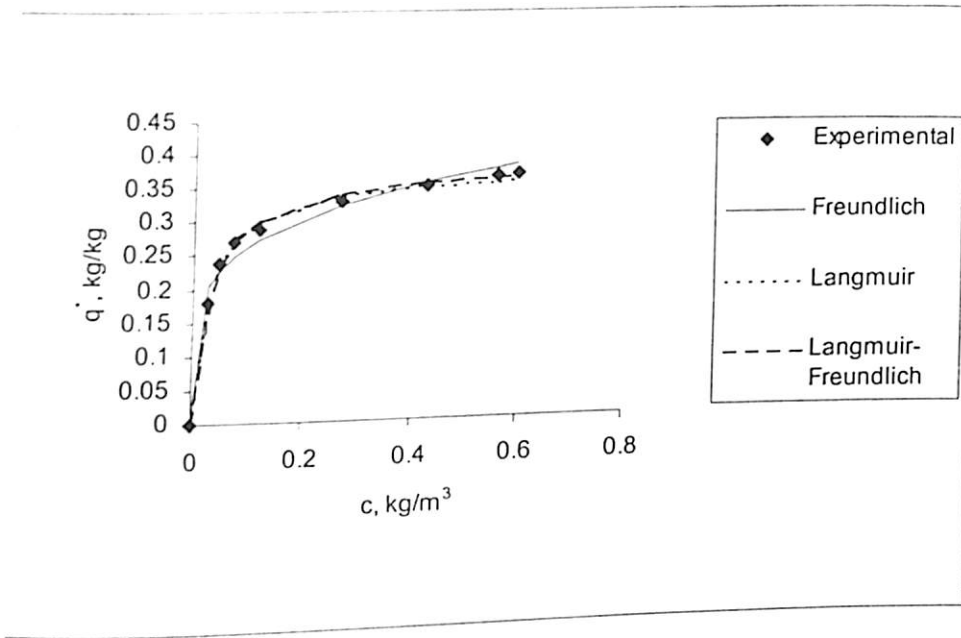


Figure 4.1.9: Comparison of different isotherm models' predictions with experimental equilibrium data of ethyl acetate in E-merck 5A molecular sieves at 35 deg C

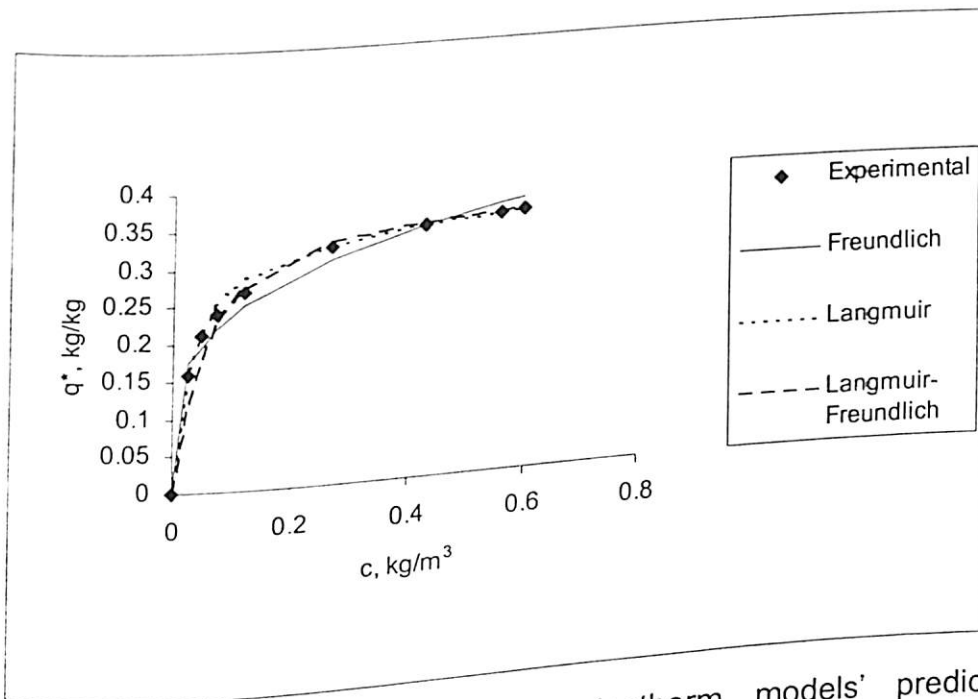


Figure 4.1.10: Comparison of different isotherm models' predictions with experimental equilibrium data of ethyl acetate in E-merck 5A molecular sieves at 40 deg C

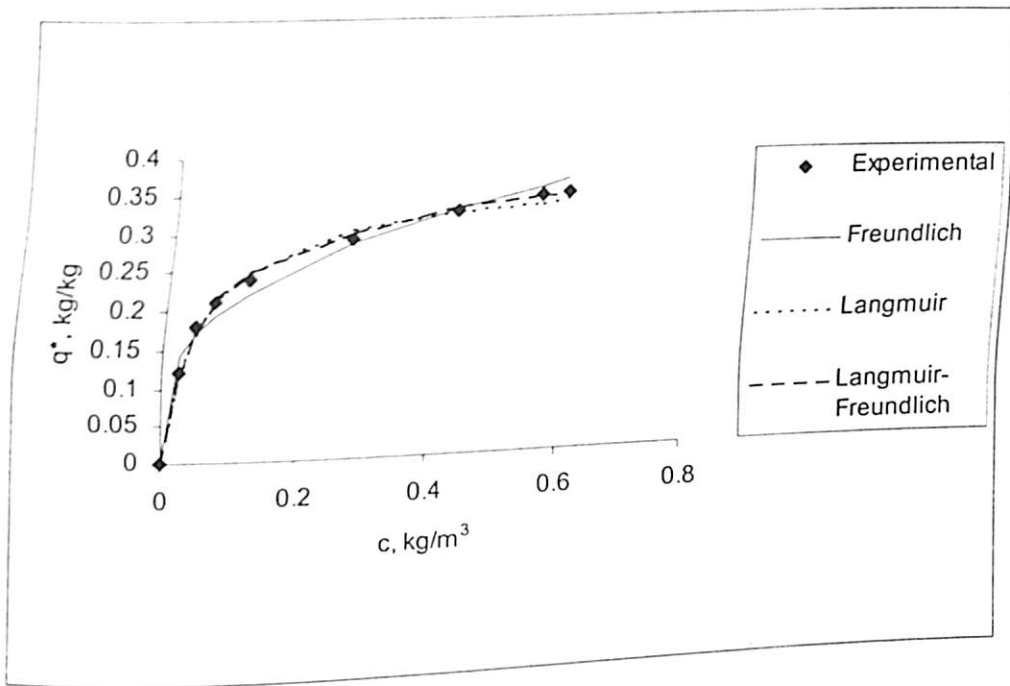


Figure 4.1.11: Comparison of different isotherm models' predictions with experimental equilibrium data of ethyl acetate in E-merck 5A molecular sieves at 45 deg C

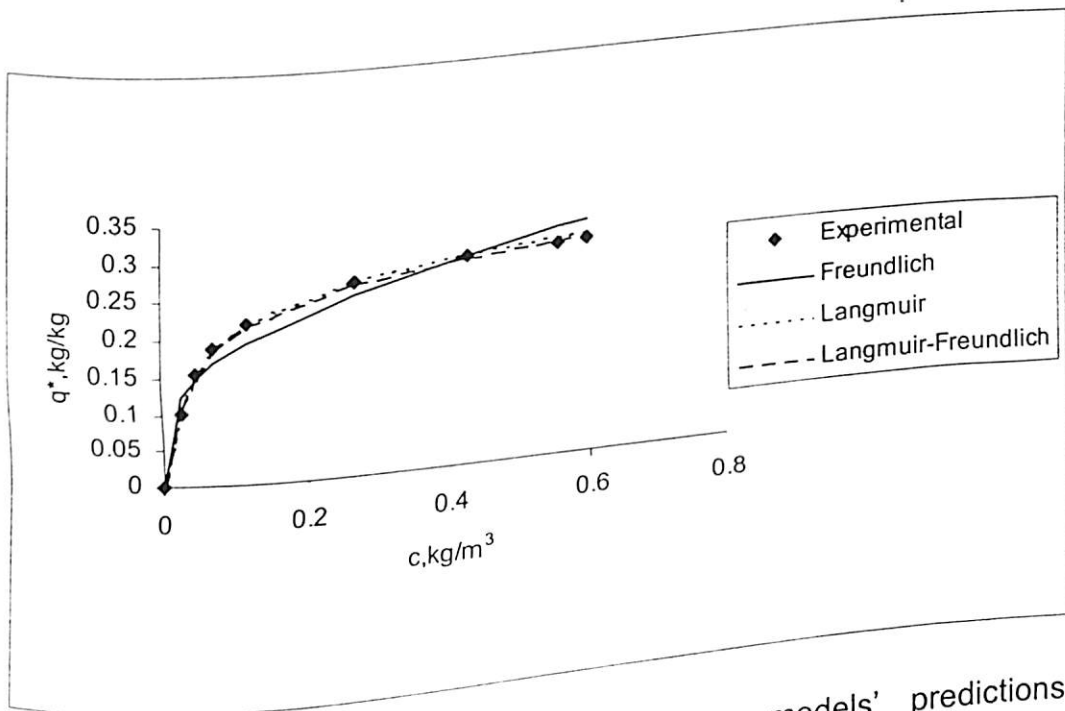


Figure 4.1.12: Comparison of different isotherm models' predictions with experimental equilibrium data of ethyl acetate in E-merck 5A molecular sieves at 55 deg C

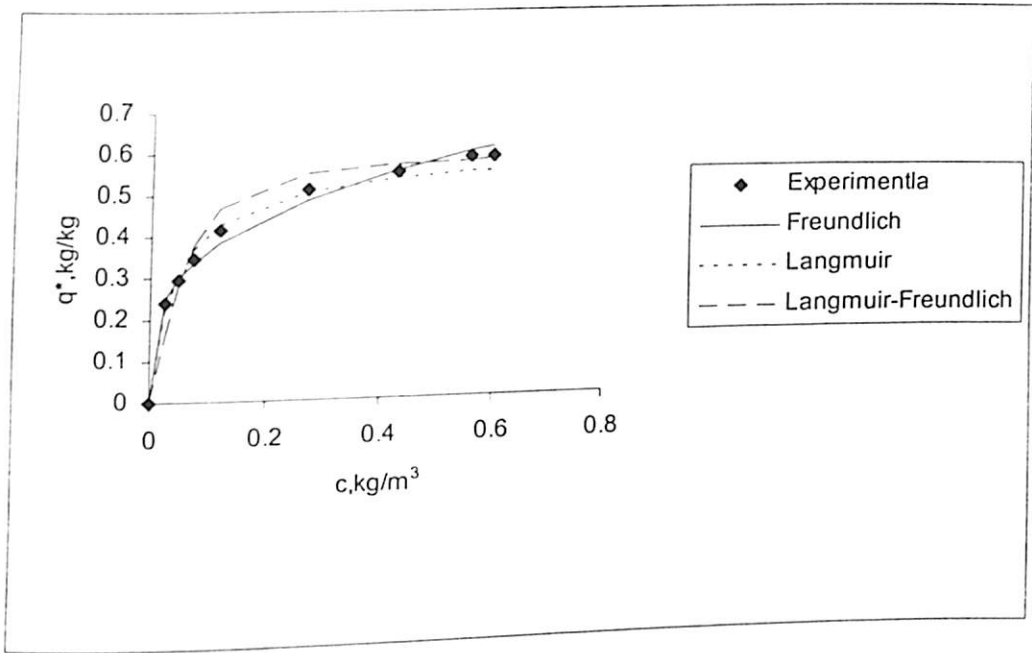


Figure 4.1.13: Comparison of different isotherm models' predictions with experimental equilibrium data of ethyl acetate in E-merck 13X molecular sieves at 35 deg C

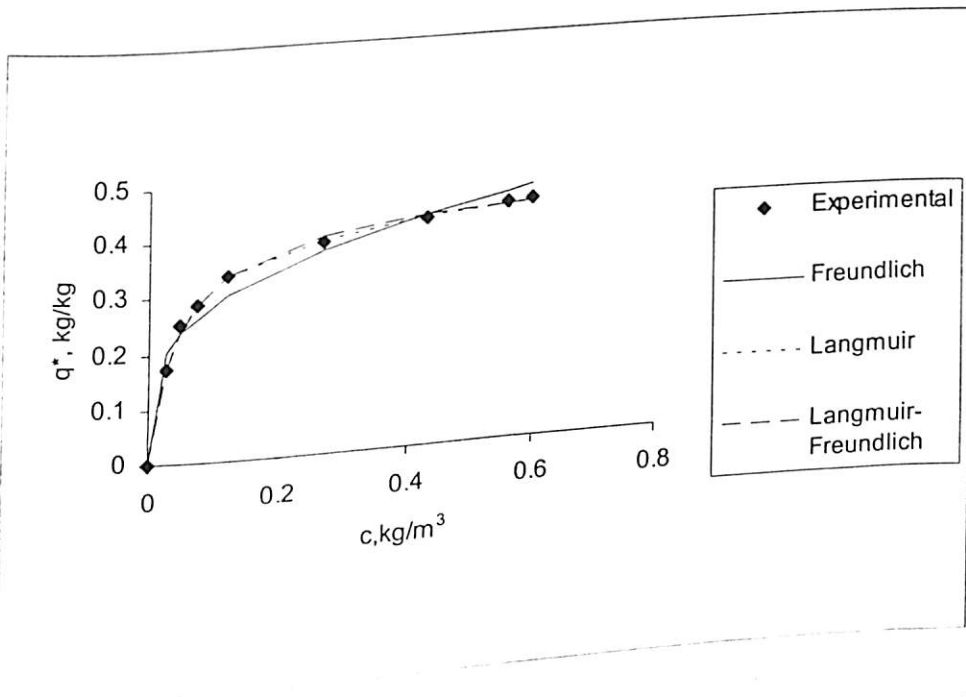


Figure 4.1.14: Comparison of different isotherm models' predictions with experimental equilibrium data of ethyl acetate in E-merck 13X molecular sieves at 45 deg C

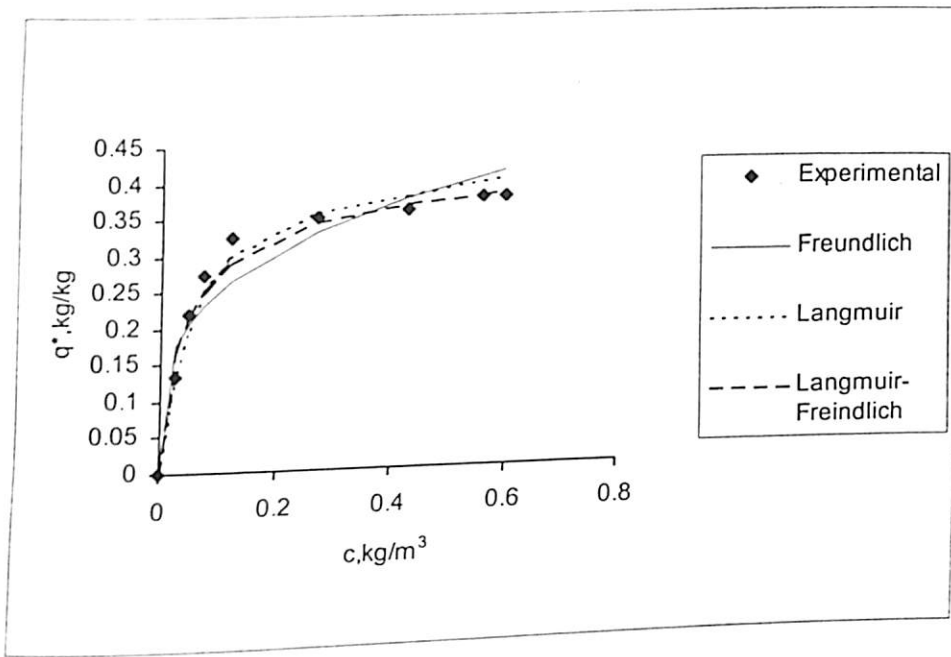


Figure 4.1.15: Comparison of different isotherm models' predictions with experimental equilibrium data of ethyl acetate in E-merck 13X molecular sieves at 55 deg C

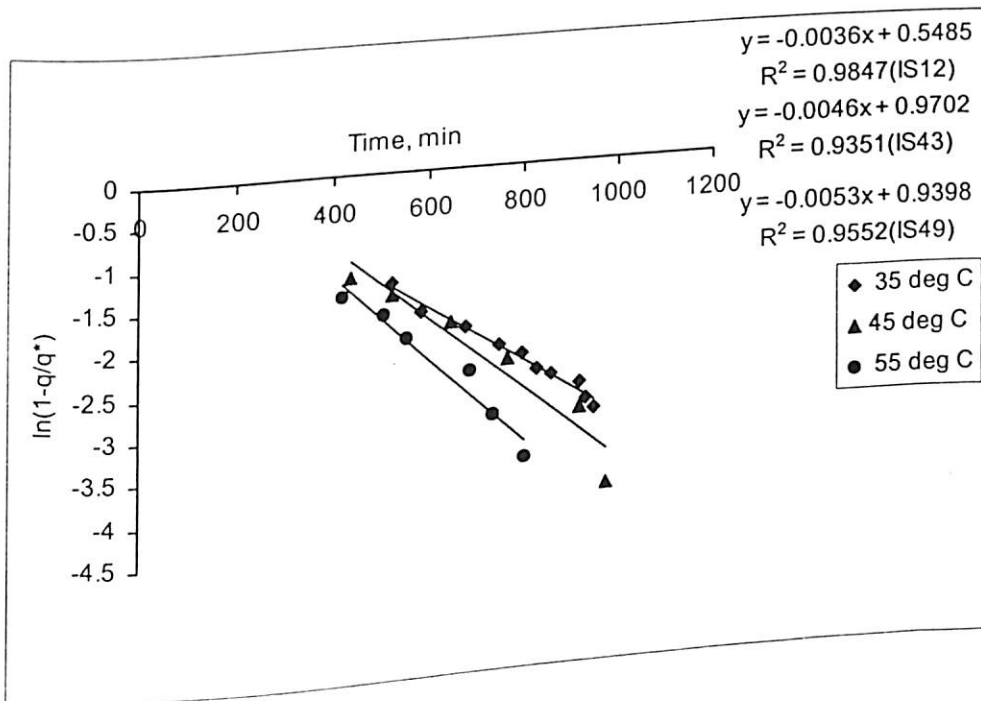


Figure 4.1.16: Determination of overall mass transfer coefficient using uptake rate for ethyl acetate in E-merck 5A molecular sieve

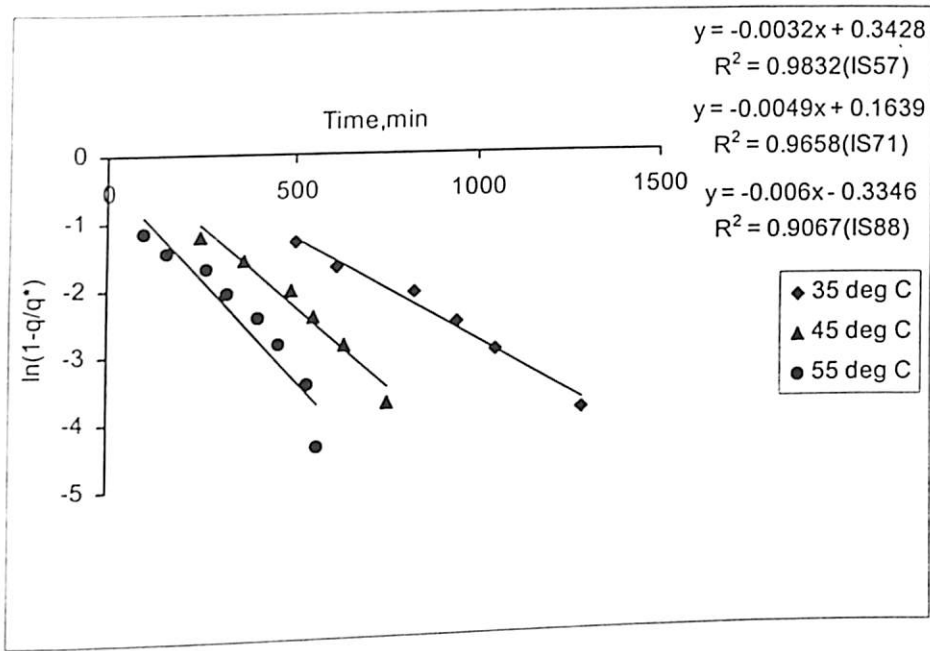


Figure 4.1.17: Determination of overall mass transfer coefficient using uptake rate for ethyl acetate in E-merck 13x molecular sieve

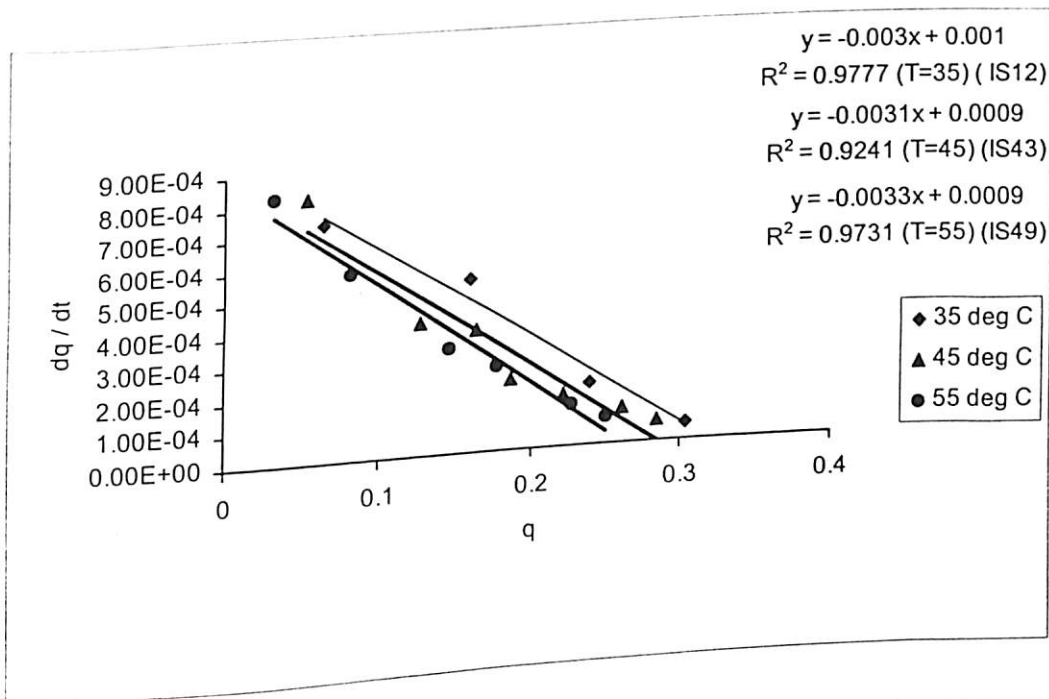


Figure 4.1.18: Determination of overall mass transfer coefficient using LDF model in E-merck 5A molecular sieve

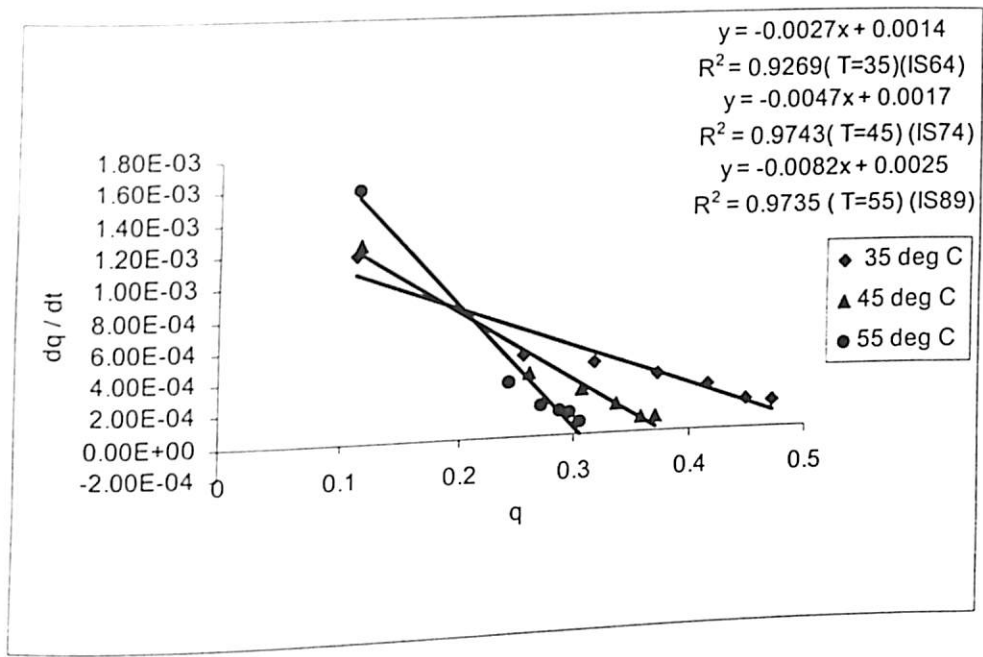


Figure 4.1.19: Determination of overall mass transfer coefficient using LDF model in E-merck 13X molecular sieve

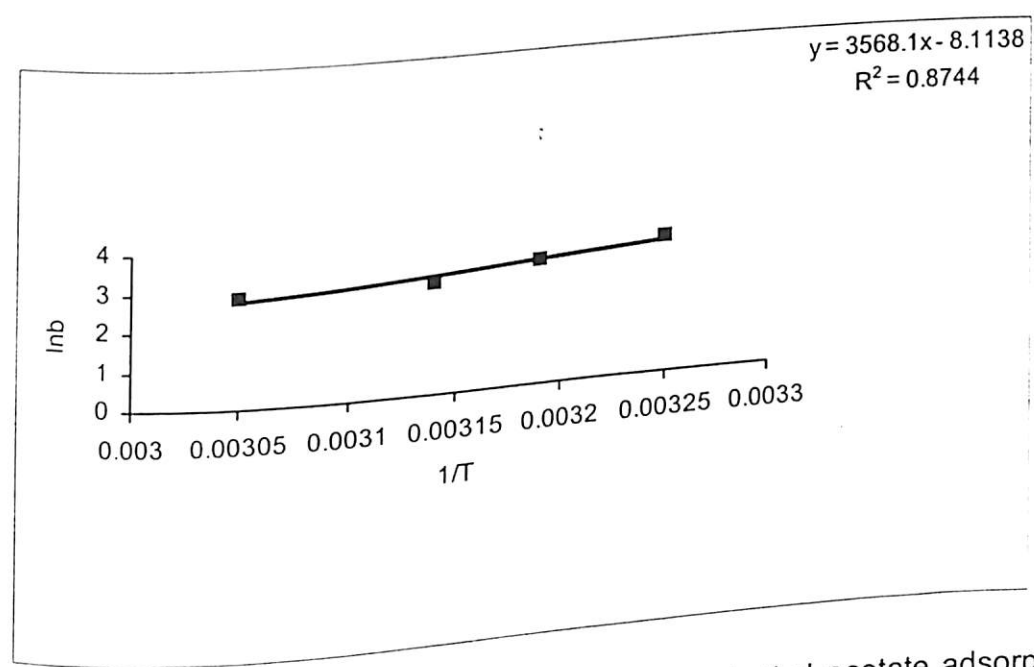


Figure 4.1.20: Determination of heat of adsorption of ethyl acetate adsorption in E-merck 5A molecular sieves based on Langmuir model

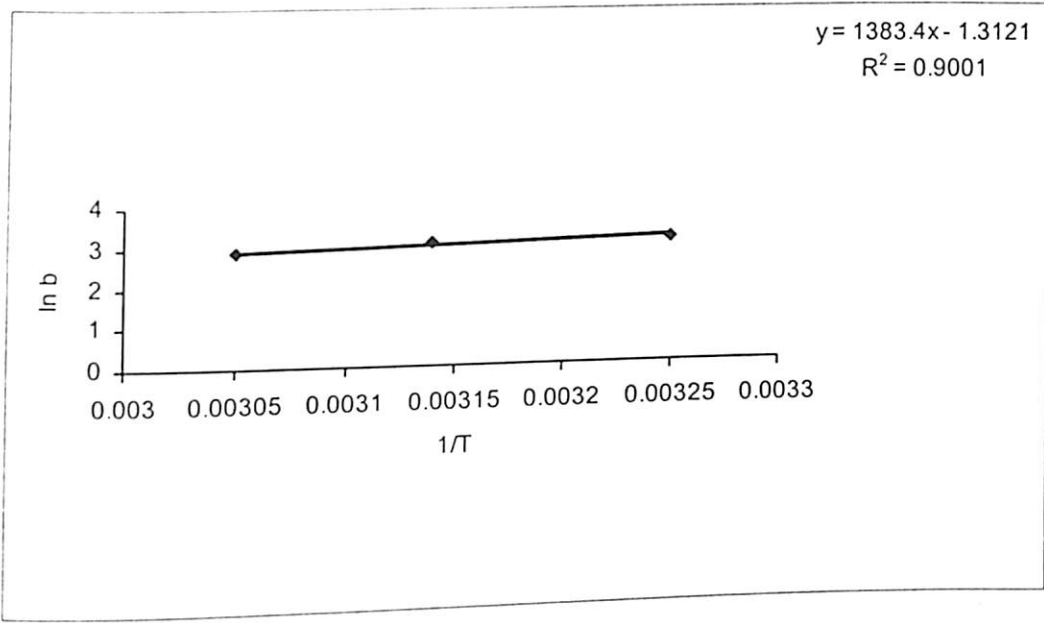


Figure 4.1.21: Determination of heat of adsorption of ethyl acetate adsorption in E-merck 13X molecular sieves based on Langmuir model

4.2 Dynamic Studies

4.2.1 Introduction

Realizing the importance of the dynamic studies as has been discussed in chapter III, both experimental and theoretical dynamic studies have been performed in this research work and the results of the said study have been reported in this section.

The results are presented in the form of concentration and temperature breakthrough curves in case of EA-E-merck 13X molecular sieve system. In case of EA-E-merck 5A system, the results have only been the concentration breakthrough curves as there have been insignificant rise in temperature during adsorption for the system within the range of the variables studied. These concentrations and temperatures at the bed exit are non-dimensionalized with respect to inlet concentration and inlet gas temperature respectively.

Section 4.2.2 presents the results of the experimentally observed dynamic behaviour of EA adsorption on E-merck 5A and 13X molecular sieves with the variation of certain input variables and analyses the same.

Later, in section 4.2.3, results of the dynamic behaviour from experiments and model simulation have been compared in terms of standard deviation to validate the model. This has been used to establish the quality of the model for the successful prediction of the experimental results.

Finally, section 4.2.4 discusses the effects of varying the model input parameters on the adsorption dynamic behaviour of EA. This is done to identify the relatively important parameters and their effects to influence the design aspects of the adsorber bed.

4.2.2 Experimental Results

Experiments have been conducted to study the dynamic behavior of ethyl acetate adsorption on E-merck 5A and 13X molecular sieves. Effects of changes in input variables such as inlet superficial velocity, inlet concentration of EA and bed height have been analyzed and discussed in detail. Also the adsorption behavior between the sieves has been compared.

The range of variables studied during the experimentations has been presented in Table 4.2.2.1. The operating conditions for each experimental run have been shown in Tables 4.2.2.2 and 4.2.2.3. The exit concentration and temperature histories have been presented for each experimental run in Appendix - III

4.2.2.1 Adsorption on 5A and 13X molecular sieves

The results of ethyl acetate adsorption on E-merck 5A and 13X molecular sieves are presented as concentration breakthrough curves in Figures 4.2.2.1 and 4.2.2.2. The operating conditions for these cases are nearly identical for comparison of the results. The corresponding temperature breakthrough curves have not been presented here, as there is no significant rise of temperature in case of 5A sieve.

The concentration breakthrough curve in 5A molecular sieve shows a flatter and much earlier breakthrough indicating that the 5A molecular sieve has lower adsorption capacity compared to the 13X molecular sieve. The comparatively steep concentration breakthroughs in case of 13X sieve may be attributed to the shorter mass transfer zone length compared to 5A molecular sieves. This leads to the conclusion that 13X molecular sieve behaves closer to ideal behaviour than E-merck 5A molecular sieve, while adsorbing EA from air.

4.2.2.2 Effect of inlet concentration

Concentration breakthrough curves of EA during adsorption on E-merck 5A and 13X molecular sieves for different inlet concentrations of EA in air have been presented through Figures 4.2.2.3 and 4.2.2.4 respectively. The corresponding temperature breakthrough curves for 13X molecular sieves have been shown in Figure 4.2.2.5. No appreciable temperature rise has been observed for 5A molecular sieves and hence corresponding temperature breakthrough curves could not be obtained. The inlet concentration of EA has been varied while keeping other variables constant. Early concentration breakthrough observed from the Figures 4.2.2.3 and 4.2.2.4 for higher inlet adsorbate (EA) concentrations may be attributed to the fact that higher gas phase adsorbate concentration increases the mass transfer rate (adsorption rate) at the early stage of adsorption and is expected to get early and steep breakthroughs. Corresponding higher and higher temperature rise, in case of 13X, as a result of higher adsorption rate has also been observed from the Figure 4.2.2.5. The higher bed temperature reduces the adsorption capacity of the bed and brings out early breakthrough in case of higher inlet concentration. With passage of time the adsorption rate slows down due to partial saturation of the bed, showing flatter breakthrough in the rear portion of the concentration breakthrough curve. Thus, the difference between the concentration breakthrough curves narrows down after the breakthrough point and finally reaches the saturation. This has also been reflected with the gradual decrease in peak temperature with lower inlet concentration of EA and consequently lower rate of adsorption. Also the wider temperature peaks for lower inlet concentration of EA establishes the flatter concentration breakthrough behaviour. In the case of 5A molecular sieve, the insignificant temperature rise may be due to comparatively less saturation adsorption capacity (poor adsorption characteristic) of the EA-5A molecular sieve system. Lower saturation adsorption capacity

reduces the rate of adsorption leading to lower temperature rise, which reduces further due to convective transport of heat with the fluid.

4.2.2.3 Effect of Inlet velocity

Adsorption experiments have been carried out at different velocities while the other parameters are kept constant. This leads to variations in the turbulence inside the bed interstices, affecting the mass transfer rate and the residence time within the bed.

The concentration breakthrough curves for 5A and 13X molecular sieves at different inlet fluid velocities have been presented through Figures 4.2.2.6 and 4.2.2.7 respectively. Corresponding temperature breakthrough curves for 13X molecular sieve are shown in Figure 4.2.2.8.

It can be observed from the figures, that with decrease in velocity, the breakthrough occurs late, and almost a proportionate increase in breakthrough time with decrease in velocity (constant pattern behaviour). There have been no significant differences of the pattern of the breakthrough curves for both the molecular sieves.

The primary effect of the inlet gas velocity is on the rate of the movement of mass transfer zone (MTZ). The movement of MTZ is directly related to inlet gas velocity. This, in turn, results in early breakthroughs with increasing velocity. A similar nature of the breakthrough curves in the case of both the sieves indicates that mass transfer rate is not sensitive to velocity. This leads to a conclusion that the adsorption process is probably controlled by pore diffusion and not by external film mass transfer (Ghoshal et al., 1999). The corresponding temperature breakthrough curve for 13X molecular sieve shows slightly higher temperature rise and a little narrower peak for higher velocity. Faster movement of the MTZ at higher velocity may be responsible for the narrower peak. The lower peak height at lower velocity

may be due to higher heat loss from the system, as residence time for heat transfer becomes more with lower velocity.

4.2.2.4 Effect of bed height

The adsorption experiments have been carried out with different bed heights (L) while other variables are held constant. The bed length variation keeping other variables constant changes the residence time of the fluid within the bed.

Figures 4.2.2.9 and 4.2.2.10 show the concentration breakthrough curves in case of 5A and 13X molecular sieves respectively for different bed heights. The corresponding temperature breakthrough curve in case of 13X molecular sieve has been presented in Figure 4.2.2.11.

It can be observed from the figures that with increasing bed length the breakthrough curves are shifted to the right with higher breakthrough and saturation time and almost same temperature peak. Nature of the figures also remains the same. For a long bed, the mass transfer zone will be contained within the bed. In such cases the concentration breakthrough profile will remain unchanged with change in bed length (constant pattern behavior). The effects of bed length will only be due to axial dispersion for beds of shorter length (Ghoshal et al, 1999). Almost similar nature of the breakthrough curves as already mentioned indicates insignificant effect of axial dispersion on the changes of bed length. For different bed lengths the ethyl acetate concentration breakthrough curves for both the adsorbents show a reasonable breakthrough time, indicating that the mass transfer zone is contained within the bed due to higher affinity of both the sieves for EA. Again, comparatively flatter breakthrough in 5A supports the stronger adsorption behavior of EA on 13X in comparison to itself.

4.2.3 Validation of the Model

Mathematical models in the form of partial differential equations for transient mass and energy balances of adsorbate (ethyl acetate) in the gas and solid phases over an elemental section of an adsorption column and the corresponding discretisation for numerical solution have been presented in chapter –II. Langmuir type adsorption isotherm has been considered for the model since the Langmuir model best explained the experimental equilibrium data as discussed in section 4.1. Values of the input parameters used for simulation are presented in Table 4.2.3.1 for both 5A and 13X molecular sieves. The values of mass transfer coefficient, heat of adsorption, and Langmuir constants are determined from equilibrium and kinetic studies described in chapter III. The other physicochemical and transport properties are collected from literature.

Validity of the model has been attempted through the comparison of the concentration and temperature histories measured at the end of the bed with those obtained from the proposed model. The model has been simulated after taking values of the input parameters such as Langmuir constant, equilibrium adsorption capacity, heat of adsorption and overall mass transfer coefficients as have been calculated from equilibrium studies. A quantitative assessment of the quality of the model has been made by calculating standard deviation at each experimental point. The deviation statistics are presented in Tables 4.2.3.2 and 4.2.3.3 for E-merck 5A and 13X molecular sieves respectively.

In case of 5A, the model simulation with the calculated heat of adsorption values (as calculated from equilibrium studies) shows much higher temperature rise (10 to 12 °C). This is not the case, as observed experimentally may be attributed to the fact of over prediction of the heat of adsorption values from the experimental equilibrium studies. In case of 5A breakthrough experiments the temperature rise has been found to be around 1 – 2 deg C only.

The comparable size of ethyl acetate molecules with pore size of 5A molecular sieves corresponds to higher resistance for the mass transfer. This implies that ethyl acetate is weakly adsorbed in 5A molecular sieves, which has also been observed from the flatter concentration breakthrough curves. Poorer adsorption capacity would be associated with lower heat of adsorption. Hence, the model has also been simulated with several lower values of heat of adsorption for all the cases of experimental dynamic studies in 5A (Table 4.2.2.2). It has been found that when the heat of adsorption was decreased to 75000 J/kg, the temperature rise was about 2 to 3 °C for all the cases. Thus, the simulated results with heat of adsorption value (75000 J/kg) not only satisfy the observed temperature rise, they also well predicts the experimental concentration breakthrough curves for 5A – EA system. Therefore, in all the validation results shown pictorially for 5A molecular sieve, predictions by author's experimentally calculated heat of adsorption values and the reduced heat of adsorption values have been presented. In both the predictions the concentration breakthrough curves have not been influenced much due to the change of heat of adsorption values.

Figures 4.2.3.1, 4.2.3.3 and 4.2.3.5 are sample plots presenting the experimental concentration breakthrough curves in case of E-merck 5A molecular sieves for ethyl acetate adsorption with corresponding values predicted from the model. Corresponding temperature breakthrough curves are shown in Figures 4.2.3.2, 4.2.3.4, and 4.2.3.6 respectively. The predicted results for concentration breakthroughs are in good agreement with the experimental results for a major portion of the breakthrough curves. In all cases the model is found to under predict the concentration at the very initial stages of breakthrough and at the saturation level. While the assumption of complete radial mixing may be one factor for the deviation, the other factor may be that at very low concentration and at the saturation level measurement of concentration has been possibly associated with experimental error. Table

4.2.3.2 shows the standard deviation of predicted results (for unchanged and changed values of heat of adsorption) from experimental data.

Figures 4.2.3.7, 4.2.3.9 and 4.2.3.11 present the experimental concentration breakthrough curves for E-merck 13X molecular sieves for ethyl acetate adsorption with corresponding values predicted from the models with and without axial dispersion terms. Corresponding temperature breakthrough curves are shown in Figures 4.2.3.8, 4.2.3.10, and 4.2.3.12. It has been found, both from concentration and temperature breakthrough curves, that the model without axial dispersion of heat and mass shows good agreement with the experimental results. But there is poor agreement between experimental and predicted results using model with axial dispersion of heat and mass. In both the cases the overall mass transfer coefficient have been increased to $5.0 \times 10^{-4} \text{ s}^{-1}$, which is higher than the calculated values as reported in section 4.1 (around $2.0 \times 10^{-4} \text{ s}^{-1}$). Sample plots of predictions of concentration and temperature breakthrough curves by the model with calculated overall mass transfer coefficient ($2.0 \times 10^{-4} \text{ s}^{-1}$) showed poor fitting and are presented through Figures 4.2.3.13 and 4.2.3.14 respectively. The simulated results with the increased value of overall mass transfer coefficient for 13X very well predict the experimental concentration and temperature breakthrough data. This indicates that the kinetics studies for 13X sieve may have under predicted the value of overall mass transfer coefficient. Whereas in case of 5A the calculated overall mass transfer coefficient $1.5 \times 10^{-4} \text{ s}^{-1}$ from the experimental data (explained in section 4.1) gave a reasonably good fitting with the experimental results. Better suitability of higher mass transfer coefficient and no axial dispersion terms in the model may lead to a conclusion that adsorption of ethyl acetate in 13X molecular sieve is an example of strong adsorption phenomenon, closer to ideal adsorption behavior, in comparison to adsorption in 5A

molecular sieve. Table 4.2.3.3 shows the standard deviation of predicted results (for cases of with and without axial dispersion term) from experimental data.

4.2.4 Simulation studies

The effects of different input parameters, describing the geometric, thermophysical and transport properties of the system of study, in the developed mathematical model have been studied in this section. The mathematical model based on linear driving force (LDF) approximation used for the simulation studies have been developed in chapter II. This includes the axial dispersion of heat and mass. The adsorption equilibrium is described by Langmuir adsorption equilibrium. The parameters studied are

- Adsorbate inlet concentration, c_0
- Inlet superficial velocity, v_0
- Bed length, L
- Bed diameter, D
- Overall mass transfer coefficient, k
- Saturation Capacity q_s
- Heat of adsorption, $(-\Delta H)$
- Bed to wall heat transfer coefficient, h_w
- Solid to gas heat transfer coefficient, h
- Axial Dispersion Coefficient, D_a

The mathematical model has been simulated with different values of the above parameters to know the effect of each of them on the adsorption dynamics. This information is helpful in understanding the similar adsorption systems and provides guidelines during the design and operation of such systems. Effects of all the parameters studied in this section are

investigated by simulating concentration breakthrough and temperature breakthrough curves. The variable ranges and parameter base values are given in Tables 4.2.4.1 and 4.2.4.2 respectively.

4.2.4.1 Effect of adsorbate inlet concentration, inlet superficial velocity, and bed length

The simulation results with the above variables have been obtained. The effect of variations in adsorbate inlet concentration, superficial velocity and bed length on the concentration and temperature breakthrough curves are presented in different figures as mentioned below:

Parameter	Figure number of concentration breakthrough curve	Figure number of temperature breakthrough curve
c_o	4.2.4.1	4.2.4.2
v_o	4.2.4.3	4.2.4.4
L	4.2.4.5	4.2.4.6

The concentration and temperature breakthrough curves obtained from the simulation results with the above variables have similar trends as have been found in case of experimental results. The nature and trend of such results have already been explained and discussed under section 4.2.2.

the major variation has been expected in the temperature breakthrough curves. Heat transfer area has been taken as the solid to wall surface area. It has been found that temperature rise increases with increase in column diameter (Figure 4.2.4.8). For same inlet velocity, higher bed diameter increases the net through put with square of bed diameter and as the amount of adsorbent per unit cross-sectional area is also more the heat generation in the bed increases, which doesn't get transferred through the wall totally leading to accumulation of energy. For lower diameter this accumulation of energy becomes lower and increases with increase in bed diameter as discussed. Again, at higher temperature adsorption becomes poorer due to decrease in adsorption capacity and hence the concentration breakthrough is expected to be flatter due to decrease in rate of adsorption. But increase in rate due to increase in amount of adsorbent per unit cross-sectional might not have allowed any change in the concentration breakthroughs with change in bed diameter. Under totally adiabatic condition, the temperature rise would be higher. This in turn helps in desorption of the bed. Hence, suitable heat removal machinery should be accompanied with industrial scale adsorptive separation, where adsorber diameter is quite high, if concentrated only to have better adsorption performance in the bed.

4.2.4.3 Effect of overall mass transfer coefficient, k

Mass transfer coefficient is indicative of strong or poor adsorptivity of adsorbate in the adsorbent. Mass transfer coefficient may be improved either by making bigger pore sizes facilitating mechanism of transport or by improving the adsorbate-adsorbent affinity through adsorbate surface modifications. In case of any adsorber design, higher mass transfer coefficient is desired to have better adsorption behaviour. In contrast, a higher temperature peak is undesirable because it reduces the adsorption capacity of the bed. So, a study on the

effect of the mass transfer coefficient helps to find out the nature of the changes in the *concentration and temperatures breakthrough* curves and thereafter the design considerations.

Higher mass transfer coefficient leads to smaller *Mass Transfer Zone (MTZ) length* because of higher rate of mass transfer. This, in turn, makes the concentration breakthrough steeper indicating strong adsorption behavior (Figure 4.2.4.9). This phenomenon is also revealed through temperature breakthrough curves (Figure 4.2.4.10), where with increase in mass transfer coefficient the temperature peak gets higher and narrower. This may also be attributed to the fact that an increased rate of mass transfer with higher mass transfer coefficient is responsible for higher heat generation. Thus the accumulation of heat in gas phase is also high leading to a higher temperature of the gas phase. The narrow peak is obviously because of the smaller MTZ length.

4.2.4.4 Effect of Saturation Adsorption Capacity, q_s

Saturation adsorption capacity of the adsorbent decides the maximum amount of the adsorbate that can be adsorbed. Saturation adsorption capacity can be improved by replacing with a better adsorbent, increasing the adsorption surface area per unit volume of the adsorbent and by surface modification of the adsorbent, where the forces of attraction are increased to withhold more layers of adsorbate molecules. Thus, higher saturation adsorption capacity enables more amount of adsorbate to be adsorbed per unit amount of the adsorbent. This in turn reduces the velocity of the mass transfer zone. So, a delayed concentration as well as temperature breakthrough with constant pattern are expected and have been observed through Figures 4.2.4.11 and 4.2.4.12 respectively. The constant pattern behavior suggests, as expected, that mechanism of mass and heat transfer do not get disturbed with changes in the saturation adsorption capacity. It has also been found that the temperature peak rises slightly (Figure 4.2.4.12) with increase in the values of saturation adsorption capacity. This

may be attributed to the fact that with increase in the saturation adsorption capacity more amount of adsorbate gets adsorbed generating more amount of energy. The rate of generation of this enhanced energy could be more than the rate of energy transfers via different mechanism, as being discussed in the model development. This results in accumulation of extra energy reflected through rise in temperature peak.

4.2.4.5 Effect of heat of adsorption, $(-\Delta H)$

Higher value of heat of adsorption is responsible for generation of more heat. As this cannot be removed at the rate it is generated, a higher temperature rise results. It is also obvious that at higher temperature the adsorbent capacity decreases and poor adsorption behavior is expected. This is reflected through the flatter breakthrough curves. The concentration breakthrough curves in the present investigation (Figure 4.2.4.13) do not show the same behaviour rather it shows a reverse trend. Whereas the temperature breakthrough (Figure 4.2.4.14) shows the expected trend as discussed. This contradictory observation may be explained as follows. The Langmuir constant b is a function of b_0 and $(-\Delta H)$ (Eq. 2.3). With increase in heat of adsorption the equilibrium capacity also increases when b_0 is a constant. The positive impact towards adsorption through increase in equilibrium adsorption capacity *at a particular concentration becomes more significant over the negative impact of the higher temperature.* Thus the higher heat of adsorption values makes the concentration breakthrough steeper with delayed breakthrough time. As because amount adsorbed is increased and heat of adsorption values are also increased, the temperature peak is also increased. However, it can also be observed that change in heat of adsorption values does not show constant pattern behaviour both for concentration and temperature breakthrough curves which has been discussed in case of effect of saturation adsorption capacity under section 4.2.4.4. In fact, it is seen that with lower heat of adsorption values, the concentration curves

become flatter, showing weak adsorption behaviour with wide and low peak for temperature breakthrough curves. Though higher heat of adsorption (when Langmuir constant b is kept independent) value is expected to make the system more non-ideal by making the concentration breakthrough flatter with high and narrow peak temperature breakthrough curves, the reverse observation in case of concentration breakthrough in the present case is due to change of b , the Langmuir constant with heat of adsorption.

4.2.4.6 Effect of bed to wall heat transfer coefficient h_w

Wall heat transfer coefficient is expected to have direct impact on temperature breakthrough curves and indirect impact on concentration breakthrough curves. Figures 4.2.4.15 and 4.2.4.16 represent the effects of bed to wall heat transfer coefficient h_w on simulated concentration and temperature breakthrough curves respectively while other parameters are kept constant. With smaller values of h_w , the breakthrough time decreases and also the concentration breakthrough curve becomes flatter in latter part of the breakthrough curve. This may be attributed to the fact that with smaller values of h_w , the rate of heat loss from the bed to wall decreases resulting in more accumulation of energy. This in turn increases the temperature of the bed and gas. The corresponding width of the temperature breakthrough curve also becomes wider. Decreased capacity of the adsorbents due to increase in temperature of the bed as is evident from the gas phase temperature breakthrough curves (Figure 4.2.4.16) decreases the driving force for adsorption. Thus, with the decreased rate of adsorption the system takes more time for saturation resulting in a flatter concentration breakthrough curve. The above study, thus, suggests that instead of using an adiabatic process, a suitable design of heat removal arrangement from the bed would improve the efficiency of the bed, when only adsorption is concerned.

4.2.4.7 Solid to gas heat transfer coefficient, h

The simulated results with different values of h have been obtained and compared in terms of concentration and temperature breakthrough curves as shown in Figures 4.2.4.17 and 4.2.4.18 respectively. It may be observed from the figures that the solid gas heat transfer coefficient does not influence significantly the concentration and temperature breakthrough curves within the range of the study.

4.2.4.8 Effect of axial dispersion coefficient, D_a

Figures 4.2.4.19 and 4.2.4.20 show the effects of D_a values on simulated concentration, and temperature breakthrough curves respectively while the other parameters are kept constant. Change in mass transfer zone length is reflected through change in D_a . It is observed that the concentration breakthrough curve becomes steeper while the temperature peak becomes narrower with a higher peak for lower values of D_a . This may be attributed to the fact that decreases in D_a , also leads to decreases in mass transfer zone length. This in turn helps the system behaving more close to ideal adsorption situation making the concentration breakthrough curve steeper. Again, with decrease in D_a , delayed breakthrough is expected. But higher temperature rise makes the breakthrough earlier. These two counteracting effects might not have allowed major differences in the breakthrough times due to change in D_a values. Similarly, with higher dispersion coefficient the concentration breakthrough expands showing a flatter curve and the temperature peak broadens with a lower peak value. This may be attributed to the fact that with increase in dispersion coefficient the mass transfer zone length increases due to axial mixing and the system behaves like a poorer adsorbate-adsorbent system.

4.2.5 Conclusions from dynamic studies

The following conclusions may be drawn from the dynamic studies that include experimental study, model validation and dynamic simulation studies.

- In case of EA-E-merck 5A system there have been insignificant rise in temperature.
- E-merck 13X molecular sieve behaves closer to ideal behaviour than E-merck 5A molecular sieve, while adsorbing EA from air, establishing itself as stronger adsorbent than 5A.
- Early concentration breakthrough has been observed with higher inlet adsorbate (EA) concentrations due to increased mass transfer rate (adsorption rate) at the early stage of adsorption. With time the adsorption rate slows down and breakthrough reaches to saturation after a longer time.
- The constant pattern breakthrough curves for both the molecular sieves with change in inlet velocity indicate that mass transfer rate is probably controlled by pore diffusion and not by external film mass transfer. The lower temperature peak height at lower velocity may be due to more heat loss from the system as residence time for heat transfer increases with lower velocity.
- The constant pattern breakthrough curves with increasing bed lengths indicate insignificant effect of axial dispersion on the changes of bed length. The mass transfer zone is probably contained within the bed (in the range of the experiments) due to higher affinity of both the sieves for EA.
- In case of 5A, the predicted results for concentration breakthroughs are in good agreement with the experimental results for a major portion of the breakthrough curves with the calculated overall mass transfer coefficient value. But the temperature breakthrough curves are better matched with heat of adsorption was decreased to

75000 J/kg, which is lower than the experimentally calculated value 337000 J/kg

(Table 4.1.12).

- In case of 13X, the model without axial dispersion shows a better match than that with axial dispersion. The increased value of overall mass transfer coefficient ($5.0 \times 10^{-4} \text{ s}^{-1}$) as model input, which is higher than the calculated values ($(1.0 - 2.0) \times 10^{-4} \text{ s}^{-1}$) better predicts the experimental data.
- Changes in bed diameter do not significantly influence the concentration breakthrough curves. But, larger bed diameter increases the bed temperature and adsorption becomes poorer due to decrease in adsorption capacity. Hence, suitable heat removal arrangement is needed for better adsorption performance in the bed where adsorber diameter is quite more.
- Higher mass transfer coefficient leads to smaller MTZ length because of higher rate of mass transfer. This, in turn, makes the concentration breakthrough steeper, indicating strong adsorption behaviour, which is also revealed through temperature breakthrough curves where with increase in mass transfer coefficient temperature peak is higher and narrower. So, the study on the effect of the mass transfer coefficient helps to find out the nature of the changes in the concentration and temperatures breakthrough curves and thereafter the design considerations.
- Higher saturation adsorption capacity is always desired for any industrial scale separation. Saturation adsorption capacity can be improved by replacing the existing adsorbent with a better adsorbent, increasing the adsorption surface area per unit volume of the adsorbent and by surface modification of the adsorbent. The constant pattern behaviour suggests that mechanism of mass and heat transfer do not get disturbed with changes in the saturation adsorption capacity.

- With lower heat of adsorption values, the concentration curves become flatter showing weak adsorption behaviour with wide and low peak for temperature breakthrough curves. Though higher heat of adsorption (when Langmuir constant b is kept independent) value is expected to make the system more non-ideal by making the concentration breakthrough flatter, with high and narrow peak in temperature breakthrough curves, the reverse observation in case of concentration breakthrough in the present case is due to change of b with heat of adsorption.
- Changes in values of h_w do not significantly influence the concentration breakthrough curves. *Smaller values of h_w increases the temperature of the bed and gas leading to higher and wider temperature peak.*
- The solid-gas heat transfer coefficient does not influence significantly the concentration and temperature breakthrough curves within the range of the study.
- With increase in mass axial dispersion coefficient, the mass transfer zone length increases due to axial mixing and the system behaves like a poorer adsorbate-adsorbent system, which is not desirable for design of an efficient adsorber.

Table 4.2.2.1: Variables Studied in Packed Bed Adsorption Experiments

System	Molecular sieve	Variable	Range of study
Ethyl Acetate (EA)- Air	E-merck 5A and 13X	Inlet concentration of EA (c_o), kg/m^3	0.22-0.71
		Inlet velocity (v_o) $\times 10^3$, m/s	2.88-14.8
		Bed height (L), m	0.06-0.18

Table 4.2.2.2: Operating conditions for Adsorption of Ethyl Acetate on E-merck 5A Molecular sieves

Run No.	Inlet EA concentration (c_o), kg/m^3	Inlet velocity (v_o), $\times 10^3$, m/s	Bed height (L), m	$T_{g_o} = T_{s_o}$, $^{\circ}\text{C}$
DS3	0.60	8.0	0.18	34
DS 4	0.37	4.6	0.18	32
DS 5	0.23	2.88	0.18	32
DS 7	0.37	2.88	0.18	32
DS 9	0.37	8.0	0.06	32
DS 10	0.37	4.6	0.18	34
DS 11	0.37	8.0	0.12	32
DS 12	0.71	4.6	0.18	32
DS 13	0.37	8.0	0.18	32
DS 14	0.22	9.0	0.18	32
	0.25			

Table 4.2.2.3: Operating conditions for Adsorption of Ethyl Acetate on E-merck 13X Molecular sieves

Run No.	Inlet EA concentration (c_o), kg/m^3	Inlet velocity (v_o), $\times 10^3$, m/s	Bed height (L), m	$T_{g_o} = T_{s_o}$, $^{\circ}\text{C}$
DS15	0.60	8.0	0.18	34
DS 16	0.50	8.0	0.18	34
DS 17	0.71	8.0	0.18	34
DS 18	0.37	8.0	0.18	32
DS 19	0.30	9.0	0.18	33
DS 20	0.37	4.6	0.18	32
DS 21	0.37	8.0	0.12	34
DS 22	0.60	8.0	0.06	34
DS 24	0.37	14.8	0.18	32

Table 4.2.3.1: Values of Model input Parameters for Simulation of Experimental Runs

Basic Parameters	E-merck 5A	E-merck 13X
Inlet concentration, kg of EA / m ³ of fluid	0.22-0.71	0.30-0.71
Superficial Velocity, m/sec x 10 ³	2.88-9.0	4.6-14.8
Bed Length, m x 10 ²	6-18	6-18
Adsorption bed diameter, m x 10 ²	10	10
Molecular weight of fluid, kg	29.0	29.0
Molecular weight of EA, kg	88.0	88.0
Average particle diameter, m	0.00158	0.00158
Fluid viscosity kg/m/sec x 10 ⁵	1.86	1.86
Adsorbate molecular diffusivity, m ² /sec x 10 ⁶	8.9	8.9
Bed voidage	0.4	0.4
Inlet fluid temperature, K	305-307	305-307
Initial solid temperature, K	305-307	1524.0
Particle external surface area, m ² /m ³ of bed	1524.0	1.165
Fluid density, kg/m ³ of fluid	1.165	600
Solid density kg/m ³ of bed	650	1006
Fluid specific heat, J/kg/K	1006	1050
Solid specific heat, J/kg/K	1050	0.0267
Fluid thermal conductivity, J/m/sec/K	0.0267	5.0
Overall mass transfer coefficient, 1/sec x 10 ⁴	1.5	18.0
Wall to bed heat transfer coefficient, J/m ² /sec/K	15.0	1.30689
Heat of adsorption, J/kg x 10 ⁻⁵	0.75	0.587, 0.269
Langmuir constants, q _s , b	0.372, 35.70	94.477
Universal gas constant, J/kg/K	94.477	

Table 4.2.3.2: Statistical Analysis Results: Model vs. Experiment (E-merck 5A molecular sieves)

Run No.	Std. Dev. (Simulation with calculated heat of adsorption value) for concentration breakthrough curves	Std. Dev. (Simulation with decreased heat of adsorption value) for concentration breakthrough curves
DS3	0.028	0.024
DS4	0.009	0.0085
DS5	0.0093	0.009
DS7	0.0099	0.0095
DS9	0.021	0.017
DS10	0.027	0.025
DS11	0.056	0.055
DS12	0.007	0.0093
DS13	0.033	0.014
DS14	0.044	0.05

Table 4.2.3.3: Statistical Analysis Results: Model vs. Experiment (E-merck 13X molecular sieves)

Run No.	Std. Dev. (With axial dispersion)		Std. Dev. (Without axial dispersion)	
	Concentration Breakthrough	Temperature Breakthrough	Concentration Breakthrough	Temperature Breakthrough
DS15	0.022	0.0026	0.016	0.00084
DS16	0.012	0.0016	0.01	0.00057
DS17	0.028	0.0027	0.015	0.0010
DS18	0.024	0.0013	0.0154	0.0010
DS19	0.031	0.0007	0.027	0.00064
DS20	0.08	0.001	0.0044	0.00067
DS21	0.028	0.0032	0.017	0.003
DS22	0.042	0.005	0.034	0.0024
DS24	0.033	0.0022	0.03	0.0019

Table 4.2.4.1 Variables with Range of Values used for Theoretical Study of Ethyl Acetate Adsorption

Variables	Range of Values
Inlet concentration, kg of EA / m ³ of fluid	0.2 - 0.71
Superficial Velocity, m/sec x 10 ³	4.0 - 9.0
Bed Length, m x 10 ²	6 - 24
Adsorption bed diameter, m x 10 ²	2.5 - 10
Mass transfer coefficient, k, 1/sec x 10 ⁴	0.9 - 10
Saturation capacity, q _s , kg adsorbate/ kg adsorbent	0.4 - 0.64
Heat of Adsorption, (-ΔH), J/kg x 10 ⁻⁵	0.5 - 2.0
Bed to wall heat transfer coefficient, h _w , J/m ² /sec/K	0 - 25
Solid-fluid heat transfer coefficient, h _w , J/m ² /sec/K	10 - 60
Dispersion coefficient, D _a , m ² /sec x 10 ⁴	0 - 3.12

Table 4.2.4.2 Base Values of Model Input Parameters for Ethyl Acetate Adsorption

Parameters	Base Values
	0.60
Inlet concentration, kg of EA / m ³ of fluid	8.0
Superficial Velocity, m/sec x 10 ³	18.0
Bed Length, m x 10 ²	10.0
Adsorption bed diameter, m x 10 ²	26.9
Langmuir Constant, b ₀ , m ³ /kg x 10 ²	5.0
Mass transfer coefficient, k, 1/sec x 10 ⁴	0.587
Saturation capacity, q _s , kg adsorbate/ kg adsorbent	1.30689
Heat of Adsorption, (-ΔH), J/kg x 10 ⁻⁵	15.0
Bed to wall heat transfer coefficient, h _w , J/m ² /sec/K	60.0
Solid-fluid heat transfer coefficient, h, J/m ² /sec/K	2.86
Dispersion coefficient, D _a , m ² /sec x 10 ⁴	

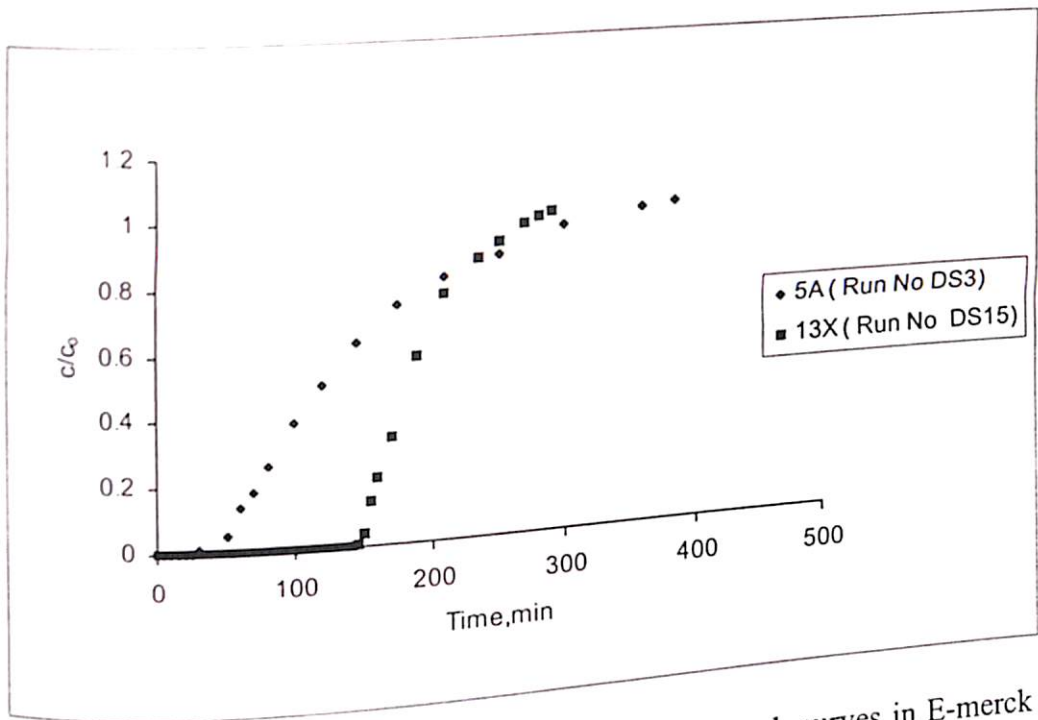


Figure 4.2.2.1: Comparison between concentration breakthrough curves in E-merck 5A and 13X molecular sieves for ethyl acetate adsorption

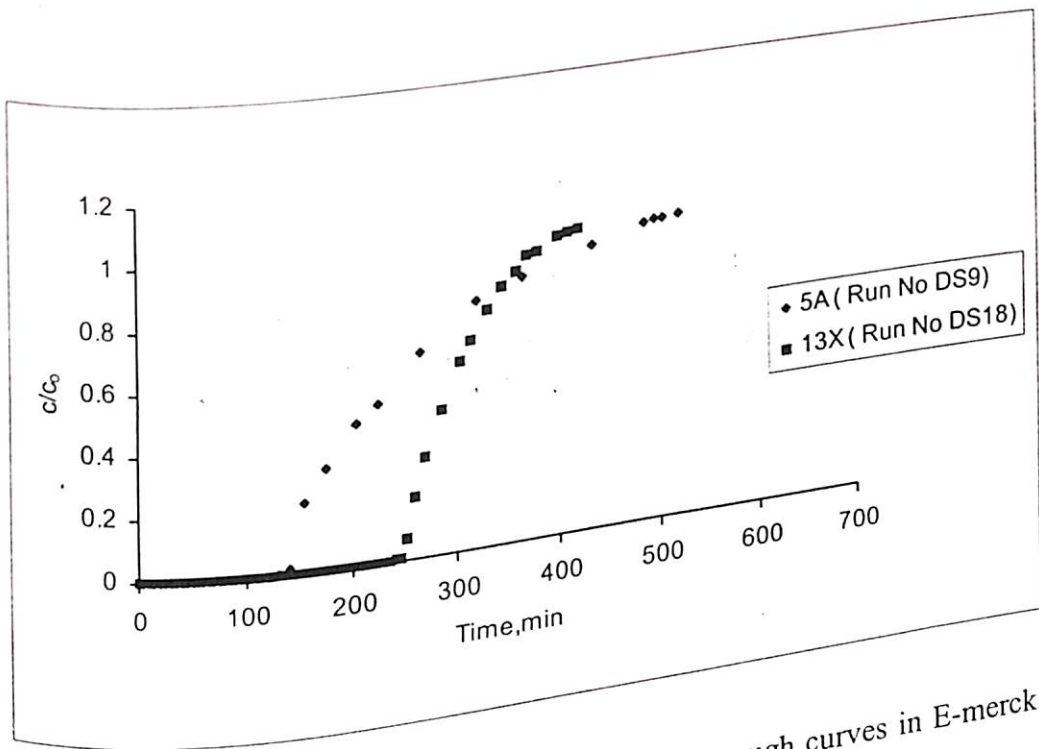


Figure 4.2.2.2: Comparison between concentration breakthrough curves in E-merck 5A and 13X molecular sieves for ethyl acetate adsorption

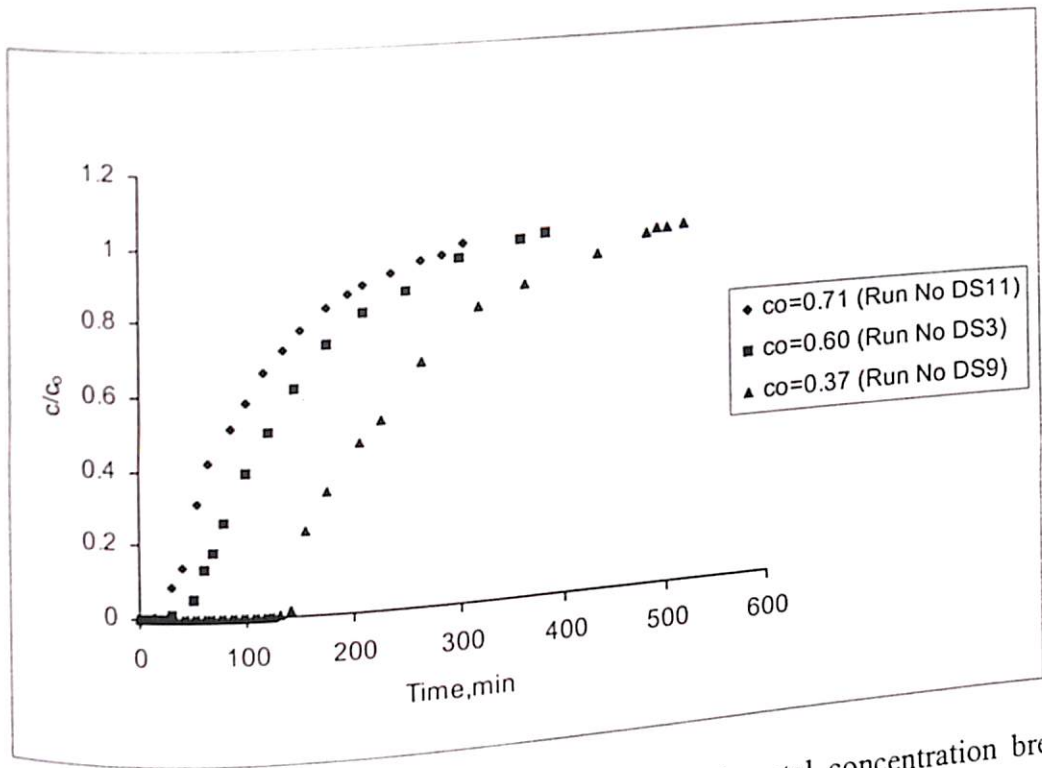


Figure 4.2.2.3: Effect of inlet concentration on experimental concentration breakthrough curves in E-merck 5A molecular sieve of ethyl acetate in air

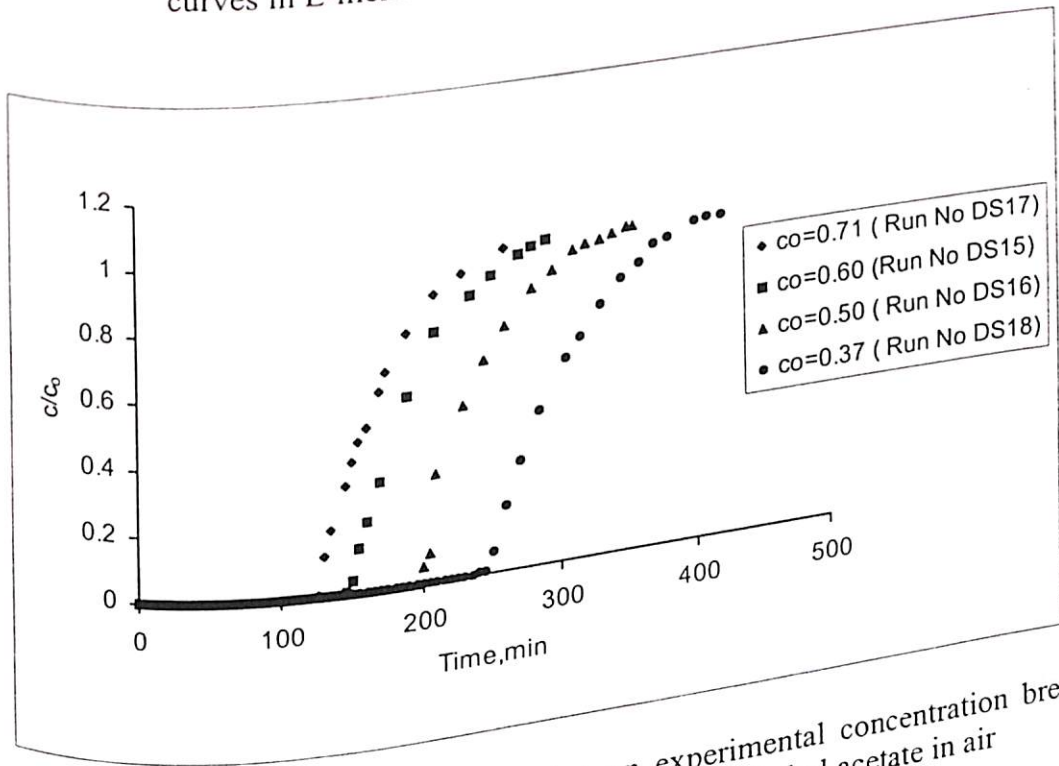


Figure 4.2.2.4: Effect of inlet concentration on experimental concentration breakthrough curves in E-merck 13X molecular sieve of ethyl acetate in air

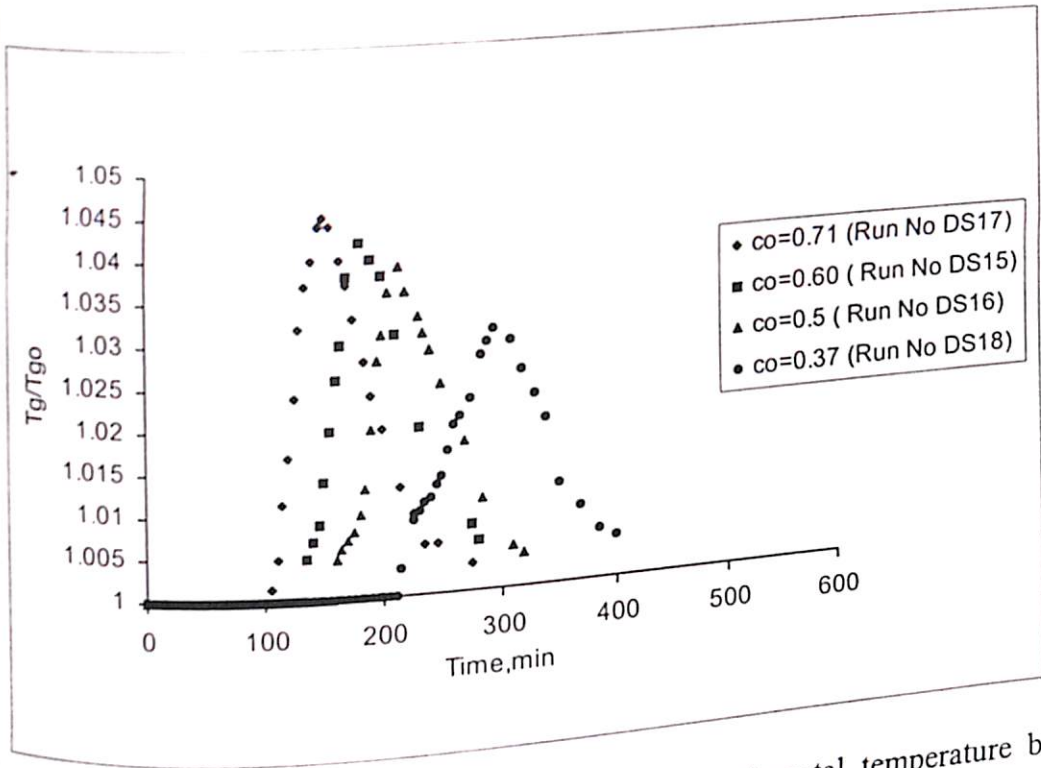


Figure 4.2.2.5: Effect of inlet concentration on experimental temperature breakthrough curves in E-merck 13X molecular sieve of ethyl acetate in air

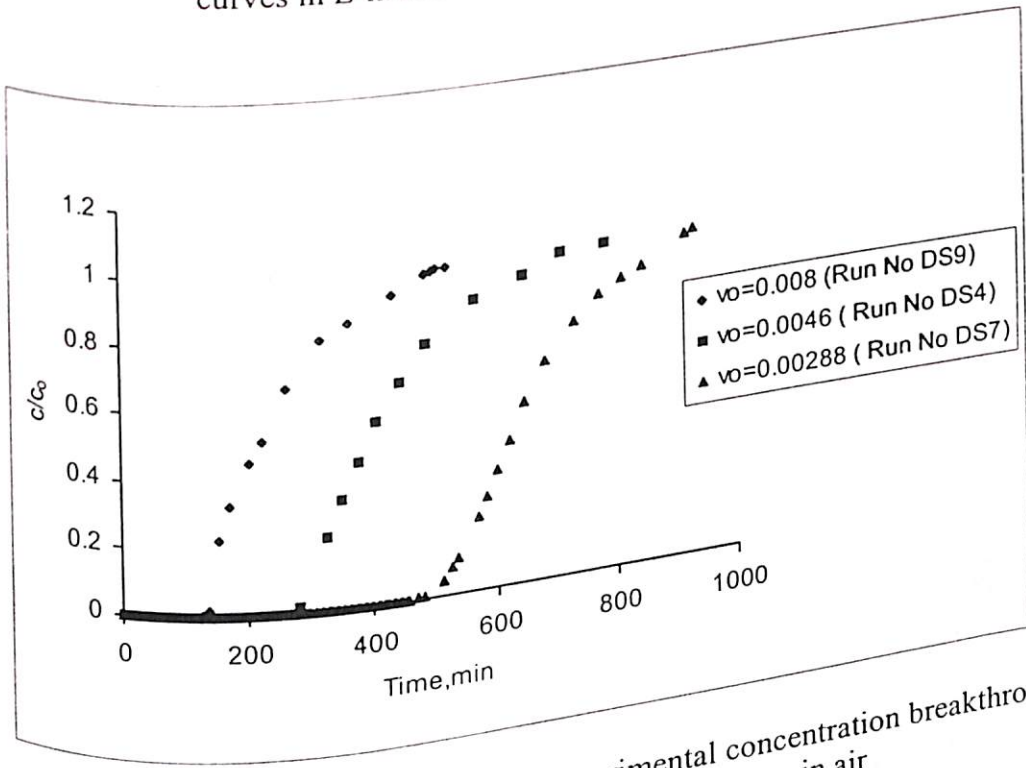


Figure 4.2.2.6: Effect of inlet velocity on experimental concentration breakthrough curves in E-merck 5A molecular sieve of ethyl acetate in air

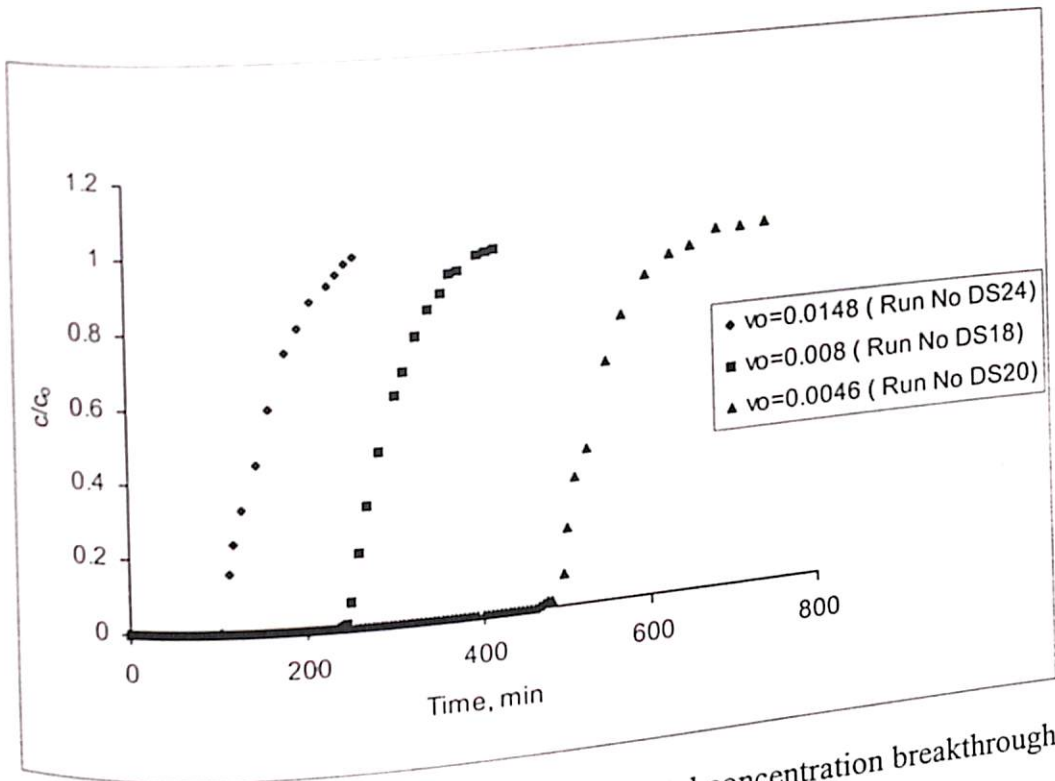


Figure 4.2.2.7: Effect of inlet velocity on experimental concentration breakthrough curves in E-merck 13X molecular sieve of ethyl acetate in air

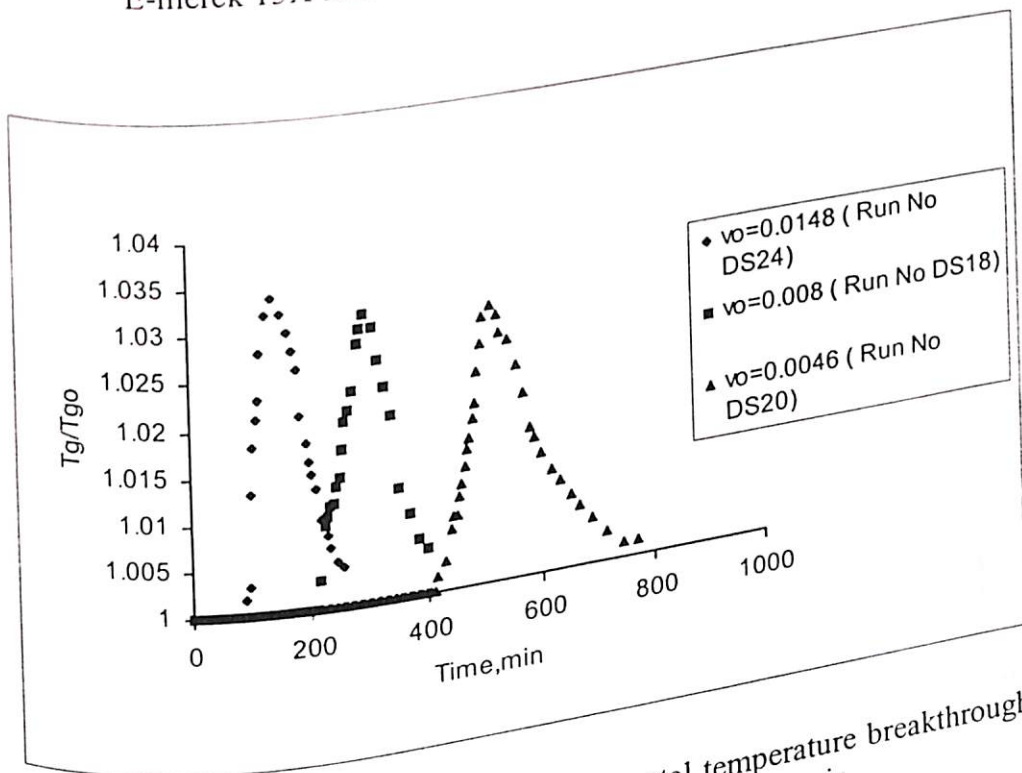


Figure 4.2.2.8: Effect of inlet velocity on experimental temperature breakthrough curves in E-merck 13X molecular sieve of ethyl acetate in air

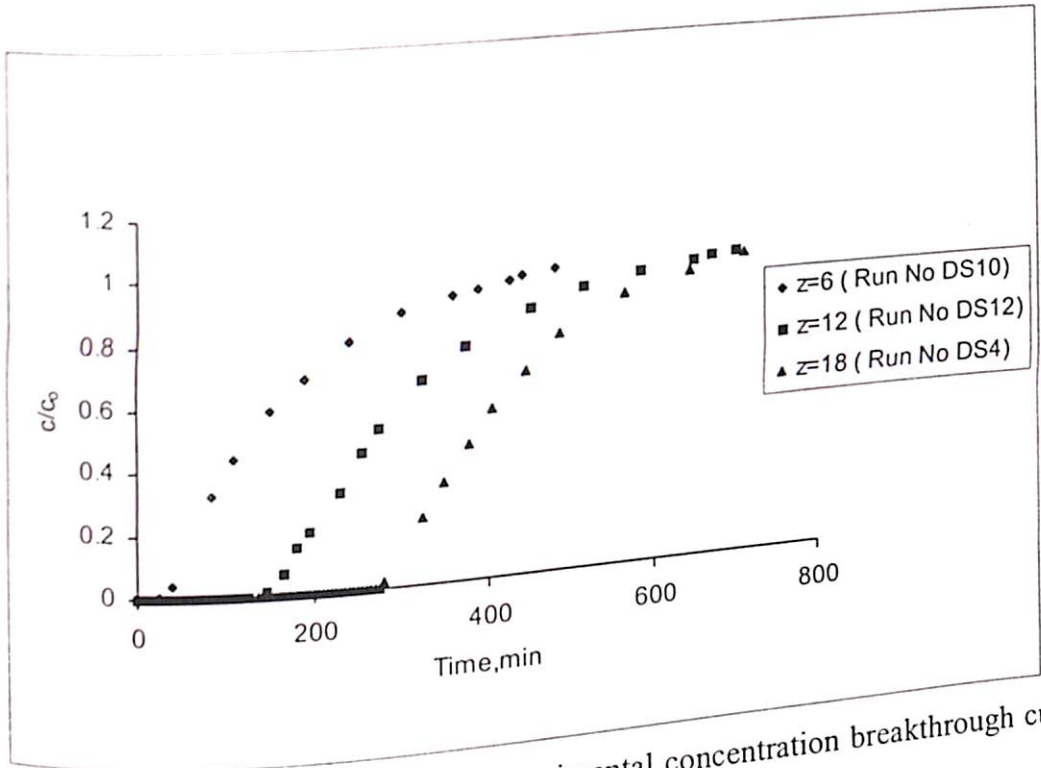


Figure 4.2.2.9: Effect of bed heights on experimental concentration breakthrough curves in E-merck 5A molecular sieve of ethyl acetate in air

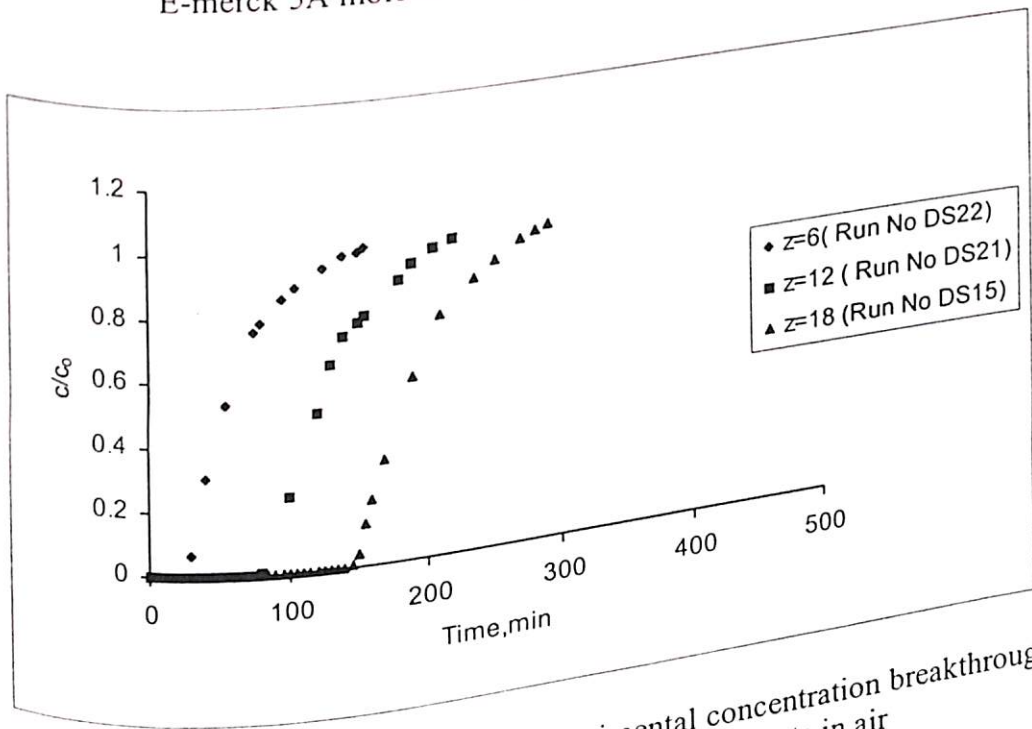


Figure 4.2.2.10: Effect of bed heights on experimental concentration breakthrough curves in E-merck 13X molecular sieve of ethyl acetate in air

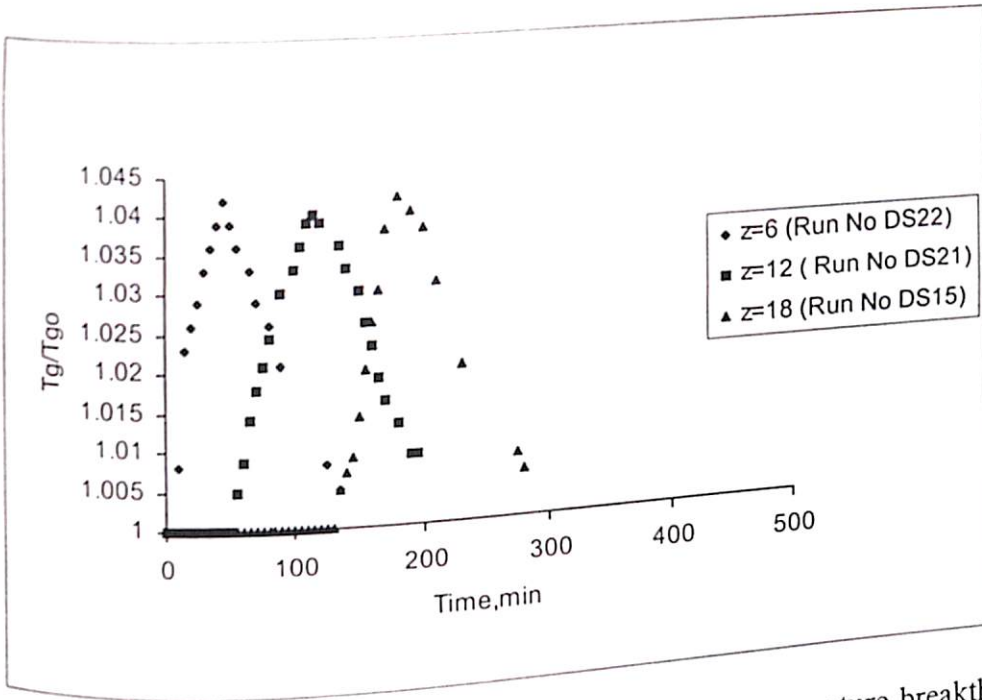


Figure 4.2.2.11: Effect of bed heights on experimental temperature breakthrough curves in E-merck 13X molecular sieve of ethyl acetate in air

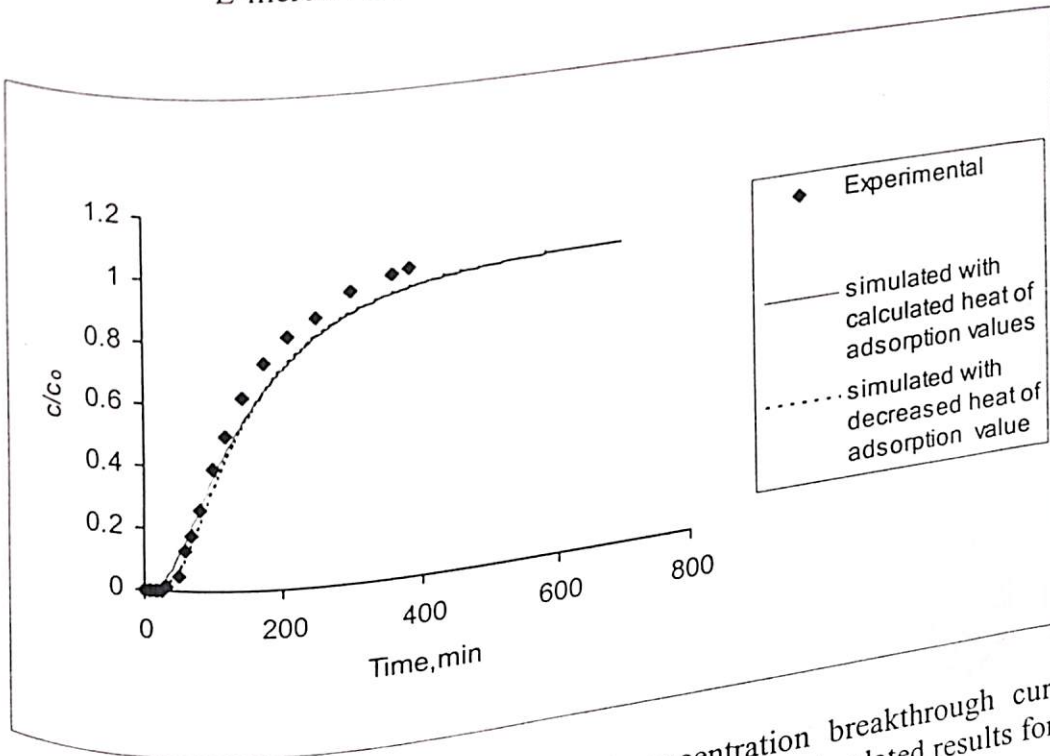


Figure 4.2.3.1: Comparison of experimental concentration breakthrough curve of ethyl acetate in E-merck 5A molecular sieve with simulated results for run DS3

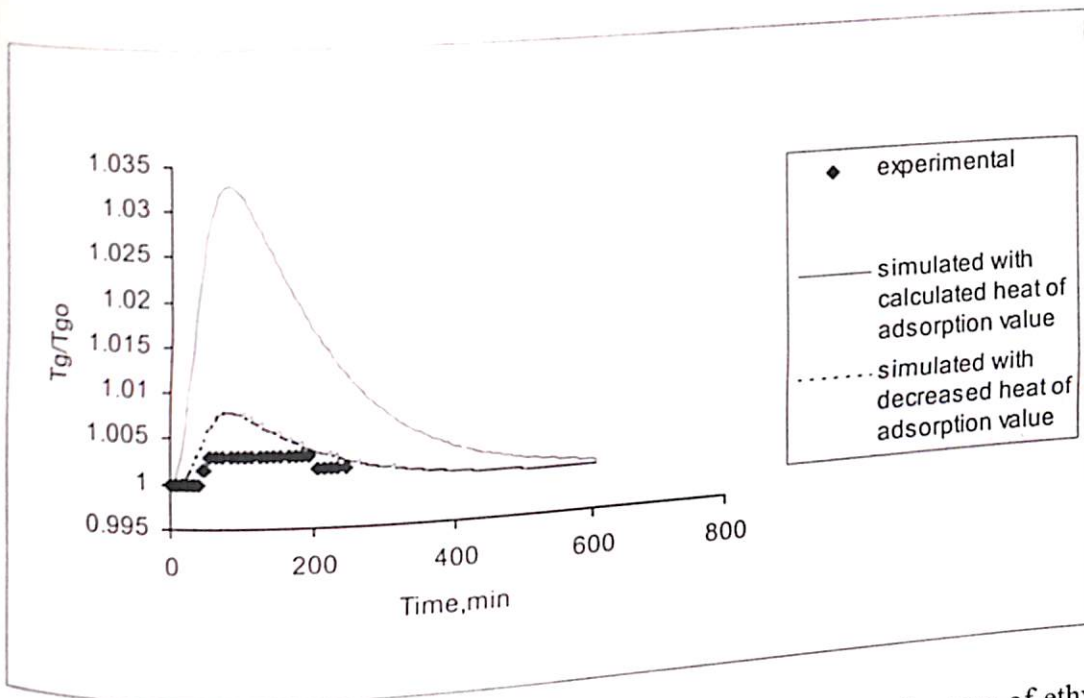


Figure 4.2.3.2: Comparison of experimental temperature breakthrough curve of ethyl acetate in E-merck 5A molecular sieve with simulated results for run DS3

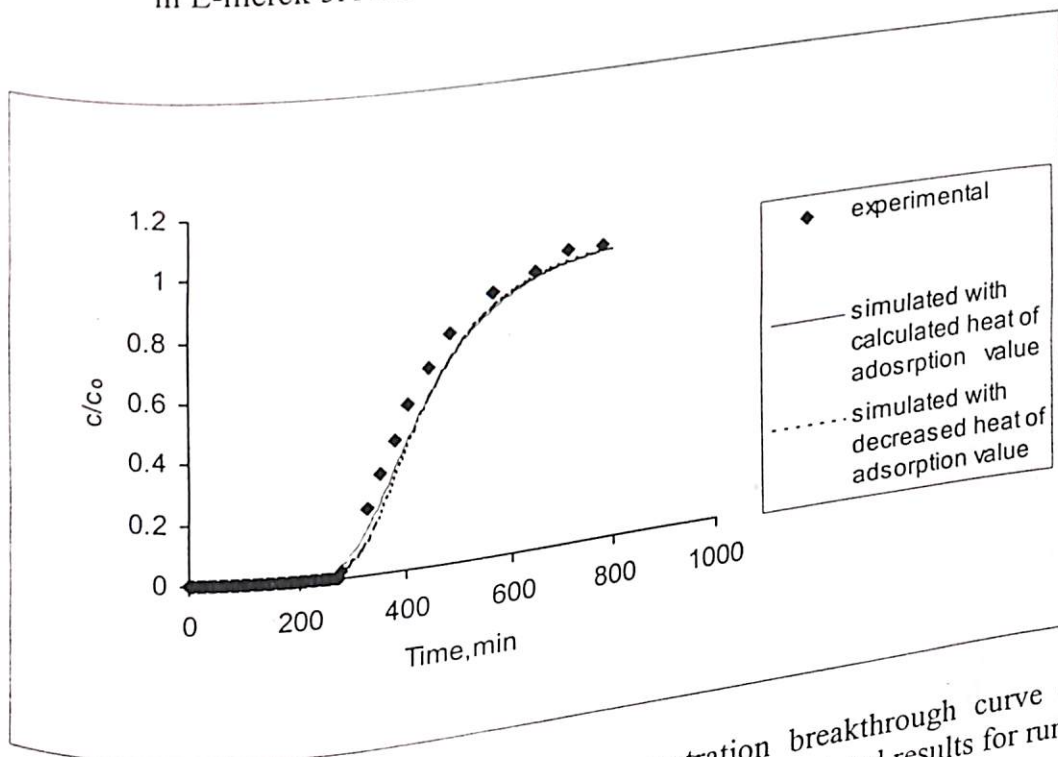


Figure 4.2.3.3: Comparison of experimental concentration breakthrough curve of ethyl acetate in E-merck 5A molecular sieve with simulated results for run DS4

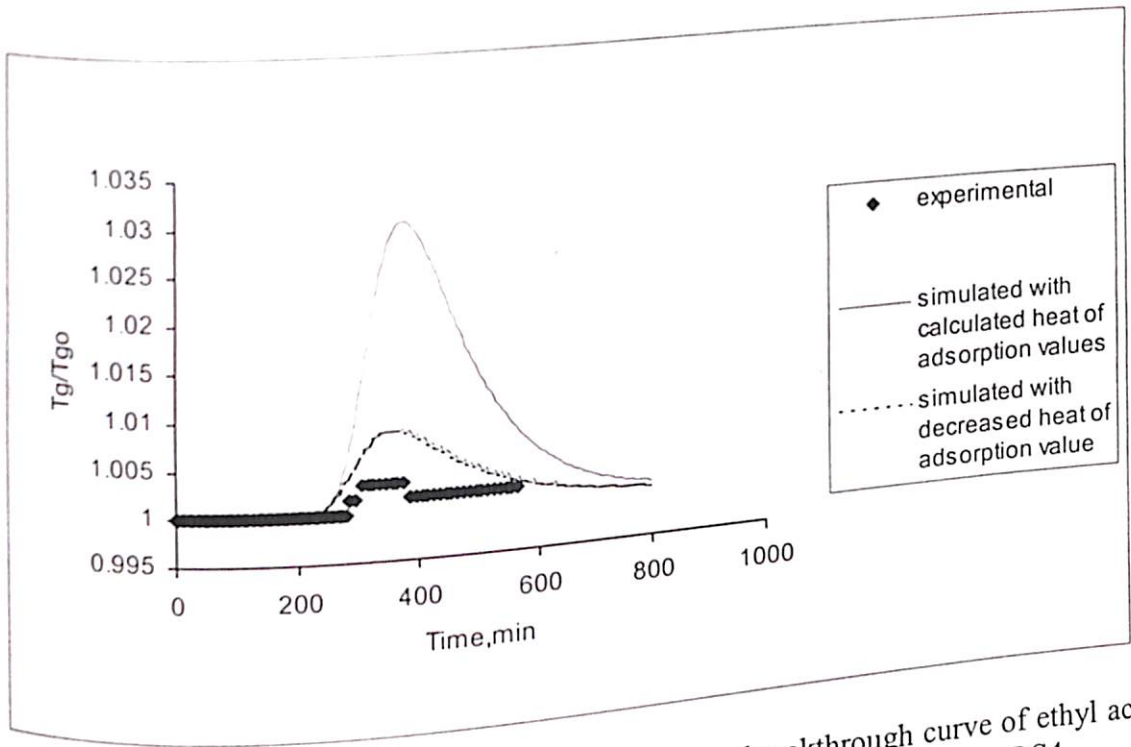


Figure 4.2.3.4: Comparison of experimental temperature breakthrough curve of ethyl acetate in E-merck 5A molecular sieve with simulated results for run DS4

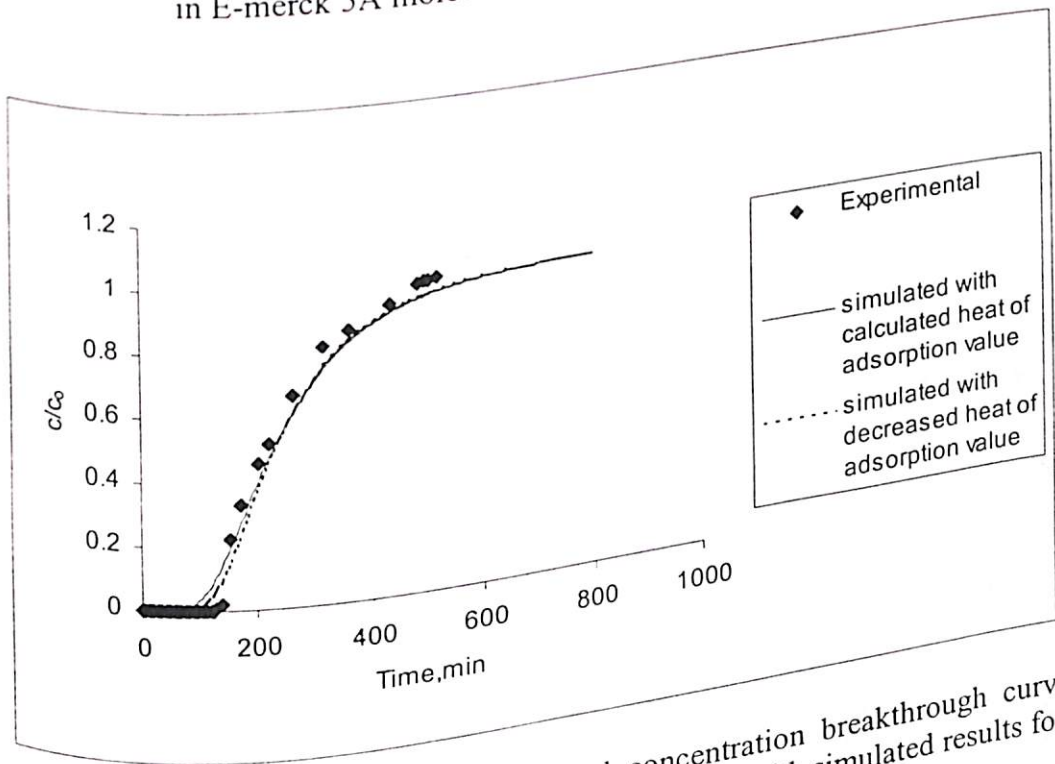


Figure 4.2.3.5: Comparison of experimental concentration breakthrough curve of ethyl acetate in E-merck 5A molecular sieve with simulated results for run DS9

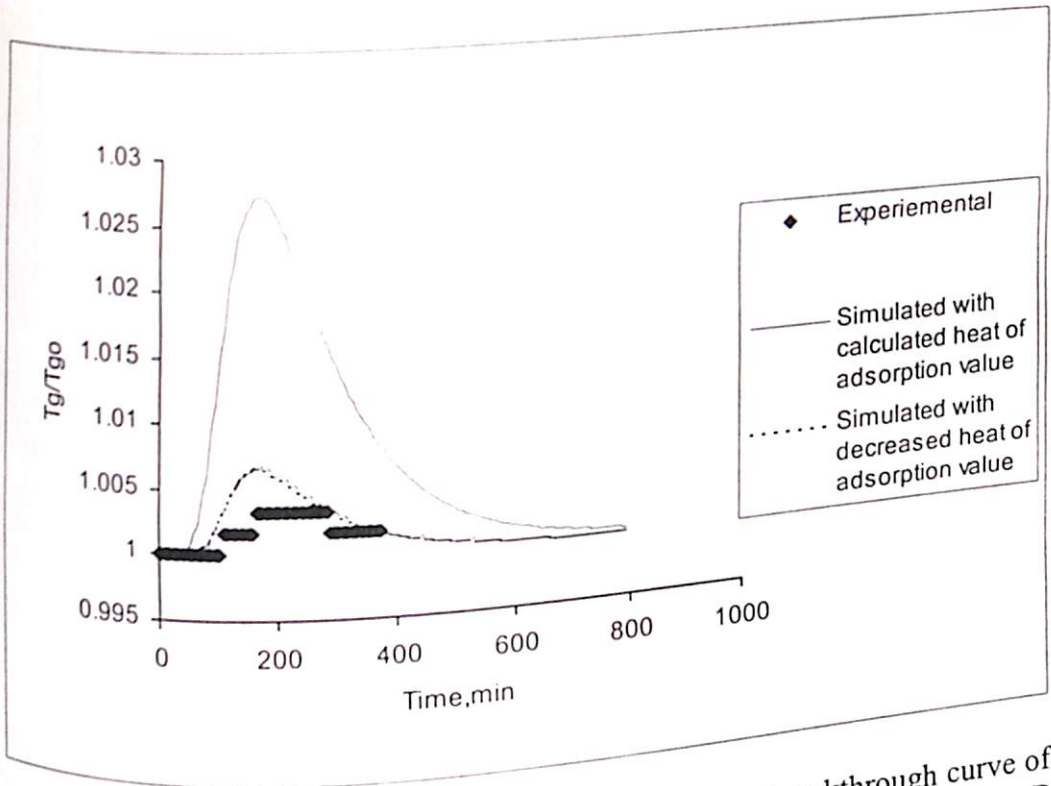


Figure 4.2.3.6: Comparison of experimental temperature breakthrough curve of ethyl acetate in E-merck 5A molecular sieve with simulated results for run DS9

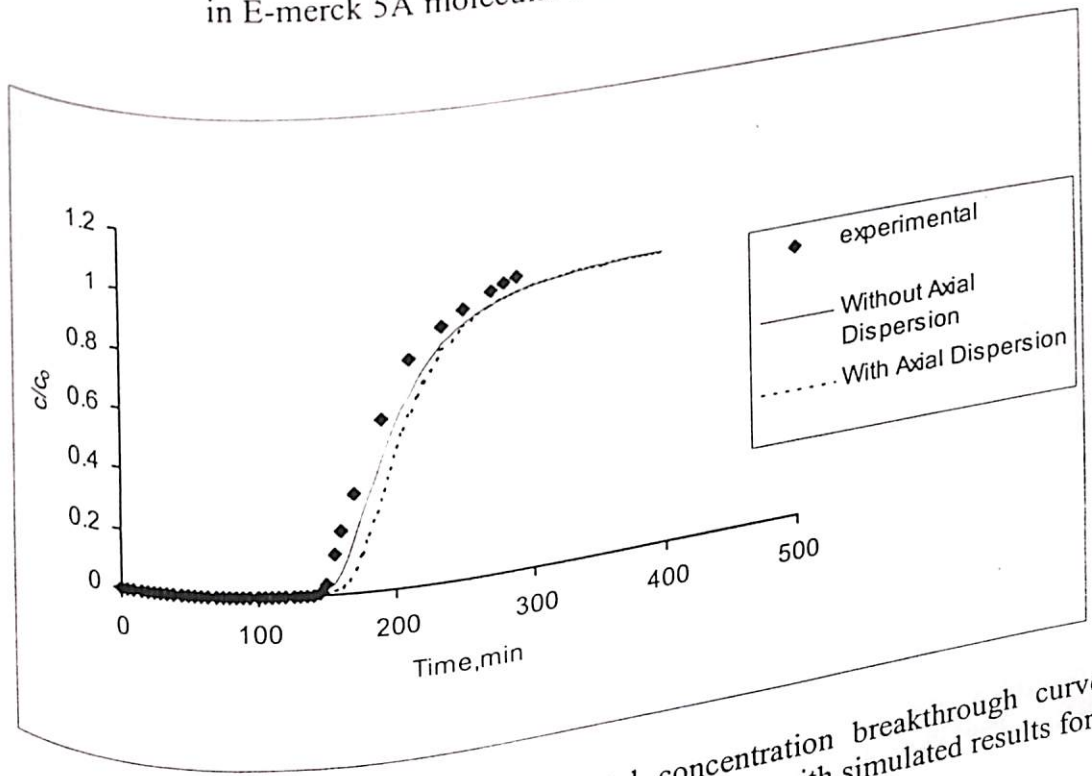


Figure 4.2.3.7: Comparison of experimental concentration breakthrough curve of ethyl acetate in E-merck 13X molecular sieve with simulated results for run DS15

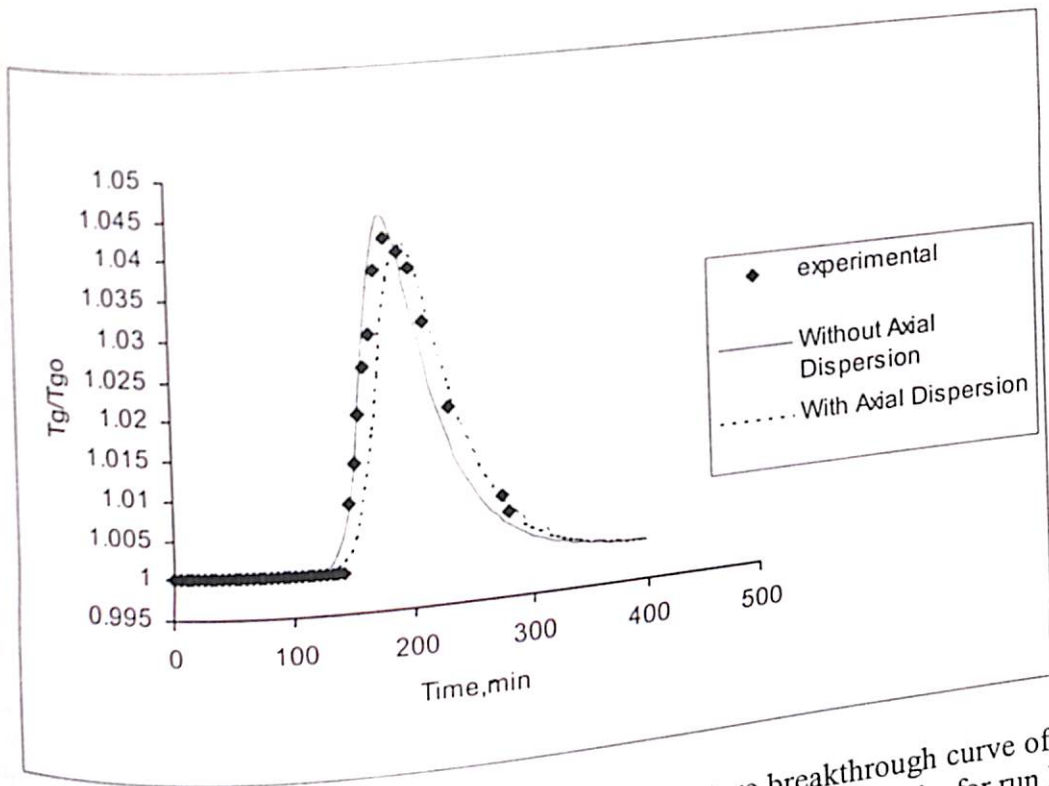


Figure 4.2.3.8: Comparison of experimental temperature breakthrough curve of ethyl acetate in E-merck 13X molecular sieve with simulated results for run DS15

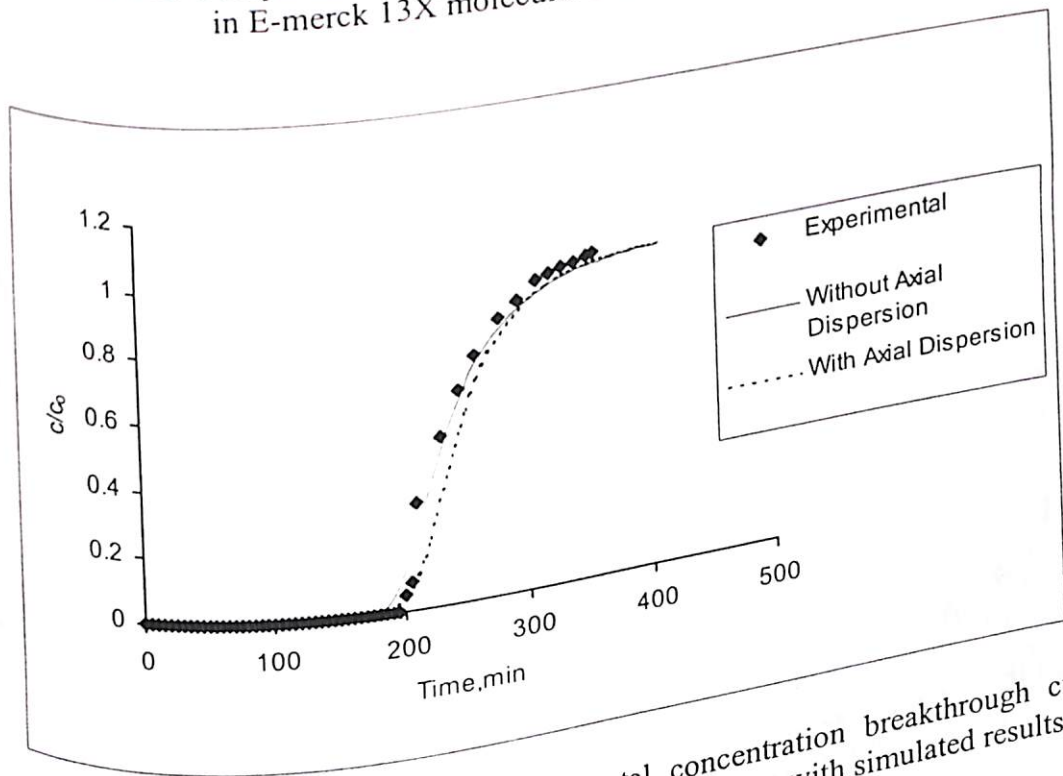


Figure 4.2.3.9: Comparison of experimental concentration breakthrough curve of ethyl acetate in E-merck 13X molecular sieve with simulated results for run DS16

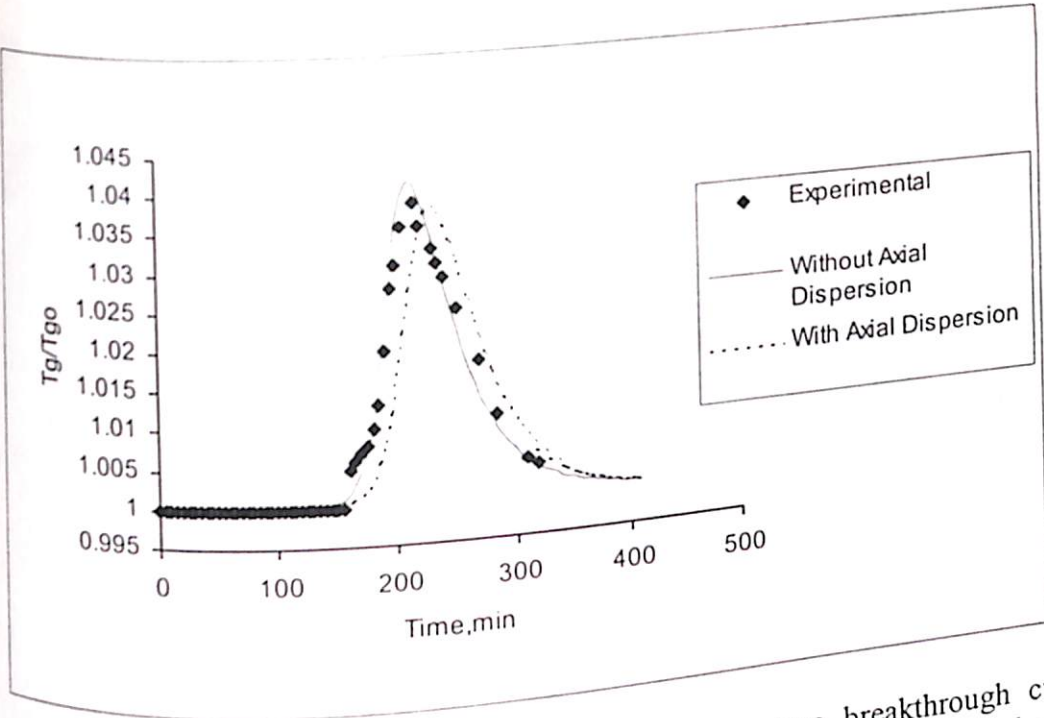


Figure 4.2.3.10: Comparison of experimental temperature breakthrough curve of ethyl acetate in E-merck 13X molecular sieve with simulated results for run DS16

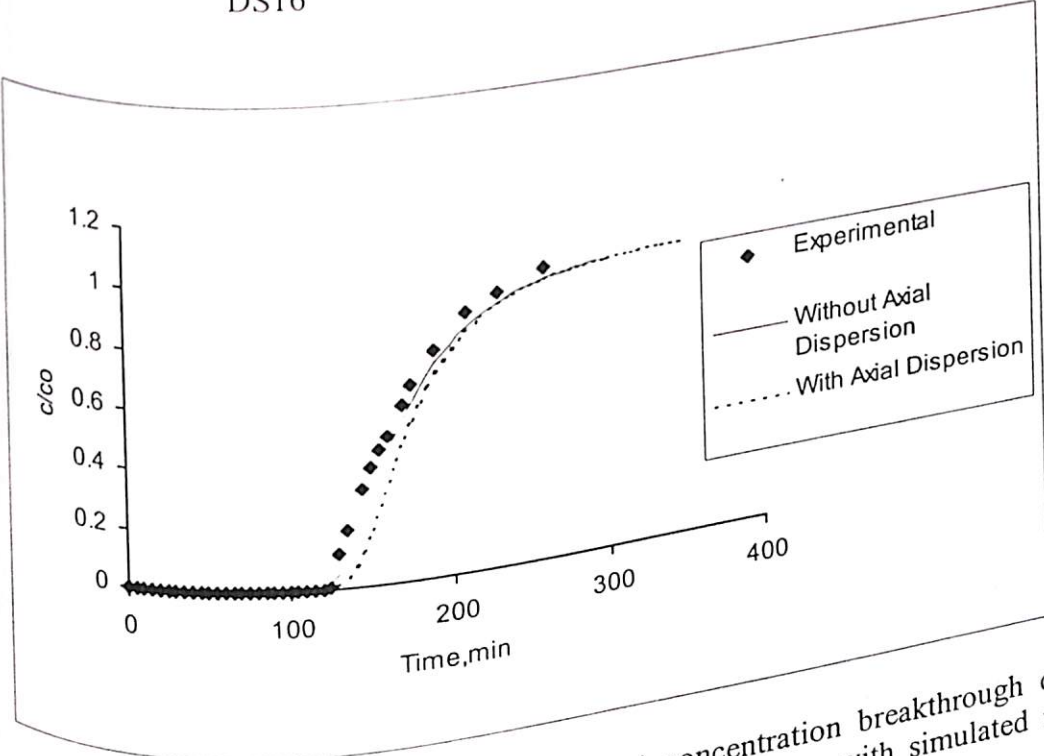


Figure 4.2.3.11: Comparison of experimental concentration breakthrough curve of ethyl acetate in E-merck 13X molecular sieve with simulated results for run DS17

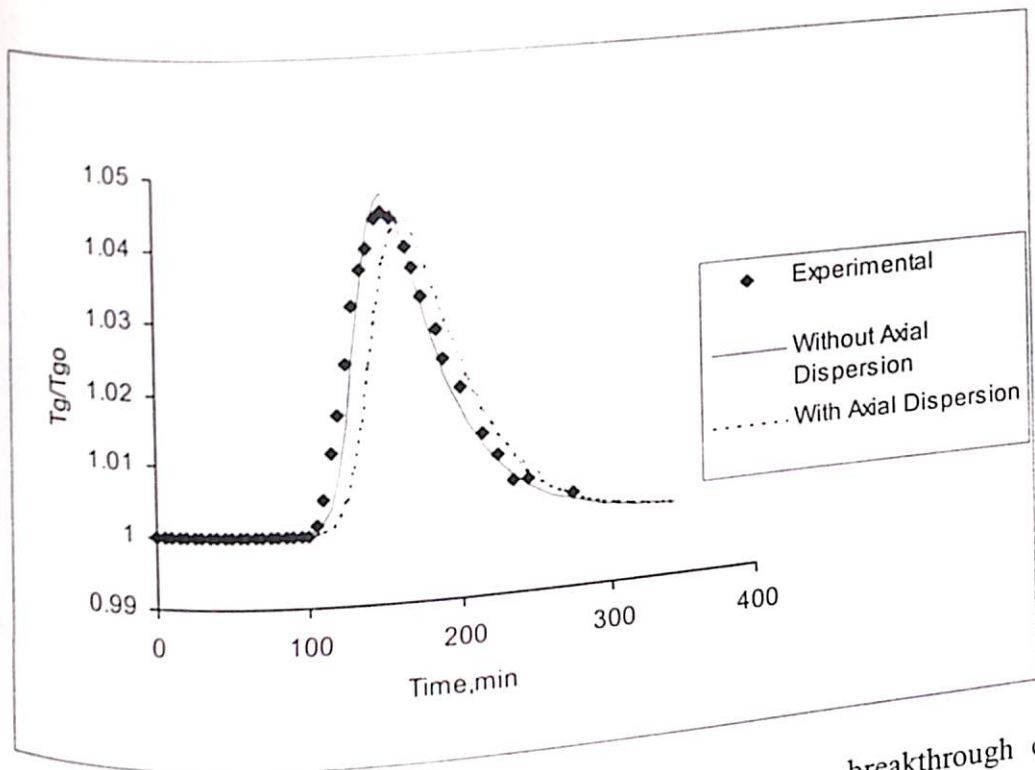


Figure 4.2.3.12: Comparison of experimental temperature breakthrough curve of ethyl acetate in E-merck 13X molecular sieve with simulated results for run DS17

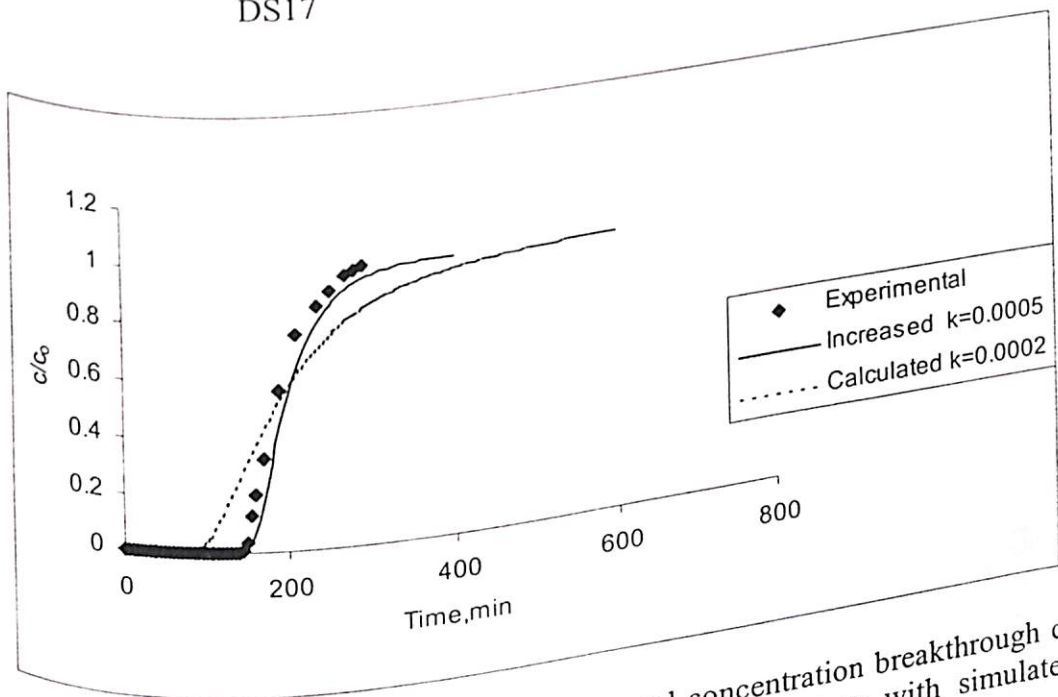


Figure 4.2.3.13 Comparison of experimental concentration breakthrough curve of ethyl acetate in E-merck 13X molecular sieve with simulated results for increased k and calculated k for run DS 15

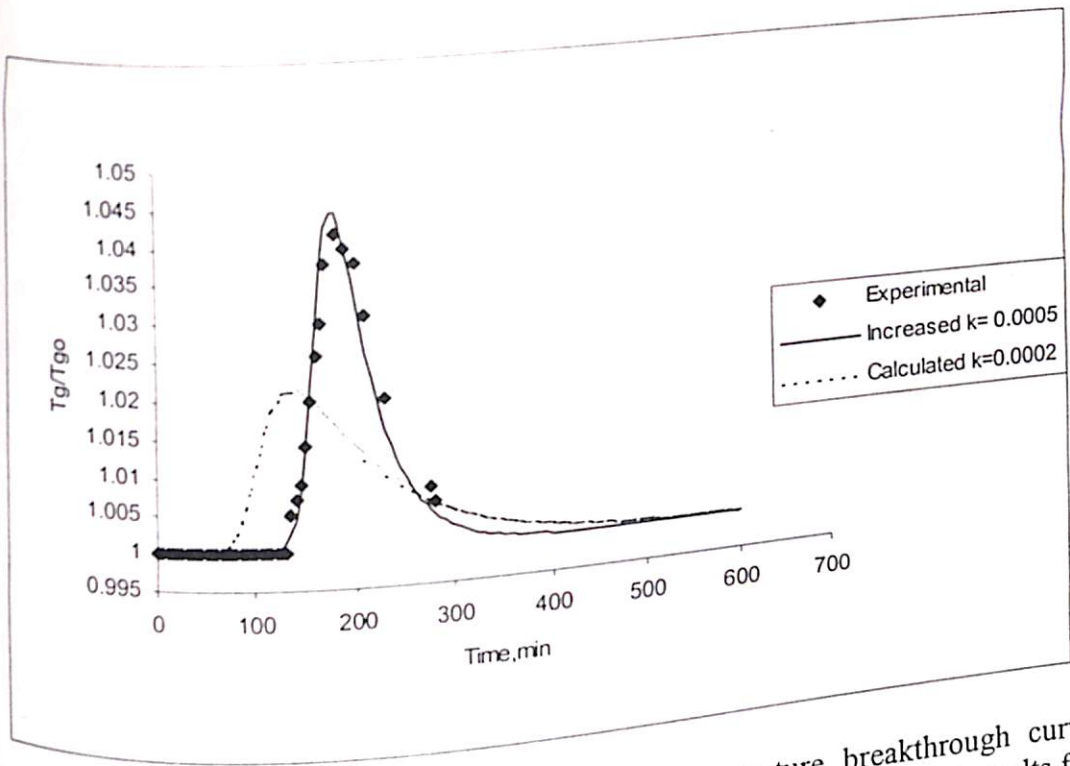


Figure 4.2.3.14 Comparison of experimental temperature breakthrough curve of ethyl acetate in E-merck 13X molecular sieve with simulated results for increased k and calculated k for run DS 15

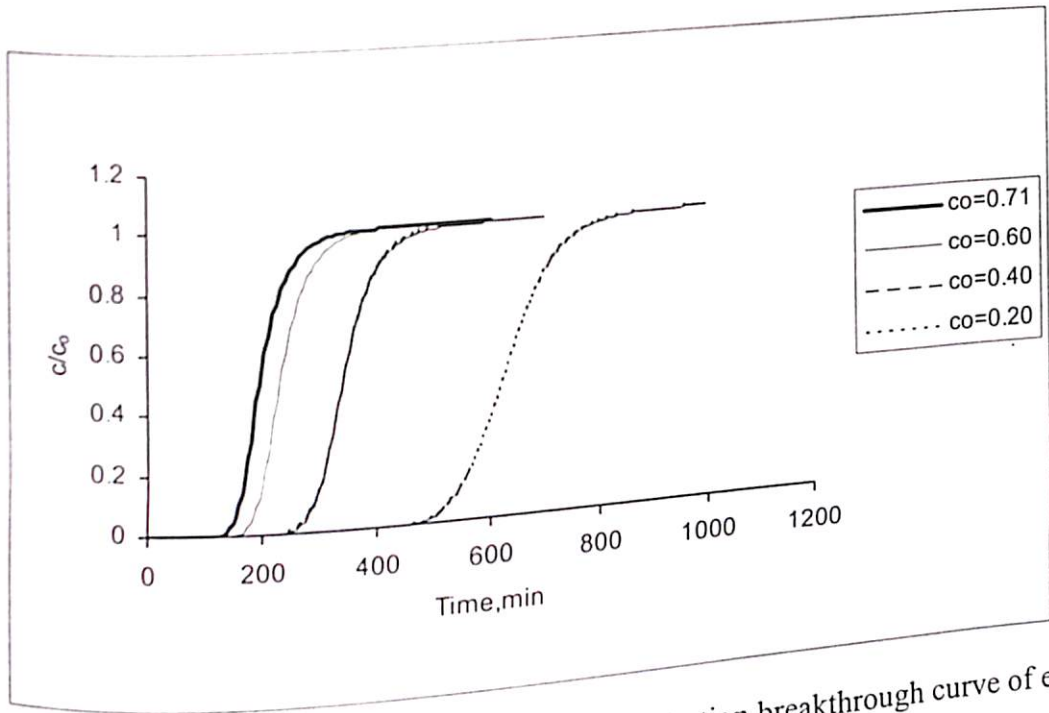


Figure 4.2.4.1: Effect of inlet concentration on concentration breakthrough curve of ethyl acetate

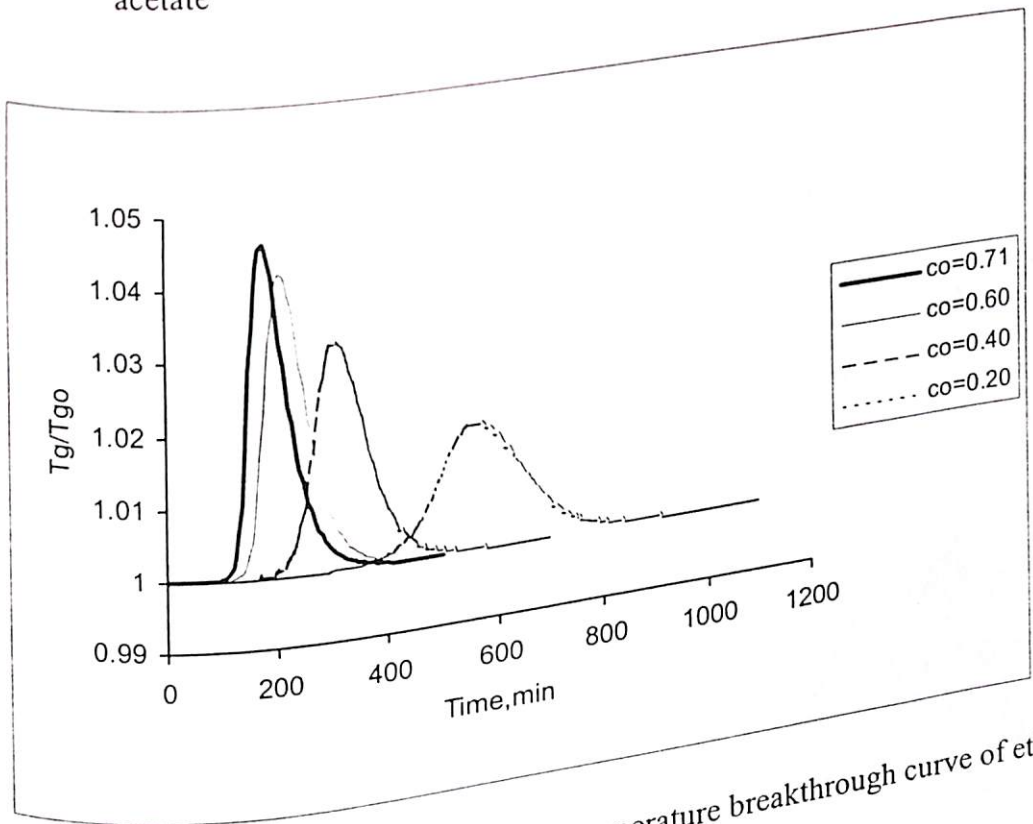


Figure 4.2.4.2: Effect of inlet concentration on temperature breakthrough curve of ethyl acetate

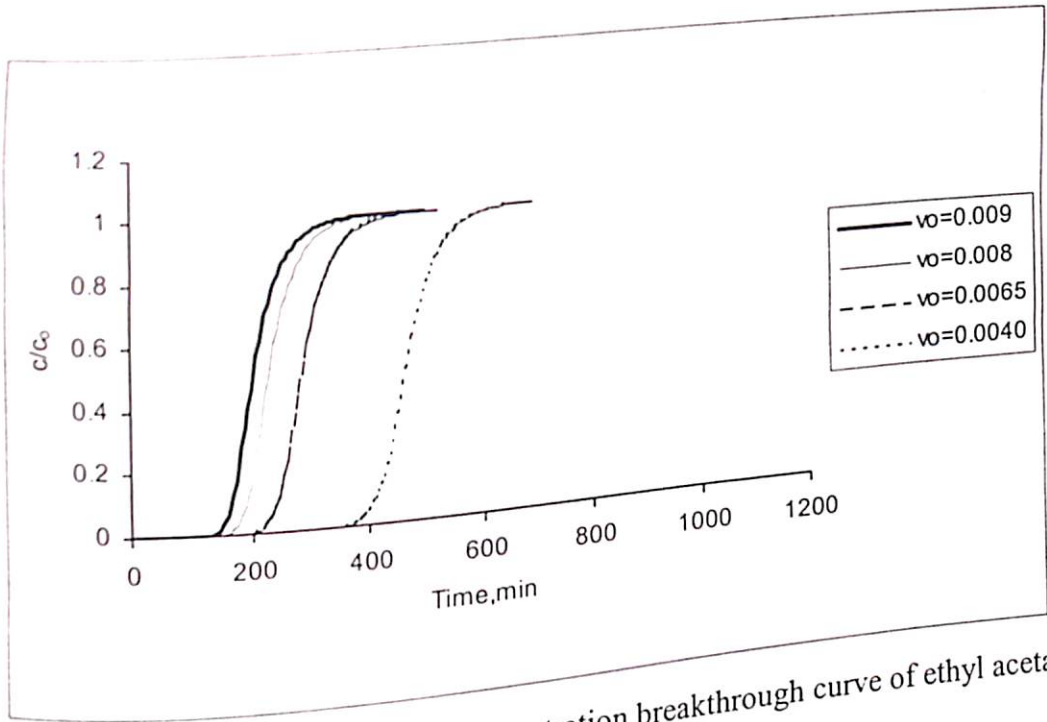


Figure 4.2.4.3: Effect of inlet velocity on concentration breakthrough curve of ethyl acetate

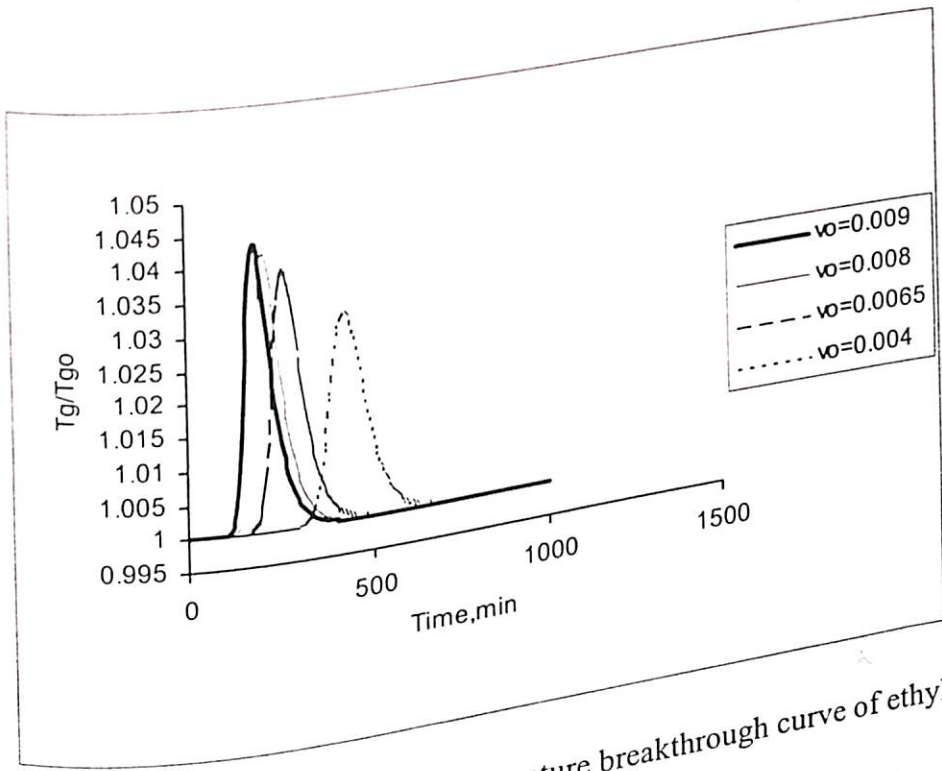


Figure 4.2.4.4: Effect of inlet velocity on temperature breakthrough curve of ethyl acetate

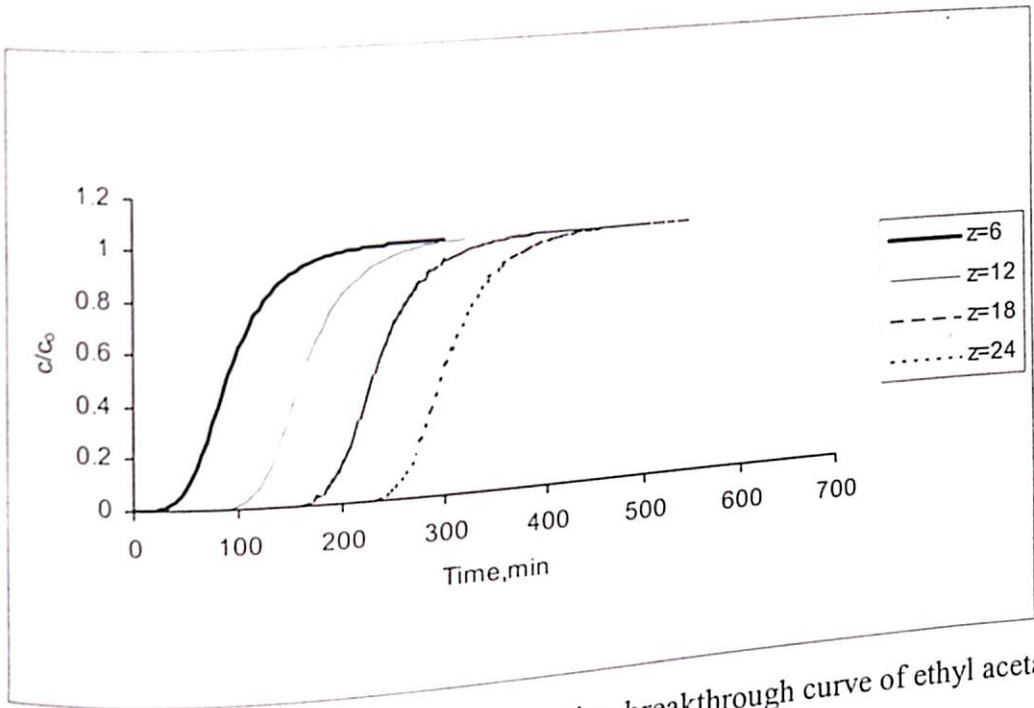


Figure 4.2.4.5: Effect of bed height on concentration breakthrough curve of ethyl acetate

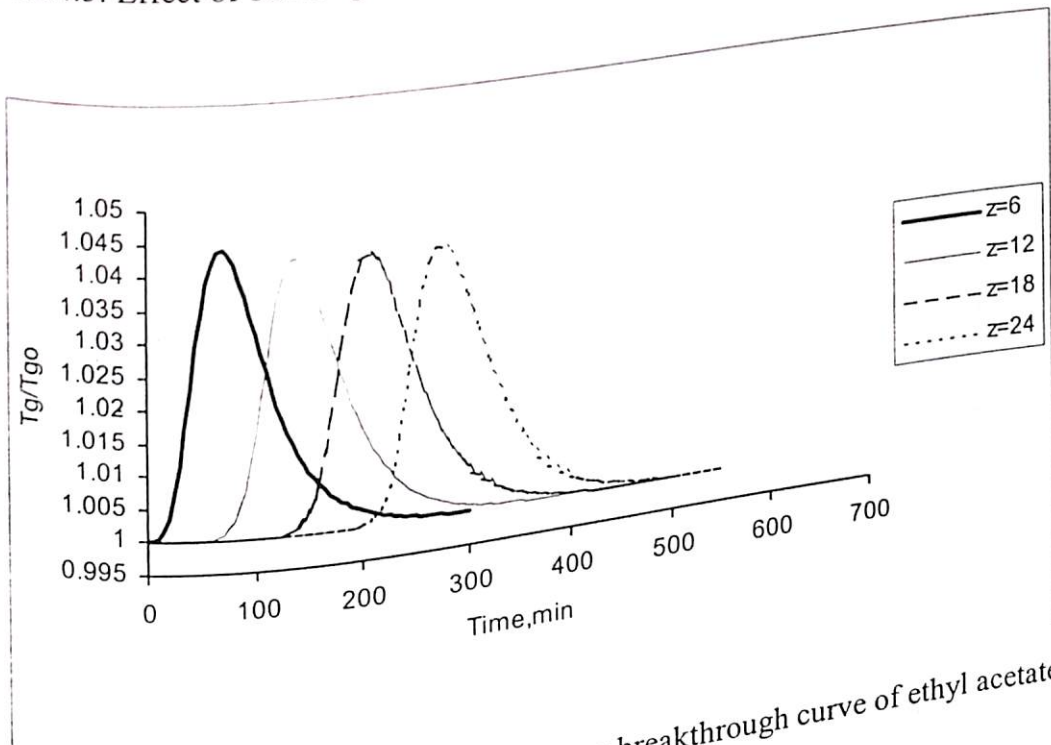


Figure 4.2.4.6: Effect of bed height on temperature breakthrough curve of ethyl acetate

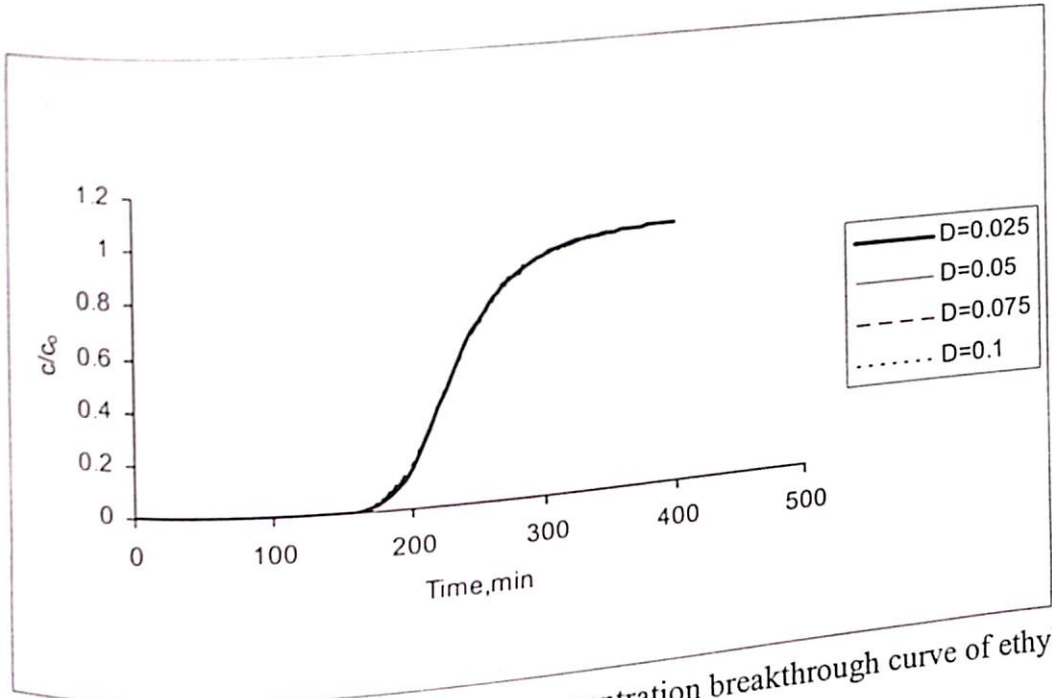


Figure 4.2.4.7: Effect of bed diameter on concentration breakthrough curve of ethyl acetate

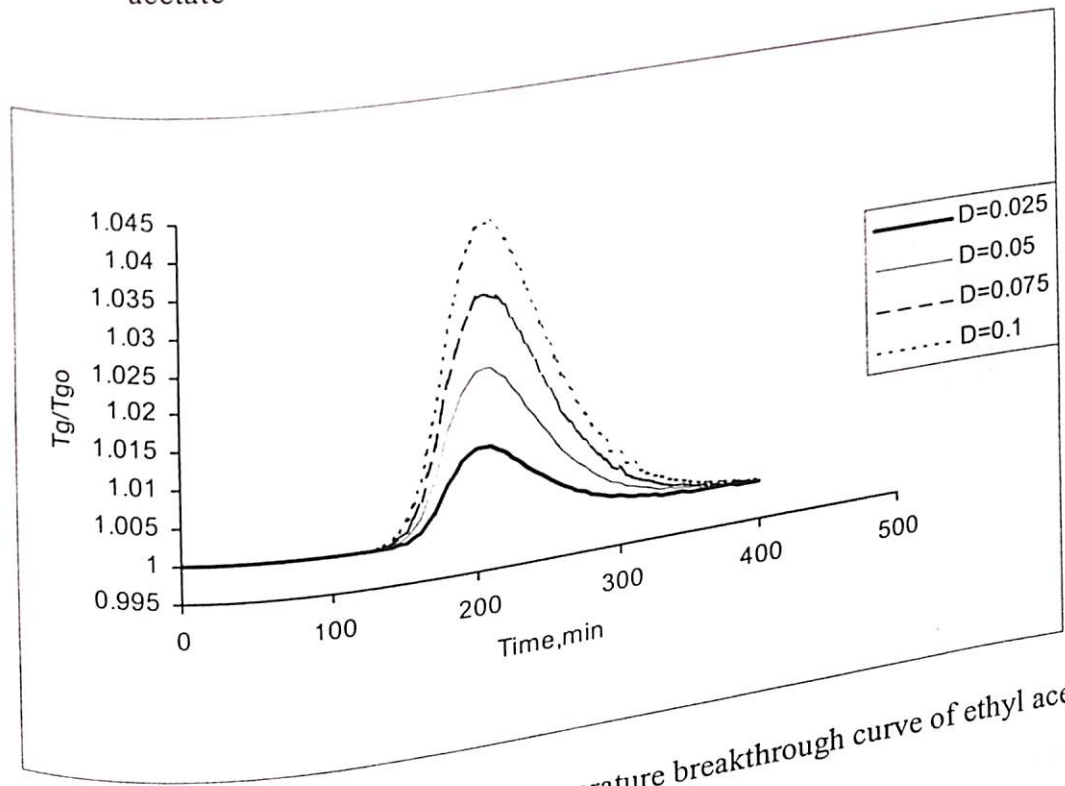


Figure 4.2.4.8: Effect of bed diameter on temperature breakthrough curve of ethyl acetate

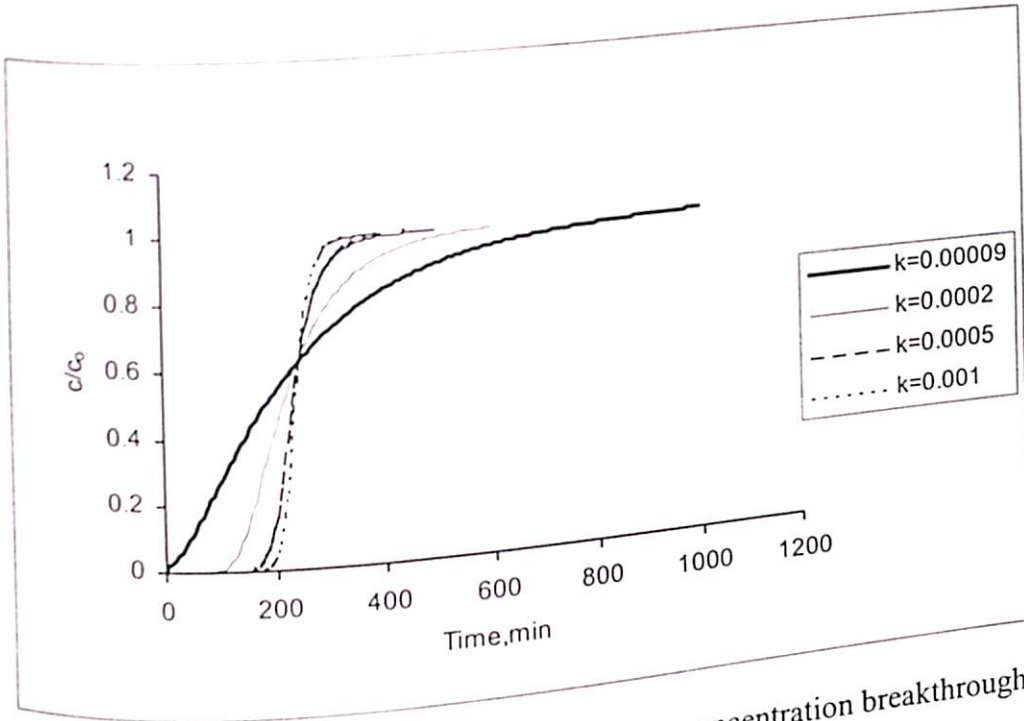


Figure 4.2.4.9: Effect of mass transfer coefficient on concentration breakthrough curve of ethyl acetate

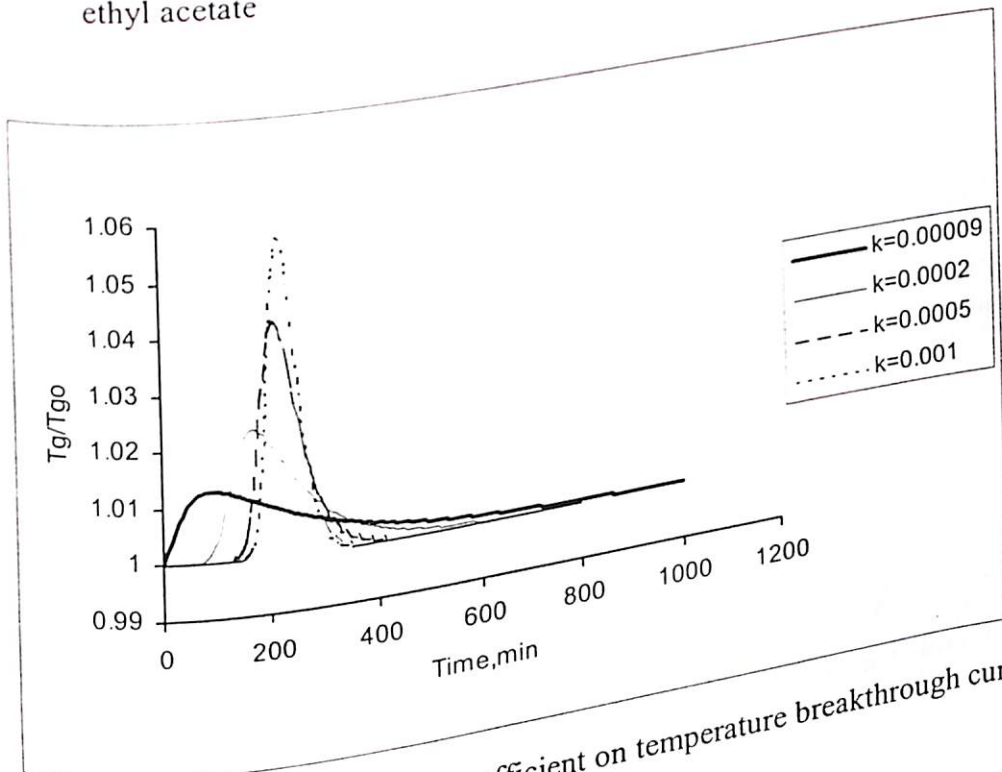


Figure 4.2.4.10: Effect of mass transfer coefficient on temperature breakthrough curve of ethyl acetate

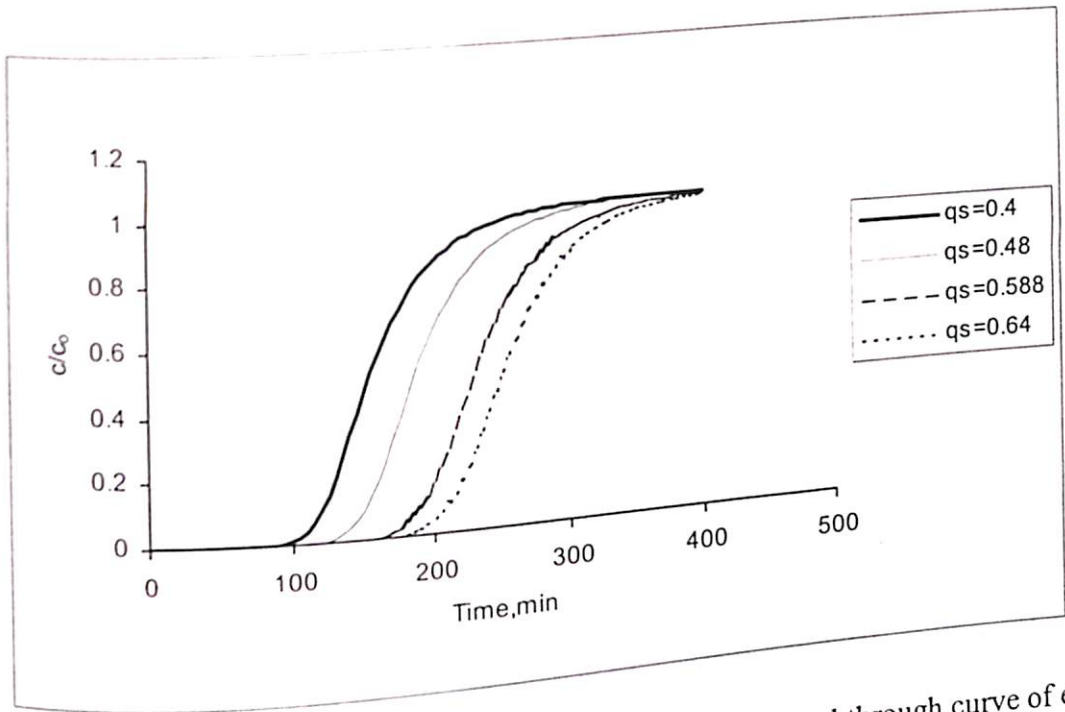


Figure 4.2.4.11: Effect of saturation capacity on concentration breakthrough curve of ethyl acetate

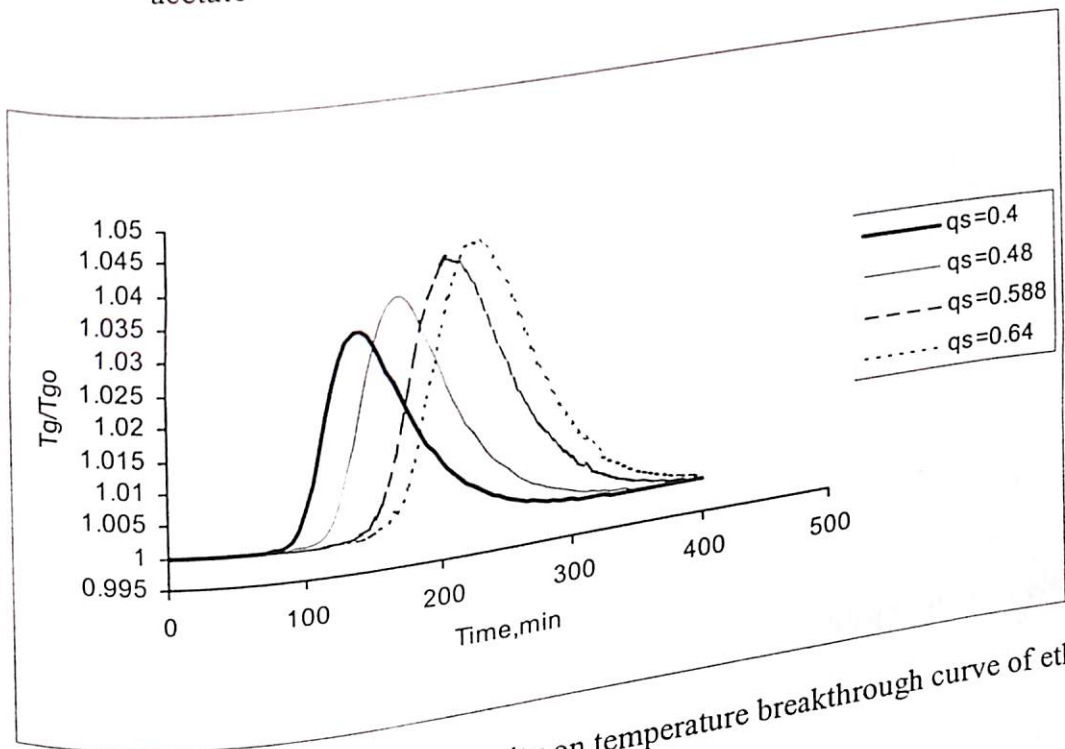


Figure 4.2.4.12: Effect of saturation capacity on temperature breakthrough curve of ethyl acetate

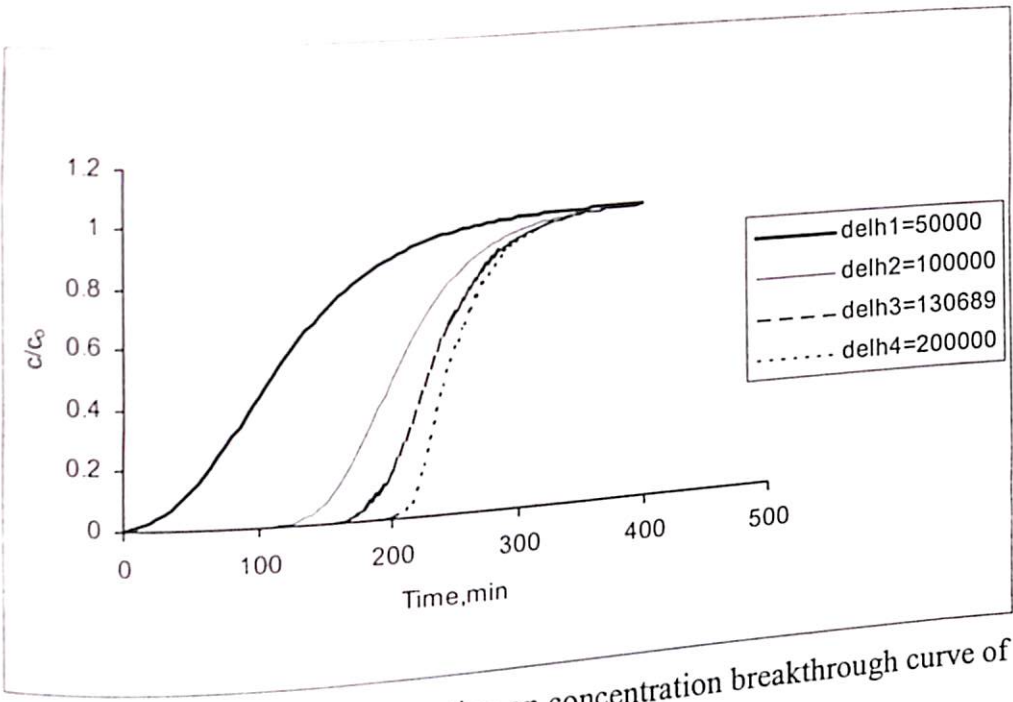


Figure 4.2.4.13: Effect of heat of adsorption on concentration breakthrough curve of ethyl acetate

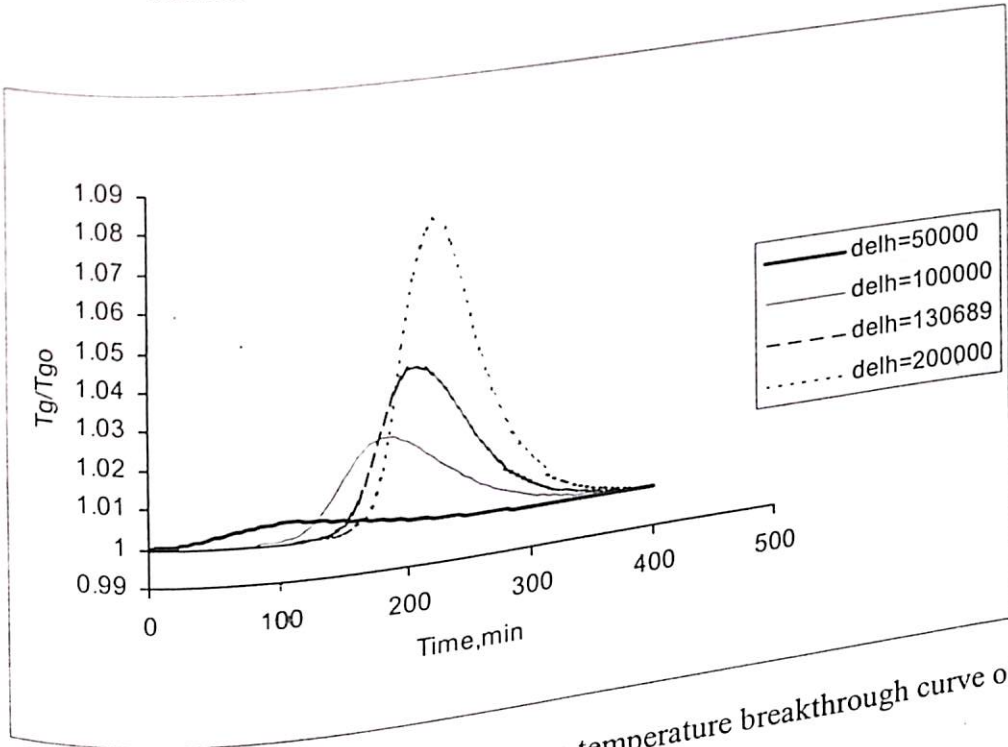


Figure 4.2.4.14: Effect of heat of adsorption on temperature breakthrough curve of ethyl acetate

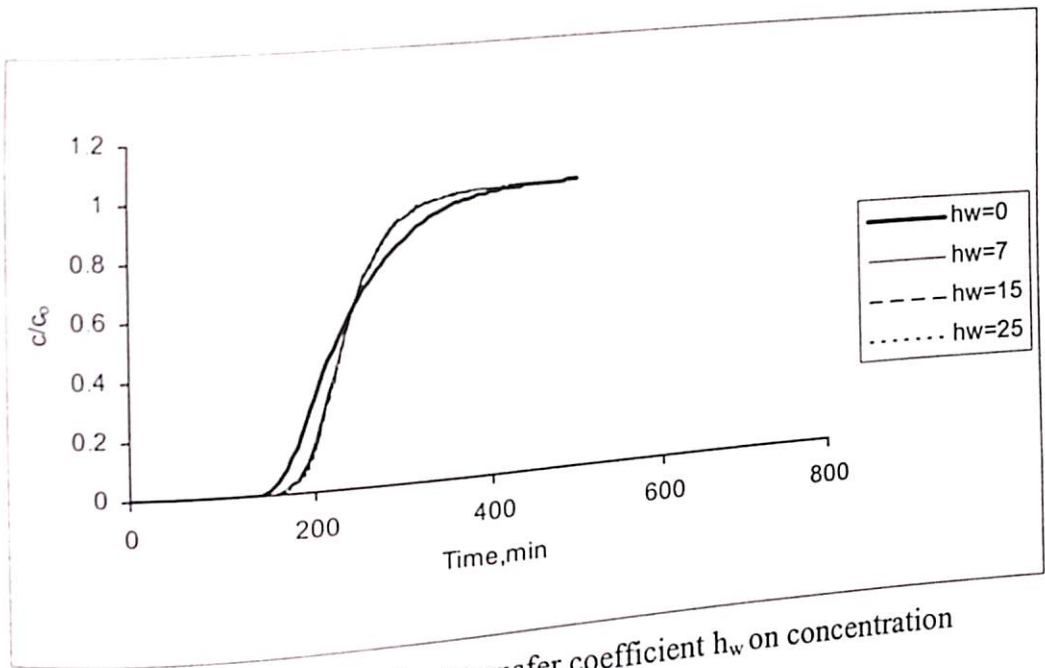


Figure 4.2.4.15: Effect of bed to wall heat transfer coefficient h_w on concentration breakthrough curve of ethyl acetate

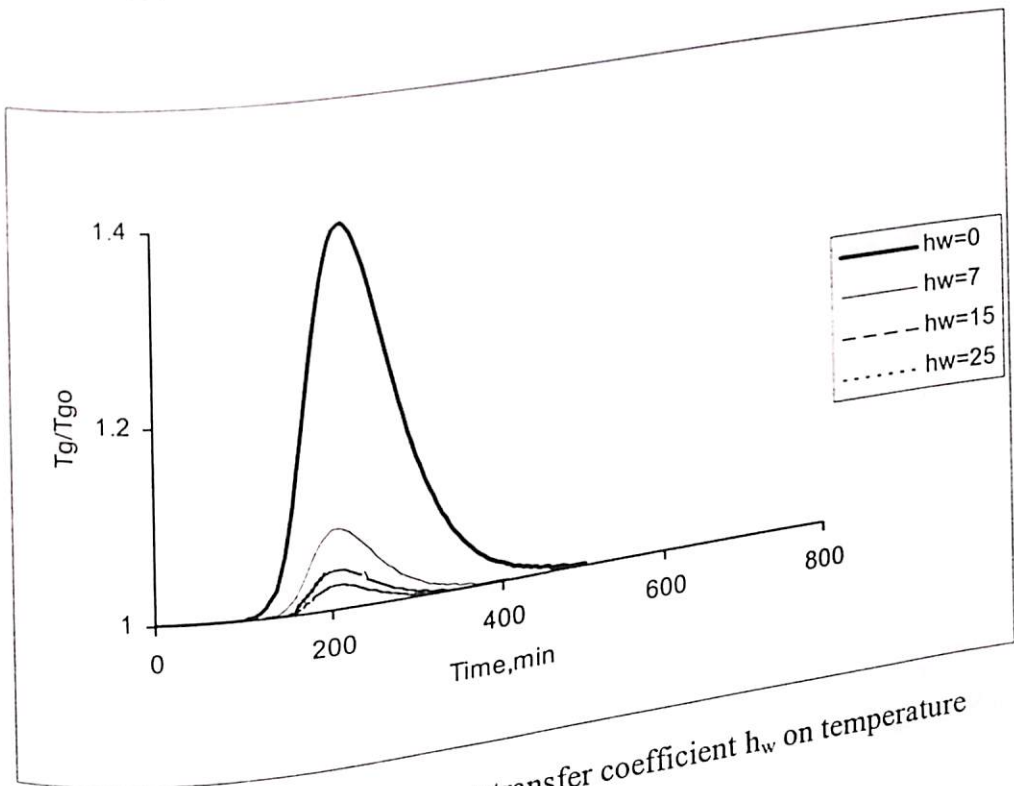


Figure 4.2.4.16: Effect of bed to wall heat transfer coefficient h_w on temperature breakthrough curve of ethyl acetate

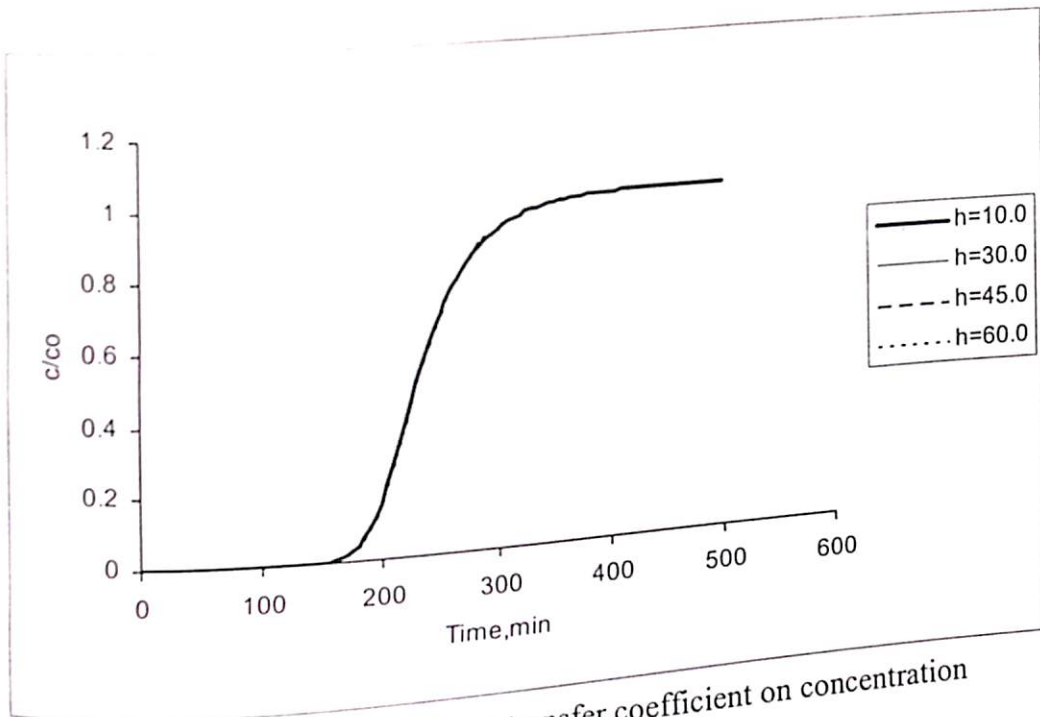


Figure 4.2.4.17: Effect of solid to fluid heat transfer coefficient on concentration breakthrough curve of ethyl acetate

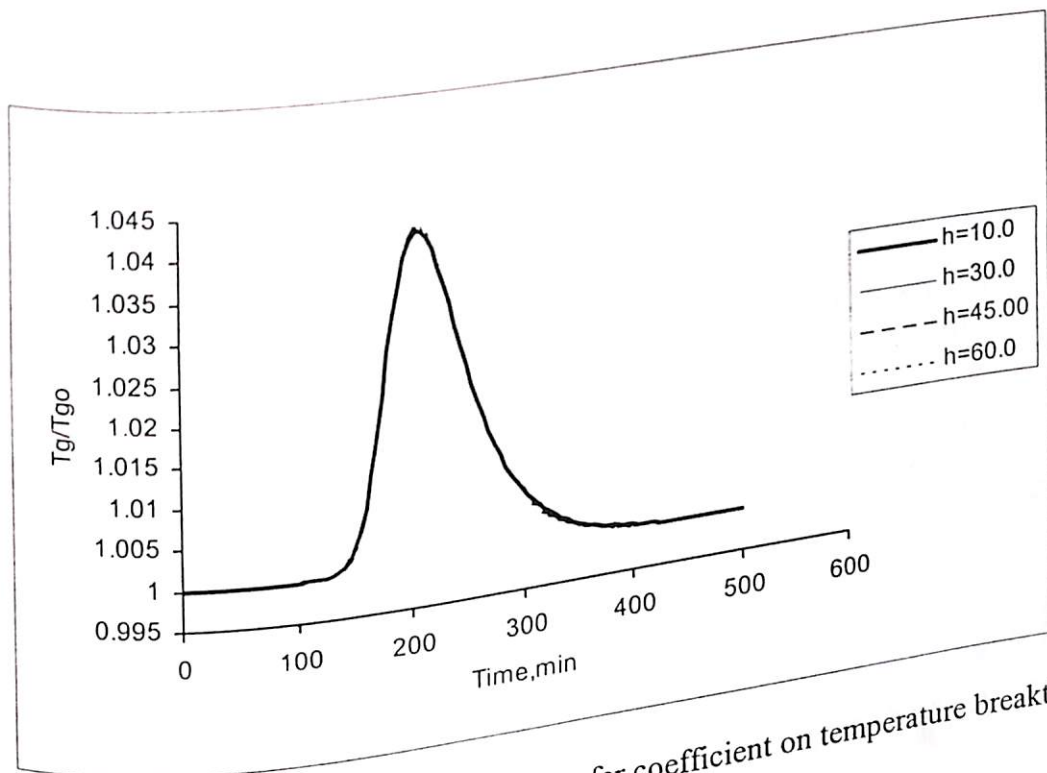


Figure 4.2.4.18: Effect of solid to fluid heat transfer coefficient on temperature breakthrough curve of ethyl acetate

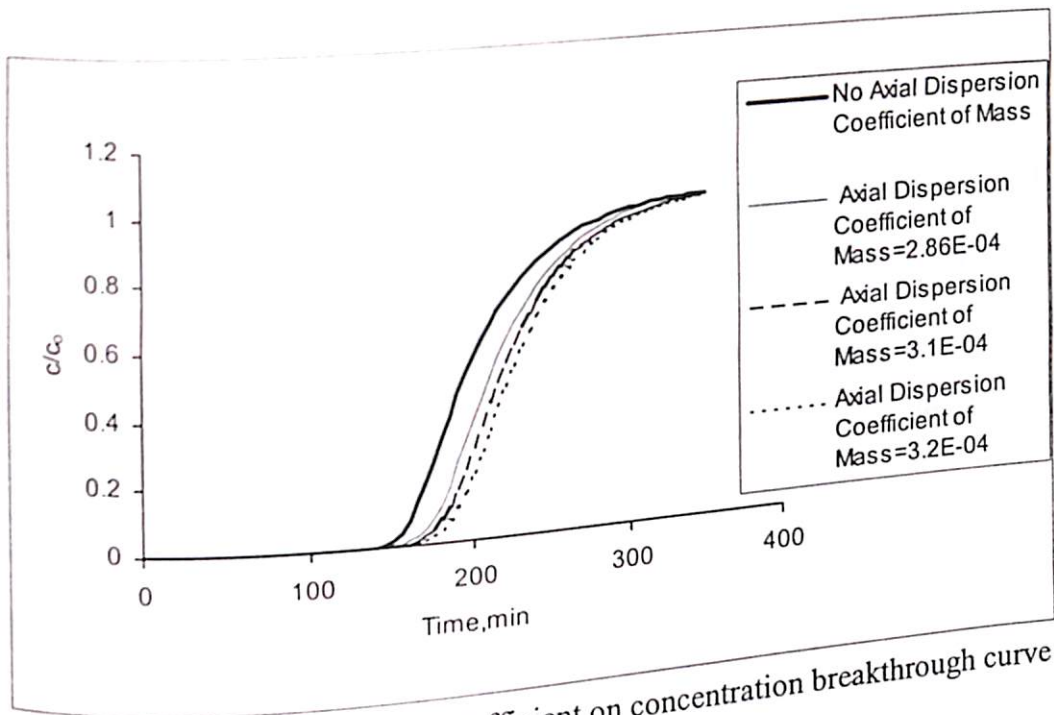


Figure 4.2.4.19: Effect of dispersion coefficient on concentration breakthrough curve of ethyl acetate

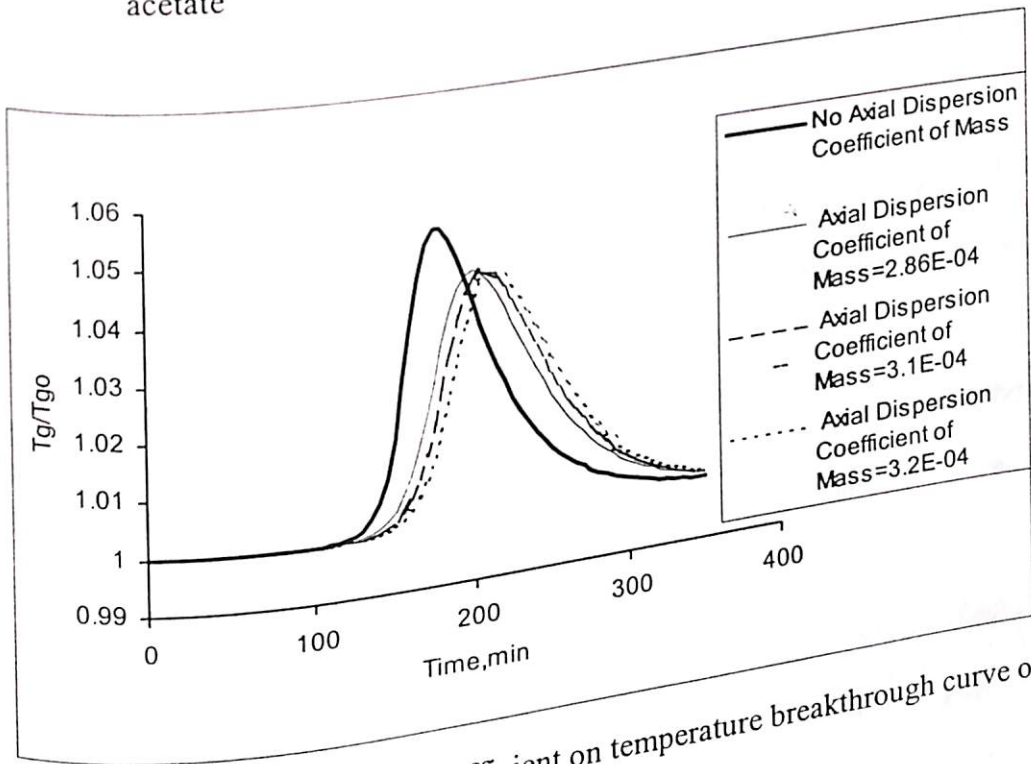


Figure 4.2.4.20: Effect of dispersion coefficient on temperature breakthrough curve of ethyl acetate

CONCLUSIONS

Adsorption behaviour of ethyl acetate (EA) from air on molecular sieves (E-merck 5A and 13X) has been studied through experimental investigation on equilibrium and kinetics and through both experimental and theoretical investigations on dynamic adsorption. A nonisothermal, nonadiabatic mathematical model has been developed and the parameters determined from the equilibrium adsorption studies have been used as model input for theoretical investigation of the dynamic adsorption behaviour.

Based on the analysis of the results on equilibrium and kinetic studies of ethyl acetate adsorption on E-merck 5A and 13X molecular sieves the following conclusions are drawn:

- The isotherms for ethyl acetate on E-merck 5A and 13X molecular sieves are typically of Brunauer Type - I.
- Of the three isotherm models tested (Freundlich, Langmuir and Langmuir-Freundlich isotherm models) Langmuir isotherm model best explains the equilibrium adsorption behaviour of EA on E-merck 5A and 13X molecular sieves.
- Equilibrium adsorption capacity of ethyl acetate in E-merck 13X molecular sieve is higher than E-merck 5A molecular sieve at all concentrations and temperatures of study.
- Mass transfer coefficient determined by both the Uptake and LDF methods shows no significant dependence on the flow rate, leading to a conclusion that mass transfer is controlled by pore diffusion. Also, no significant effect of concentration of EA on mass transfer coefficient has been observed.
- Mass transfer coefficient obtained by Uptake method is of the order of 10^{-4} s^{-1} . In general, LDF method gives slightly lower values of overall mass transfer coefficient

in comparison to those by the Uptake method. Though the Uptake method is the established method for determining the values of overall mass transfer coefficient, LDF method also can be an alternative to Uptake method if provided with properly designed data collection and analysis unit.

- Heat of adsorption values in both the sieves has been of the order of 10^5 J/kg

The following conclusions may be drawn from the dynamic studies that include experimental study, model validation and dynamic simulation studies:

- E-merck 13X molecular sieve behaves closer to ideal behaviour than E-merck 5A molecular sieve, while adsorbing EA from air, establishing itself as stronger adsorbent than 5A molecular sieve.
- Early concentration breakthrough has been observed with higher inlet adsorbate (EA) concentrations due to increased mass transfer rate (adsorption rate) at the early stage of adsorption.
- Constant pattern breakthrough curves have been observed with the changes of inlet adsorbate (EA) concentration, inlet velocity, and saturation adsorption capacity.
- Constant pattern breakthrough curves for both the molecular sieves with change in inlet velocity establish the fact that mass transfer rate is controlled by pore diffusion.
- The constant pattern breakthrough curves with change in bed lengths indicate insignificant effect of axial dispersion establishing the fact that the mass transfer zone is contained within the bed (in the range of the experiments) due to higher affinity of both the sieves for EA.
- The constant pattern breakthrough curves with change in saturation adsorption mechanism of mass and heat transfer do not get disturbed with

- In case of 5A molecular sieve, the predicted results for concentration breakthroughs are in good agreement with the experimental results for a major portion of the breakthrough curves. But the temperature breakthrough curves are better matched with decreased heat of adsorption value (75000 J/kg), which is lower than the experimentally calculated value (337000 J/kg).
- In case of 13X molecular sieve, the model without axial dispersion shows a better match than that with axial dispersion. The increased value of overall mass transfer coefficient ($5.0 \times 10^{-4} \text{ s}^{-1}$) as model input, which is higher than the calculated values ($(1.0 - 2.0) \times 10^{-4} \text{ s}^{-1}$) better predicts the experimental data.
- Changes in values of the of bed diameter, bed to wall heat transfer coefficient, and solid - gas heat transfer coefficient don't significantly influence the concentration breakthrough curves. But, increased fluid phase temperature has been observed for higher bed diameter and lower bed to wall heat transfer coefficient. Hence, suitable heat removal arrangement should be installed in industrial adsorptive system to achieve better adsorption performance of the bed.
- Higher mass transfer coefficient indicates strong adsorption system. So, study on the effect of the mass transfer coefficient helps to find out the nature of the changes in the concentration and temperature breakthrough curves and thereafter the design considerations.
- Higher mass axial dispersion coefficient is not desirable for design of an efficient adsorber as the system behaves poorly under this condition.

SCOPE FOR FUTURE WORK

- In case of industrial adsorber with large diameter bed, this model could be extended by incorporating the radial dispersion.
- A random/normal porosity distribution in the bed may be incorporated in the model.
- The thermophysical properties may be upgraded in the model due to change in temperature for getting more accurate information.
- Exhaustive experiments on equilibrium studies using grounded sieves of different sizes may give further insight on the kinetics of adsorption.
- Equilibrium isotherm data of many volatile organic compounds (VOCs) are not available in the literature. Therefore, similar studies can be performed, which is essential for theoretical study on the dynamics of separation of VOCs from mixture.
- Several other adsorbents including the activated carbon can be tested to identify the most efficient adsorbent based on the adsorbates.
- Wide range of experiments with adsorption-desorption cycle and the corresponding theoretical study would give the actual picture of thermodynamic optimization of the process especially, in terms of cycle time optimization.
- New synthetic adsorbents with better selectivity and/or efficiency can be developed.

REFERENCES

- Bhole, A.G. & Parwate, A.V. (1998). "Legislation on environmental protection in India", *Journal of IAEM*, 25, 104-108.
- Blocki, S.W. (1993). "Hydrophobic zeolite adsorption: A proven advancement in solvent separation technology", *Environmental Progress*, 12, 226-237.
- Butt, J.B. (1980). "Reaction Kinetics and Reactor Design", *Prentice Hall, Englewood, Cliffs, NJ Publishers*.
- Cal, M.P., Larson, S.M., & Rood, M.J. (1994). "Experimental and modeled results describing the adsorption of acetone and benzene onto activated carbon fibers", *Environmental Progress*, 13(1), 26-30.
- Cantrell, C. J., (1982). "Vapor recovery for refineries and petrochemical plants", *Chemical Engineering Progress*, 10, 56-60.
- Cheng, Z.M., Yu, F.D., Grevillot, G., Luo, L., Tondeur, D. & Yuan, W.K. (2002). "Redistribution of adsorbed VOCs in activated carbon under electrochemical desorption", *AIChE Journal*, 48(5), 1132.
- Choudary, N.V., Kumar. P., Bhat, T.S.G., Cho, S.H., Han, S.S. & Kim, J.N. (2002). "Adsorption of light hydrocarbon gases on alkene-selective adsorbent", *Industrial Engineering and Chemistry Research*, 41(11), 2728 - 2734.
- Costa, E., Calleja, G., Jimenez, A. & Pau, J. (1991). "Adsorption equilibrium of ethylene, propane, propylene, carbon dioxide, and their mixtures on 13X zeolite", *Journal of Chemical Engineering Data*, 36, 218-224.
- Deng, S.G., & Lin, Y.S. (1995). "Sulphur dioxide sorption properties and thermal stability of hydrophobic zeolites", *Industrial Engineering and Chemistry Research*, 34(11), 4063-4070.

- Ding, L.P., Bhatia, S.K. & Liu, F. (2002). "Kinetics of adsorption on activated carbon: application of heterogeneous vacancy theory", *Chemical Engineering Science*, 57(18), 3909-3928.
- Dolidovich, A.F., Akhremkova, G.S. & Efremtsev, V.S. (1999). "Novel technologies of VOC decontamination in fixed, moving and fluidized catalyst-adsorbent beds", *The Canadian Journal of Chemical Engineering*, 77, 342-354.
- Farooq, S. & Ruthven, D.M. (1990). "Heat effects in adsorption column dynamics: 2 Experimental validation of the one-dimensional Model", *Industrial Engineering and Chemistry Research*, 29(6), 1084-1090.
- Ghoshal, A. K. (1997). "Studies on adsorption of carbon dioxides and moisture in molecular sieves" Ph.D. Thesis, IIT Kharagpur.
- Ghoshal, A. K., Samanta, A. N. & Maiti, B. R. (1999). "Experimental study on the simultaneous adsorption of carbon dioxide and moisture from nitrogen in Linde 5A molecular sieves", *The Canadian Journal of Chemical Engineering*, 77(10), 997 - 1002.
- Ghoshal, A.K. & Manjare, S.D. (2002). "Selection of appropriate adsorption technique for recovery of VOCs: An analysis", *Journal of Loss Prevention in the Process Industries*, 15, 413-421.
- Grande, C.A., Gigola, C. & Rodrigues, A.E. (2002). "Adsorption of propane and propylene in pellets and crystals of 5A zeolite", *Industrial Engineering and Chemistry Research*, 41(1), 85-92.
- Grant, W. M. (1986). "Toxicology of the Eye", *John Wiley & Sons*, New York.
- Gupta, V.K. & Verma, N. (2002) "Removal of volatile organic compounds by cryogenic condensation followed by adsorption", *Chemical Engineering Science*, 57(14), 2679 - 2696.

- Hathaway, G. J., Proctor, N. H., Hughes, J. P., & Fischman, M. L. (1991). "Proctor and Hughes' Chemical Hazards of the Workplace", *John Wiley & Sons*, New York,
- Huang, C. C., Hwu, T.L. & Hsia, Y.S. (1993). "Recovery of acetone vapor by a thermal swing adsorber with activated carbon", *Journal of Chemical Engineering of Japan*, 26(1), 21-27.
- Huang, M. C., Chou, C. H. & Teng, H. (2002). "Pore-size effects on activated - carbon capacities for volatile organic compound adsorption", *AIChE Journal*, 48(8), 1804-1809.
- Hwang, K.S., Choi, D.K., Gong, S.Y. & Cho, S.Y. (1997). "Adsorption and thermal regeneration of methylene chloride vapor on an activated carbon bed", *Chemical Engineering Science*, 52(7), 1111-1123.
- Jasra, R.V. & Bhat, T.S.G. (1987) "Sorption kinetics of higher n-paraffins on zeolite molecular sieve 5A", *Industrial Engineering and Chemistry Research*, 26(12), 2544-2546.
- Khan, F.I. & Ghoshal, A.K. (2000) "Removal of volatile organic compounds from polluted air", *Journal of Loss Prevention in the Process Industries*, 13, 527-545.
- Khan, F.I., Ghoshal, A.K. & Manjare, S.D. (1999) "VOC chemistry in atmosphere and its control", In *Proceedings of National Conference on Industries and Environment*, Karad, Dec 28-30.
- Kubota, K., Nakajima, K., Ono, Y. & Hayashi, S. (1989). "Adsorption characteristics of propylene on molecular sieve 4A", *Separation Science and Technology*, 24(9&10), 709-719.
- Liu, Y. & Ritter, J.A. (1996). "Pressure swing adsorption- solvent vapor recovery: process dynamics and parametric study", *Industrial Engineering and Chemistry Research*, 35(7), 2299-2312.

- Lo, I. M.-C., Cheng-Hao, L. & Liljestrand, H. M. (1996). "Tricaprylmethylammonium bentonite complexes as adsorbents for benzene, toluene, ethyl benzene and xylene" *Water Science & Technology*, 34(7/8), 319-325.
- Lyandres, S., Meardon, J. & Rees, J. (1989). "Evaluation of membrane processes for the reduction of trace organic contaminants", *Environmental Progress*, 8(4), 239-244.
- Malek, A. & Farooq, S. (1996) "Comparison of Isotherm models for hydrocarbon adsorption on Activated Carbon", *AIChE Journal*, 42(11), 3191-3200.
- Martinez, G.M. & Basmadjian, D. (1996). "Towards a general gas adsorption isotherm", *Chemical Engineering Science*, 51(7), 1043-1054.
- Moretti, E.C. (2002). "Reduce VOC and HAP emissions", *Chemical Engineering Progress*, 98(6), 30-40.
- NLM (1992). "Hazardous Substances Data Bank: Ethyl Acetate". Bethesda, MD: National Library of Medicine.
- Olivier, M.G., Berlier, K. & Jadot, R. (1994). "Adsorption of butane, 2-methylpropane, and 1-butene on activated carbon", *Journal of Chemical Engineering Data*, 39, 770-773.
- Padin, J., Rege, S.U., Yang, R.T. & Cheng, L.S. (2000). "Molecular sieve sorbents for kinetic separation of propane/propylene", *Chemical Engineering Science*, 55, 4525-4535.
- Pezolt, D. C., Collick, S. J., Johnson, H. A. & Robbins, L.A. (1997). "Pressure swing adsorption for VOC recovery at gasoline loading terminals", *Environmental Progress*, 16(1), 16-19.
- Prasetyo, I., Do, H.D. & Do, D.D. (2002). "Surface diffusion of strong adsorbing vapors on porous carbon", *Chemical Engineering Science*, 57(1), 133-141.
- Ray, I. & Altshuer, B. (1997). "Adsorption with activated carbon", *Chemical Processing*, 11, 32-36.

- Riekert, L. (1971). "Rates of sorption and diffusion of hydrocarbon in zeolites", *AICHE Journal*, 17(2), 446 - 454.
- Ritter, J.A. & Yang, R.T. (1991). "Pressure swing adsorption: experimental and theoretical study on air purification and vapor recovery", *Industrial Engineering and Chemistry Research*, 30(5), 1023-1032.
- Ruddy, E.N. & Carroll, L.A. (1993). "Select the best VOC control strategy", *Chemical Engineering Progress*, 89, 28-35.
- Ruhl, M.J. (1993) "Recover VOCs via adsorption on activated carbon", *Chemical Engineering Progress*, 89, 37-41.
- Ruthven, D.M., & Loughlin, K. F. (1971). "The effect of crystallite shape and size distribution on diffusion measurements in molecular sieves", *Chemical Engineering Science*, 26(5), 577-584
- Ruthven, D.M., & Loughlin, K. F. (1972). "The diffusional resistance of molecular sieve pellets", *Canadian Journal of Chemical Engineering*, 50, 550-552
- Ruthven, D.M. & Doetisch, I.H. (1976). "Diffusion of hydrocarbons in 13X zeolite", *AICHE Journal*, 22(5), 882-886.
- Ruthven, D.M. (1984). "Principles of Adsorption and Adsorption Processes", John Wiley & Sons, USA
- Ruthven, D.M., Farooq, S. & Knaebel, K.S. (1994). "Pressure Swing Adsorption", *VCH Publishers, New York*.
- Ruthven, D.M. & Sircar, S. (1995). "Design of membrane and PSA process for bulk gas separation", *AICHE Symposium Series No 304*, 91, 29-37.
- Ruthven, D.M. & Kaul, B.K. (1996). "Adsorption of n-hexane and intermediate molecular weight aromatic hydrocarbons on LaY zeolite", *Industrial Engineering and Chemistry*

- Sax, N.I. & Lewis, R.J. (1989). "Dangerous Properties of Industrial Materials", *Van Nostrand Reinhold Company*, New York.
- Serbezov, A.S. & Sotirchos, S.V. (1997). "Mathematical modeling of the adsorptive separation of multicomponent gaseous mixtures", *Chemical Engineering Science*, 52(1), 79-91.
- Silva, J.A.C., & Rodrigues, A.E. (1997). "Sorption and diffusion of n-pentane in pellets of 5A zeolite", *Industrial Engineering and Chemistry Research*, 36(2), 493-500.
- Silva, J.A.C. & Rodrigues, A.E. (1997). "Equilibrium and kinetics of n-Hexane sorption in pellets of 5A zeolite", *AIChE Journal*, 43(10), 2524-2534.
- Silva, J.A.C. & Rodrigues, A.E. (1997). "Fixed-bed adsorption of n-pentane /isopentane mixtures in pellets of 5A zeolite", *Industrial Engineering and Chemistry Research*, 36(9), 3769-3777.
- Silva, F.A.D. & Rodrigues, A.E. (1999). "Adsorption equilibria and kinetics for propylene and propane over 13X and 4A zeolite pellets", *Industrial Engineering and Chemistry Research*, 38(5), 2051-2057.
- Singh, K.P., Mohan, D., Tandon, G.S. & Gupta, G.S.D. (2002) "Vapor-phase adsorption of hexane and benzene on activated carbon fabric cloth: equilibria and rate studies", *Industrial Engineering and Chemistry Research*, 41(10), 2480-2486.
- Sowerby, B. & Crittenden, B.D. (1988). "Vapor phase separation of alcohol-water mixtures by adsorption onto silicalite", *Gas Separation & Purification*, 2(12), 177-183.
- Stenzel, M.H. (1993). "Remove organics by activated carbon adsorption", *Chemical Engineering Progress*, 89(4), 36-43.
- Suyadal, Y., Erol, M. & Oguz, H. (2000). "Deactivation Model for the adsorption of Trichloroethylene Vapor on an Activated Carbon Bed", *Industrial Engineering and Chemistry Research*, 39(3), 724-730.

- Takeuchi, Y., Hayato, N., Miyata, S.A. & Harada, A. (1995). "Adsorption of 1-butanol and p-xylene vapour and their mixtures with high silica zeolites", *Separation Technology*, 5, 23-34.
- Tan, C.S. & Liou, D.C. (1988). "Desorption of ethyl acetate from activated carbon by supercritical carbon dioxide", *Industrial Engineering and Chemistry Research*, 27(6), 988-991.
- Technical Links to Safety and Health Topics (2003) "US Department of Labor, Occupational Safety & Health Administration"
<http://www.osha.gov/SLTC/healthguidelines/ethylacetate/recognition.html>
- Triebe, R.W., Tezel, F.H. & Khulbe, K.C. (1996). "Adsorption of methane, ethane, and ethylene on molecular sieve zeolites", *Gas Separation Purification*, 10(1), 81-84
- William, J.C. & Lead, P.E. (1997). "VOC control strategies in plant design", *Chemical Processing: Project Engineering Annual*, 44-44.
- Yang, R.T. (1987). "Gas Separation by Adsorption Processes", *Imperial College Press*, London.
- Yeh, Y.T. & Yang, R.T. (1989). "Diffusion in zeolites containing mixed cations", *AIChE Journal*, 35(10), 1659-1666.
- Yun, J.H., Choi, D.K. & Kim, S.H. (1998). "Adsorption of organic solvent vapors on hydrophilic Y-type zeolite", *AIChE Journal*, 44(6), 1344-1350.
- Yun, J.H., Choi, D.K. & Kim, S.H. (1998). "Adsorption equilibria of chlorinated organic solvents onto activated carbon", *Industrial Engineering and Chemical Research*, 37(4), 1422-1427.
- Yun, J.H. & Choi, D.K. (1997). "Adsorption isotherms of benzene and methyl benzene vapours on activated carbon", *Journal of Chemical Engineering Data*, 42, 894-896.

Zhou, L., Sun, Y., & Zhou, Y. (2002). "Enhancement of the methane storage on activated carbon by preadsorbed water", *AIChE Journal*, 48(10), 2412-2416.

Appendix I

Determination of ethyl acetate vapor concentration in the air stream

Ethyl acetate vapor concentration in the air stream was determined as per following procedure.

Concentration calculation contains two steps:

- Concentration of EA in the vapour in EA bottle
- Concentration of EA in the syringe after dilution, which will give the final concentration of EA.

Concentration of EA in the vapour in EA Bottle:

Antoine equation was used to determine the vapor pressure of ethyl acetate at the operating temperature.

The equation is

$$\ln(p^*) = A - \frac{B}{C + T}$$

For temperature range of 260-385 K the constants A, B, and C for ethyl acetate are

$$A=16.15, B = 2790.50, C = - 57.15$$

At 307 K the vapor pressure calculated from above equation is 145.66 mm Hg.

According to Daltons law, Partial pressure = Total pressure * gas phase mole fraction.

For pure liquid, according to Raoult's law, Partial pressure = Vapor pressure

So for pure ethyl acetate, using Dalton's law

Ethyl acetate mole fraction in air, $y = \text{partial pressure} / \text{total pressure}$

Therefore $y = 145.66 / 760 = 0.2$ mole fraction of pure ethyl acetate at ambient condition (307

K) in the bottle assuming the air in the bottle is fully saturated.

Final EA concentration:

Say A volume % of air - EA mixture from the bottle is present in the 100 unit volume of the syringe containing air-EA in bottle and free air from ambient.

So, EA present is $A*y/100$ moles of final EA and air mixture

EA concentration = $(A*y * 88 * 1.165)/(100 * 29.1)$ in g/litre = kg/m^3

Where, molecular weight of ethyl acetate and air are 88 and 29.1 respectively and density of air is 1.165 kg/m^3

Sample calculation of ethyl acetate vapor concentration in syringe using GC for Run no DS15.

85-volume percentage of ethyl acetate was taken from EA bottle in GC syringe (capacity of syringe was $500 \mu\text{l}$). The area of the peak for standard obtained from GC was 3242.83 mv-sec and the area of the peak for column inlet sample was 3237.82 mv-sec .

Concentration of standard is $(85*0.2*88*1.165)/(100*29.1) = 0.60 \text{ kg/m}^3$.

The sample concentration was calculated using following formula.

$$\text{concentration of sample} \rightarrow \frac{\text{area of sample}}{\text{area of standard}} \times \text{concentration of standard}$$

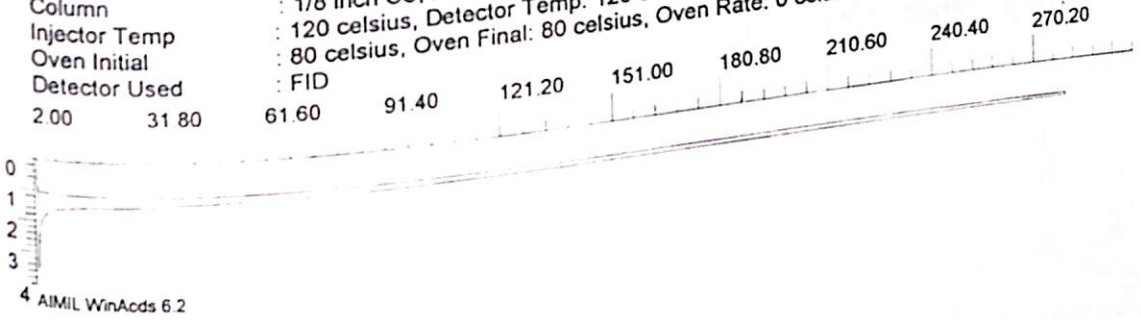
For DS run15 the calculated inlet concentration was 0.60 Kg/m^3

The standard area peak and sample area peak are shown below.

May 13 2003 15:25:29

Chromatogram for : ethylacetate adsorption bed
Chart speed : 0.50 cm/min.
File Name : C:\WINDOWS\13x.cds
Last save date : Sep 25 2002 15:20:30
13X Molecular Sieve

Carrier : Nitrogen @ 30 ml/min
Oxidant : Oxygen @ 300 ml/min
Fuel : Hydrogen @ 30 ml/min
Column : 1/8 inch SS, Packing:
Injector Temp : 120 celsius, Detector Temp: 120 celsius
Oven Initial : 80 celsius, Oven Final: 80 celsius, Oven Rate: 0 celsius/minute
Detector Used : FID



4 AIMIL WinAcids 6.2

May 13 2003 15:25:04

RAN Report for : ethylacetate adsorption bed
File Name : C:\WINDOWS\13x.cds
Last save date : Sep 25 2002 15:20:30
13X Molecular Sieve

Carrier : Nitrogen @ 30 ml/min
Oxidant : Oxygen @ 300 ml/min
Fuel : Hydrogen @ 30 ml/min
Column : 1/8 inch SS, Packing:
Injector Temp : 120 celsius, Detector Temp: 120 celsius
Oven Initial : 80 celsius, Oven Final: 80 celsius, Oven Rate: 0 celsius/minute
Detector Used : FID

Peak No	RT min:sec	Height mV	Area mV-sec	Amount % Area	Name
1	00 : 42	0.111	1.199	0.037	
2	00 : 58	0.285	1.174	0.036	
3	01 : 11	276.776	3242.831	99.927	

Total Area : 3245.204 mV-Sec

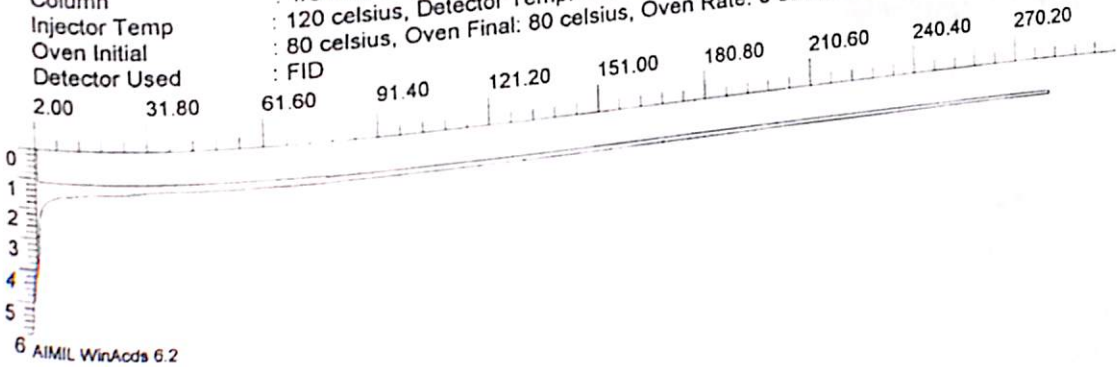
AIMIL WinAcids 6.2

Figure AI-1: GC peak for standard sample and area of the peak.

May 13 2003 15:28:05

Chromatogram for : ethylacetate adsorption bed
Chart speed : 0.50 cm/min.
File Name : C:\WINDOWS\13x.cds
Last save date : Sep 25 2002 20:27:32
13X Molecular Sieve

Carrier : Nitrogen @ 30 ml/min
Oxidant : Oxygen @ 300 ml/min
Fuel : Hydrogen @ 30 ml/min
Column : 1/8 inch SS, Packing:
Injector Temp : 120 celsius, Detector Temp: 120 celsius
Oven Initial : 80 celsius, Oven Final: 80 celsius, Oven Rate: 0 celsius/minute
Detector Used : FID



May 13 2003 15:27:42

RAN Report for : ethylacetate adsorption bed
File Name : C:\WINDOWS\13x.cds
Last save date : Sep 25 2002 20:27:32
13X Molecular Sieve

Carrier : Nitrogen @ 30 ml/min
Oxidant : Oxygen @ 300 ml/min
Fuel : Hydrogen @ 30 ml/min
Column : 1/8 inch SS, Packing:
Injector Temp : 120 celsius, Detector Temp: 120 celsius
Oven Initial : 80 celsius, Oven Final: 80 celsius, Oven Rate: 0 celsius/minute
Detector Used : FID

Peak No	RT min:sec	Height mV	Area mV-sec	Amount % Area	Name
1	00 : 29	0.128	0.470	0.014	
2	00 : 45	0.094	0.681	0.021	
3	01 : 00	0.214	1.050	0.032	
4	01 : 12	277.584	3237.823	99.779	
5	02 : 44	0.259	4.962	0.153	

Total Area : 3244.986 mV-Sec

AIMIL WinAcids 6.2

Figure AI-2: GC peak for column inlet sample and area of the peak.

APPENDIX-II

Experimental Equilibrium data

A) System: 5A-Ethyl Acetate, Temperature: 35⁰C

Run Number: IS1, Flow rate: 2×10^{-6} m³/sec, Inlet Concentration: 0.66 kg/m³

LDF method

Amount adsorbed (g/g)	0.078	0.105	0.1206	0.126	0.127	0.128
Time (min)	90	210	510	690	730	765
Average adsorbed, q	0.039	0.0915	0.1128	0.1233	0.1265	0.1275
$\frac{dq}{dt} \times 10^4$	4.375	0.71	0.583	0.8	0.285	-

Uptake curve method

$\ln(1-q/q^*)$	-1.716	-2.851	-4.158	-4.852
Time (min)	210	510	690	730

Run Number: IS 2, Flow rate: 2×10^{-6} m³/sec, Inlet concentration: 0.65kg/m³

LDF method

Amount adsorbed (g/g)	0.0733	0.0782	0.089	0.0989	0.1111	0.1135	0.1171	0.125	0.134	0.141
Time (min)	195	270	435	565	675	715	745	785	820	845
Average adsorbed, q	0.036	0.0757	0.083	0.094	0.105	0.1123	0.1153	0.121	0.129	0.137
$\frac{dq}{dt} \times 10^4$	5.3	0.44	0.846	1.0	1.825	1.0	1.42	1.78	3.2	-

Uptake curve method

$\ln(1-q/q^*)$	-1.208	-1.551	-1.635	-1.775	-2.176	-3.003
Time (min)	565	675	715	745	785	820

Run Number: IS3, Flow rate: 4×10^{-6} m³/sec, Inlet concentration: 0.13kg/m³

LDF method

Amount adsorbed (g/g)	0.145	0.157	0.163
Time (min)	285	525	675
Average adsorbed, q	0.0725	0.151	0.16
$\frac{dq}{dt} \times 10^4$			

Uptake curve method

$\ln(1-q/q^*)$	-2.165	-3.182	-5.322
Time (min)	285	525	675

Run Number: IS4, Flow rate: $4 \times 10^{-6} \text{ m}^3/\text{sec}$, Inlet concentration: 0.23 kg/m^3

LDF method										
Amount adsorbed (g/g)	0.092	0.124	0.159	0.173	0.176	0.184	0.188	0.190	0.1902	0.191
Time (min)	145	280	490	595	670	780	820	840	875	885
Average adsorbed, q	0.046	0.11	0.142	0.166	0.175	0.18	0.186	0.189	0.1901	0.1906
$\frac{dq}{dt} \times 10^4$	4.74	1.52	2.28	1.20	0.45	1.5	0.314	0.5	0.125	
Uptake curve method										
$\ln(1-q/q^*)$	-1.786	-2.362	-2.544	-3.306	-4.154	-5.252	-5.475			
Time (min)	490	595	670	780	820	840	875			

Run Number: IS5, Flow rate: $1.49 \times 10^{-6} \text{ m}^3/\text{sec}$, Inlet concentration: 0.44 kg/m^3

LDF method			
Amount adsorbed (g/g)	0.109	0.115	0.157
Time (min)	150	300	405
Average adsorbed, q	0.0545	0.112	0.136
$\frac{dq}{dt} \times 10^4$	3.83	2.28	-
Uptake curve method			-1.318
$\ln(1-q/q^*)$	-1.185	150	300
Time (min)			

Run Number: IS6, Flow rate: $1.49 \times 10^{-6} \text{ m}^3/\text{sec}$, Inlet concentration: 0.70 kg/m^3

LDF method									
Amount adsorbed (g/g)	0.033	0.037	0.049	0.057	0.0575	0.059	0.0615	0.0633	
Time (min)	210	295	480	615	700	720	755	830	
Average adsorbed, q	0.016	0.035	0.043	0.053	0.0572	0.058	0.0603	0.062	
$\frac{dq}{dt} \times 10^4$	2.23	0.43	0.74	0.5	0.375	0.657	0.23	-	
Uptake curve method						-2.689	-3.560		
$\ln(1-q/q^*)$	-1.487	-2.307	700	-2.390	720	755			
Time (min)	480	615	700	720	755				

Run Number: IS7, Flow rate: $1.49 \times 10^{-6} \text{ m}^3/\text{sec}$, Inlet concentration: 0.35 kg/m^3

LDF method											
Amount adsorbed (g/g)	0.108	0.143	0.159	0.174	0.1811	0.1889	0.195	0.197	0.215	0.216	0.2169
Time (min)	135	255	345	515	585	645	685	720	915	945	975
Average adsorbed, q	0.054	0.125	0.151	0.166	0.177	0.185	0.192	0.196	0.206	0.209	0.213
$\frac{dq}{dt} \times 10^4$	5.92	2.9	0.88	1.57	1.33	1.75	1.14	0.51	1.0	1.33	
Uptake curve method								-2.388	-4.737	-5.485	
$\ln(1-q/q^*)$	-1.321	-1.621	-1.801	-2.047	-2.293	720	915	945			
Time (min)	345	515	585	645	685	720	915	945			

Run Number: IS8, Flow rate: $1.49 \times 10^{-6} \text{ m}^3/\text{sec}$, Inlet concentration: 0.33 kg/m^3

LDF method											
Amount adsorbed (g/g)	0.095	0.117	0.131	0.142	0.148	0.152	0.158	0.160	0.185	0.192	0.203
Time (min)	120	180	235	345	440	525	615	645	735	780	810
Average adsorbed, q	0.047	0.106	0.124	0.136	0.145	0.15	0.155	0.159	0.173	0.188	0.197
$\frac{dq}{dt} \times 10^4$	9.83	3.3	1.09	0.95	0.588	0.55	1.33	1.55	3.33	3.0	-

Uptake curve method				
$\ln(1-q/q^*)$	-1.202	-1.305	-1.381	-1.506
Time (min)	345	440	525	615
				-1.552
				645
				-2.423
				735
				-2.915
				780

Run Number: IS9, Flow rate: $0.86 \times 10^{-6} \text{ m}^3/\text{sec}$, Inlet concentration: 0.53 kg/m^3

LDF method							
Amount adsorbed (g/g)		0.0745	0.0892	0.1090	0.1414	0.1472	0.2043
Time (min)		165	240	335	515	575	620
Average adsorbed, q		0.0373	0.0818	0.0991	0.1252	0.1443	0.1757
$\frac{dq}{dt} \times 10^4$		5.93	1.82	1.45	3.18	6.97	-

Uptake curve method		
$\ln(1-q/q^*)$		-1.1780
Time (min)		515
		-1.2747
		575

Run Number: IS10, Flow rate: $0.86 \times 10^{-6} \text{ m}^3/\text{sec}$, Inlet concentration: 0.38 kg/m^3

LDF method											
Amount adsorbed (g/g)	0.0639	0.0723	0.0803	0.0933	0.0997	0.1027	0.1074	0.1145	0.1254	0.1274	0.1316
Time (min)	160	240	335	450	515	555	600	750	850	870	920
Average adsorbed, q	0.0319	0.0681	0.076	0.087	0.096	0.1012	0.1051	0.111	0.119	0.126	0.129
$\frac{dq}{dt} \times 10^4$	4.52	0.83	0.96	1.38	1.3	0.87	0.393	0.8	3.5	0.6	-

Uptake curve method				
$\ln(1-q/q^*)$	-1.234	-1.417	-1.515	-1.693
Time (min)	450	515	555	600
				-2.046
				750
				-3.055
				850
				-3.445
				870

Run Number: IS11, Flow rate: $0.86 \times 10^{-6} \text{ m}^3/\text{sec}$, Inlet concentration: 0.18 kg/m^3

LDF method								
Amount adsorbed (g/g)	0.1706	0.1789	0.206	0.214	0.2318	0.2452	0.259	0.2631
Time (min)	130	200	325	415	525	620	730	775
Average adsorbed, q	0.085	0.175	0.192	0.21	0.223	0.238	0.252	0.261
$\frac{dq}{dt} \times 10^4$	12.86	1.361	2.0	1.18	1.58	1.27	2.0	0.44
Amount adsorbed (g/g)	0.2637	0.2781	0.2793	0.2815	0.2851			
Time (min)	820	920	940	965	995			
Average adsorbed, q	0.263	0.271	0.278	0.28	0.2833			
$\frac{dq}{dt} \times 10^4$	0.8	1.16	0.5	1.1	-			
Uptake curve method								
$\ln(1-q/q^*)$	-1.282	-1.388	-1.677	-1.966	-2.391	-2.562	-2.589	-3.707
Time (min)	325	415	525	620	730	775	820	920
								-3.895
								940
								965
								-4.372

Run Number: IS12, Flow rate: $4.0 \times 10^{-6} \text{ m}^3/\text{sec}$, Inlet concentration: 0.27 kg/m^3

LDF method								
Amount adsorbed (g/g)	0.128	0.187	0.22	0.263	0.273	0.288	0.293	0.3
Time (min)	135	265	345	525	585	675	745	795
Average adsorbed, q	0.064	0.16	0.203	0.24	0.268	0.281	0.291	0.296
$\frac{dq}{dt} \times 10^4$	7.38	5.4	2.05	1.94	-	-	-	-
Amount adsorbed (g/g)	0.303	0.305	0.31	0.312	0.313	0.313	0.33	
Time (min)	825	855	915	930	945	1145		
Average adsorbed, q	0.302	0.304	0.307	0.311	0.313	0.319		
$\frac{dq}{dt} \times 10^4$	-	0.52	-	-	-	-	-	-
Uptake curve method								
$\ln(1-q/q^*)$	-1.30	-1.67	-1.90	-2.13	-2.27			
Time (min)	525	585	675	745	795			
$\ln(1-q/q^*)$	-2.47	-2.54	-2.66	-2.85	-2.97			
Time (min)	825	855	915	930	945			

Run Number: IS13, Flow rate: $1.49 \times 10^{-6} \text{ m}^3/\text{sec}$, Inlet concentration: 0.36 kg/m^3

LDF method									
Amount adsorbed (g/g)	0.102	0.173	0.21	0.225	0.255	0.275	0.29	0.2956	0.302
Time (min)	105	220	280	345	420	510	615	710	780
Average adsorbed, q	0.051	0.137	0.192	0.217	0.24	0.265	0.283	0.293	0.298
$\frac{dq}{dt} \times 10^4$	7.48	9.16	3.85	3.06	2.77	1.71	1.05	0.71	2.5
Uptake curve method									
$\ln(1-q/q^*)$	-1.277	-1.699	-2.132	-2.652	-2.946	-3.44	-3.664		
Time (min)	345	420	510	615	710	780	800		
$\ln(1-q/q^*)$	-3.664	-4.357	-4.261	-4.356	-4.644	-5.406			
Time (min)	830	860	885	905	920	935			

Run Number: IS14, Flow rate: $4 \times 10^{-6} \text{ m}^3/\text{sec}$, Inlet concentration: 0.14 kg/m^3

LDF method									
Amount adsorbed (g/g)	0.157	0.184	0.198	0.217	0.233	0.254	0.27	0.277	0.28
Time (min)	160	225	280	340	410	515	600	660	725
Average adsorbed, q	0.078	0.17	0.191	0.207	0.225	0.244	0.262	0.274	0.278
$\frac{dq}{dt} \times 10^4$	14.75	3.82	2.67	2.57	1.81	2.11	2.0	0.615	1.43
Uptake curve method									
$\ln(1-q/q^*)$	-1.4	-1.655	-2.136	-2.772	-3.265	-3.583	-4.564		
Time (min)	340	410	515	600	660	725	760		

Run Number: IS15, Flow rate: $1.49 \times 10^{-6} \text{ m}^3/\text{sec}$, Inlet concentration: 0.027 kg/m^3

LDF method									
Amount adsorbed (g/g)	0.072	0.114	0.117	0.13	0.14	0.158	0.163	0.167	
Time (min)	195	260	310	360	415	505	590	680	
Average adsorbed, q	0.036	0.093	0.115	0.124	0.135	0.149	0.161	0.165	
$\frac{dq}{dt} \times 10^4$	8.76	4.4	1.8	2.0	1.55	1.41	0.6	-	
Amount adsorbed (g/g)	0.17	0.175	0.176	0.176	0.177	0.178	0.18	0.181	
Time (min)	770	790	820	845	890	915	930	930	
Average adsorbed, q	0.168	0.173	0.175	0.176	0.177	0.179	0.1805	-	
$\frac{dq}{dt} \times 10^4$	-	0.535	-	-	-	-	-	-	

Uptake curve method

$\ln(1-q/q^*)$	-1.37	-1.73	-2.20	-2.43	-2.63	-3.11
Time (min)	415	505	590	680	770	790

$\ln(1-q/q^*)$	-3.4	-3.58	-3.81	-4.50
Time (min)	820	845	890	915

Run Number: IS16, Flow rate: $0.975 \times 10^{-6} \text{ m}^3/\text{sec}$, Inlet concentration: 0.047 kg/m^3

LDF method

Amount adsorbed (g/g)	0.056	0.092	0.12	0.14	0.16	0.175	0.185	0.2
Time (min)	85	180	275	355	470	550	590	735
Average adsorbed, q	0.028	0.074	0.106	0.13	0.15	0.167	0.18	0.193
$\frac{dq}{dt} \times 10^4$	4.84	3.36	3.0	1.89	-	1.4	-	1.32

Amount adsorbed (g/g)	0.215	0.2151	0.22	0.222	0.225	0.24
Time (min)	840	880	920	945	990	1240
Average adsorbed, q	0.207	0.2151	0.2175	0.221	0.223	0.2325
$\frac{dq}{dt} \times 10^4$	-	-	0.46	-	-	-

Uptake curve method

$\ln(1-q/q^*)$	-1.19	-1.39	-1.63	-1.98	-2.26	-2.37	-2.54	-2.65	-3.47
Time (min)	550	590	735	840	880	920	945	990	1240

Run Number: IS17, Flow rate: $0.86 \times 10^{-6} \text{ m}^3/\text{sec}$, Inlet concentration: 0.073 kg/m^3

LDF method

Amount adsorbed (g/g)	0.098	0.13	0.168	0.18	0.211	0.222	0.234	0.243
Time (min)	150	220	310	360	475	540	615	700
Average adsorbed, q	0.049	0.114	0.149	0.174	0.195	0.216	0.228	0.238
$\frac{dq}{dt} \times 10^4$	9.3	3.9	2.78	-	2.35	-	1.16	-

Amount adsorbed (g/g)	0.25	0.251	0.258	0.265	0.2675	0.2686	0.27
Time (min)	770	805	930	975	1010	1035	1055
Average adsorbed, q	0.246	0.2505	0.2545	0.2615	0.266	0.268	0.2693
$\frac{dq}{dt} \times 10^4$	0.76	-	-	0.975	-	-	-

Uptake curve method

$\ln(1-q/q^*)$	-1.28	-1.86	-2.13	-2.42	-2.62	-2.86	-3.46	-4.2
Time (min)	475	540	615	700	770	805	930	975

Run Number: IS18, Flow rate: $7.0 \times 10^{-6} \text{ m}^3/\text{sec}$, Inlet concentration: 0.56 kg/m^3

LDF method

Amount adsorbed (g/g)	0.149	0.193	0.212	0.236	0.25	0.283	0.2936	0.3
Time (min)	125	213	271	327	385	564	624	684
Average adsorbed, q	0.0725	0.171	0.2025	0.224	0.243	0.2665	0.2883	0.2968
$\frac{dq}{dt} \times 10^4$	11.2	4.65	-	3.27	1.97	-	-	-

Amount adsorbed (g/g)	0.328	0.335	0.353	0.3560	0.36	0.362
Time (min)	744	824	964	1004	1034	1059
Average adsorbed, q	0.314	0.3315	0.344	0.3545	0.358	0.361
$\frac{dq}{dt} \times 10^4$	1.55	-	-	1.18	-	-

Uptake curve method

$\ln(1-q/q_0)$	-1.33	-1.60	-1.71	-2.02	-2.47	-3.0	-3.87
Time (min)	564	624	684	744	824	964	1004

Run Number: IS19, Flow rate: $4.0 \times 10^{-6} \text{ m}^3/\text{sec}$, Inlet concentration: 0.12 kg/m^3

LDF method

Amount adsorbed (g/g)	0.1378	0.17	0.19	0.207	0.24	0.257	0.274	0.2811	0.29
Time (min)	160	238	302	371	539	617	710	790	970
Average adsorbed, q	0.0689	0.1539	0.18	0.1985	0.2235	0.2485	0.2655	0.277	0.2855
$\frac{dq}{dt} \times 10^4$	10.75	4.08	1.83	-	1.44	-	-	-	-

Uptake curve method

$\ln(1-q/q_0)$	-1.15	-1.47	-1.94	-2.47	-3.10	-4.16
Time (min)	371	539	617	710	790	970

Run Number: IS20, Flow rate: $6.5 \times 10^{-6} \text{ m}^3/\text{sec}$, Inlet concentration: 0.60 kg/m^3

LDF method

Amount adsorbed (g/g)	0.133	0.183	0.22	0.25	0.3	0.324	0.339	0.35	0.363	0.365	0.366
Time (min)	160	245	310	380	550	630	725	785	965	1005	1038
Average adsorbed, q	0.0665	0.158	0.2	0.235	0.275	0.312	0.319	0.344	0.356	0.364	0.3655
$\frac{dq}{dt} \times 10^4$	10.76	6.46	5.0	3.08	-	2.06	-	0.85	-	-	-

Uptake curve method

$\ln(1-q/q_0)$	-1.39	-1.91	-2.05	-2.81	-3.60
Time (min)	550	630	725	785	965

Run Number: IS21, Flow rate: $4.34 \times 10^{-6} \text{ m}^3/\text{sec}$, Inlet concentration: 0.43 kg/m^3

LDF method							
Amount adsorbed (g/g)	0.158	0.232	0.288	0.314	0.3314	0.35	0.352
Time (min)	115	235	390	490	610	805	875
Average adsorbed, q	0.079	0.195	0.26	0.301	0.323	0.3417	0.351
$\frac{dq}{dt} \times 10^4$	9.7	4.19	4.1	1.83	0.96	-	-
Uptake curve method						-2.50	-3.53
$\ln(1-q/q^*)$	-1.34		-1.93		610	805	
Time (min)	390		490				

Run Number: IS22, Flow rate: $4 \times 10^{-6} \text{ m}^3/\text{sec}$, Inlet concentration: 0.27 kg/m^3

LDF method					
Amount adsorbed (g/g)	0.128	0.1669	0.198	0.206	0.21
Time (min)	115	235	390	490	548
Average adsorbed, q	0.064	0.14745	0.18245	0.202	0.208
$\frac{dq}{dt} \times 10^4$	6.92	2.25	2.0	1.03	
Uptake curve method				-2.862	-3.961
$\ln(1-q/q^*)$	-1.583		390	490	
Time (min)	235				

B) System : 5A-Ethyl Acetate, Temperature: 40°C

Run Number: IS23, Flow rate: $0.86 \times 10^{-6} \text{ m}^3/\text{sec}$, Inlet concentration: 0.073 kg/m^3

LDF method										
Amount adsorbed (g/g)	0.05	0.073	0.107	0.135	0.164	0.203	0.223	0.229	0.235	0.24
Time (min)	35	66	123	176	243	381	438	490	530	600
Average adsorbed, q	0.025	0.0615	0.09	0.121	0.149	0.184	0.213	0.226	0.232	0.237
$\frac{dq}{dt} \times 10^4$	11.77	5.0	4.92	-	3.28	-	2.5	1.5	0.71	-
Uptake curve method										
$\ln(1-q/q')$	-1.45		-2.18		-2.84		-3.4		-4.38	
Time (min)	381		438		490		530		600	

Run Number: IS24, Flow rate: $7.0 \times 10^{-6} \text{ m}^3/\text{sec}$, Inlet concentration: 0.56 kg/m^3

LDF method										
Amount adsorbed (g/g)	0.127	0.196	0.255	0.296	0.32	0.33	0.344	0.3467	0.3497	0.351
Time (min)	60	118	204	322	424	524	651	704	761	818
Average adsorbed, q	0.063	0.1615	0.225	0.275	0.308	0.325	0.337	0.345	0.348	0.35
$\frac{dq}{dt} \times 10^4$	17.0	7.38	4.23	3.23	1.7	0.95	0.778	-	-	-
Uptake curve method										
$\ln(1-q/q')$	-1.53		-2.1		-2.60		-3.22		-4.06	
Time (min)	322		424		524		651		704	

Run Number: IS25, Flow rate: $0.975 \times 10^{-6} \text{ m}^3/\text{sec}$, Inlet concentration: 0.047 kg/m^3

LDF method										
Amount adsorbed (g/g)	0.07	0.09	0.106	0.12	0.14	0.173	0.184	0.198	0.204	0.21
Time (min)	120	178	237	296	355	474	533	592	625	651
Average adsorbed, q	0.035	0.08	0.098	0.113	0.13	0.156	0.178	0.191	0.201	0.204
$\frac{dq}{dt} \times 10^4$	7.75	3.05	2.71	-	2.69	-	2.37	-	-	-
Uptake curve method										
$\ln(1-q/q')$	-1.36		-1.88		-2.40		-3.15		-3.55	
Time (min)	474		533		592		625		651	

Run Number: IS26, Flow rate: $6.5 \times 10^{-6} \text{ m}^3/\text{sec}$, Inlet concentration: 0.60 kg/m^3

LDF method										
Amount adsorbed (g/g)	0.161	0.238	0.282		0.3277		0.34		0.347	0.354
Time (min)	170	290	385		535		595		640	730
Average adsorbed, q	0.0805	0.199	0.26		0.304		0.33		0.3435	0.351
$\frac{dq}{dt} \times 10^4$	6.97	6.42	2.93		2.41		-		-	-
Uptake curve method										
$\ln(1-q/q')$	-1.33		-1.96		-2.69		-3.51		-4.38	
Time (min)	385		535		595		640		730	

Run Number: IS27, Flow rate: $4.0 \times 10^{-6} \text{ m}^3/\text{sec}$, Inlet concentration: 0.27 kg/m^3

LDF method										
Amount adsorbed (g/g)	0.1373	0.18	0.203	0.233	0.253	0.2674	0.2899	0.305	0.3135	0.32
Time (min)	165	285	380	530	635	725	875	1000	1100	1200
Average adsorbed, q	0.069	0.159	0.191	0.218	0.243	0.26	0.279	0.297	0.3092	0.317
$\frac{dq}{dt} \times 10^4$	7.5	3.1	2.1	-	1.5	-	1.16	-	-	-
Uptake curve method										
$\ln(1-q/q^*)$	-1.14	-1.42	-1.67	-2.05	-2.63	-3.38				
Time (min)	530	635	725	875	1000	1100				

Run Number: IS28, Flow rate: $4.0 \times 10^{-6} \text{ m}^3/\text{sec}$, Inlet concentration: 0.12 kg/m^3

LDF method										
Amount adsorbed (g/g)	0.042	0.091	0.168	0.2063	0.238	0.259	0.263	0.266	0.267	
Time (min)	60	163	346	449	584	764	819	879	939	
Average adsorbed, q	0.021	0.066	0.129	0.187	0.222	0.248	0.261	0.2645	0.2665	
$\frac{dq}{dt} \times 10^4$	4.36	3.44	2.84	-	-	2.36	0.458	-	-	
Uptake curve method										
$\ln(1-q/q^*)$	-1.20	-1.78	-2.64	-3.79	-4.67					
Time (min)	449	584	764	819	879					

Run Number: IS29, Flow rate: $4.34 \times 10^{-6} \text{ m}^3/\text{sec}$, Inlet concentration: 0.43 kg/m^3

LDF method										
Amount adsorbed (g/g)	0.161	0.202	0.25	0.303	0.32	0.328	0.332	0.34		
Time (min)	135	210	315	500	605	665	740	920		
Average adsorbed, q	0.0805	0.1815	0.226	0.2765	0.3115	0.324	0.33	0.336		
$\frac{dq}{dt} \times 10^4$	13.5	4.24	2.72	2.23	-	-	0.33	-		
Uptake curve method										
$\ln(1-q/q^*)$	-1.67	-2.45	-3.056	-3.53						
Time (min)	500	605	665	740						

Run Number: IS30, Flow rate: $1.49 \times 10^{-6} \text{ m}^3/\text{sec}$, Inlet concentration: 0.027 kg/m^3

LDF method								
Amount adsorbed (g/g)	0.0638	0.0825	0.097	0.1225	0.136	0.14	0.145	0.15
Time (min)	120	180	240	360	480	540	660	780
Average adsorbed, q	0.0319	0.0732	0.089	0.109	0.129	0.138	0.1425	0.147
$\frac{dq}{dt} \times 10^4$	6.88	2.63	1.66	1.11	-	-	0.375	-

Uptake curve method			
$\ln(1-q/q^*)$	-1.18	-1.72	-2.11
Time (min)	360	480	540
			-2.38
			660
			-2.75
			780

Run Number: IS31, Flow rate: $0.86 \times 10^{-6} \text{ m}^3/\text{sec}$, Inlet concentration: 0.12 kg/m^3

LDF method								
Amount adsorbed (g/g)	0.0465	0.06	0.078	0.1076	0.122	0.1377	0.1516	0.1628
Time (min)	135	225	340	485	565	645	790	890
Average adsorbed, q	0.02325	0.05325	0.069	0.0928	0.115	0.13	0.14465	0.1572
$\frac{dq}{dt} \times 10^4$	3.33	1.37	1.64	2.775	1.875	1.01	1.25	1.058

Uptake curve method			
$\ln(1-q/q^*)$	-1.11	-1.42	-1.79
Time (min)	565	645	790
			-2.26
			890
			-3.6
			1010

Run Number: IS32, Flow rate: $0.86 \times 10^{-6} \text{ m}^3/\text{sec}$, Inlet concentration: 0.12 kg/m^3

LDF method								
Amount adsorbed (g/g)	0.0024	0.0307	0.062	0.073	0.083	0.0958	0.1074	0.1188
Time (min)	85	230	420	478	554	674	754	874
Average adsorbed, q	0.0012	0.0154	0.0463	0.0675	0.078	0.0896	0.1016	0.1131
$\frac{dq}{dt} \times 10^4$	0.976	1.63	3.655	1.38	0.97	1.5	0.958	1.48

Uptake curve method			
$\ln(1-q/q^*)$	-1.55	-2.06	-2.66
Time (min)	754	874	934
			-4.57
			994

Run Number: IS33, Flow rate: $4 \times 10^{-6} \text{ m}^3/\text{sec}$, Inlet concentration: 0.27 kg/m^3

LDF method

Amount adsorbed (g/g)	0.045	0.0749	0.086	0.1064	0.1185	0.1285	0.138	0.145	0.1478
Time (min)	200	300	425	545	665	755	955	1025	1055
Average adsorbed, q	0.0225	0.0599	0.0804	0.0962	0.112	0.1235	0.13325	0.1415	0.1464
$\frac{dq}{dt} \times 10^4$	3.742	1.64	1.32	1.32	1.28	0.4875	1.178	1.63	-

Uptake curve method

$\ln(1-q/q^*)$	-1.23	-1.56	-1.94	-2.52	-3.4
Time (min)	545	665	755	955	1025

Run Number: IS34, Flow rate: $4 \times 10^{-6} \text{ m}^3/\text{sec}$, Inlet concentration: 0.27 kg/m^3

LDF method

Amount adsorbed (g/g)	0.12468	0.174	0.205	0.222	0.245	0.2615	0.2655
Time (min)	170	280	400	510	650	855	880
Average adsorbed, q	0.06234	0.149	0.1895	0.2735	0.2335	0.253	0.2635
$\frac{dq}{dt} \times 10^4$	7.88	3.375	7.64	2.86	0.951	4.2	-

Uptake curve method

$\ln(1-q/q^*)$	-1.478	-1.8	-2.56	-4.19
Time (min)	400	510	650	855

C) System: 5A-Ethyl Acetate, Temperature: 45°C

Run Number: IS35, Flow rate: $1.49 \times 10^{-6} \text{ m}^3/\text{sec}$, Inlet concentration: 0.027 kg/m^3

LDF method

Amount adsorbed (g/g)	0.034	0.047	0.061	0.066	0.085	0.096	0.1044	0.11	0.1168	0.12
Time (min)	105	155	245	325	490	570	640	715	830	880
Average adsorbed, q	0.017	0.0405	0.054	0.0635	0.0755	0.0905	0.1	0.107	0.1134	0.1184
$\frac{dq}{dt} \times 10^4$	4.7	1.5	1.18	1.115	-	-	-	0.69	-	-

Uptake curve method

$\ln(1-q/q^*)$	-1.38	-1.75	-2.156	-2.77	-3.84
Time (min)	570	640	715	830	880

Run Number: IS36, Flow rate: $0.975 \times 10^{-6} \text{ m}^3/\text{sec}$, Inlet concentration: 0.047 kg/m^3

LDF method							
Amount adsorbed (g/g)	0.087	0.122	0.1377	0.159	0.167	0.1737	0.18
Time (min)	180	300	360	480	540	630	810
Average adsorbed, q	0.0435	0.1045	0.13	0.1483	0.163	0.17	0.176
$\frac{dq}{dt} \times 10^4$	5.08	4.25	1.52	1.44	-	0.33	-
Uptake curve method							
$\ln(1-q/q^*)$	-1.28	-1.74	-2.35	-2.89	-3.80		
Time (min)	360	480	540	630	810		

Run Number: IS37, Flow rate: $0.86 \times 10^{-6} \text{ m}^3/\text{sec}$, Inlet concentration: 0.073 kg/m^3

LDF method							
Amount adsorbed (g/g)	0.093	0.133	0.158	0.17	0.184	0.189	0.2
Time (min)	150	255	340	420	505	585	655
Average adsorbed, q	0.0465	0.113	0.1455	0.164	0.177	0.1865	0.1945
$\frac{dq}{dt} \times 10^4$	6.33	3.8	1.67	-	-	1.088	-
Uptake curve method							
$\ln(1-q/q^*)$	-1.18	-1.52	-1.85	-2.19	-2.6	-3.74	
Time (min)	340	420	505	585	655	755	

Run Number: IS38, Flow rate: $4.34 \times 10^{-6} \text{ m}^3/\text{sec}$, Inlet concentration: 0.43 kg/m^3

LDF method							
Amount adsorbed (g/g)	0.173	0.211	0.25	0.283	0.3	0.313	0.32
Time (min)	184	271	390	540	630	690	780
Average adsorbed, q	0.0865	0.192	0.2305	0.2665	0.2915	0.3065	0.3165
$\frac{dq}{dt} \times 10^4$	12.33	3.23	2.4	2.08	-	-	0.647
Uptake curve method							
$\ln(1-q/q^*)$	-1.24	-1.73	-2.23	-2.92	-3.76		
Time (min)	390	540	630	690	780		

Run Number: IS39, Flow rate: $7.0 \times 10^{-6} \text{ m}^3/\text{sec}$, Inlet concentration: 0.56 kg/m^3

LDF method							
Amount adsorbed (g/g)	0.157	0.195	0.237	0.267	0.28	0.311	0.329
Time (min)	120	170	245	335	410	530	650
Average adsorbed, q	0.0785	0.176	0.216	0.252	0.2735	0.2955	0.32
$\frac{dq}{dt} \times 10^4$	19.5	6.13	4.0	2.23	-	1.97	-
Uptake curve method							
$\ln(1-q/q^*)$	-1.33	-1.60	-1.98	-2.72	-3.68		
Time (min)	335	410	530	650	725	782	810

Run Number: IS40, Flow rate: $4.0 \times 10^{-6} \text{ m}^3/\text{sec}$, Inlet concentration: 0.12 kg/m^3

LDF method								
Amount adsorbed (g/g)	0.0648	0.1284	0.178	0.193	0.216	0.2277	0.235	0.24
Time (min)	90	210	370	430	550	670	790	910
Average adsorbed, q	0.0324	0.096	0.1532	0.1855	0.2045	0.2218	0.2314	0.237
$\frac{dq}{dt} \times 10^4$	5.3	3.6	2.85	-	1.44	0.8	0.47	-
Uptake curve method						-2.57	-3.32	
$\ln(1-q/q^*)$	-1.48		-1.91		670	790		
Time (min)	430		550					

Run Number: IS41, Flow rate: $1.49 \times 10^{-6} \text{ m}^3/\text{sec}$, Inlet concentration: 0.36 kg/m^3

LDF method								
Amount adsorbed (g/g)	0.0976	0.135	0.151	0.18	0.192	0.208	0.210	0.22
Time (min)	145	245	305	420	500	605	665	725
Average adsorbed, q	0.048	0.116	0.143	0.165	0.186	0.2	0.209	0.215
$\frac{dq}{dt} \times 10^4$	6.8	4.5	1.91	2.63	1.33	1.5	1.0	1.1
Amount adsorbed (g/g)	0.222	0.227	0.232	0.234	0.237			
Time (min)	780	870	910	945	975			
Average adsorbed, q	0.221	0.224	0.229	0.233	0.235			
$\frac{dq}{dt} \times 10^4$	0.33	1.25	1.14	0.66	-			
Uptake curve method								
$\ln(1-q/q^*)$	-1.425	-1.661	-2.101	-2.172	-2.635	-2.76	-3.165	-3.858
Time (min)	420	500	605	665	725	780	870	910
								945
								-4.369

Run Number: IS42, Flow rate: $1.49 \times 10^{-6} \text{ m}^3/\text{sec}$, Inlet concentration: 0.047 kg/m^3

LDF method											
Amount adsorbed (g/g)	0.0945	0.111	0.135	0.1478	0.163	0.174	0.184	0.188	0.193	0.208	0.211
Time (min)	190	245	335	380	475	545	600	660	715	830	865
Average adsorbed, q	0.0473	0.103	0.123	0.141	0.1554	0.168	0.179	0.186	0.1905	0.2005	0.209
$\frac{dq}{dt} \times 10^4$	10.13	2.22	4.0	1.51	1.8	2.0	1.16	0.82	0.87	2.43	-
Amount adsorbed (g/g)											
Time (min)											
Average adsorbed, q											
$\frac{dq}{dt} \times 10^4$											
Uptake curve method											
$\ln(1-q/q^*)$	-1.2		-1.48		-1.74		-2.05		-2.2		-2.4
Time (min)	380		475		545		600		660		715

Run Number: IS43, Flow rate: $4.0 \times 10^{-6} \text{ m}^3/\text{sec}$, Inlet concentration: 0.27 kg/m^3

LDF method											
Amount adsorbed (g/g)	0.10476	0.15	0.1788	0.195	0.2137	0.232	0.2548	0.269	0.284	0.287	0.291
Time (min)	120	210	300	360	435	525	645	765	915	975	1035
Average adsorbed, q	0.053	0.127	0.164	0.1869	0.204	0.223	0.2434	0.262	0.276	0.285	0.289
$\frac{dq}{dt} \times 10^4$	8.22	4.11	3.81	2.18	-	1.625	-	1.095	-	0.66	-
Uptake curve method											
$\ln(1-q/q^*)$	-1.20	-1.45	-1.81	-2.3	-2.96	-3.88					
Time (min)	435	525	645	765	915	975					

Run Number: IS44, Flow rate: $6.5 \times 10^{-6} \text{ m}^3/\text{sec}$, Inlet concentration: 0.60 kg/m^3

LDF method							
Amount adsorbed (g/g)	0.177	0.2613	0.2935	0.325	0.338	0.342	0.345
Time (min)	165	300	390	615	720	795	855
Average adsorbed, q	0.0885	0.22	0.2774	0.31	0.332	0.34	0.343
$\frac{dq}{dt} \times 10^4$	9.74	6.4	1.65	-	0.815	-	-
Uptake curve method							
$\ln(1-q/q^*)$	-1.63	-2.29	-3.28	-4.23			
Time (min)	390	615	720	795			

D) System: 5A-Ethyl Acetate, Temperature: 55°C

Run Number: IS45, Flow rate: $1.49 \times 10^{-6} \text{ m}^3/\text{sec}$, Inlet concentration: 0.027 kg/m^3

LDF method								
Amount adsorbed (g/g)	0.0456	0.0645	0.0775	0.0855	0.0955	0.0985	0.1011	0.102
Time (min)	65	125	207	275	375	425	480	565
Average adsorbed, q	0.0228	0.0551	0.071	0.0815	0.0905	0.097	0.0998	0.1015
$\frac{dq}{dt} \times 10^4$	5.38	1.76	-	0.9	0.885	-	0.2	-
Uptake curve method								
$\ln(1-q/q^*)$	-1.19	-1.60	-2.18	-3.01	-3.84			
Time (min)	207	275	375	425	480			

Run Number: IS46, Flow rate: $0.975 \times 10^{-6} \text{ m}^3/\text{sec}$, Inlet concentration: 0.047 kg/m^3

LDF method									
Amount adsorbed (g/g)	0.070	0.084	0.0989	0.1243	0.1337	0.1364	0.145	0.155	
Time (min)	170	240	300	460	527	590	650	710	810
Average adsorbed, q	0.035	0.077	0.0914	0.1116	0.129	0.135	0.141	0.1475	0.153
$\frac{dq}{dt} \times 10^4$	6.0	2.4	1.66	-	0.975	-	0.75	-	-
Uptake curve method									
$\ln(1-q/q^*)$	-1.27	-1.78	-2.04	-2.4	-3.03				
Time (min)	460	527	590	650	710				

Run Number: IS43, Flow rate: $4.0 \times 10^{-6} \text{ m}^3/\text{sec}$, Inlet concentration: 0.27 kg/m^3

LDF method

Amount adsorbed (g/g)	0.10476	0.15	0.1788	0.195	0.2137	0.232	0.2548	0.269	0.284	0.287	0.291
Time (min)	120	210	300	360	435	525	645	765	915	975	1035
Average adsorbed, q	0.053	0.127	0.164	0.1869	0.204	0.223	0.2434	0.262	0.276	0.285	0.289
$\frac{dq}{dt} \times 10^4$	8.22	4.11	3.81	2.18	-	1.625	-	1.095	-	0.66	-

Uptake curve method

$\ln(1-q/q^*)$	-1.20	-1.45	-1.81	-2.3	-2.96	-3.88
Time (min)	435	525	645	765	915	975

Run Number: IS44, Flow rate: $6.5 \times 10^{-6} \text{ m}^3/\text{sec}$, Inlet concentration: 0.60 kg/m^3

LDF method

Amount adsorbed (g/g)	0.177	0.2613	0.2935	0.325	0.338	0.342	0.345
Time (min)	165	300	390	615	720	795	855
Average adsorbed, q	0.0885	0.22	0.2774	0.31	0.332	0.34	0.343
$\frac{dq}{dt} \times 10^4$	9.74	6.4	1.65	-	0.815	-	-

Uptake curve method

$\ln(1-q/q^*)$	-1.63	-2.29	-3.28	-4.23
Time (min)	390	615	720	795

D) System: 5A-Ethyl Acetate, Temperature: 55°C

Run Number: IS45, Flow rate: $1.49 \times 10^{-6} \text{ m}^3/\text{sec}$, Inlet concentration: 0.027 kg/m^3

LDF method

Amount adsorbed (g/g)	0.0456	0.0645	0.0775	0.0855	0.0955	0.0985	0.1011	0.102
Time (min)	65	125	207	275	375	425	480	565
Average adsorbed, q	0.0228	0.0551	0.071	0.0815	0.0905	0.097	0.0998	0.1015
$\frac{dq}{dt} \times 10^4$	5.38	1.76	-	0.9	0.885	-	0.2	-

Uptake curve method

$\ln(1-q/q^*)$	-1.19	-1.60	-2.18	-3.01	-3.84
Time (min)	207	275	375	425	480

Run Number: IS46, Flow rate: $0.975 \times 10^{-6} \text{ m}^3/\text{sec}$, Inlet concentration: 0.047 kg/m^3

LDF method

Amount adsorbed (g/g)	0.070	0.084	0.0989	0.1243	0.1337	0.1364	0.145	0.15	0.155
Time (min)	170	240	300	460	527	590	650	710	810
Average adsorbed, q	0.035	0.077	0.0914	0.1116	0.129	0.135	0.141	0.1475	0.153
$\frac{dq}{dt} \times 10^4$	6.0	2.4	1.66	-	0.975	-	0.75	-	-

Uptake curve method

$\ln(1-q/q^*)$	-1.27	-1.78	-2.04	-2.4	-3.03
Time (min)	460	527	590	650	710

Run Number: IS47, Flow rate: $0.86 \times 10^{-6} \text{ m}^3/\text{sec}$, Inlet concentration: 0.073 kg/m^3

LDF method								
Amount adsorbed (g/g)	0.064	0.092	0.1161	0.1511	0.163	0.175	0.18	0.1903
Time (min)	80	140	205	320	410	450	500	560
Average adsorbed, q	0.032	0.078	0.104	0.1336	0.157	0.169	0.1775	0.185
$\frac{dq}{dt} \times 10^4$	7.66	4.0	2.57	2.14	-	-	-	-
Uptake curve method								
$\ln(1-q/q^*)$	-1.21	-1.74	-2.18	-2.7	-3.6			
Time (min)	320	410	450	500	560			

Run Number: IS48, Flow rate: $4.0 \times 10^{-6} \text{ m}^3/\text{sec}$, Inlet concentration: 0.12 kg/m^3

LDF method								
Amount adsorbed (g/g)	0.0589	0.0865	0.1069	0.124	0.154	0.1644	0.171	0.1819
Time (min)	80	147	207	267	387	452	512	572
Average adsorbed, q	0.0294	0.0727	0.0967	0.115	0.139	0.159	0.167	0.176
$\frac{dq}{dt} \times 10^4$	6.46	4.0	3.05	2.0	1.79	-	-	-
Amount adsorbed (g/g)			0.1878	0.206	0.2157	0.22		
Time (min)			642	782	882	942		
Average adsorbed, q			0.1848	0.197	0.2108	0.22		
$\frac{dq}{dt} \times 10^4$			1.07	-	-	-		
Uptake curve method								
$\ln(1-q/q^*)$	-1.28	-1.42	-1.61	-1.83	-2.26	-3.17		
Time (min)	452	512	572	642	782	882		

Run Number: IS49, Flow rate: $4.0 \times 10^{-6} \text{ m}^3/\text{sec}$, Inlet concentration 0.27 kg/m^3

LDF method								
Amount adsorbed (g/g)	0.0627	0.0997	0.1321	0.161	0.194	0.208	0.221	0.235
Time (min)	60	120	180	265	360	420	505	555
Average adsorbed, q	0.0313	0.0812	0.1159	0.146	0.177	0.2014	0.2146	0.228
$\frac{dq}{dt} \times 10^4$	8.32	5.78	3.54	3.26	2.61	-	-	1.28
Amount adsorbed (g/g)			0.248	0.254	0.261	0.265		
Time (min)			685	735	800	880		
Average adsorbed, q			0.2415	0.251	0.257	0.263		
$\frac{dq}{dt} \times 10^4$			-	0.83	-	-		
Uptake curve method								
$\ln(1-q/q^*)$	-1.43	-1.66	-1.97	-2.42	-2.94	-3.5		
Time (min)	420	505	555	685	735	800		

Run Number: IS50, Flow rate: $4.34 \times 10^{-6} \text{ m}^3/\text{sec}$, Inlet concentration: 0.43 kg/m^3

LDF method									
Amount adsorbed (g/g)	0.073	0.1255	0.1601	0.1893	0.2142	0.239	0.261	0.275	0.285
Time (min)	60	125	185	250	310	375	435	505	560
Average adsorbed, q	0.0365	0.0993	0.143	0.175	0.202	0.226	0.25	0.268	0.28
$\frac{dq}{dt} \times 10^4$	9.66	7.28	4.92	4.5	3.69	3.23	-	2.18	-
Uptake curve method									
$\ln(1-q/q')$	-1.23			-1.57		-2.1		-2.82	
Time (min)	310			375		435		505	

Run Number: IS51, Flow rate: $7.0 \times 10^{-6} \text{ m}^3/\text{sec}$, Inlet concentration: 0.56 kg/m^3

LDF method												
Amount adsorbed (g/g)	0.1106	0.1441	0.176	0.199	0.226	0.243	0.2462	0.263	0.269	0.279	0.288	
Time (min)	95	155	210	270	345	410	485	565	627	731	835	
Average adsorbed, q	0.055	0.127	0.161	0.187	0.213	0.234	0.244	0.255	0.266	0.274	0.284	
$\frac{dq}{dt} \times 10^4$	12.0	6.18	4.33	3.47	3.23	1.33	1.22	-	-	0.96	-	
Uptake curve method												
$\ln(1-q/q')$	-1.34			-1.67		-1.87		-2.17		-2.57		-3.02
Time (min)	345			410		485		565		627		731

Run Number: IS52, Flow rate: $6.5 \times 10^{-6} \text{ m}^3/\text{sec}$, Inlet concentration: 0.60 kg/m^3

LDF method											
Amount adsorbed (g/g)	0.067	0.105	0.1366	0.1625	0.192	0.219	0.2421	0.266	0.284	0.289	0.291
Time (min)	60	120	180	222	325	415	490	600	690	730	790
Average adsorbed, q	0.034	0.086	0.1208	0.149	0.177	0.206	0.231	0.254	0.275	0.2865	0.29
$\frac{dq}{dt} \times 10^4$	8.67	5.8	3.875	-	2.8	-	-	2.5	-	0.58	-
Uptake curve method											
$\ln(1-q/q')$	-1.23			-1.6		-2.06		-2.9		-4.16	
Time (min)	415			490		600		690		730	

B) System : 13X-Ethyl Acetate, Temperature: 35°C

Run Number: IS53, Flow rate: $6.5 \times 10^{-6} \text{ m}^3/\text{sec}$, Inlet Concentration: 0.60 kg/m^3

LDF method

Amount adsorbed (g/g)	0.259	0.350	0.3845	0.444	0.4756	0.5036	0.5276	0.566	0.577	0.584
Time (min)	135	250	307	437	522	587	667	847	907	937
Average adsorbed, q	0.1295	0.304	0.3672	0.414	0.4598	0.489	0.5016	0.5468	0.5715	0.5805
$\frac{dq}{dt} \times 10^4$	15.17	11.08	3.6	5.4	4.49	1.575	2.5	4.11	3.0	-

Uptake curve method

$\ln(1-q/q^*)$	-1.23	-1.55	-1.82	-1.96	-2.75	-3.84
Time (min)	437	522	587	667	847	907

Run Number: IS54, Flow rate: $4.0 \times 10^{-6} \text{ m}^3/\text{sec}$, Inlet Concentration: 0.27 kg/m^3

LDF method

Amount adsorbed (g/g)	0.254	0.284	0.35	0.41	0.439	0.448	0.467	0.506
Time (min)	160	240	335	587	700	777	855	960
Average adsorbed, q	0.127	0.269	0.317	0.380	0.424	0.44	0.457	0.48
$\frac{dq}{dt} \times 10^4$	17.75	5.05	2.5	3.9	2.07	2.18	2.19	-

Uptake curve method

$\ln(1-q/q^*)$	-0.98	-1.39	-1.82	-2.04	-2.33
Time (min)	335	587	700	777	855

Run Number: IS55, Flow rate: $8.0 \times 10^{-6} \text{ m}^3/\text{sec}$, Inlet Concentration: 0.27 kg/m^3

LDF method

Amount adsorbed (g/g)	0.207	0.270	0.327	0.416	0.475	0.494	0.498	0.508
Time (min)	145	240	355	602	910	1000	1035	1115
Average adsorbed, q	0.1035	0.2385	0.2985	0.3715	0.445	0.484	0.496	0.503
$\frac{dq}{dt} \times 10^4$	14.21	5.22	2.955	2.4	4.33	3.4	0.875	-

Uptake curve method

$\ln(1-q/q^*)$	-1.31	-2.08	-3.05	-3.74
Time (min)	602	910	1000	1035

Run Number: IS56, Flow rate: $0.86 \times 10^{-6} \text{ m}^3/\text{sec}$, Inlet Concentration: 0.047 kg/m^3

LDF method								
Amount adsorbed (g/g)	0.058	0.087	0.1285	0.155	0.193	0.208	0.238	0.255
Time (min)	235	387	502	620	736	870	980	1015
Average adsorbed, q	0.029	0.0725	0.107	0.142	0.174	0.20	0.223	0.246
$\frac{dq}{dt} \times 10^4$	2.86	3.0	2.96	2.76	1.94	2.09	2.3	-
							-3.34	
							980	1015

Uptake curve method

$\ln(1-q/q^*)$	-1.15	-1.53	-2.07					
Time (min)	736	870	980					

Run Number: IS57, Flow rate: $4.0 \times 10^{-6} \text{ m}^3/\text{sec}$, Inlet Concentration: 0.12 kg/m^3

LDF method								
Amount adsorbed (g/g)	0.169	0.23	0.2843	0.325	0.353	0.377	0.391	0.416
Time (min)	140	260	385	500	612	823	945	1050
Average adsorbed, q	0.0845	0.1995	0.2572	0.3047	0.339	0.365	0.384	0.395
$\frac{dq}{dt} \times 10^4$	9.58	4.6	4.08	3.125	1.23	1.55	1.04	0.52
							-2.98	-3.89
							1050	1290

Uptake curve method

$\ln(1-q/q^*)$	-1.32	-1.7	-2.1	-2.56				
Time (min)	500	612	823	945				

Run Number: IS58, Flow rate: $0.86 \times 10^{-6} \text{ m}^3/\text{sec}$, Inlet Concentration: 0.047 kg/m^3

LDF method								
Amount adsorbed (g/g)	0.089	0.1106	0.1248	0.1489	0.168	0.196	0.2407	0.2589
Time (min)	120	220	315	415	505	605	835	925
Average adsorbed, q	0.044	0.0998	0.117	0.136	0.158	0.182	0.218	0.249
$\frac{dq}{dt} \times 10^4$	5.58	1.81	1.9	2.44	2.4	1.56	3.44	1.83
							-3.1	
							835	925

Uptake curve method

$\ln(1-q/q^*)$	-1.2	-1.80						
Time (min)	605	835						

Run Number: IS59, Flow rate: $1.49 \times 10^{-6} \text{ m}^3/\text{sec}$, Inlet Concentration: 0.027 kg/m^3

LDF method								
Amount adsorbed (g/g)	0.1236	0.166	0.192	0.209	0.225	0.231	0.238	
Time (min)	120	220	315	415	550	625	725	
Average adsorbed, q	0.0618	0.1448	0.179	0.2	0.217	0.228	0.2345	
$\frac{dq}{dt} \times 10^4$	8.3	3.6	2.1	1.26	1.46	0.65	-	

Uptake curve method

$\ln(1-q/q^*)$	-1.39	-1.83	-2.43	-3.17	-4.2
Time (min)	315	415	550	625	725

Run Number: IS60, Flow rate: $7.0 \times 10^{-6} \text{ m}^3/\text{sec}$, Inlet Concentration: 0.56 kg/m^3

LDF method

Amount adsorbed (g/g)	0.1818	0.271	0.348	0.4265	0.469	0.498	0.5426	0.5632	0.582	0.583
Time (min)	122	242	362	482	602	672	812	937	1002	1042
Average adsorbed, q	0.0909	0.226	0.309	0.387	0.447	0.483	0.5203	0.5529	0.5726	0.5825
$\frac{dq}{dt} \times 10^4$	11.25	6.9	6.5	5.0	5.14	2.66	2.608	3.01	2.475	-

Uptake curve method

$\ln(1-q/q^*)$	-1.45	-1.76	-2.23	-2.96	-4.03
Time (min)	602	672	812	937	1002

Run Number: IS61, Flow rate: $4.34 \times 10^{-6} \text{ m}^3/\text{sec}$, Inlet Concentration: 0.43 kg/m^3

LDF method

Amount adsorbed (g/g)	0.316	0.404	0.469	0.5086	0.534	0.546	0.55
Time (min)	123	243	363	483	603	723	963
Average adsorbed, q	0.158	0.360	0.4365	0.488	0.5213	0.54	0.548
$\frac{dq}{dt} \times 10^4$	16.8	6.4	4.29	2.8	1.55	0.33	-

Uptake curve method

$\ln(1-q/q^*)$	-1.57	-2.18	-2.95	-4.0
Time (min)	363	483	603	723

Run Number: IS62, Flow rate: $5.5 \times 10^{-6} \text{ m}^3/\text{sec}$, Inlet Concentration: 0.09 kg/m^3

LDF method

Amount adsorbed (g/g)	0.208	0.2357	0.266	0.289	0.318	0.328	0.332	0.336
Time (min)	120	220	340	460	585	700	855	915
Average adsorbed, q	0.104	0.2218	0.251	0.277	0.303	0.323	0.33	0.334
$\frac{dq}{dt} \times 10^4$	11.78	2.43	2.17	2.08	1.74	0.452	0.66	-

Uptake curve method

$\ln(1-q/q^*)$	-1.2089	-1.5686	-1.9669	-2.9267	-3.7376	-4.4308
Time (min)	220	340	460	585	700	855

Run Number: IS63, Flow rate: $0.975 \times 10^{-6} \text{ m}^3/\text{sec}$, Inlet Concentration: 0.047 kg/m^3

LDF method

Amount adsorbed (g/g)	0.2056	0.2213	0.2386	0.241	0.2545	0.267
Time (min)	120	220	340	460	560	700
Average adsorbed, q	0.1028	0.2134	0.229	0.239	0.247	0.261
$\frac{dq}{dt} \times 10^4$	11.06	1.3	0.833	0.8	1.0	-

Uptake curve method

$\ln(1-q/q^*)$	-1.46	-1.765	-2.241	-2.329	-3.061
Time (min)	120	220	340	460	560

Run Number: IS64, Flow rate: $4.0 \times 10^{-6} \text{ m}^3/\text{sec}$, Inlet Concentration: 0.27 kg/m^3

LDF method

Amount adsorbed (g/g)	0.223	0.287	0.346	0.397	0.436	0.462	0.482	0.501	0.508
Time (min)	120	240	360	480	605	720	845	965	1015
Average adsorbed, q	0.112	0.255	0.3165	0.3715	0.416	0.449	0.472	0.492	0.504
$\frac{dq}{dt} \times 10^4$	11.9	5.125	4.58	3.56	2.86	1.84	1.66	-	-

Uptake curve method

$\ln(1-q/q^*)$	-1.31	-1.71	-2.15	-2.65	-3.45
Time (min)	480	605	720	845	965

Run Number: IS65, Flow rate: $0.975 \times 10^{-6} \text{ m}^3/\text{sec}$, Inlet Concentration: 0.047 kg/m^3

LDF method

Amount adsorbed (g/g)	0.179	0.2228	0.2458	0.255	0.265	0.272	0.277	0.281	0.29
Time (min)	35	115	200	260	335	395	445	490	635
Average adsorbed, q	0.089	0.2009	0.2343	0.2504	0.26	0.2685	0.2745	0.279	0.2855
$\frac{dq}{dt} \times 10^4$	13.8	4.03	2.68	1.28	1.41	1.2	1.0	0.45	-

Uptake curve method

$\ln(1-q/q^*)$	-1.14	-1.59	-1.91	-2.15	-2.44	-2.71	-2.97	-3.54
Time (min)	115	200	260	335	395	445	490	635

Run Number: IS66, Flow rate: $0.86 \times 10^{-6} \text{ m}^3/\text{sec}$, Inlet Concentration: 0.073 kg/m^3

LDF method

Amount adsorbed (g/g)	0.2066	0.2550	0.285	0.301	0.312	0.319	0.326	0.335	0.34	0.345
Time (min)	65	165	250	310	370	430	500	600	660	780
Average adsorbed, q	0.103	0.231	0.27	0.293	0.306	0.315	0.323	0.331	0.337	0.343
$\frac{dq}{dt} \times 10^4$	12.78	4.611	3.83	2.25	1.5	1.0	0.8	1.13	0.43	-

Uptake curve method

$\ln(1-q/q^*)$	-1.53	-1.89	-2.2	-2.44	-2.75	-3.20	-3.76
Time (min)	250	310	370	430	500	600	660

C) System: 13X-Ethyl Acetate, Temperature: 45°C

Run Number: IS67, Flow rate: $1.49 \times 10^{-6} \text{ m}^3/\text{sec}$, Inlet Concentration: 0.027 kg/m^3

LDf method

Amount adsorbed (g/g)	0.074	0.104	0.1376	0.152	0.16	0.1664	0.17	0.174
Time (min)	60	150	270	390	460	570	750	870
Average adsorbed, q	0.037	0.089	0.1208	0.1448	0.156	0.1632	0.1682	0.172
$\frac{dq}{dt} \times 10^4$	5.77	2.65	2.0	1.02	-	0.30	-	-

Uptake curve method

$\ln(1-q/q^*)$	-1.18	-1.78	-2.27	-2.80	-3.40
Time (min)	270	390	460	570	750

Run Number: IS68, Flow rate: $6.5 \times 10^{-6} \text{ m}^3/\text{sec}$, Inlet Concentration: 0.12 kg/m^3

LDf method

Amount adsorbed (g/g)	0.186	0.224	0.254	0.287	0.3143	0.3221	0.3256	0.33
Time (min)	120	240	345	470	590	710	830	890
Average adsorbed, q	0.093	0.205	0.239	0.2705	0.3006	0.3182	0.323	0.3278
$\frac{dq}{dt} \times 10^4$	9.33	2.72	2.52	2.51	1.47	0.4	0.8	-

Uptake curve method

$\ln(1-q/q^*)$	-1.468	-2.037	-3.045	-3.732	-4.317
Time (min)	345	470	590	710	830

Run Number: IS69, Flow rate: $4.34 \times 10^{-6} \text{ m}^3/\text{sec}$, Inlet Concentration: 0.43 kg/m^3

LDf method

Amount adsorbed (g/g)	0.259	0.309	0.3403	0.376	0.3906	0.396	0.402	0.41	0.415
Time (min)	135	260	380	535	655	770	840	940	1090
Average adsorbed, q	0.1295	0.284	0.3246	0.358	0.3833	0.393	0.399	0.406	0.408
$\frac{dq}{dt} \times 10^4$	12.36	3.38	2.15	2.10	0.84	0.857	0.36	-	-

Uptake curve method

$\ln(1-q/q^*)$	-1.15	-1.52	-1.98	-2.57	-2.94	-3.255	-3.83
Time (min)	260	380	535	655	770	840	940

Run Number: IS70, Flow rate: $8.0 \times 10^{-6} \text{ m}^3/\text{sec}$, Inlet Concentration: 0.12 kg/m^3

LDf method

Amount adsorbed (g/g)	0.251	0.279	0.304	0.319	0.325	0.328	0.333
Time (min)	145	265	385	505	580	635	720
Average adsorbed, q	0.125	0.265	0.2915	0.3115	0.322	0.326	0.3305
$\frac{dq}{dt} \times 10^4$	11.67	2.21	1.67	1.4	0.73	0.53	-

Uptake curve method

$\ln(1-q/q^*)$	-1.401	-1.819	-2.441	-3.169	-3.728	-4.198
Time (min)	145	265	385	505	580	635

Run Number: IS71, Flow rate: $4.0 \times 10^{-6} \text{ m}^3/\text{sec}$, Inlet Concentration: 0.12 kg/m^3

LDF method

Amount adsorbed (g/g)	0.219	0.256	0.281	0.303	0.3112	0.323	0.334	0.336
Time (min)	125	245	365	490	550	635	750	820
Average adsorbed, q	0.1095	0.237	0.268	0.292	0.307	0.317	0.328	0.335
$\frac{dq}{dt} \times 10^4$	10.62	2.58	1.92	2.5	1.17	0.96	1.0	-

Uptake curve method

$\ln(1-q/q^*)$	-1.22	-1.60	-2.03	-2.45	-2.87	-3.74
Time (min)	245	365	490	550	635	750

Run Number: IS72, Flow rate: $0.975 \times 10^{-6} \text{ m}^3/\text{sec}$, Inlet Concentration: 0.047 kg/m^3

LDF method

Amount adsorbed (g/g)	0.198	0.205	0.222	0.231	0.242	0.247	0.251
Time (min)	125	245	365	485	550	630	745
Average adsorbed, q	0.099	0.2015	0.213	0.226	0.236	0.245	0.249
$\frac{dq}{dt} \times 10^4$	4.6	-	1.2	-	1.62	0.347	-

Uptake curve method

$\ln(1-q/q^*)$	-1.62	-1.88	-2.3	-2.82	-3.73
Time (min)	245	365	485	550	630

Run Number: IS73, Flow rate: $7.0 \times 10^{-6} \text{ m}^3/\text{sec}$, Inlet Concentration: 0.56 kg/m^3

LDF method

Amount adsorbed (g/g)	0.259	0.319	0.362	0.390	0.425	0.428	0.435
Time (min)	90	205	320	425	535	690	810
Average adsorbed, q	0.129	0.289	0.341	0.376	0.407	0.426	0.432
$\frac{dq}{dt} \times 10^4$	13.91	4.52	3.33	2.82	1.22	0.5	-

Uptake curve method

$\ln(1-q/q^*)$	-1.53	-2.0	-2.74	-3.87
Time (min)	320	425	535	690

Run Number: IS74, Flow rate: $4.0 \times 10^{-6} \text{ m}^3/\text{sec}$, Inlet Concentration: 0.27 kg/m^3

LDF method

Amount adsorbed (g/g)	0.233	0.289	0.326	0.349	0.366	0.374	0.387
Time (min)	75	190	305	410	520	675	795
Average adsorbed, q	0.1165	0.261	0.307	0.337	0.357	0.370	0.381
$\frac{dq}{dt} \times 10^4$	12.56	4.0	2.85	1.81	0.84	0.92	-

Uptake curve method

$\ln(1-q/q^*)$	-1.12	-1.57	-2.046	-2.56	-3.12
Time (min)	190	305	410	520	675

Run Number: IS75, Flow rate: $6.0 \times 10^{-6} \text{ m}^3/\text{sec}$, Inlet Concentration: 0.073 kg/m^3

LDF method

Amount adsorbed (g/g)	0.213	0.239	0.259	0.267	0.290	0.299	0.305
Time (min)	120	220	310	390	485	565	705
Average adsorbed, q	0.106	0.226	0.249	0.263	0.278	0.294	0.302
$\frac{dq}{dt} \times 10^4$	12.0	2.56	1.75	1.58	2.0	0.57	-

Uptake curve method

$\ln(1-q/q^*)$	-1.198	-1.53	-1.892	-2.083	-3.0
Time (min)	120	220	310	390	485

Run Number: IS76, Flow rate: $0.86 \times 10^{-6} \text{ m}^3/\text{sec}$, Inlet Concentration: 0.073 kg/m^3

LDF method

Amount adsorbed (g/g)	0.208	0.223	0.2337	0.240	0.25	0.272	0.276	0.277	0.282	0.285
Time (min)	70	130	190	235	325	475	565	605	705	845
Average adsorbed, q	0.104	0.216	0.228	0.237	0.245	0.261	0.274	0.276	0.2795	0.2835
$\frac{dq}{dt} \times 10^4$	18.66	2.0	2.0	0.88	1.06	1.44	0.5	0.2	-	-

Uptake curve method

$\ln(1-q/q^*)$	-1.41	-1.61	-1.78	-1.96	-2.47	-3.25	-3.45	-4.04
Time (min)	130	190	235	325	475	565	605	705

Run Number: IS77, Flow rate: $8.0 \times 10^{-6} \text{ m}^3/\text{sec}$, Inlet Concentration: 0.12 kg/m^3

LDF method

Amount adsorbed (g/g)	0.2206	0.248	0.2664	0.278	0.298	0.320	0.333	0.346	0.348
Time (min)	45	120	180	255	345	460	530	597	695
Average adsorbed, q	0.11	0.234	0.257	0.272	0.288	0.309	0.326	0.339	0.347
$\frac{dq}{dt} \times 10^4$	16.53	3.83	2.0	1.77	1.83	2.43	1.94	0.816	-

Uptake curve method

$\ln(1-q/q^*)$	-1.247	-1.444	-1.605	-1.929	-2.5	-3.106	-4.898
Time (min)	120	180	255	345	460	530	597

Run Number: IS78, Flow rate: $4.0 \times 10^{-6} \text{ m}^3/\text{sec}$, Inlet Concentration: 0.43 kg/m^3

LDF method

Amount adsorbed (g/g)	0.248	0.281	0.2981	0.324	0.348	0.371	0.382	0.395	0.399	0.402	0.405	0.406
Time (min)	85	155	215	285	405	515	700	785	865	905	965	1025
Average adsorbed, q	0.124	0.264	0.289	0.31	0.335	0.359	0.376	0.388	0.397	0.401	0.403	0.405
$\frac{dq}{dt} \times 10^4$	20.0	4.17	3.0	2.08	2.18	0.95	1.34	1.125	1.0	0.33	0.33	-

Uptake curve method

$\ln(1-q/q^*)$	-1.179	-1.324	-1.595	-1.948	-2.452	-2.833	-3.602	-4.108	-4.676	-6.217
Time (min)	155	215	285	405	515	700	785	865	905	965

Run Number: IS79, Flow rate: $6.5 \times 10^{-6} \text{ m}^3/\text{sec}$, Inlet Concentration: 0.60 kg/m^3

LDF method

Amount adsorbed (g/g)	0.2548	0.2996	0.3486	0.3896	0.408	0.423	0.438	0.44
Time (min)	40	90	161	230	290	350	450	510
Average adsorbed, q	0.1274	0.277	0.3241	0.369	0.398	0.416	0.431	0.439
$\frac{dq}{dt} \times 10^4$	29.92	6.63	5.68	-	3.0	1.5	1.33	-

Uptake curve method

$\ln(1-q/q^*)$	-1.33	-1.82	-2.35	-2.90	-3.88
Time (min)	161	230	290	350	450

D) System: 13X-Ethyl Acetate, Temperature: 55°C

Run Number: IS80, Flow rate: $0.975 \times 10^{-6} \text{ m}^3/\text{sec}$, Inlet Concentration: 0.047 kg/m^3

LDF method

Amount adsorbed (g/g)	0.189	0.2	0.209	0.215	0.218
Time (min)	95	195	265	345	405
Average adsorbed, q	0.094	0.194	0.204	0.212	0.2165
$\frac{dq}{dt} \times 10^4$	10.0	1.42	1.0	1.0	--

Uptake curve method

$\ln(1-q/q^*)$	-2.21	-2.75	-3.59
Time (min)	195	265	345

Run Number: IS81, Flow rate: $0.975 \times 10^{-6} \text{ m}^3/\text{sec}$, Inlet Concentration: 0.047 kg/m^3

LDF method

Amount adsorbed (g/g)	0.206	0.219	0.227	0.231	0.238	0.239	0.245
Time (min)	95	195	270	345	405	490	540
Average adsorbed, q	0.103	0.2125	0.223	0.229	0.2395	0.238	0.242
$\frac{dq}{dt} \times 10^4$	10.95	1.4	0.8	1.75	0.148	-	-

Uptake curve method

$\ln(1-q/q^*)$	-2.02	-2.41	-2.73	-3.79
Time (min)	195	270	345	405

Run Number: IS82, Flow rate: $0.86 \times 10^{-6} \text{ m}^3/\text{sec}$, Inlet Concentration: 0.073 kg/m^3

LDF method

Amount adsorbed (g/g)	0.1852	0.1978	0.2148	0.2236	0.234	0.24	0.245	0.255	0.265	0.274
Time (min)	45	92	195	255	315	430	520	600	700	870
Average adsorbed, q	0.0926	0.1915	0.2063	0.2192	0.2288	0.237	0.2425	0.25	0.26	0.27
$\frac{dq}{dt} \times 10^4$	21.0	1.44	2.15	1.6	0.71	0.611	-	-	-	-

Uptake curve method

$\ln(1-q/q^*)$	-1.20	-1.39	-1.61	-1.80	-2.0	-2.16	-2.43	-2.97
Time (min)	92	195	255	315	430	520	600	700

Run Number: IS83, Flow rate: $1.51 \times 10^{-6} \text{ m}^3/\text{sec}$, Inlet Concentration: 0.092 kg/m^3

LDF method

Amount adsorbed (g/g)	0.212	0.226	0.2478	0.252	0.265	0.272	0.281	0.301
Time (min)	45	87	195	255	315	430	520	680
Average adsorbed, q	0.106	0.219	0.2369	0.249	0.258	0.268	0.276	0.291
$\frac{dq}{dt} \times 10^4$	26.9	1.65	2.02	1.5	0.87	0.88	0.937	-

Uptake curve method

$\ln(1-q/q^*)$	-1.218	-1.389	-1.733	-1.815	-2.123	-2.339	-2.711
Time (min)	45	87	195	255	315	430	520

Run Number: IS84, Flow rate: $7.0 \times 10^{-6} \text{ m}^3/\text{sec}$, Inlet Concentration: 0.56 kg/m^3

LDF method

Amount adsorbed (g/g)	0.2153	0.2513	0.305	0.328	0.342	0.365	0.371	0.375	0.376
Time (min)	87	192	432	572	634	767	802	827	857
Average adsorbed, q	0.1076	0.233	0.26	0.316	0.335	0.354	0.368	0.373	0.3755
$\frac{dq}{dt} \times 10^4$	4.41	-	4.0	3.06	1.96	-	1.36	-	-

Uptake curve method

$\ln(1-q/q^*)$	-1.175	-1.83	-2.21	-2.83	-3.85
Time (min)	432	572	634	767	802

Run Number: IS85, Flow rate: $4.0 \times 10^{-6} \text{ m}^3/\text{sec}$, Inlet Concentration: 0.073 kg/m^3

LDF method

Amount adsorbed (g/g)	0.2307	0.243	0.2805
Time (min)	85	103	242
Average adsorbed, q	0.115	0.237	0.262
$\frac{dq}{dt} \times 10^4$	67.77	1.79	-

Uptake curve method

$\ln(1-q/q^*)$	-1.728	-2.012
Time (min)	85	103

Run Number: IS86, Flow rate: $4.0 \times 10^{-6} \text{ m}^3/\text{sec}$, Inlet Concentration: 0.092 kg/m^3

LDf method

Amount adsorbed (g/g)	0.2215	0.2368	0.2529	0.2645	0.2695	0.2812	0.2877	0.2934	0.2979	0.299
Time (min)	45	120	181	250	305	365	430	495.0	550	670
Average adsorbed, q	0.1107	0.229	0.245	0.258	0.267	0.2753	0.284	0.2905	0.2956	0.2989
$\frac{dq}{dt} \times 10^4$	15.77	2.6	1.88	1.64	1.38	1.34	1.0	0.93	0.275	-

Uptake curve method

$\ln(1-q/q')$	-1.341	-1.558	-1.853	-2.136	-2.289	-2.774	-3.202	-3.831	-5.01
Time (min)	45	120	181	250	305	365	430	495	550

Run Number: IS87, Flow rate: $4.34 \times 10^{-6} \text{ m}^3/\text{sec}$, Inlet Concentration: 0.43 kg/m^3

LDf method

Amount adsorbed (g/g)	0.2249	0.2615	0.283	0.3069	0.3243	0.335	0.3525	0.356	0.36
Time (min)	38	105	165	230	290	350	415	465	515
Average adsorbed, q	0.1124	0.243	0.272	0.2949	0.3156	0.3296	0.3437	0.354	0.358
$\frac{dq}{dt} \times 10^4$	19.49	4.83	3.52	3.45	2.33	2.16	1.43	-	-

Uptake curve method

$\ln(1-q/q')$	-1.41	-1.71	-2.1	-2.47	-3.1	-4.1
Time (min)	165	230	290	350	415	465

Run Number: IS88, Flow rate: $4.0 \times 10^{-6} \text{ m}^3/\text{sec}$, Inlet Concentration: 0.12 kg/m^3

LDf method

Amount adsorbed (g/g)	0.2034	0.2417	0.255	0.276	0.2906	0.3015	0.3086	0.3186	0.322	0.324
Time (min)	30	95	156	260	320	400	460	535	565	600
Average adsorbed, q	0.1017	0.223	0.248	0.265	0.283	0.296	0.305	0.3136	0.320	0.323
$\frac{dq}{dt} \times 10^4$	18.95	4.09	1.63	3.0	1.63	1.5	1.14	1.21	-	-

Uptake curve method

$\ln(1-q/q')$	-1.16	-1.45	-1.70	-2.06	-2.45	-2.84	-3.44	-4.39
Time (min)	95	156	260	320	400	460	535	565

Run Number: IS89, Flow rate: $4.0 \times 10^{-6} \text{ m}^3/\text{sec}$, Inlet Concentration: 0.27 kg/m^3

LDf method

Amount adsorbed (g/g)	0.2293	0.258	0.283	0.2907	0.3029	0.3067	0.322	0.333	0.35
Time (min)	65	145	225	310	370	430	550	610	685
Average adsorbed, q	0.1146	0.243	0.2707	0.2871	0.296	0.3048	0.314	0.327	0.339
$\frac{dq}{dt} \times 10^4$	16.05	3.46	1.93	1.48	1.46	0.76	2.17	1.6	-

Uptake curve method

$\ln(1-q/q')$	-1.18	-1.48	-1.72	-1.87	-2.046	-2.27	-2.72
Time (min)	145	225	310	370	430	550	610

Run Number: IS90, Flow rate: $6.5 \times 10^{-6} \text{ m}^3/\text{sec}$, Inlet Concentration: 0.60 kg/m^3

LDF method												
Amount adsorbed (g/g)	0.216	0.252	0.271	0.2931	0.316	0.329	0.337	0.343	0.350	0.363	0.372	0.377
Time (min)	45	115	165	265	330	390	450	530	590	650	700	745
Average adsorbed, q	0.108	0.234	0.261	0.2821	0.302	0.320	0.333	0.34	0.346	0.356	0.37	0.375
$\frac{dq}{dt} \times 10^4$	18.0	5.4	2.63	-	-	2.13	1.15	-	-	1.47	-	-

Uptake curve method												
$\ln(1-q/q)$	-1.18	-1.38	-1.61	-1.89	-2.15	-2.32	-2.50	-2.89	-3.98			
Time (min)	165	265	330	390	450	530	590	650	700			

Run Number: IS91, Flow rate: $1.49 \times 10^{-6} \text{ m}^3/\text{sec}$, Inlet Concentration: 0.027 kg/m^3

LDF method							
Amount adsorbed (g/g)	0.084	0.0948	0.1098	0.119	0.125	0.13	0.135
Time (min)	50	110	210	270	330	400	450
Average adsorbed, q	0.042	0.089	0.102	0.114	0.122	0.127	0.133
$\frac{dq}{dt} \times 10^4$	7.83	1.3	2.0	1.33	0.66	-	-

Uptake curve method							
$\ln(1-q/q)$	-1.40	-1.86	-2.34	-2.82			
Time (min)	210	270	330	400			

APPENDIX-III

Experimental Dynamic Adsorption Data for Ethyl Acetate Adsorption on
E-merck 5A and 13X Molecular Sieves

System: 5A-Ethyl Acetate,

Run Number: DS3, T_{go} : 34 °C, Inlet velocity 0.008 m/s, c_o : 0.60 kg/m³, Height of bed: 18 cm

Concentration Breakthrough data

Time (min)	5	30	50	60	70	80	100	120	145	175	210	250	300	360	385
c/c_o	0.0	0.011	0.05	0.133	0.18	0.26	0.39	0.51	0.62	0.73	0.812	0.866	0.945	0.988	0.998

Temperature Breakthrough data

Time (min)	5	30	45	50	60	70	80	100	175	205	250	300	360	385
T_g/T_{go}	1	1	1.002	1.002	1.003	1.003	1.003	1.003	1.003	1.002	1.002	1.002	1.002	1.002

Run Number: DS4, T_{go} : 32 °C, Inlet velocity 0.0046 m/s, c_o : 0.372 kg/m³, Height of bed: 18 cm

Concentration Breakthrough data

Time (min)	275	280	325	350	380	405	445	485	565	645	710	780
c/c_o	0.0	0.021	0.22	0.33	0.44	0.55	0.66	0.77	0.88	0.93	0.985	0.99

Temperature Breakthrough data

Time(min)	275	285	305	350	385	400	450	500	550	570
T_g/T_{go}	1	1.0016	1.0032	1.0032	1.0016	1.0016	1.0016	1.0016	1.0016	1.0016

Run Number: DS5, T_{go} : 32 °C, Inlet velocity 0.00288 m/s, c_o : 0.23 kg/m³, Height of bed: 18 cm

Concentration Breakthrough data

Time (min)	800	835	850	865	885	895	905	910	930	940	985	1020
c/c_o	0.0	0.0054	0.02	0.03	0.045	0.1	0.15	0.20	0.25	0.3	0.4	0.5
Time(min)	1065	1085	1115	1160	1215	1230	1245	1275				
c/c_o	0.65	0.69	0.77	0.88	0.925	0.95	0.975	0.984				

Run Number: DS7 T_{go} : 32 °C, Inlet velocity 0.00288 m/s, c_o : 0.372 kg/m³, Height of bed: 18 cm

Concentration Breakthrough data

Time (min)	400	455	470	480	510	525	535	570	585	600	620	645	680
c/c_o	0.0	0.002	0.0033	0.0093	0.044	0.08	0.11	0.22	0.28	0.355	0.44	0.543	0.66
Time(min)			730	770	810	845	915	930					
c/c_o			0.77	0.84	0.876	0.9	0.98	0.99					

Run Number: DS9 T_{go} : 32 °C, Inlet velocity 0.008 m/s, c_o : 0.372 kg/m³, Height of bed: 18 cm

Concentration Breakthrough data

Time(min)	125	130	140	155	175	205	225	265	320	365	435	485	495	505	520
c/c_o	0.0	0.0035	0.018	0.23	0.33	0.46	0.52	0.67	0.81	0.86	0.93	0.977	0.984	0.988	0.991

Run Number: DS10 T_{go} : 32 °C, Inlet velocity 0.0046 m/s, c_o : 0.372 kg/m³, Height of bed: 6 cm

Concentration Breakthrough data

Time(min)	25	40	55	85	110	150	190	240	300	360	390	425	440	480
c/c_o	0.0084	0.044	0.11	0.33	0.44	0.59	0.69	0.8	0.88	0.92	0.935	0.955	0.966	0.985

Run Number: DS11 T_{go} : 34 °C, Inlet velocity 0.008 m/s, c_o : 0.71 kg/m³, Height of bed: 18 cm

Concentration Breakthrough data

Time(min)	15	30	40	55	65	85	100	115	135	150	175	195
c/c_o	0.0043	0.088	0.14	0.31	0.42	0.51	0.58	0.665	0.72	0.775	0.83	0.867

Time(min)	210	235	265	285	305
c/c_o	0.89	0.92	0.944	0.96	0.986

Run Number: DS12 T_{go} : 32 °C, Inlet velocity 0.0046 m/s, c_o : 0.372 kg/m³, Height of bed: 12 cm

Concentration Breakthrough data

Time (min)	125	145	165	180	195	230	255	275	325	375
c/c_o	0.0033	0.0144	0.067	0.15	0.2	0.32	0.44	0.52	0.66	0.76

Time (min)	450	515	585	650	670	700
c/c_o	0.86	0.991	0.95	0.965	0.98	0.99

Run Number: DS13 T_{go} : 32 °C, Inlet velocity 0.008 m/s, c_o : 0.22 kg/m³, Height of bed: 18 cm

Concentration Breakthrough data

Time(min)	140	155	170	205	230	250	300	350	455	520	590	655	675	705
c/c_o	0.078	0.153	0.256	0.303	0.44	0.545	0.66	0.764	0.85	0.911	0.95	0.965	0.98	0.99

System: 13X-Ethyl Acetate,

Run Number: DS15, T_{go} : 34 °C, Inlet velocity: 0.008 m/sec, c_o : 0.60 kg/m³, Height of bed: 18 cm

Concentration Breakthrough data

Time(min)	125	145	150	155	160	170	190	210	235	250	270	280	290
c/c_o	0	0.0043	0.0386	0.133	0.21	0.33	0.573	0.76	0.86	0.91	0.96	0.98	0.994

Temperature Breakthrough data

Time (min)	135	140	145	150	155	160	165	170	180	190	200	210	230	275	280
T_g/T_{go}	1.005	1.007	1.009	1.014	1.02	1.026	1.03	1.038	1.042	1.04	1.038	1.031	1.02	1.008	1.006

Run Number: DS16, T_{go} : 34 °C, Inlet velocity: 0.008 m/sec, c_o : 0.50 kg/m³, Height of bed: 18 cm

Concentration Breakthrough data

Time(min)	190	195	200	205	210	230	245	260	280	295	310	320	330	340	350	355
c/c_o	0.0	0.0018	0.05	0.09	0.33	0.52	0.65	0.75	0.85	0.9	0.95	0.96	0.97	0.98	0.993	0.995

Temperature Breakthrough data

Time (min)	160	165	170	175	180	185	190	195	200	205
T_g/T_{go}	1.0048	1.006	1.007	1.008	1.01	1.013	1.02	1.028	1.031	1.036

Time (min)	215	220	230	235	240	250	270	285	310	320
T_g/T_{go}	1.039	1.036	1.033	1.031	1.029	1.025	1.018	1.011	1.005	1.004

Run Number: DS17, T_{go} : 34 °C, Inlet velocity: 0.008 m/sec, c_o : 0.71 kg/m³, Height of bed: 18 cm

Concentration Breakthrough data

Time(min)	100	125	130	135	145	150	155	160	170	175	190	210	230	260
c/c_o	0.0	0.0076	0.12	0.2	0.33	0.4	0.46	0.5	0.6	0.66	0.77	0.88	0.93	0.987

Temperature Breakthrough data

Time (min)	100	105	110	115	120	125	130	135	140	145	150
T_g/T_{go}	1.0	1.0016	1.005	1.011	1.017	1.024	1.032	1.037	1.04	1.044	1.045

Time (min)	155	165	170	175	185	190	200	215	225	235	245	275
T_g/T_{go}	1.044	1.04	1.037	1.033	1.028	1.024	1.02	1.013	1.0098	1.006	1.006	1.0032

Run Number: DS18, T_{go} : 32 °C, Inlet velocity: 0.008 m/sec, c_o : 0.372 kg/m³, Height of bed: 18 cm

Concentration Breakthrough data

Time(min)	230	240	245	250	260	270	285	305	315	330	345	360	370	380	400	410	420
c/c_o	0.0	0.003	0.009	0.066	0.2	0.327	0.47	0.62	0.68	0.77	0.84	0.88	0.93	0.94	0.98	0.985	0.99

Temperature Breakthrough data

Time (min)	200	215	225	230	235	240	245	250	255	260	265	275
T_g/T_{go}	1.0	1.0032	1.009	1.01	1.011	1.0114	1.013	1.014	1.017	1.02	1.021	1.023

Time (min)	285	290	295	310	320	330	350	370	385	400
T_g/T_{go}	1.028	1.029	1.031	1.029	1.026	1.023	1.012	1.009	1.006	1.005

Run Number: DS19, T_{go} : 33 °C, Inlet velocity: 0.0148 m/sec, c_o : 0.3 kg/m³, Height of bed: 18 cm

Concentration Breakthrough data

Time (min)	120	125	135	145	155	165	175	195	205	225	255	280	325	335	345	360
c/c_o	0	0.0044	0.118	0.234	0.35	0.45	0.485	0.62	0.72	0.78	0.875	0.94	0.97	0.984	0.992	0.995

Temperature Breakthrough data

Time (min)	90	100	110	115	120	135	155	160	165	175	185	200	205	210
T_g/T_{go}	1	1.0014	1.002	1.004	1.006	1.011	1.0196	1.023	1.026	1.028	1.032	1.03	1.028	1.026

Time (min)	215	220	225	235	240	250	255	265	275	290	310	330
T_g/T_{go}	1.024	1.023	1.021	1.0195	1.018	1.016	1.015	1.013	1.011	1.008	1.0032	1.0032

Run Number: DS20, T_{go} : 32 °C, Inlet velocity: 0.0046 m/sec, c_o : 0.372 kg/m³, Height of bed: 18 cm

Concentration Breakthrough data

Time (min)	450	460	465	470	475	480	495	500	510	525	550	570	600	630	655	685
c/c_o	0.0	0.0024	0.0067	0.011	0.016	0.02	0.084	0.21	0.35	0.423	0.66	0.78	0.88	0.93	0.95	0.986

Temperature Breakthrough data

Time (min)	400	415	430	440	445	450	455	460	465	470	480	490	500	515
T_g/T_{go}	0	1.0016	1.0032	1.0065	1.0078	1.008	1.01	1.0114	1.013	1.015	1.018	1.023	1.029	1.03

Time (min)	525	530	560	580	600	620	635	650	665	690	715	745
T_g/T_{go}	1.029	1.027	1.023	1.016	1.013	1.011	1.0098	1.008	1.0065	1.0049	1.0032	1.0016

Run Number: DS21, T_{go} : 34 °C, Inlet velocity: 0.008 m/sec, c_o : 0.60 kg/m³, Height of bed: 12 cm

Concentration Breakthrough data

Time (min)	75	80	100	120	130	140	150	155	180	190	205	220
c/c_o	0.0	0.0053	0.238	0.493	0.64	0.73	0.77	0.79	0.89	0.933	0.973	0.993

Temperature Breakthrough data

Time (min)	50	55	60	65	70	75	80	90	100	110	115
T_g/T_{go}	1.0	1.0049	1.0088	1.014	1.018	1.021	1.0245	1.03	1.033	1.036	1.039

Time (min)	120	135	140	150	155	160	165	170	180	190	195
T_g/T_{go}	1.04	1.036	1.033	1.03	1.026	1.023	1.019	1.016	1.013	1.009	1.009

Run Number: DS22, T_{go} : 34 °C, Inlet velocity: 0.008 m/sec, c_o : 0.60 kg/m³, Height of bed: 6 cm

Concentration Breakthrough data

Time(min)	20	25	30	40	55	75	80	95	105	125	140	150	155
c/c_o	0	0.0021	0.067	0.31	0.533	0.76	0.79	0.86	0.893	0.95	0.98	0.986	0.997

Temperature Breakthrough data

Time (min)	5	10	15	20	25	30	35	40	45	50	55	65	70	80	90	125	135
T_g/T_{go}	1.0	1.008	1.023	1.026	1.029	1.033	1.036	1.039	1.042	1.039	1.036	1.033	1.029	1.026	1.021	1.008	1.005

Run Number: DS24, T_{g0} : 32 °C, Inlet velocity: 0.0148 m/sec, c_0 : 0.372 kg/m³, Height of bed: 18 cm

Concentration Breakthrough data

Time(min)	100	105	115	120	130	145	160	180	195	210	230	240	250	260
c/c_0	0.0	0.0033	0.16	0.24	0.33	0.45	0.6	0.75	0.81	0.88	0.92	0.95	0.98	0.99

Temperature Breakthrough data

Time (min)	80	90	95	100	105	110	115	120	130	140	155
T_g/T_{g0}	1.0	1.0019	1.0032	1.013	1.018	1.021	1.023	1.028	1.031	1.034	1.032

Time (min)	165	175	180	185	195	200	205	210	220	230	235	245
T_g/T_{g0}	1.03	1.028	1.026	1.021	1.018	1.016	1.015	1.013	1.0098	1.008	1.0065	1.005

ERRATA

Page No.	Line No.	Corrections
151	3 rd from top	In place of 1997, should be read as 1997,a
151	6th from top	In place of 1997, should be read as 1997,b
151	8th from top	In place of 1997, should be read as 1997,c
152	4 th from bottom	Journal name should be read as Industrial and Engineering Chemistry Research
54	9th line from top	Eq (2.23), second term on right hand side did not include ϵ , It is typing mistake. ϵ should be included in second term on right hand side.
Name of Journal, Industrial and Engineering Chemistry Research is wrongly typed, as Industrial Engineering and Chemistry Research should be read as Industrial and Engineering Chemistry Research.		